© Copyright 2022

Minyong Lee

Biocementation for Liquefaction Mitigation: Examining Response, Development, and Deployment

Minyong Lee

A dissertation

submitted in partial fulfillment of the

requirements for the degree of

Doctor of Philosophy

University of Washington

2022

Reading Committee:

Michael Gomez, Chair

Brett Maurer

Pedro Arduino

Program Authorized to Offer Degree:

Civil and Environmental Engineering

University of Washington

Abstract

Biocementation for Liquefaction Mitigation:
Examining Response, Development, and Deployment

Minyong Lee

Chair of the Supervisory Committee:
Michael Gomez
Department of Civil and Environmental Engineering

Microbially Induced Calcite Precipitation (MICP) is an environmentally conscious soil improvement technique that can improve the geotechnical properties of granular soils through the precipitation of $CaCO_3$ minerals on soil particle surfaces and contacts. The resulting biocementation affords significant improvements in soil shear strength and initial shear stiffness, while achieving minor reductions in soil hydraulic conductivity and porosity. The process has been investigated for wide variety of geotechnical and geoenvironmental applications, however, perhaps most notably the technology has been proposed for the mitigation of earthquake-induced soil liquefaction. Despite extensive demonstrations at the laboratory scale, critical gaps regarding our understanding of the undrained cyclic behavior of biocemented soils, the efficacy of treatment techniques at meter-scale, and the management of generated aqueous nitrogen by-products has

limited practical adoption of the technology for liquefaction mitigation purposes. In this research, a series of experiments at both centimeter- and meter-scales were performed in combination with reactive transport modeling in order to (1) further characterize the liquefaction behaviors of biocemented sands including triggering and post-triggering responses, (2) develop new techniques that can control the enrichment of indigenous ureolytic microorganisms to improve cementation spatial uniformity and extent, (3) identify post-treatment processes by which ammonium by-products can be effectively removed, and (4) evaluate the success of the developed treatment techniques when applied over meter-scale treatment distances. The results of this work suggest that (1) the liquefaction triggering resistance of biocemented soils can be significantly improved with the addition of even small magnitudes of cementation (ΔV_s > 25 m/s), however, improvements in post-triggering behaviors require higher magnitudes of cementation (ΔV_s > 50 to 150 m/s), which can improve larger-strain behaviors by densifying soils in addition to providing interparticle bonding and cemented particle coatings, (2) enrichment techniques can be modified to regulate stimulated bulk ureolytic activities with the ability to achieve improved spatial control of the biocementation process, (3) ammonium by-products can be successively removed from soil particle surfaces and pore fluids using post-treatment rinse injections containing cations that permit improved cation exchange with sorbed ammonium masses, and (4) developed techniques can be successfully up-scaled to uniformly improve soils over meter-scale distances, effectively remove generated ammonium by-products, and realize mechanical enhancements far exceeding those needed for most liquefaction mitigation applications. The primary outcomes of this research identify novel and effective field-ready treatment techniques for stimulated MICP as well as provide new understandings regarding the deployment of MICP at meter-scale and the liquefaction

behaviors of biocemented soils, ultimately furthering the development of the technology for practical liquefaction mitigation applications.

TABLE OF CONTENTS

List of Figures ix

List of Tables xx

Acknowledgements xxii

Chapter 1. Introduction 1

Chapter 2. Research Objectives and Scope 10

2.1 Research Objectives 10

2.2 Research Activities 11

Chapter 3. Background and Literature Review 18

3.1 Introduction to MICP 18

3.2 Biological Strategies for MICP 20

3.3 Treatment Processes and Related Monitoring Methods 22

3.4 Mechanical Enhancements Resulting from Biocementation 24

3.5 Large-Scale Demonstrations 28

3.6 Knowledge Gaps and Remaining Challenges 31

Chapter 4. Effect of Light Biocementation on the Liquefaction Triggering and Post-Triggering Behavior of Loose Sands 36

4.1 Introduction 37

4.2 Materials and Methods 43

4.2.1 Sand Material 43

4.2.2 Direct Simple Shear Apparatus 44
4.2.3 Specimen Preparation 45
4.2.4 Biocementation Treatments 47
4.2.5 Shear and Compression Wave Velocity Measurements 50
4.2.6 Undrained Cyclic Shearing 50
4.2.7 Undrained Monotonic Shearing 51
4.2.8 $CaCO_3$ Content Measurements 52
4.2.9 SEM Imaging 52
4.3 Results 53
4.3.1 Summary of Undrained Cyclic Tests 53
4.3.2 Biocementation-induced Changes in V_s, D_r, and Soil Microstructure 56
4.3.3 Effect of Biocementation on Pre-Triggering Behaviors 59
4.3.4 Effect of Biocementation on Post-Triggering Behaviors 70
4.3.5 Summary of Undrained Monotonic Tests 75
4.3.6 Effect of Biocementation on Undrained Monotonic Behaviors 76
4.4 Conclusions 79
Chapter 5. Improving the Spatial Control of Soil Biocementation using Indigenous Microorganisms: Column Experiments and Reactive Transport Modeling 81
5.1 Introduction 82
5.2 Materials and Methods 87
5.2.1 Soil Materials 87
5.2.2 Centimeter-scale Soil Column Specimens 87
5.2.3 Treatment Injections 88

5.2.4 Aqueous Sampling 89
5.2.5 Aqueous Measurements 90
5.2.6 Shear Wave Velocity Measurements 90
5.2.7 Soil Sampling and $CaCO_3$ Content Measurements 91
5.2.8 Previous Meter-scale Soil Column Experiments 91
5.2.9 PHREEQC Modeling 92
5.3 Results and Discussion 95
5.3.1 Set A Centimeter-scale Soil Column Experiments 95
5.3.2 Set B Centimeter-scale Soil Column Experiments 99
5.3.3 Summary of Ureolytic Rates Obtained in Centimeter-scale Soil Column Experiments 104
5.3.4 Reactive Transport Simulations 107
5.3.5 Characterizing Biocementation Treatment Conditions and Outcomes 114
5.3.6 Practical Implications of Reduced Reaction Rates 120
5.4 Conclusions 122
Chapter 6. Investigating Ammonium By-Product Removal Following Stimulated Ureolytic Microbially-Induced Calcite Precipitation 125
6.1 Introduction 126
6.2 Materials and Methods 129
6.2.1 Soil Column Specimens 129
6.2.2 Treatment Injections 130
6.2.3 Shear Wave Velocity Measurements 132
6.2.4 Aqueous Chemical Measurements 132

6.2.5 Ammonium Bromide Tracer Testing 133
6.2.6 Unconfined Compressive Strength Measurements 134
6.2.7 Calcite Content Measurements 134
6.3 Results and Discussion 135
6.3.1 Ammonium Bromide Tracer Testing 135
6.3.2 Aqueous Solution Chemistry 137
6.3.3 Shear Wave Velocity 138
6.3.4 Ammonium Removal 140
6.3.5 Unconfined Compressive Strength 142
6.3.6 Calcite Content 143
6.4 Conclusions 144

Chapter 7. Examination of Rinse Injection Strategies for Removal of Ammonium By-products Following Biocemenatation Soil Improvement 146

7.1 Introduction 147
7.2 Materials and Methods 153
7.2.1 Soil Materials 153
7.2.2 Soil Columns Specimens 154
7.2.3 Treatment Injections 155
7.2.4 Passive Tracer Testing 156
7.2.5 Treatment Schemes 156
7.2.6 Aqueous Samples 161
7.2.7 Aqueous Chemical Measurements 162
7.2.8 Shear Wave Velocity Measurements 163

7.2.9 Post-treatment Soil Sampling 163
7.2.10 Soil NH_4^+ Extractions 164
7.2.11 Soil $CaCO_3$ Content Measurements 165
7.3 Results 165
7.3.1 Passive Tracer Testing 165
7.3.2 Biogeochemical & Mechanical Changes During Biocementation 167
7.3.3 NH_4^+ Removal During Rinse Injections 170
7.3.4 NH_4^+ Removal Achieved Following Rinsing 177
7.3.5 Effect of Rinsing on Cementation Integrity 186
7.4 Conclusions 191

Chapter 8. Meter-Scale Biocementation Experiments to Advance Process Control and Reduce Impacts: Examining Spatial Control, Ammonium By-Product Removal, and Chemical Reductions 195

8.1 Introduction 196
8.2 Experimental Objectives and Development 200
8.2.1 Experimental Development 200
8.2.2 Control of Stimulated Ureolysis 200
8.2.3 Ammonium By-product Removal 201
8.2.4 Solution Optimization 201
8.2.5 Reactive Transport Pre-modeling 202
8.2.6 Experiment Objectives 203
8.2.7 Experiment Rationale 203
8.3 Materials and Methods 206

8.3.1 Meter-scale Soil Columns 206
8.3.2 Treatment Application System 207
8.3.3 Treatment Schemes 208
8.3.4 Soil Materials 209
8.3.5 Treatment Solutions 210
8.3.6 Passive Tracer Measurements 211
8.3.7 Aqueous Sampling 211
8.3.8 Shear Wave Velocity Measurements 212
8.3.9 Hydraulic Conductivity Measurements 212
8.3.10 Biological Measurements 213
8.3.11 Soil Sample Measurements 213
8.3.12 Chemical Measurements 214
8.4 Results and Discussion 215
8.4.1 Passive Tracer Testing 215
8.4.2 Biological Monitoring 216
8.4.3 Shear Wave Velocity Measurements 219
8.4.4 Calcite Content Measurements 221
8.4.5 Hydraulic Conductivity Measurements 224
8.4.6 Ammonium By-Product Removal 225
8.5 Conclusions 226
Chapter 9. Investigating Ammonium By-product Removal for Ureolytic Biocementation Using Meter-scale Experiments 229
9.1 Introduction 230

9.2 Materials and Methods 234
9.2.1 Soil Materials 234
9.2.2 Soil Columns 235
9.2.3 Saturation and Bromide Passive Tracer Testing 237
9.2.4 Treatment Injections 238
9.2.5 Aqueous Sampling 240
9.2.6 Shear Wave Velocity Measurements 241
9.2.7 Aqueous Measurements 241
9.2.8 Cation Exchange Capacity and Exchangeable Cation Measurements 242
9.2.9 Soil Sampling and Soil NH_4^+ Measurements 243
9.3 Results and Discussion 244
9.4 Conclusions 261
Chapter 10. Effect of Biocementation on the Liquefaction Behavior of Ottawa F-65 Sand 263
10.1 Introduction 264
10.2 Materials and Methods 270
10.2.1 Sand Material 270
10.2.2 Direct Simple Shear Apparatus 271
10.2.3 Specimen Preparation 271
10.2.4 Biocementation Treatments 273
10.2.5 Shear and Compression Wave Velocity Measurements 275
10.2.6 Drained and Undrained Monotonic Shearing 276
10.2.7 Undrained Cyclic Shearing 277
10.2.8 Dry Density & $CaCO_3$ Content Measurements 278

10.3 Results and Discussion 279
10.3.1 Changes in Specimen V_s, $CaCO_3$ Contents, & Dry Densities with Biocementation 279
10.3.2 Effect of Biocementation on Drained Monotonic Behaviors 280
10.3.3 Effect of Biocementation on Undrained Monotonic Behaviors 285
10.3.4 Determination of 0.25 Cycle Triggering Resistances From Undrained Cyclic & Monotonic Tests 291
10.3.5 Effect of Biocementation on Undrained Cyclic Behaviors 294
10.3.6 Effect of Biocementation on Pre-triggering Behaviors 301
10.3.7 Effect of Biocementation on Post-triggering Behaviors 310
10.4 Conclusions 321
Chapter 11. Future Work 325
11.1 Continued Characterization of the Undrained Cyclic Behavior and Dynamic Properties of Biocemented Sands 325
11.2 Optimization of Rinse Injection Sequencing and Solution Compositions for Post-treatment Ammonium By-product Removal 326
11.3 Investigation of Biological Nitrogen Transformations for By-product Management 327
11.4 Deployment, Monitoring, and Verification of Biocementation at Field-scale 327
Bibliography 329
Appendix A. Chapter 5 Supplementary Tables and Figures 361
Appendix B. Chapter 7 Supplementary Figure 366
Appendix C. Chapter 10 Supplementary Tables 367

LIST OF FIGURES

Figure 3.1. Overview of the MICP process including the (a) MICP reaction network, (b) scanning electron microscope images of biocemented sands, and (c) an image of a biocemented sand column after failure following an unconfined compression test. 20

Figure 4.1. Images of the (a) direct simple shear (DSS) testing apparatus, treatment application set-up, bender-extender element monitoring system, and (b) DSS specimen configuration including saturation and treatment application ports and ring retainment system.... 44

Figure 4.2. Relationships between cementation-induced shear wave velocity increases (ΔV_s), soil $CaCO_3$ contents, and changes in soil total relative densities (ΔD_r) for all biocemented and uncemented loose ($D_{r\ initial} \approx 30\%$) Ottawa F-65 specimens subjected to undrained cyclic and monotonic loading. 57

Figure 4.3. Scanning electron microscope (SEM) images of (a, b) untreated Ottawa F-65 sand, and biocemented Ottawa F-65 sand specimens with ΔV_s increases of (c, d) 36 m/s and (e, f) 77 m/s. 58

Figure 4.4. Results from undrained cyclic DSS tests performed on loose ($D_{r\ initial} \approx 30\%$) Ottawa F-65 specimens of varying cementation levels (assessed by ΔV_s) subjected to a CSR of 0.2. Plots in each column show: (i) shear stress versus vertical effective stress, (ii) shear stress versus shear strain, (iii) shear stress versus cycle number, and (iv) r_u ($=\Delta u/\sigma'_{v\ initial}$) versus cycle number. 60

Figure 4.5. Number of cycles from (a) $r_u = 0$ to 0.475 and (b) $r_u = 0.475$ to 0.95, and (c) the ratio [cycles from $r_u = 0$ to 0.475 / cycles from $r_u = 0.475$ to 0.95] versus ΔV_s from cementation for loose (D_r initial $\approx 30\%$) biocemented specimens. Number of cycles (d) from $r_u = 0$ to 0.475 and (e) from $r_u = 0.475$ to 0.95, and (f) the ratio [cycles from $r_u = 0$ to 0.475 / cycles from $r_u = 0.475$ to 0.95] versus total D_r for all biocemented and uncemented specimens with varying relative densities. 61

Figure 4.6. Evolution of maximum excess pore pressure ratios ($r_u = \Delta u/\sigma'_{v\ initial}$) with shear strain for loose specimens of varying-cementation levels subjected to a CSR of 0.2, wherein the maximum excess pore pressure ratio (r_u) is the largest r_u value that a specimen has experienced

prior to achieving different shear strains. Plots present similar data for shear strains from 0% to (a) 3% and (b) 15%. Data points were evaluated at discrete increments of 0.05% shear strain. 63

Figure 4.7. Number of cycles to 3% SASS versus number of cycles to $r_u = 0.95$ for specimens of varying biocementation (as indicated by ΔV_s) subjected to different applied CSRs. A 1:1 trendline is provided to compare criteria. 65

Figure 4.8. Number of cycles to 3% SASS versus (a) ΔV_s from biocementation and (b) $CaCO_3$ contents for loose ($D_{r\ initial} \approx 30\%$) specimens of varying biocementation. (c) Number of cycles to 3% SASS versus total relative densities (D_r) for all biocemented and uncemented specimens of varying D_r. 66

Figure 4.9. Relationships between (a) applied CSRs versus number of cycles to 3% SASS and (b) improvement ratios ($N_{3\%\ SASS\ Cemented}$ / $N_{3\%\ SASS\ Uncemented}$) versus applied CSRs for loose ($D_{r\ initial} \approx 30\%$) specimens of varying biocementation levels (ΔV_s = 0, 10, 25, 50, 75, 100 m/s). 68

Figure 4.10. Number of cycles from 3% to 9% SASS versus (a) ΔV_s from cementation for loose ($D_{r\ initial} \approx 30\%$) specimens of varying biocementation and (b) D_r for all biocemented specimens and uncemented specimens prepared at varying D_r. (c) Number of cycles from 3% SASS to 24% DASS versus ΔV_s from cementation for loose ($D_{r\ initial} \approx 30\%$) specimens of varying biocementation. 72

Figure 4.11. Reconsolidation strains versus (a) ΔV_s from cementation for loose ($D_{r\ initial} \approx 30\%$) specimens of varying biocementation levels and (b) total D_r for all biocemented loose specimens and uncemented specimens prepared at varying initial D_r. 73

Figure 4.12. Shear wave velocity changes (ΔV_s) following shearing and reconsolidation events versus shear wave velocity increases (ΔV_s) from cementation for loose ($D_{r\ initial} \approx 30\%$) specimens of varying cementation with different applied CSRs. Data points plotting near the 1:1 trendline suggest that increases in V_s from cementation were eliminated following shearing and reconsolidation events. 74

Figure 4.13. Results from undrained monotonic tests on loose ($D_{r\ initial} \approx 30\%$) specimens of varying biocementation levels including plots of (a) shear stresses versus shear strains, (b) shear stresses versus vertical effective stresses, and (c) excess pore water pressures (Δu) versus shear strains. 77

Figure 4.14. Relationships between applied CSRs required to achieve 3% SASS in 0.25 cycles and ΔV_s from cementation for loose ($D_{r\ initial} \approx 30\%$) specimens of varying cementation as determined from both undrained monotonic and cyclic DSS tests. 78

Figure 5.1. Solution urea concentrations (mM) in time during the **(a)** 2nd, **(b)** 4th, and **(c)** 6th stimulation injection and the **(d)** 3rd, **(e)** 6th, **(f)** 8th, and **(g)** 10th cementation injection for all set A columns. Urea concentrations supplied in injected solutions were 50 mM during stimulation and 350 mM during cementation. 94

Figure 5.2. Normalized urea degradation ($\Delta C/C_o$) observed after 24-hour injection and retention periods during all **(a)** stimulation and **(b)** cementation injections in set A columns. 96

Figure 5.3. Soil $CaCO_3$ contents versus distance from injection location for all experiment set A columns. Provided error bars indicate ± one standard deviation for all measurements. 97

Figure 5.4. Solution urea concentrations (mM) in time during the **(a)** 2nd and **(b)** 6th stimulation injection and the **(c)** 1st, **(d)** 5th, and **(e)** 9th cementation injection for all set B columns. Urea concentrations provided in injected solutions were 50 mM during stimulation and 250 mM during cementation. 99

Figure 5.5. Normalized urea degradation ($\Delta C/C_o$) observed 24-hours after all **(a)** stimulation and **(b)** cementation injections and 48-hours after all **(c)** cementation injections in set B columns. 101

Figure 5.6. Soil column shear wave velocities (V_s) measured immediately before all injections during experiment set B at the mid-height of columns. 103

Figure 5.7. Soil column $CaCO_3$ contents versus distance from injection location for all experiment set B columns. Provided error bars indicate ± one standard deviation for all measurements. 104

Figure 5.8. Bulk V_{max} values versus supplied YE concentrations obtained during select stimulation and cementation injections for all soil columns from experiment set **(a)** A and **(b**) B. 106

Figure 5.9. Comparison of normalized urea concentrations (C/C_0) in time from the 0.01 g/L YE daily, 0.07 g/L YE alternating, and 0.2 g/L YE daily columns from set A during cementation injection 8 with simulated trends from PHREEQC models assuming bulk V_{max} values of 6.4, 28.8, or 108.8 mM urea/hr. 108

Figure 5.10. Simulated soil column $CaCO_3$ distributions **(a, b, c)** immediately after injections and **(d, e, f)** following reaction completion for select injection rates including **(a, d)** 0.06 PV/hr

(50 mL/min), **(b, e)** 0.3 PV/hr (250 mL/min) and **(c, f)** 1.8 PV/hr (1500 mL/min) for the three different ureolytic reaction rates (as described by YE additions). 110

Figure 5.11. Results from soil column simulations for different injection rates and ureolytic reaction rates (as described by YE additions) including: average $CaCO_3$ contents in columns **(a)** immediately after injections and **(b)** after reaction completion, **(c)** differences between column average $CaCO_3$ contents after injections and after reaction completion, $CaCO_3$ contents after reaction completion at the column **(d)** inlet and **(e)** outlet, and (**f)** outlet-to-inlet $CaCO_3$ content ratios after reaction completion versus injection rates. 112

Figure 5.12. Results from soil column simulation's for different injection rates and ureolytic reaction rates (as described by YE additions) including: average $CaCO_3$ contents in columns **(a)** immediately after injections and **(b)** after reaction completion, **(c)** differences between average $CaCO_3$ contents in columns after injections and after reaction completion, $CaCO_3$ contents after reaction completion at the column **(d)** inlet and **(e)** outlet, and (**f)** outlet-to-inlet $CaCO_3$ content ratios after reaction completion versus dimensionless reaction-to-injection duration ratios. 114

Figure 5.13. (a, c) Soil column $CaCO_3$ content distributions versus distance and **(b, d)** cumulative $CaCO_3$ content distributions versus normalized distance for **(a, b)** simulations with the highest (0.01 g/L YE daily, injection rate = 1.8 PV/hr) and lowest (0.2 g/L YE daily, injection rate = 0.06 PV/hr) reaction-to-injection duration ratios and **(c, d)** low and high ureolytic rate physical meter-scale experiments by San Pablo et al. (2020) involving a constant flow rate (0.48 PV/hr). Nonuniformity area (NA) values are indicated as shaded areas between respective cumulative $CaCO_3$ content distributions and dashed line trends expected for full uniformity (NA = 0%). 116

Figure 5.14. Nonuniformity area parameters determined from cumulative $CaCO_3$ distributions for all soil column simulations and low and high ureolytic rate physical meter-scale experiments by San Pablo et al. (2020) versus **(a)** reaction-to-injection duration ratios and **(b)** outlet-to-inlet $CaCO_3$ ratios. 119

Figure 5.15. Results from extended 15-meter-long soil column simulations including: **(a)** the percentage of supplied Ca^{2+} that was precipitated within the 3.67-meter-long column previously considered, and the treatment distances over which $CaCO_3$ contents exceeded **(b)** 0.25% and **(c)** 0.1% by mass versus reaction-to-injection duration ratios. 121

Figure 6.1. Spatial contours of total NH_4^+ concentrations during and after treatment injections in a meter-scale experiment involving stimulated ureolytic MICP indicated NH_4^+ concentrations exceeding 500 mM when urea concentrations of 350 mM were applied (Gomez et al. 2017). 128

Figure 6.2. Soil columns received solutions using a peristaltic pump and included sampling ports and bender elements at mid-height for monitoring of V_s and pore fluid chemistry during treatments. 131

Figure 6.3. (a) Normalized concentrations of bromide (Br^-) and total ammonium (NH_4^+) measured during 59 mM NH_4Br tracer testing, (b) cumulative mmol of bromide and ammonium determined from measured effluent concentrations and injected volumes. 135

Figure 6.4. (a) Solution pH and (b) urea measurements during stimulation and cementation phases. 137

Figure 6.5. Shear wave velocities (V_s) measured in all soil columns during stimulation, cementation, and ammonium removal rinse phases. 138

Figure 6.6. Aqueous total ammonium (NH_4^+/NH_3) concentrations at mid-height in soil columns during ammonium removal rinse injections and the 103-day solution retention period. 140

Figure 6.7. Solution pH values at mid-height in soil columns during ammonium removal rinse injections and the 103-day solution retention period. 142

Figure 6.8. Average calcite contents for column sections versus distance from injection port (error bars represent one standard deviation from average values). 144

Figure 7.1. Images of (a) soil column experiments with treatment application and shear wave velocity monitoring system and (b) a single soil column with loading frame, sampling and treatment ports, and bender element sensors. 155

Figure 7.2. Measurements of normalized effluent Br^- concentrations (C/C_0) versus injected volume obtained during passive tracer testing for twelve select soil column specimens. 166

Figure 7.3. Measurements of **(a)** normalized 24 hour urea degradation ($\Delta C/C_0$) and **(b)** pre-treatment solution pH obtained from mid-height column sampling ports for all stimulation and cementation treatments. 167

Figure 7.4. Shear wave velocities (V_s) measured at column mid-heights during all stimulation and cementation treatments. V_s measurements for C-Ca-200-E1 were not obtained beyond the 7th cementation injection due to sensor failure. 169

Figure 7.5. Measurements of aqueous NH_4^+ concentrations in column effluent solutions during continuous-rinse injections for **(a)** all continuous columns, **(b)** continuous columns receiving Ca^{2+}-based rinse solutions, **(c)** continuous columns receiving Na^+-based rinse solutions, and **(d)** continuous columns receiving rinse solutions with 200 mM of various cations. Effluent concentrations were not measured for columns with staged injections. 171

Figure 7.6. Measurements of mid-height aqueous NH_4^+ concentrations versus rinse injection volume for **(a)** all continuous and staged injection columns, **(b)** all columns receiving Ca^{2+}-based rinse solutions, **(c)** all columns receiving Na^+-based rinse solutions, and **(d)** all columns receiving rinse solutions with 200 mM concentrations of various cations. 174

Figure 7.7. Measurements of solution pH obtained from mid-height column sampling ports during rinse injections versus injected volume. 177

Figure 7.8. Measurements of **(a)** aqueous NH_4^+ concentrations versus column lengths, **(b)** sorbed NH_4^+ versus aqueous NH_4^+ concentrations (log-scale), **(c)** sorbed NH_4^+ concentrations versus column lengths, and **(d)** sorbed NH_4^+ masses versus aqueous NH_4^+ concentrations (linear-scale). Data included from recent meter-scale experiments (Lee et al. 2019b) involved the same Concrete Sand material and was obtained following continuous rinse injections of 200 mM $CaCl_2$ solutions. 180

Figure 7.9. Comparisons of **(a)** aqueous NH_4^+ removal, **(b)** sorbed NH_4^+ removal, and **(c)** total NH_4^+ removal in all columns as a function of column length. Removal was determined by comparing aqueous and sorbed NH_4^+ concentrations in all columns following rinsing to values measured in the single column receiving no rinse injections (No Rinse). 184

Figure 7.10. Shear wave velocity changes (ΔV_s) measured at column mid-heights during rinsing versus injected volume. 186

Figure 7.11. Summary of **(a)** soil column $CaCO_3$ contents by mass versus column length and **(b)** mid-height shear wave velocities (V_s) versus average soil column $CaCO_3$ contents by mass. 189

Figure 8.1. (a) Schematic of columns outlining locations of sampling ports and bender elements, treatment application systems, and the injected solution direction, (b) meter-scale column set-up, and (c) bender element pairs and sampling ports during soil placement. 205

Figure 8.2. Schedule of soil column treatments including treatment durations and type of treatment for each respective column. Black horizontal lines indicate when treatments were injected. 207

Figure 8.3. Measurements of C/C_0 versus injected volume from column outlet wells during passive tracer tests wherein a 15 mM NaBr solution was injected and rinsed with de-ionized (DI) water. 215

Figure 8.4. Aqueous cell densities versus distance from injection location for all columns during initial conditions (after saturation) and at the end of the 1st, 4th, and 9th cementation treatment. 216

Figure 8.5. Concentrations of aqueous urea in time at all port locations in all columns during the 9th cementation treatment. 217

Figure 8.6. Spatial contours of soil V_s for all columns after the 1st, 5th, and 9th cementation injection. 219

Figure 8.7. Increase in V_s in time at all sensor locations for all columns showing the progression of V_s with number of cementation treatments. 220

Figure 8.8. Comparison of calcite content spatial measurements with trend line interpretations for (a) Concrete Sand with different biological treatment types and (b) for low ureolytic rate stimulation treatments for different sands. 221

Figure 8.9. (a) Normalized shear wave velocity increases ($\Delta V_s/V_{s\ uncemented}$) versus soil calcite contents for columns with Concrete Sand with different biological treatment types and (b) columns with low ureolytic rate stimulation treatments for different sands. An interpreted linear trend line is shown on both plots for Concrete Sand columns. 223

Figure 8.10. Soil hydraulic conductivities along column lengths during the 1st, 5th, and 9th cementation injection. 224

Figure 8.11. Aqueous ammonium concentrations versus distance from injection location for all columns at 0 min, 700 min, and 1440 min after the start of the ammonium by-product removal injections. 226

Figure 9.1. Overview of meter-scale experiments including: (a) schematic of meter-scale soil columns with treatment application systems, sampling ports, and bender element locations, (b) images of soil columns during treatments, (c) treatment solution injection systems, and (d) biocemented soil materials during post-rinsing soil sampling. 237

Figure 9.2. Measurements of normalized bromide concentrations (C/C_0) versus injected volume during passive tracer testing for (a) Column 1 and 2, (b) Column 3 and 5, and (c) Column 4 with PHREEQC modelled comparisons. 247

Figure 9.3. Changes in aqueous NH_4^+ concentrations in time at all aqueous sampling port locations during the ninth cementation treatment. 249

Figure 9.4. Measurements of outlet well (a) solution pH and (b) aqueous NH_4^+ concentrations versus injected rinse solution volume with PHREEQC modeled passive tracer comparisons. 249

Figure 9.5. Contours of aqueous NH_4^+ concentrations within columns at all sampling port locations at various times during rinse injections. Measurement times after start of injections and cumulative injected rinse volumes are provided. 252

Figure 9.6. Changes in aqueous NH_4^+ concentrations following a 12 hour stop flow period after rinsing versus column length for all columns. 254

Figure 9.7. (a) Final NH_4^+ removal following the 12-hour stop flow period (in percent) versus column length and (b) cumulative NH_4^+ removal (in percent) versus rinse injection time. 255

Figure 9.8. Comparison of aqueous NH_4^+ concentrations between solution samples obtained from aqueous sampling ports (after the 12 hour stop flow period) and physical soil samples obtained post-rinsing. 256

Figure 9.9. (a) Sorbed NH_4^+ masses versus column lengths, (b) sorbed NH_4^+ masses as a percentage of soil CEC versus column lengths, (c) sorbed NH_4^+ masses versus aqueous NH_4^+ concentrations, and (d) "effective" aqueous NH_4^+ concentrations versus column lengths. 257

Figure 9.10. Soil shear wave velocities (V_s) versus column lengths for all columns before cementation, after cementation and immediately before rinsing, and after rinsing. 259

Figure 9.11. Changes in soil shear wave velocities (V_s) for all bender element sensor locations in all columns versus time since the start of rinsing injections. 261

Figure 10.1. Relationships between cementation-induced shear wave velocity increases (ΔV_s), soil $CaCO_3$ contents, and changes in dry densities ($\Delta\rho_{dry}$) for all biocemented and uncemented loose ($D_{r\ initial} \approx 30\%$) Ottawa F-65 specimens..... 279

Figure 10.2. Results from drained monotonic tests for biocemented loose ($D_{r\ initial} \approx 30\%$) specimens treated to varying cementation levels and uncemented specimens prepared to varying initial densities including plots of **(a)** shear stress versus shear strain, **(b)** shear stress versus shear strain (in log-scale), and **(c)** axial strain versus shear strain. All tests were performed under a constant vertical effective stress of 100 kPa..... 283

Figure 10.3. Results from undrained monotonic tests for biocemented loose ($D_{r\ initial} \approx 30\%$) specimens treated to varying cementation levels and uncemented specimens prepared to varying densities ($D_{r\ initial} \approx 30$ to 70%) including plots of **(a)** shear stress versus shear strain, **(b)** shear stress versus vertical effective stress, **(c)** stress-normalized shear stress versus shear strain, and **(d)** excess pore water pressure (Δu) versus shear strain. All tests were performed at an initial vertical effective stress of 100 kPa and were sheared under constant volume conditions. 288

Figure 10.4. Applied CSRs required to achieve trigger liquefaction (3% SASS) in 0.25 cycles versus **(a)** ΔV_s values from cementation for loose ($D_{r\ initial} \approx 30\%$) uncemented and biocemented specimens of varying cementation levels and **(b)** dry density values for uncemented specimens of varying initial densities determined from a combination of both undrained monotonic and undrained cyclic DSS tests. 291

Figure 10.5. Results from undrained cyclic DSS tests performed on loose ($D_{r\ initial} \approx 30\%$) Ottawa F-65 specimens of varying cementation levels (assessed by ΔV_s) subjected to a CSR of **(a, b)** 0.15, **(c, d)** 0.75, and **(e, f)** 1.5. Plots show **(i)** shear stress versus vertical effective stress, **(ii)** shear stress versus shear strain, **(iii)** shear stress versus cycle number, and **(iv)** r_u ($= \Delta u/\sigma'_{vo}$) versus cycle number. 300

Figure 10.6. Changes in maximum excess pore pressure ratios ($r_u = \Delta u/\sigma'_{vo}$) with shear strain for loose specimens of varying cementation levels subjected to CSRs of **(a, b)** 0.75 and **(c, d)** 1.5. The maximum excess pore pressure ratio (r_u) indicates the largest r_u value that a specimen has experienced prior to achieving different shear strain magnitudes. Plots present similar data for shear strains from **(a, c)** 0 to 3% and **(b, d)** 0 to 15%. Data points were evaluated at discrete shear strain increments of 0.05%. 302

Figure 10.7. Comparison of liquefaction triggering criteria including number of cycles to 3% SASS versus number of cycles to r_u = 0.95 for tests involving loose specimens at varying biocementation levels (as indicated by ΔV_s) subjected to different applied CSRs. Points plotting near the 1:1 trendline provided are reflective of perfect agreement between criteria. 303

Figure 10.8. Number of cycles to 3% SASS versus **(a)** ΔV_s from biocementation and **(b)** $CaCO_3$ contents for loose ($D_{r\ initial} \approx 30\%$) specimens of varying biocementation levels... 305

Figure 10.9. Relationships between applied CSRs versus number of cycles to 3% SASS for loose ($D_{r\ initial} \approx 30\%$) biocemented specimens of varying biocementation levels (ΔV_s = 25, 50, 100, 200, 300, 400, 500 m/s) and uncemented specimens prepared to varying initial dry densities. 308

Figure 10.10. Number of cycles from **(a, b)** 3% to 9% SASS and **(c, d)** 3% SASS to 24% DASS versus **(a, c)** ΔV_s from cementation for loose ($D_{r\ initial} \approx 30\%$) specimens of varying biocementation levels and **(c, d)** dry density for all biocemented specimens and uncemented specimens prepared at varying initial dry densities. 310

Figure 10.11. (a) Post-triggering shear strain ($\gamma_{postliq}$) and **(b)** stress-normalized post-triggering shear strain ($\gamma_{postliq}/\tau_{cyc}$) accumulation versus number of applied loading cycles ($N_{cyc,\ post\ liq}$) for select undrained cyclic DSS tests prepared to five different cementation levels ($\Delta V_s \approx$ 0, 100, 150, 200, 500 m/s) and subjected to different applied cyclic shear stresses (i.e., CSRs). Data presented follows the framework proposed by Tasiopoulou et al. (2019). 314

Figure 10.12. Post-triggering compliance rates versus **(a)** ΔV_s from cementation for loose ($D_{r\ initial} \approx 30\%$) Ottawa F-65 specimens of varying biocementation levels, **(b)** dry densities for all biocemented specimens and uncemented Ottawa F-65 specimens prepared at varying initial dry densities including uncemented Ottawa F-65 sands from other studies, and **(c)** total relative densities for all biocemented specimens and uncemented Ottawa F-65 specimens prepared at varying initial dry densities including various other uncemented sands compiled by Tasiopoulou et al. (2019). 316

Figure 10.13. Vertical reconsolidation strains versus **(a)** ΔV_s from cementation for loose ($D_{r\ initial} \approx 30\%$) specimens of varying biocementation levels and **(b)** dry density differences for all biocemented loose specimens and uncemented specimens prepared to varying initial densities. 318

Figure 10.14. Shear wave velocity changes (ΔV_s) following shearing and reconsolidation events versus shear wave velocity increases (ΔV_s) from cementation for loose ($D_{r\ initial} \approx 30\%$) specimens of varying cementation subjected to different applied CSRs. Data points plotting near the 1:1 trendline suggest that increases in V_s from cementation were eliminated following shearing and reconsolidation events. 321

LIST OF TABLES

Table 4.1. Summary of Uncemented Undrained Cyclic Test Results..... 53
Table 4.2. Summary of Results from Biocemented Undrained Cyclic Tests 55
Table 4.3. Summary of Results from Undrained Monotonic Tests 76
Table 5.1. Summary of PHREEQC 3.67-meter Soil Column Simulations..... 109
Table 7.1. Summary of MICP Treatment Solution Compositions for All Columns..... 159
Table 7.2. Summary of Rinse Injections for All Columns Including Solution Constituents and Injection Sequences 161
Table 7.3. Summary of Post-rinsing Aqueous and Sorbed NH_4^+ Concentrations for All Columns 179
Table 8.1. Summary of Column Soil Properties 209
Table 8.2. Summary of Solution Chemical Compositions and Treatment Injections.... 210
Table 8.3. Comparison of Actual and Theoretical Calcite Contents (CC) for Columns 222
Table 9.1. Summary of Soil Properties 235
Table 9.2. Summary of Soil Column Properties and PHREEQC Model Parameters 235
Table 9.3. Summary of Solution Constituents and Injection Schemes for All Columns240
Table 9.4. Summary of Cation Exchange Capacity and Exchangeable Cation Analyses for Sands 245
Table 10.1. Summary of Initial and Post-cementation Properties and Shearing and Post-shearing Behaviors for Drained Monotonic Tests Performed on Biocemented Loose Specimens and Uncemented Specimens at Varying Initial Densities..... 282
Table 10.2. Summary of Initial and Post-treatment Specimen Properties and Shearing and Post-shearing Behaviors for Undrained Monotonic Tests Performed on Biocemented Loose Specimens and Uncemented Specimens at Varying Initial Densities..... 287
Table 10.3. Summary of Specimen Initial Properties, Applied Loadings, and Pre-triggering and Post-triggering Behaviors for Undrained Cyclic Tests Performed on Uncemented Specimens at Varying Initial Densities 296

Table 10.4. Summary of Specimen Initial and Post-treatment Properties, Applied Loadings, and Pre-triggering and Post-triggering Behaviors for Undrained Cyclic Tests Performed on Biocemented Loose Specimens 297

Table 10.5. Fitted Parameters for Liquefaction Resistance Curves for Uncemented Specimens at Varying Initial Densities and Biocemented Specimens at Various ΔV_s Increases. 310

ACKNOWLEDGEMENTS

First of all, I would like to thank my adviser, Professor Mike Gomez. He has been a perceptive adviser, a thoughtful mentor, and a supportive friend since we have met. All of the work presented herein was achieved thanks to his insight, motivation, encouragement, patience, and support. When I had questions, he was the one who helped provide answers. When I was experiencing challenges, he was the one who helped me. I feel grateful to have him not only as my adviser but also as my mentor and friend for the rest of my life.

I would also like to express my gratitude to my committee members, Professor Brett Maurer, Professor Pedro Arduino, and Professor Drew Gorman-Lewis for their guidance, advice, and feedback which helped improve my research, my dissertation, and myself.

I would also like to sincerely thank several professors at UC Davis, Professor Jason DeJong, Professor Douglas Nelson, and Professor Katerina Ziotopoulou. I learnt a lot from their insights, vision, experiences, and support. Also, I would like to thank my friends and colleagues at UC Davis, including Alexandra San Pablo, Charles Graddy, Maya El Kortbawi, Francisco Humire, and others. I would especially like to thank Alex and Charlie for their advice and support which kept encouraging me.

I would like to thank my current and former lab mates at the UW Biogeotechnics Lab, including Bruna Ribeiro, Trent Shepherd, Dellen Behrend, Andrea Mattson, Robert Burdalski, Samantha Muchongwe, Colin Kolbus, Carson Valente, Lucas Lindberg, Carson Cheung, and Tyler Wilcox.

I would also like to extend my thanks to other friends and colleagues at the University of Washington, including Long Chen, Andrew Makdisi, John Schobert, Mertcan Geyin, Ryan Rasanen, Hangyu Kim, Danbi Won, Jaehyun Lee, and Minjae Park for their help throughout my journey.

Lastly, I would like to thank my family who show me endless support and love. Their support and love make me proud of who I am now, and I will do my best to keep making them proud of me. I appreciate my adorable wife who is the one and only for her patience, support, and love.

Finally, I would like to thank and acknowledge the financial support provided for this research by the National Science Foundation (NSF) under NSF Cooperative Agreement No. EEC-1449501 and NSF Award ECI-1824647 as well as the University of Washington. I appreciate all of the opportunities provided to me by the Center for Bio-mediated and Bio-inspired Geotechnics (CBBG), which allowed me to experience and learn diverse new research topics as well as provided valuable life skills including those related to communication and leadership as well as improving ethics, equality, and diversity. I feel very fortunate to have been able to be involved in CBBG during my Ph.D. journey.

DEDICATION

To my parents, Youngsoo Lee and Hongkum Lee, and my lovely wife, Nara Jung.

Chapter 1. INTRODUCTION

Although traditionally somewhat conservative with respect to adopting and apply new technologies, the field of geotechnical engineering has been increasingly forced to rethink its current practices to address emergent challenges related to climate change and natural hazards, all within the context of new constraints related to environmental impacts and financial costs. Recently the field of biogeotechnics has sought to address these challenges through a variety of technologies that either draw inspiration and extract principles from natural systems to identify processes and technologies that can achieve enhanced material efficiency and performance (bio-inspired) or the use of biological agents directly to complete some biological or chemical process of engineering significance (bio-mediated) (DeJong & Kavazanjian 2019). In all cases, biogeotechnical technologies acknowledge that natural systems have evolved over geologic time and therefore can provide insights and opportunities to improve business-as-usual practices including designing and building civil infrastructure with less energy and materials, remediating and/or preserving existing geosystems, and discovering new technologies and processes by which the performance and efficacy of geotechnical systems and design methods can be improved (Mitchell & Santamarina 2005).

The most mature of these technologies, leverage soil microbial enzymatic and metabolic processes to generate a variety of different by-products including inorganic mineral phases, organic polymers, and compressible gases, that can alter soil engineering behaviors for a variety of different purposes (DeJong et al. 2010; 2013). These processes known more broadly as bio-mediated soil improvement methods offer the potential to achieve transformative reductions in environmental

impacts and costs when compared to traditional processes that oftentimes rely on high mechanical energy and energy-intensive materials such as Portland Cement to improve soil engineering behaviors. The most well-researched of these bio-mediated soil improvement methods are those which involve the generation of calcium carbonate ($CaCO_3$) minerals. Although a variety of different microbial processes can be used to generate the alkalinity required for $CaCO_3$ precipitation, to-date the majority of these technologies have either used microbial urea hydrolysis (Ferris et al. 1997; Stocks-Fischer et al. 1999; DeJong et al. 2006; Gomez et al. 2017) or microbial denitrification (van Paassen et al. 2017; Wang et al. 2020). One such process, Microbially Induced Carbonate Precipitation (MICP), has been researched for over two decades and uses urea hydrolyzing bacteria to enable $CaCO_3$ precipitation and the improvement of granular soils when solutions enriched with urea and calcium salts are supplied (Ferris et al. 1997; Stocks-Fischer et al. 1999; DeJong et al. 2006). Although first demonstrated by Ferris et al. (1997) for petroleum recovery applications, researchers such as Whiffin et al. (2007) and DeJong et al. (2006) further investigated the potential of the MICP process for geotechnical applications. Collectively, this research demonstrated the ability of ureolytic bacteria (bacteria with intracellular urease enzymes) to generate $CaCO_3$ minerals capable of coating soil particle surfaces, binding particles at interparticle contacts, and densifying geomaterials through the filling of existing void space. As the technology progressed, an expanding body of research further illustrated the utility of the process for applications including general soil improvement (Martinez and DeJong 2009; van Paassen et al. 2010; Montoya & DeJong 2015; Feng and Montoya 2016; Gomez et al. 2017; Lin et al. 2016; Gao et al. 2019; Riveros and Sadrekarimi 2020a; Xiao et al. 2020; and many others), liquefaction mitigation (Montoya et al. 2013; Simatupang and Okamura 2017; Simatupang 2018; Darby et al. 2019; Zamani and Montoya 2019; Riveros and Sadrekarimi 2020b; and many others),

remediation of concrete materials (Ramakrishnan et al. 1998, 2001; Ramachandran et al. 2001; De Muynck et al. 2008), slope stability enhancement (Zamani et al. 2018), erosion prevention and seepage control (Gomez et al. 2015; Montoya et al. 2018; Tao et al. 2018; Ghasemi and Montoya 2020), divalent contaminant immobilization (Fujita et al. 2004; Bhattacharya et al. 2018; He et al. 2019; Jiang et al. 2019), and sustainable construction material development (Bernardi et al. 2014; Fang et al. 2021), among other uses.

Of these applications, the potential of MICP to provide an effective and environmentally-conscious liquefaction mitigation approach has arguably received the most interest from the geotechnical community, likely due to ability of MICP to (1) enable improvement of soils underlying existing infrastructure, (2) maintain initial soil permeabilities thereby allowing for repeated treatments and improved pore pressure dissipation during earthquake loading, and (3) the remarkable improvement of soil undrained behaviors with the addition of relatively small magnitudes of cementing minerals. Although our fundamental understanding of the underlying microbial and geochemical processes, the engineering behavior of biocemented soils, and the application of MICP to field sites has advanced significantly, critical gaps have remained in our understanding of the applicability of MICP for the mitigation of soil liquefaction. These gaps include: (1) how the undrained cyclic response of biocemented soils may shift as a function of biocementation levels, loading magnitudes, relative densities, confining stresses, and other field-representative factors, (2) how treatment techniques can be modified and developed to afford improved spatial uniformity, treatment extent, and effective by-product management for field treatment scenarios, and (3) how processes developed at the centimeter-scale can be deployed at more practical length scales wherein environmental variables including oxygen availability, nutrient limitations, temperature

reductions, and inherent soil heterogeneity, among other factors may complicate and compromise the performance of laboratory-developed techniques.

The research presented in this dissertation focuses on addressing knowledge gaps related to the application of MICP for the mitigation of earthquake-induced soil liquefaction. These gaps reside primarily in one of three main categories: (1) response: the characterization of the mechanical behavior of biocemented soils, (2) development: the identification and development of field-ready treatment techniques capable of improving the success of MICP applications at field-scale including enhancements in spatial control and by-product management, and (3) deployment: the realization and application of techniques developed at bench-scale to more practical meter-scale testing venues wherein the success and limitations of such processes can be better characterized and understood. More specifically, the research performed and presented in this dissertation is organized as follows:

Chapter 2 presents an overview of the proposed research program, including primary objectives, research activities, and the research scope.

Chapter 3 presents a brief review of past studies on MICP ground improvement with focus on our current understanding of liquefaction behaviors, treatment techniques including those involving the enrichment of native soil microorganisms and the removal of ammonium by-products, and past studies examining the success of MICP in meter-scale experiments and field site deployments. A broad overview of the MICP reaction network, mechanisms by which MICP can alter granular soil behaviors, biological treatment approaches, and monitoring methods are also provided.

Chapter 4 presents insights from a series of direct simple shear tests aimed at improving our understanding of the undrained cyclic response of poorly-graded clean sands at the transition from uncemented to cemented conditions. Biocemented specimens consisted of loose (D_r = 30%) Ottawa F-65 sand and were cemented to achieve varying shear wave velocity improvements ranging from a ΔV_s of 0 to 100 m/s and subjected to varying cyclic loading magnitudes. Liquefaction triggering and post-triggering behaviors were evaluated with changes in loading demands and cementation levels and compared to untreated soils of varying initial densities to compare effect of cementation to that of densification. This chapter was published as a journal paper entitled, "Effect of Light Biocementation on the Liquefaction Triggering and Post-Triggering Behavior of Loose Sands", in the *Journal of Geotechnical and Geoenvironmental Engineering*. The paper was authored by Minyong Lee, Michael Gomez, Maya El Kortbawi, and Katerina Ziotopoulou.

Chapter 5 presents results from a series of experiments aimed at understanding the potential of modified treatment techniques to control the enrichment of indigenous ureolytic microorganisms and resulting urea hydrolysis reaction rates. In these experiments, bulk urea hydrolysis rates were controlled through changes in supplied nutrient concentrations that controlled resulting ureolytic cell densities. Differences in achieved ureolytic rates were then further shown to alter resulting cementation distributions through a series of numerical experiments, which considered varying transport conditions. This chapter was submitted as a journal paper entitled, "Improving the Spatial Control of Soil Biocementation using Indigenous Microorganisms: Column Experiments and Reactive Transport Modeling" to *Engineering Geology*. The paper was authored by (in-order)

Minyong Lee, Michael G. Gomez, Charles M.R. Graddy, Alexandra C.M. San Pablo, Jason T. DeJong, and Douglas C. Nelson.

Chapter 6 presents an investigation of the ability of post-treatment rinse injections to remove generated ammonium by-products following biocementation. Soil column experiments considered the removal of generated ammonium using rinse solutions of varying ionic strength and pH intended to evaluate how rinse solution composition may alter the transport of ammonium ions in biocemented soils. The transport of ammonium was characterized relative to passive bromide ions using passive tracer testing and the integrity of cementation during rinsing was monitored using both shear wave velocity and soil $CaCO_3$ content measurements. This chapter was published as a conference paper entitled, "Investigating Ammonium By-Product Removal following Stimulated Ureolytic Microbially-Induced Calcite Precipitation", in the *Proceedings of GeoCongress 2019*. The paper was authored by (in-order) Minyong Lee, Colin M. Kolbus, Andres D. Yepez, and Michael G. Gomez.

Chapter 7 further explored the modification of by-product removal techniques considered earlier in Chapter 6. Soil column experiments were used to examine the effect of changes in rinse injection sequences, rinse solution composition, and various other factors intended to alter cation exchange between cations supplied in rinse solutions and sorbed ammonium masses remaining on soil surfaces following MICP treatments. The objective of this work was to minimize the required energy (pumping effort) and materials (chemical reagents) required for a given removal magnitude. This chapter was submitted as a journal paper entitled, "Examination of Rinse Injection Strategies

for Removal of Ammonium By-products Following Biocementation Soil Improvement" to *Engineering Geology*. The paper was authored by (in-order) Minyong Lee and Michael G. Gomez.

Chapter 8 presents results from a series of meter-scale experiments aimed at understanding the deployment of rate control techniques developed in Chapter 5 and their ability to alter resulting cementation distributions over meter-scale treatment distances. In this study, five 3.7-meter long horizontal columns containing three different natural sands received augmentation and stimulation treatments intended to achieve lower and higher ureolytic rates. Experiments successfully demonstrated earlier trends demonstrated in numerical models and confirmed that lower ureolytic rates could enable improved cementation extent and uniformity when compared to higher ureolytic rates, which localized cementation near injection sources. This chapter entitled, "Meter-Scale Biocementation Experiments to Advance Process Control and Reduce Impacts: Examining Spatial Control, Ammonium By-Product Removal, and Chemical Reductions" is authored by (in-order) Alexandra C.M. San Pablo, Minyong Lee, Charles M.R. Graddy, Colin M. Kolbus, Mahanoor Khan, Atefeh Zamani, Nina Martin, Catalina Acuff, Jason T. DeJong, Michael G. Gomez, and Douglas C. Nelson and was published in *Journal of Geotechnical and Geoenvironmental Engineering*.

Chapter 9 presents an investigation of ammonium by-product removal in the same meter-scale experiments described in Chapter 8. The performed study examined the removal of ammonium by-products from soil pore fluids and sorbed phases during rinse injections as well as the impact of differences in soil cation exchange capacities. Obtained measurements from the soil column experiments were compared to a passive tracer model and further demonstrated that ammonium

transport was retarded due to soil-ion interactions. Removal efficacy from soil surfaces and pore fluids were also quantified. This chapter was published as a journal paper entitled, "Investigating Ammonium By-product Removal for Ureolytic Biocementation Using Meter-scale Experiments", in *Scientific Reports*. The paper was authored by (in-order) Minyong Lee, Michael G. Gomez, Alexandra C.M. San Pablo, Colin M. Kolbus, Charles M.R. Graddy, Jason T. DeJong, Douglas C. Nelson.

Chapter 10 presents insights from a series of direct simple shear tests aimed at improving our understanding of the undrained and drained shearing behaviors of biocemented poorly graded clean sands at cementation levels corresponding to ΔV_s increases from 0 to 500 m/s and $CaCO_3$ contents from 0 to 5% by mass. Tests specifically examined the effect of cementation and loading magnitude on the liquefaction triggering and post-triggering behavior of loose biocemented Ottawa F-65 sand specimens and compared responses to similar uncemented specimens prepared to varying initial densities. Differences in triggering resistances, post-triggering shear strain accumulation, reconsolidation vertical strains, and ΔV_s changes after shearing as a function of cementation level and loading magnitudes were compared between biocemented and uncemented specimens. Liquefaction resistance curves were developed for different cementation levels with increases in CSR power law curve a- and b-values observed with increasing cementation. Although lightly cemented specimens had post-triggering behaviors comparable to uncemented specimens, more highly cemented specimens ($\Delta V_s > 50$ m/s) achieved detectable post-triggering behavioral enhancements attributable to the densification of specimens from added mineral solids, with additional benefits afforded by cemented bonds and particle coatings observed at higher

cementation levels (ΔV_s > 150 m/s). This chapter will be submitted as a journal paper to *Soil Dynamics and Earthquake Engineering* and be authored by Minyong Lee and Michael Gomez.

Lastly, **Chapter 11** presents some final suggestions for future work related to further examining the response, development, and deployment of biocementation soil improvement for liquefaction mitigation purposes.

Chapter 2. RESEARCH OBJECTIVES AND SCOPE

2.1 Research Objectives

The primary objectives of this research program are (1) to characterize the **response** of biocemented sandy soils subjected to undrained cyclic loading events relevant to the mitigation of earthquake-induced soil liquefaction, (2) identify and **develop** novel treatment strategies that can be used to successfully deploy biocementation soil improvement for practical meter-scale applications, and (3) to **deploy** developed treatment strategies through meter-scale and field-representative experiments to assess the developed methods and enable more widespread practical adoption of biocementation for liquefaction mitigation applications. Although MICP has been proposed for liquefaction mitigation applications by a variety of researchers, surprisingly, critical gaps have remained in our understanding of the liquefaction behavior of these materials and the processes by which they can be successfully implemented at field-sites. The current research program first reviews past advancements in MICP technology specifically with respect to our understanding of liquefaction behaviors, treatment techniques, and meter-scale applications. Following this, a comprehensive series of undrained cyclic direct simple shear tests were performed to explore the liquefaction triggering and post-triggering behaviors of clean poorly graded loose sands at low cementation levels intended to improve our understanding of how such behaviors evolve at the transition from uncemented to biocemented conditions including the behaviors of naturally cemented sands. Subsequently, a series of experiments were performed to evaluate how microbial reaction rates can be manipulated to control spatial distributions of cementation at meter-scale using both soil column physical experiments and reactive transport numerical modeling with the ultimate goal of enhancing cementation uniformity. Next, a series of

soil column experiments were performed to examine the removal of ammonium by-products produced during the MICP process. These experiments considered post-treatment rinse injections which altered geochemical conditions within columns through modification of solution pH and addition of cations intended to promote ammonium removal from cemented materials via cation exchange. Next, a series of five 3.7-meter-long soil column experiments were performed to upscale rate control and by-product removal techniques developed in earlier column experiments. Experiments both characterized cementation progression and uniformity as well as post-treatment by-product removal from soil surfaces and pore fluids. Lastly, the liquefaction behaviors of more heavily biocemented soils (ΔV_s = 100 m/s to 500 m/s) were examined to improve our understanding of how triggering and post-triggering behaviors continue to evolve with added cementation due to increases in cemented bonding (i.e., cohesion), increases in soil particle angularity and surface roughness, as well as cementation-induced densification due to added mineral solids.

2.2 Research Activities

The above research objectives were accomplished by performing the following research activities briefly described below:

- **Activity 1. Review of Past Literature & Findings** – A review of past studies related to: (i) the characterization of the liquefaction behavior of biocemented geomaterials, (ii) treatment techniques for enhanced spatial uniformity and enrichment of indigenous microorganisms, (iii) quantification and management of aqueous ammonium concentrations including those related to biocementation and agricultural applications, and

(iv) the up-scaling and monitoring of biocementation soil improvement was completed. The literature review was used to identify knowledge gaps in these areas and develop the research program performed and reported on in this dissertation.

- **Activity 2. Evaluating the Liquefaction Triggering and Post-Triggering Behavior of Lightly Cemented Sands Using Microbially Induced Calcite Precipitation (ΔV_s = 0 to 100 m/s)** – While much work has been done to characterize the liquefaction behavior of biocemented soils in centrifuge and triaxial experiments, most studies have involved higher cementation levels that have not always been characterized using consistent metrics (e.g. V_s or $CaCO_3$ content) as well as involved the treated of other geomaterials than clean sands. In order to improve our understanding of the behavior of loose sands near the transition from uncemented to biocemented states, a series of 28 undrained cyclic direct simple shear tests were performed on loose biocemented Ottawa F-65 sand specimens treated to varying light biocementation levels (ΔV_s = 0 to 100 m/s) and subjected to different loading magnitudes (CSR = 0.1 to 0.3). 34 similar tests were performed on uncemented specimens prepared to different relative densities (D_r = 30 to 75%) to compare the effect of cementation to that of densification. A series of monotonic undrained tests were also performed to examine differences in peak strengths, initial stiffnesses, and dilatancy as a function of biocementation magnitudes. The performed tests improve our understanding of the liquefaction behaviors of lightly biocemented materials including pre-triggering and post-triggering responses and suggest that much lower levels of cementation than that considered previously by other researchers may be needed to dramatically improve soil liquefaction resistances.

- **Activity 3. Examining Control of Stimulated Urea Hydrolysis Rates During Biocementation Using Indigenous Microorganisms Through Soil Column Physical Experiments and Reactive Transport Modeling** – To-date much of the literature regarding biocementation has involved augmentation, the culture and injection of exogenous microorganisms with high ureolytic activity to hydrolyze supplied urea and enable the biocementation process. Under these circumstances, the applied cell densities can be used to alter the rate of urea hydrolysis reactions. During injections representative of field-scale applications, however, the balance between the reaction rate and transport rate of the injected fluids will govern where reactants will be consumed and thus the distribution of resulting $CaCO_3$ precipitates. As the process has matured, researchers have avoided the injection of non-native ureolytic bacteria and instead shown that enrichment injections can successfully select for indigenous ureolytic soil bacteria that can enable the MICP process. While high ureolytic activity can be obtained with this approach, the ability of enrichment injections to regulate ureolytic activity (via modification of ureolytic cell densities) and achieve enhanced spatial control has not yet been explored. A series of soil column experiments were completed wherein supplied nutrients (i.e., yeast extract) were varied during stimulation and cementation injections to examine how such solution modifications may be able to control resulting ureolytic activities. Although these tests were completed at centimeter-scale, in order to understand the implications of these rate changes a series of numerical reactive transport experiments were completed using a PHREEQC reactive transport model in order to examine how the balance between flow rates and reaction rates can impact resulting cementation distributions. The performed tests enhance our understanding of the ability of stimulation solution modifications to improve

the spatial control of biocementation with the ultimate goal of increasing improvement extent and uniformity at field-scale.

- **Activity 4. Preliminary Assessment of Ammonium By-product Removal via Post-treatment Rinse Injections –** The production of ammonium by-products during ureolytic biocementation has been a major challenge for the technology with respect to achieving regulatory acceptance and more widespread field-scale deployment. Although a variety of processes may be used to remove generated nitrogen by-products, perhaps the simplest approach is to injected solutions following biocementation to rinse and remove generated ammonium from cemented soils and pore fluids with subsequent treatment *ex situ* at water reclamation or other treatment facilities. While perhaps relatively straight-forward, the negative surface charge of soil minerals can sorb generated ammonium ions making the removal of such by-products increasingly challenging. In an effort to further our understanding of post-treatment ammonium removal, a series of passive tracer and rinse soil column experiments were performed to examine the transport of ammonium in biocemented soils and the removal effectiveness of rinse solutions with varying initial pH and ionic strengths. Column tests quantified both aqueous removal during rinse injections as well as potential impacts on cementation integrity. At the conclusion of these experiments, the effect of rinse solution pH and ionic strength were preliminarily characterized with later experimentation investigating these effects further.

- **Activity 5. Optimization of Post-treatment Rinse Strategies for Ammonium By-product Removal** – Following the preliminary characterizations completed in Activity 4,

a series of soil column experiments were completed to further explore several effects including: (i) the sequencing of rinse injections (i.e., one continuous 12 PV injection or twelve daily 1 PV injections), (ii) the impact of rinse solution cation type (i.e., K^+, Ca^{2+}, Na^+), (iii) the effect of cation concentration, (iv) the efficacy of deionized water rinse injections, (v) NH_4^+ removal effectiveness from both soil pore fluids and sorbed soil phases, and (vi) the impact of cation-based rinse solutions applied prior to MICP treatments, which might limit NH_4^+ sorption and improve post-treatment removal. Following these experiments, the impact of cation additions on aqueous and sorbed ammonium removal was examined and recommendations regarding cation types and injection sequencing were made. The impacts of rinse injections on cementation integrity and the potential for material dissolution were also evaluated.

- **Activity 6. Up-scaling of Urea Hydrolysis Rate Control Treatment Techniques in Meter-scale Column Tests for Enhanced Spatial Control** – Following successful identification of techniques to control ureolytic rates, a series of five 3.7-meter column experiments were performed to examine the effect of ureolytic rate changes on the distribution and extent of biocementation at meter-scale. Tested columns included specimens containing three different natural sands (Concrete Sand, Covelo Sand, Delta Sand) which received "slow ureolytic rate" treatments intended to achieve improved cementation uniformity, a single column containing Concrete Sand which received "fast ureolytic rate" treatments expected to result in greater location of cementation near the injection location, and a single column containing Concrete Sand that was augmented to compare the response of stimulated columns to that obtainable using non-native cell

injections used primarily by other research groups. Experiments considered changes in ureolytic rates across the length of columns, characterized resulting soil $CaCO_3$ contents, and examined resulting engineering improvements achieved using hydraulic conductivity and shear wave velocity measurements. The experiments provide a demonstration of the techniques developed at the centimeter-scale and suggested that such techniques can be used to achieve improved spatial uniformity and treatment extent for meter-scale applications. This was particularly noteworthy given the potential for differences in enrichment success at meter-scale due to nutrient and oxygen limitations with increases in distance from the injection locations.

- **Activity 7. Implementation and Characterization of By-product Removal Techniques in Meter-scale Column Tests** – In addition to examining the effect of various treatment strategies on biocementation improvement attainable in the five 3.7-meter column experiments described in Activity 6, an investigation of ammonium removal including removal efficacy from sorbed phases and free pore fluids was completed. Experiments involved the application of 12 PV of an alkaline calcium-enriched rinse solution intended to remove generated ammonium concentrations from soils and pore fluids. Experiments examined the impact of differences in soil cation exchange capacities as well as compared aqueous removal measured from columns to that expected from a passive tracer model. These experiments provided the first characterization of by-product removal for MICP-treated soils at the more practical meter-scale.

- **Activity 8. Investigation of Undrained Cyclic Response of Biocemented Sands: Effect of Higher Cementation Levels (ΔV_s = 100 to 500 m/s) and Cementation-induced Density Increases** – Previous direct simple shear tests characterized the liquefaction and undrained monotonic behavior of lightly biocemented sand specimens. Critical questions remained, however, regarding the influence of cementation-induced changes in dry densities, soil angularity, and cohesion on the liquefaction behaviors of these materials and the metrics by which these improvements should be judged once applied at field-scale. A series of undrained and drained monotonic and undrained cyclic tests were performed to investigate the effect of higher cementation levels, more representative of those expected to be applied for practical liquefaction mitigation purposes, on the shearing behavior of biocemented sands. The primary goal of these investigations was to improve our understanding of how biocementation-induced changes may impact triggering and post-triggering behaviors including shear strain accumulation and reconsolidation behaviors as well as to generate liquefaction-resistance curves, which can be used to inform the design of field applications. The test data generated from this work provides one of the only comprehensive investigations of the liquefaction behavior of biocemented clean sands and will be used to further inform constitutive models being developed to capture the undrained cyclic behavior of biocemented sands (e.g., PM4SandC), among other anticipated broader impacts.

Chapter 3. BACKGROUND AND LITERATURE REVIEW

3.1 Introduction to MICP

Microbially Induced Calcite Precipitation (MICP), or ureolytic biocementation, leverages microbial urea hydrolysis activity to precipitate calcium carbonate ($CaCO_3$) minerals on soil particle surfaces and contacts (Ferris et al. 1996; Stocks-Fischer et al. 1999; DeJong et al. 2006). The process has the potential to provide an environmentally beneficial alternative to other energy-intensive soil improvement methods (e.g., permeation grouting, compaction grouting, jet grouting), which primarily rely on the use of portland cement and other synthetic materials to bind and improve problematic soils. The process was first explored by Ferris et al. (1996) wherein the application of MICP was considered to cement pervious oil sands and permit enhanced petroleum recovery. Researchers later explored the process for concrete remediation (Ramachandran et al. 2001), strontium immobilization (Fujita et al. 2004), and geotechnical applications (DeJong et al. 2006; Whiffin et al. 2007), thereby catalyzing broad interest in the bio-mediated reaction for a wide variety of different civil engineering applications. The biocementation process is made possible by microorganisms containing urease enzymes, which can catalyze a hydrolysis reaction that degrades supplied urea, thereby generating ammonia and carbonic acid (Mobley et al. 1995; Stocks-Fischer et al. 1999). When produced ammonia enters free solution, it will speciate according to the surrounding solution pH, with generated ammonia reacting with water to form ammonium and hydroxide ions when surrounding solution pH is not highly alkaline. Resulting hydroxide ions promote the speciation of generated carbonic acid (H_2CO_3) to form increasing concentrations of bicarbonate (HCO_3^-) and carbonate (CO_3^{2-}) species and when sufficient calcium is supplied in treatment solutions, the product of calcium and carbonate ion activities can exceed

the solubility of $CaCO_3$ mineral phases and precipitation is initiated, thereby resulting in the formation of $CaCO_3$ minerals on soil particle surfaces and at interparticle contacts (Ferris et al. 2004; Gomez et al. 2019). **Figure 3.1** summarizes the MICP reaction network including related kinetic and equilibrium reactions and provides SEM images of biocemented sands as well as an image of a biocemented soil column following failure during mechanical testing. Although commonly referred to as generating solely calcite, $CaCO_3$ resulting from MICP may exist as various other mineral polymorphs including vaterite, aragonite, and amorphous $CaCO_3$, each of which has varying crystalline structures and chemical and mechanical properties. From a geotechnical perspective, the resulting $CaCO_3$ can coat soil particle surfaces, bind soil particle contacts, and densify soil matrices, resulting in dramatic enhancements in material shear stiffness and strength (DeJong et al. 2006; Montoya and DeJong 2015; Gomez et al. 2018a; Nafisi et al. 2020; and others) with generally only minor reductions in soil hydraulic conductivities for most soils relevant to liquefaction mitigation applications (e.g., clean sands, clean gravels) (Gomez and DeJong 2017; San Pablo et al. 2020). Improvements in soil engineering properties resulting from MICP have been considered for a variety of geotechnical applications, however, most prominently the method has been proposed for liquefaction mitigation, the primary application of interest for this research. This is likely due to a variety of reasons including (1) the ability of MICP to improve soils underneath existing infrastructure by injecting solutions with low viscosities similar to water, (2) the ability of MICP to maintain soil perviousness, thereby avoiding further issues related to more limited pore pressure dissipation during dynamic loading, and (3) the ability of small magnitudes of biocementation to dramatically alter soil undrained cyclic behaviors.

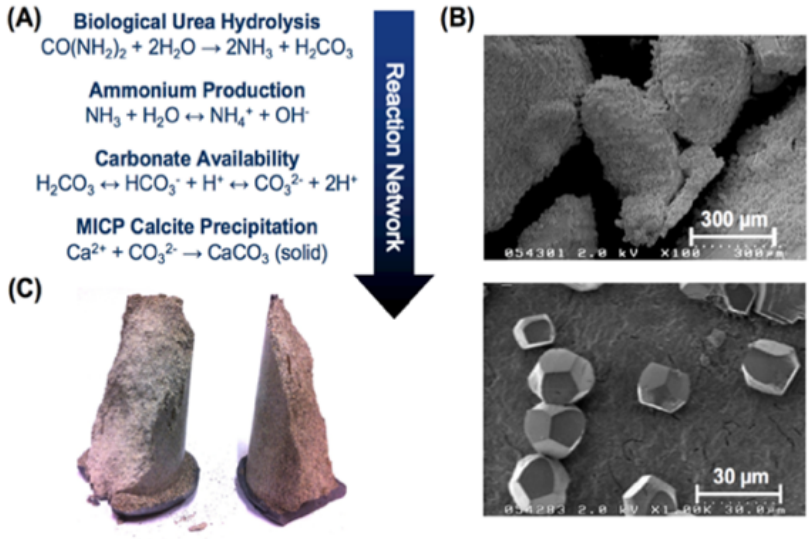

Figure 3.1. Overview of the MICP process including the (a) MICP reaction network, (b) scanning electron microscope images of biocemented sands, and (c) an image of a biocemented sand column after failure following an unconfined compression test.

3.2 Biological Strategies for MICP

Two primary methods exist by which the required microbiological activity for MICP can be achieved. Early on during the technology's development, researchers almost exclusively considered bio-augmentation, the introduction of microorganisms with desired metabolic or enzymatic capabilities into the subsurface to complete this process. In particular, many researchers cultured and injected *Sporosarcina pasteurii* (*S. pasteurii*) a gram-positive bacterium, which constitutively expresses ureolytic activity (Bang et al. 2011; DeJong et al. 2006, Gomez et al. 2015; Martinez et al. 2013; Nafisi et al. 2021; van Paassen 2011; and others) to complete MICP. Although effective at bench-scale, the bio-augmentation process requires sterile culturing procedures, transportation of bacterial inoculants to project sites, and results in issues related to spatial uniformity due to the colloidal filtration of cells in porous media, which can act to concentrate cells near injection sources (Ginn et al. 2002). In addition to high financial costs and

environmental impacts, the process can also be challenging from a regulatory perspective due to the introduction of exogenous bacterial species and the potential for related soil ecological impacts (Gomez et al. 2017).

As the technology has matured, subsequent researchers demonstrated the ability of solutions which impose selective environmental conditions while providing nutrients to enrich natural soils for indigenous ureolytic microbial communities (Gomez et al. 2017; San Pablo et al. 2020). Although extensively used in bioremediation applications, this process known as bio-stimulation, was first considered by Fujita et al. (2000; 2008) for MICP wherein microbial ureolysis was used to enable strontium coprecipitation in $CaCO_3$. Bio-stimulation offers the potential to (i) enhance MICP spatial uniformity by enriching existing soil microorganisms, (ii) reduce costs and environmental impacts by eliminating the need for and the injection of non-native microorganisms, and (iii) avoid potential regulatory concerns related to the introduction of non-native bacteria into soil systems. Through more recent investigations, stimulated microbial communities have been further characterized to understand how ubiquitous native ureolytic bacteria are in geotechnically-relevant soils (Graddy et al. 2018) as well as to further optimize solutions to improve selection for ureolytic bacteria and remove superfluous chemical reagents (Gomez et al. 2018b; 2019; San Pablo et al. 2020). While the enrichment of native ureolytic microorganisms can overcome many practical limitations associated with bio-augmentation, questions remain as to how such enrichments can be modified to better control reaction rates and the influence of field constraints, including oxygen availability and nutrient limitations, on the enrichment process.

3.3 Treatment Processes and Related Monitoring Methods

In order to evaluate the success of biocementation treatments, various geochemical, microbiological, and geotechnical metrics and methods have been used to monitor augmentation, enrichment, and cementation processes as well as characterize resulting biocemented materials. While other techniques can be used, the follow methods are leveraged in the presented research and provide insights regarding different aspect of the MICP process. During the augmentation or stimulation phase of treatments, establishment of ureolytic cell densities to complete the MICP process is desired. During this phase, treatment solutions are supplied, which include either added nutrients and urea (stimulation) or exogenous cultured bacteria (augmentation), and monitoring is completed to characterize the resulting ureolytic activities of these augmented or enriched ureolytic microorganisms. Monitoring of the augmentation and stimulation process generally includes direct measurements of aqueous urea in time, which can track changes in bulk ureolytic activity reflective of changes in ureolytic microbial densities as well as pH measurements, which can detect increases in solution pH reflective of ammonia generation and urea hydrolysis. For augmented experiments, augmented cell densities can also be quantified using optical density (OD) measurements, which can be used to characterize both injected cell densities as well as determine the cell densities retained on soil particle surfaces via measurements of generated effluent. When such measurements suggest that sufficient ureolytic activity has been achieved, the cementation process can be initiated by introducing solutions containing urea and soluble calcium. During the cementation phase of treatments, solution pH and aqueous urea measurements are continued to ensure the viability of cells and monitor geochemical changes reflective of $CaCO_3$ precipitation. The addition of aqueous calcium and carbonate measurements can also provide the opportunity to characterize solution saturation states (Ω) and the kinetics of $CaCO_3$ precipitation as enabled by

ureolytic activity. Such measurements can be performed using routine colorimetric chemical assays as well as other more sophisticated measurements including inductively-coupled mass spectrometry (ICP-MS), inorganic carbon analyses, and total alkalinity titrations.

In order to monitor and characterize mechanical enhancements resulting from the MICP process, a variety of characterization methods can be used during and after the cementation process. Specifically, during cementation injections, shear wave velocity (V_s) measurements can be used to non-destructively track the progression of cementation as reflected by soil small-strain shear stiffness (G_{max}) enhancements. The metric can be well-correlated to the amount of $CaCO_3$ precipitation generated, but also provides an indication of how effectively resulting precipitation is at binding particles and therefore can provide a more informative metric for assessing related mechanical enhancements than simple mass-based measurements. During the MICP process, shear wave velocities can increase rapidly from values near 80 to 100 m/s in the untreated condition (at 100 kPa confining stress) to over 1,500 m/s after only 15 to 20 daily cementation injections of solutions containing 250 mM calcium and urea. Beyond real-time assessment of laboratory experiments, the metric also provides a method by which field and lab results can be unified, with strong correlations between V_s and other mechanical behaviors including cone penetration resistances (q_t), liquefaction triggering resistances, and monotonic shearing behaviors, among other responses (Gomez et al. 2018a; Montoya & DeJong 2015; Montoya et al. 2013). In addition to these non-destructive geophysical measurements, treated soil materials are oftentimes characterized using mass-based soil $CaCO_3$ content measurements to assess the magnitudes of generated precipitation as well as x-ray diffraction (XRD) measurements and scanning electron microscope (SEM) images, which allow for characterization of cementation mineralogy and

morphology, respectively. Although not used routinely, measurements of aqueous ammonium in produced effluent and treated soil materials can also be used to assess the efficacy of various by-product management approaches and are used extensively in the research presented in this dissertation.

3.4 Mechanical Enhancements Resulting from Biocementation

Mechanical enhancements resulting from biocementation can be primarily attributed to the following mechanisms: (i) the generation of $CaCO_3$ bonds between soil particles that can limit soil particle movements and volumetric tendencies as well as provide tensile strength, (ii) increases in soil particle angularity, particle surface roughness, and interparticle frictional resistance through the coating of soil particle surfaces with $CaCO_3$ crystals, and (iii) increases in soil bulk dry densities through the filling of soil void space with precipitated $CaCO_3$ mineral solids thereby increasing soil dilative tendencies particularly at larger strains once cohesive bonds have failed. Each of these mechanisms contribute differently to the overall shearing behaviors of biocemented soils depending on the characteristics of the applied loadings and existing confining stresses, the magnitudes and distributions of biocementation present, and the strain levels to which such soils are subjected to. In particular, generated $CaCO_3$ bonds appear to dominate the mechanical response of biocemented soils at lower confining stresses, higher cementation levels, and smaller-strain levels wherein the integrity of brittle $CaCO_3$ bonds can be maintained. As strains increase, however, the fracturing and shearing of brittle cemented bonds allows for the mobilization of volumetric tendencies and the effect of biocementation-induced densification and surface roughness changes contributes more significantly towards altering larger-strain mechanical responses (DeJong et al. 2010; Montoya et al. 2013; Lee et al. 2021; and others).

Extensive monotonic testing by a wide variety of researchers has shown the ability of biocementation to enhance soil shear stiffnesses, peak and residual shear strengths, and volumetric behaviors during shearing as reflected by excess pore pressure changes in undrained tests and volumetric strains in drained tests (Montoya and DeJong 2015; Feng and Montoya 2016; Riveros and Sadrekarimi 2020a; Nafisi et al. 2021). Such tests have suggested that the effects of cementation become more pronounced with increases in cementation levels and reductions in confining stresses. These investigations have also considered a wide range of other factors including differences in soil gradation (Simatupang et al. 2018; Nafisi et al. 2020) and source of ureolytic activity (Bang 2009; Almaged et al. 2018), which were expected to influence the MICP geochemical process as well as cementation efficacy. Despite these more comprehensive monotonic characterizations, the undrained cyclic behavior of MICP-treated granular soils has remained relatively poorly-characterized. Of the studies that have been performed, almost all present one of two main findings, which could likely be assumed a priori: (i) the addition of biocementation can increase soil liquefaction resistances, and (ii) liquefaction behaviors correlate well with increases in biocementation magnitudes as reflected by soil V_s and/or $CaCO_3$ content increases. The influence of more critical field-representative variables including changes in confining stresses, static shear stresses, cementation levels, and relative densities, however, have remained significantly less explored for clean sands, for which the technology has been proposed extensively. Moving forward, a more extensive body of mechanical tests comparable to that which exists for clean uncemented materials will likely be needed to develop liquefaction susceptibility assessment frameworks for biocemented soils in a robust and more quantitative manner.

In spite of these gaps, several studies examining the behavior of $CaCO_3$ cemented soils have provided key insights regarding the behaviors of these materials as a function of cementation levels, confining stresses, saturation levels, and fines contents. For example, Simatupang (2018) investigated the undrained cyclic behavior of $CaCO_3$ cemented sands using enzymatically induced carbonate precipitation (EICP) in a series of cyclic triaxial tests. The tests considered different cementation levels, confining pressures, and degrees of saturation during treatments intended to alter precipitation distributions at particle contacts. While generated $CaCO_3$ bonds were shown to influence small-strain behaviors and liquefaction triggering resistances, improvements afforded by cementation were diminished at higher shear strains following triggering once bonds were damaged. Despite this, some improvements related to densification and surface roughness increases were observed at larger strains and influenced strain accumulation behaviors. Zamani and Montoya (2019) further examined the liquefaction behavior of biocemented silty sands of various fines contents. A series of undrained cyclic direct simple (DSS) tests were performed on materials treated to achieve V_s increases (ΔV_s) near 300 m/s. As expected, treated silty sands exhibited improved liquefaction resistances with reductions in excess pore pressure generation during undrained cyclic loading. Reductions in MICP improvement efficiency was also observed with increases in soil fines contents.

Furthermore, Xiao et al. (2019) investigated the liquefaction behavior of biocemented calcareous sand samples including the influence of material relative density and cementation level. A series of undrained cyclic triaxial tests were performed on uncemented specimens of different initial relative densities and cemented loose specimens with differing cementation levels. Their findings suggested that the generation of cemented bonds from MICP resulted in greater improvement of

liquefaction triggering resistances when compared to the effect of cementation-induced densification alone. Darby et al. (2019) further performed a series of centrifuge tests on biocemented Ottawa F65 sand specimens prepared loose (D_r = 38%) and treated to differing, but spatially-uniform, cementation levels corresponding to ΔV_s values of 60, 165, and 420 m/s. Specimens were characterized using cone penetration test soundings, V_s measurements, and $CaCO_3$ content measurements at various time points during treatments and repeated shaking events. Results demonstrated that biocemented specimens required higher peak base accelerations in order to trigger liquefaction, better resisted shear strain developments, and exhibited greater liquefaction resistances when subjected to repeated undrained cyclic loading events when compared to similar uncemented specimens. Zamani et al. (2021) extended these investigations and conducted similar centrifuge tests to investigate the impact of MICP treatments applied to discrete zones of soil underlying shallow foundations. Findings from these systems-level experiments highlighted the reduction in total and differential settlements for foundations wherein MICP treatments were applied to underlying soils as well as the ability of more dilative MICP treated soil zones to dampen pore pressure generation in adjacent loose sand pockets. Finally, Riveros and Sadrekarimi (2020a) examined the undrained cyclic response of biocemented Fraser River sand specimens treated to cementation levels corresponding to ΔV_s values near 90 m/s. A series of undrained cyclic direct simple shear tests were performed and increases in liquefaction triggering resistances with reductions in pore pressure generation during loadings were observed. While insightful, our understanding of how liquefaction behaviors may shift as a function of cementation levels, confining stresses, loading demands, relative densities, and other field-representative factors for clean sands has remained more limited.

3.5 Large-Scale Demonstrations

Although numerous laboratory-scale studies have been performed to optimize and develop MICP techniques, critical gaps have remained with respect to verifying that such processes can be used for field-scale applications in the presence of conditions that cannot be easily replicated in the laboratory (i.e. oxygen availability; increased solution dispersion). In an effort to better understand the ability of MICP to be applied at meter- and field-scales, researchers have performed a variety of large-scale experiments and field trials. Although others exist, the experiments most relevant to this research including those related to by-product generation, stimulation, and enhanced treatment uniformity are briefly summarized here.

Whiffin et al. (2007) completed one of the first large-scale experiments, wherein a 5-meter-long column composed of poorly-graded Itterbeck Sand (D_{10} = 0.11 mm, D_{50} = 0.17 mm, D_{90} = 0.28 mm, and D_{60}/D_{10} = 1.64) was treated using MICP via bio-augmentation (flow rate of 0.35L/hr). Their results suggested that near 80% of the injected urea was consumed in near the injection location resulting in higher and more localized soil $CaCO_3$ contents near this location. Although some $CaCO_3$ was observed along the full length of the 5-meter column, significant heterogeneity in the distribution of the achieved precipitation demonstrated a clear need for improved treatment uniformity. van Paassen et al. (2010b) performed a follow up large-scale MICP experiment involving the same poorly graded Itterbeck sand material consisting of a rectangular concrete chamber (8 m x 5.6 m x 2.5 m) that contained 100 m^3 of sand which was treated with three injection-extraction well pairs (1 m spacing between similar wells, 5 m longitudinal spacing between extraction and injection wells). The experiment was first augmented and successive cementation injections were applied using the well pairs. The experiment included 72 geophones

that were used to track V_s improvements during treatments. As expected, following treatments significant increases in soil shear stiffness and shear strength were observed with increasing biocementation, however, improvements appeared to be largely concentrated between injection wells and near the middle of the soil chamber.

van Paassen et al. (2011) later performed a field scale biocementation demonstration experiment wherein ≈ 1000 m^3 of a gravelly soil was augmented, cemented, and stabilized to permit horizontal directional drilling and installation of gas pipelines in the Netherlands. Six injection wells were installed and were surrounded by fourteen extraction wells to complete the treatment process. During the treatment process, soil electrical resistivity, shear wave velocity, cone penetration tests, static penetration tests, sonic vibration coring, and soil $CaCO_3$ content measurements were performed. Aqueous NH_4^+ concentrations in generated effluent solutions were also assessed. Unfortunately, such metrics, with the exception of the soil $CaCO_3$ content measurements, experienced challenges with respect to adequately capturing the achieved improvement. Thus, additional large-scale experiments were further performed using 1.5 m x 1.5 m x 4 m box specimens to estimate the improved strength of the biocemented soils and develop a correlation between soil shear strengths and the number of applied treatments.

Gomez et al. (2015) performed a field scale MICP test on a loose poorly graded sand at a mine site located in Saskatchewan, Canada. The field study examined the improvement of soil erosional resistance using biocementation for surface stabilization and fugitive dust control. Treatment solutions were applied using surface percolation and examined the effect of different treatment solution concentrations. Following treatments, cemented crust thickness measurements and water

jet impingement erosional tests were performed to qualitatively assess cementation distributions and erosional resistances. Dynamic cone penetrometer (DCP) measurements were also performed to evaluate changes in soil penetration resistances and discrete soil samples were collected for $CaCO_3$ content measurements. The achieved results were counter to expectations and suggested that the low concentration treatment solutions achieved the greatest measurable soil improvement up to depths near 5 cm with modest spatial variability in crust thicknesses, DCP resistances, and soil $CaCO_3$ content magnitudes.

Gomez et al. (2017) later performed large-scale tank experiments involving a poorly-graded Concrete Sand wherein two identical 0.5 m high and 1.7 m diameter tanks were either stimulated or augmented and subjected to identical cementation treatments to examine process differences, control of cementation extent with directional injections, and changes in soil microbiological, geochemical, and geotechnical attributes during the treatment process. Three treatment wells were installed in a triangular pattern with 1.2 m between wells. For every cementation treatment, only two wells would be active with one well serving as an injection well, one well serving as a production well, and the third well remaining passive. The direction of injections was altered during the treatment process, to track differences in resulting cementation magnitudes with changes in injection schemes. During all treatments, aqueous samples were collected to measure changes in pH, urea degradation, and calcite precipitation kinetics via carbonate and calcium measurements (Gomez et al. 2019). Microbiological characterizations were also completed to examine how augmented and stimulated microbial communities changed during the process (Graddy et al. 2018). Cone penetration tests soundings, shear wave velocity measurements, and $CaCO_3$ content measurements were also performed to track impacts on soil geotechnical properties

(Gomez et al. 2018a). The results suggested that for the same $CaCO_3$ content, augmented and stimulated experiments achieved similar mechanical enhancements. However, greater localization of improvement was observed in the augmentation specimen near injection wells with more diffuse improvement observed in the stimulated specimen. This primarily resulted from the higher ureolytic reaction rates observed in the augmentation specimen, which consumed injected reagents (i.e., urea, calcium) more readily near injection wells.

3.6 Knowledge Gaps and Remaining Challenges

Although the expanding body of research on biocementation has dramatically improved our collective understanding of the fundamental microbial and geochemical processes involved in MICP, the mechanical behavior of cemented geomaterials, the field-scale application of MICP, and numerous other aspects, critical knowledge gaps still remain regarding the application of MICP for practical liquefaction mitigation purposes. These gaps include: (i) the limited characterization of the liquefaction behaviors of biocemented clean loose sands, (ii) the absence of treatment techniques which can enable enhanced spatial control and uniformity of cementation over meter-scale treatment distances representative of field applications, (iii) the lack of approaches to assess and manage generated ammonium by-products and their fate following practical field implementations, and (iv) the limited understanding of how recently developed enrichment and cementation techniques may perform at more practical length-scales in the presence of field-representative constraints (i.e., oxygen and nutrient limitations, solution dispersion). Each of these aspects will be critical towards enabling the practical adoption of MICP for liquefaction mitigation purposes and are further described below.

The engineering behavior of cemented soils including biocemented (i.e., MICP, EICP), artificially-cemented (i.e., portland cement) and naturally-cemented soils have been broadly examined using a variety of different laboratory cementation processes as well as the undisturbed sampling of natural cemented soils (Frydman et al. 1980; Simatupang et al. 2018; Xiao et al. 2018; Zamani and Montoya 2019). While this existing body of research has greatly improved our understanding of the mechanical behaviors of cemented soils, the effect of cementation on clean sand liquefaction behaviors as a function of cementation levels, confining stresses, loading demands, relative densities, and other field representative factors has not yet been explored extensively. Such insights may be applicable to a wide suite of cemented geomaterials for which few characterizations exist due to sampling disturbance challenges and the limited sensitivity of large-strain penetration tests. Biocementation may therefore offer a unique opportunity to systematically examine how such behaviors transition from the uncemented to cemented condition. When considering past studies performed on biocemented soils, the majority of these studies have focused on relatively high cementation magnitudes and the effect of cementation on liquefaction triggering, however, post-triggering behaviors and the effect of lighter levels of cementation have remained largely unexplored. Furthermore, metrics used to describe generated cementation (i.e., $CaCO_3$ contents, V_s values) have lacked consistency between researchers and have therefore limited the broader conclusions that can be inferred from such tests. In order for MICP to be adopted as a practical liquefaction mitigation method, it is clear that a more comprehensive database of tests is needed, which can help guide the development of liquefaction susceptibility procedures and numerical models that can rationally account for the effect of cementation on soil liquefaction behaviors.

Previous biocementation experiments have clearly demonstrated challenges with respect to spatial uniformity, with higher cementation magnitudes generally observed near injection locations where augmented cell densities can concentrate and degrade supplied reagents more rapidly. Recent advances in biostimulation, suggest that the enrichment of indigenous microbial communities may mitigate issues related to the colloidal filtration of injected cells and thereby permit greater uniformity in biological reaction rates. To-date, stimulation techniques have targeted high ureolytic activity indicative of improved selection for ureolytic microorganisms, however, for field applications, slower transport rates may require that enriched ureolytic activities be regulated in order to ensure that desired cementation distributions and extents can be achieved. In order to modify reactive transport conditions during MICP for a variety of different field treatment scenarios, treatment techniques that can alter stimulated ureolytic activities remain needed. Such developments may not be trivial, as the mixed microbial communities present during stimulated MICP may be significantly affected by small changes in enrichment conditions.

Despite continued development of ureolytic biocementation techniques, the management and removal of produced ammonium by-products has not yet been extensively explored (Gat et al. 2017; Lee et al. 2019a; 2019b). As the technology transitions to more widespread practical adoption, methods will remain needed to quantity the production and fate of generated nitrogen species. Concentrations of generated NH_4^+ can be expected to be near twice that of the supplied urea concentrations, with magnitudes far exceeding most regulatorily acceptable levels (van Paassen 2009; El Mountassir et al. 2018; Gomez et al. 2019). If left unaddressed in treated soils and ground water, produced NH_4^+ concentrations have the potential to detrimentally impact human health and environmental quality including the potential for increased eutrophication of surface

waters (Paerl et al. 1997). Although no maximum total ammonium limits for drinking water have been established, the U.S. EPA recommends maximum total NH_4^+ concentrations for aquatic life of 17 mg/L (≈ 1 mM) and 1.9 mg/L (≈ 0.1 mM) at a pH of 7.0 for acute (1 hour) and chronic (30-day) exposure, respectively (U.S. EPA, 2013). Furthermore, although limits for total NH_4^+ in surface water bodies will be location specific, these limits generally range between 0.25 mg/L (≈ 0.01 mM) and 32.5 mg/L (≈ 1.8 mM) across the U.S. (ODHS, 2020). Lastly, the European Union has set a maximum total NH_4^+ concentration for drinking water of 0.5 mg/L (≈ 0.03 mM) (EU standards, 1998). Although acceptable NH_4^+ concentrations will depend on site-specific conditions and regulations, aqueous NH_4^+ concentrations produced during the biocementation process will likely exceed recommended concentrations by several orders of magnitude. Strategies that can enable the removal and/or *in situ* remediation of NH_4^+ by-products are therefore critical towards allowing MICP applications to be able to meet site water quality requirements and offer a truly environmentally-conscious technique.

Although developed treatment techniques can be extensively studied and demonstrated in laboratory-scale experiments, critical gaps also remain regarding how such methods may perform under more field-representative conditions. A considerable number of studies have been performed to demonstrate MICP at meter-scale, however, few have examined the process under field-representative conditions. When applied at field sites, new constraints will likely need to be addressed including those related to limited oxygen and nutrient availability, temperature reductions with depth, inherent soil heterogeneity, and site water geochemical differences. Demonstration of MICP treatment techniques under such conditions may therefore allow for the effect of such differences to be better understood and quantified as well as enable the development

of new verification techniques and an improved understanding of implementation costs and related environmental impacts. Although these knowledge gaps currently remain, as MICP technology continues to progress towards more widescale practical implementation, additional field demonstrations will provide new insights and data sets that can be used to further refine application strategies and understand the impact of field-scale factors.

Chapter 4. EFFECT OF LIGHT BIOCEMENTATION ON THE LIQUEFACTION TRIGGERING AND POST-TRIGGERING BEHAVIOR OF LOOSE SANDS

This paper has been published in the ASCE *Journal of Geotechnical and Geoenvironmental Engineering*. The paper is presented herein, with slight modifications.

Citation:

Lee, M., Gomez, M. G., El Kortbawi, M., & Ziotopoulou, K. (2022). Effect of Light Biocementation on the Liquefaction Triggering and Post-Triggering Behavior of Loose Sands. *Journal of Geotechnical and Geoenvironmental Engineering*, 148(1), 04021170.

ABSTRACT

Microbially Induced Calcite Precipitation (MICP) is an environmentally-conscious ground improvement method that can enhance the engineering properties of granular soils through the precipitation of calcium carbonate ($CaCO_3$) on soil particle surfaces and contacts. While numerous studies have shown the ability of biocementation to improve the liquefaction resistance of loose sands, the effect of light cementation levels on undrained cyclic behaviors have remained relatively unexplored. A series of undrained monotonic and cyclic direct simple shear tests were performed to examine the effect of light biocementation (ΔV_s < 100 m/s, $CaCO_3$ contents < 0.9%) on the liquefaction triggering and post-triggering behavior of loose Ottawa F-65 sand subjected to varying loading magnitudes (CSR = 0.1 to 0.3). Results suggest that the presence of light biocementation can significantly improve the liquefaction triggering resistance of loose sands with log-linear increases in the number of cycles required to trigger liquefaction, which consistently correlated with cementation-induced V_s increases. Despite these remarkable pre-triggering improvements, almost no improvements were observed in post-triggering strain accumulation and

post-cyclic reconsolidation behaviors, with V_s measurements indicating that small-strain improvements were largely erased following shearing events.

4.1 Introduction

Traditional geotechnical ground improvement methods use high mechanical energy and energy-intensive materials to improve soil engineering properties, consequently resulting in considerable greenhouse gas emissions, potential for groundwater contamination, and other impacts on environmental quality (Karol 2003; DeJong et al. 2010; Kendall et al. 2018). Sparked, in part, by increased awareness of the environmental consequences of conventional geotechnical soil improvement methods, bio-mediated soil improvement technologies have been recently developed to achieve engineering performances comparable to conventional techniques (e.g. chemical grouting, deep dynamic compaction) while achieving significant environmental benefits (Seagren and Aydilek 2010; DeJong et al. 2010; 2013). Microbially Induced Calcite Precipitation (MICP) is one such technology that can improve the engineering properties of granular soils through the precipitation of calcium carbonate ($CaCO_3$) minerals on soil particle surfaces and contacts (Ferris et al. 1996; Stocks-Fischer et al. 1999; DeJong et al. 2006). In the biocementation process, microorganisms containing urease enzymes catalyze a hydrolysis reaction that degrades supplied urea, producing carbonate ions and alkalinity (Mobley et al. 1995; Stocks-Fischer et al. 1999). When sufficient calcium ions are supplied via treatment solutions or surrounding groundwater, the production of carbonate ions from ureolysis may enable supersaturation of soil pore fluids with respect to calcium carbonate ($CaCO_3$) minerals, thereby enabling precipitation (Ferris et al. 2004; Gomez et al. 2019). Resulting biocementation can dramatically increase the shear strength and stiffness of soils (DeJong et al. 2006; Montoya and DeJong 2015; Gomez et al. 2018a; Nafisi et al.

2020) with generally only minor reductions in hydraulic conductivities for clean sandy soils (Gomez and DeJong 2017; San Pablo et al. 2020). Biocementation has been proposed for a wide range of engineering applications including geotechnical soil improvement (Martinez and DeJong 2009; van Paassen et al. 2010; Feng and Montoya 2016; Gomez et al. 2016; Lin et al. 2016; Gao et al. 2019; Xiao et al. 2020; and many others), rock fracture sealing (Cuthbert et al. 2013; Phillips et al. 2016; Minto et al. 2016), soil scour and erosion prevention (Gomez et al. 2015; Montoya et al. 2018; Tao et al. 2018; Ghasemi and Montoya 2020), divalent contaminant immobilization (Fujita et al. 2004; Bhattacharya et al. 2018; He et al. 2019; Jiang et al. 2019), concrete repair (Ramakrishnan et al. 1998, 2001; Ramachandran et al. 2001; De Muynck et al. 2008), and construction material development (Bernardi et al. 2014; Choi et al. 2016; Li et al. 2016, 2020; Xiao et al. 2019a).

Of these potential applications, MICP has been most notably proposed as an environmentally-conscious method to mitigate earthquake-induced soil liquefaction (Montoya et al. 2013; Darby et al. 2019; and others). Biocementation improves soil undrained cyclic behaviors through a variety of different mechanisms including: (1) $CaCO_3$ bonding between soil particles which limits soil particle movements and contractive tendencies during cyclic shearing, (2) increases in soil dry densities resulting from precipitated $CaCO_3$ mineral solids that "densify" soils and increase dilative tendencies at larger strains, and (3) $CaCO_3$ soil particle coatings that can increase soil particle surface roughnesses and interparticle frictional resistances. Collectively, these mechanisms suggest that at both small strains, when the integrity of cemented bonds is maintained, and at larger strains, when cemented bonds are sheared and de-structured, the presence of biocementation can improve soil shearing behaviors. While such mechanisms have been

extensively described by past researchers (DeJong et al. 2010; El Kortbawi et al. 2021; and others), the magnitudes of biocementation needed to mobilize each of these mechanisms and their respective individual and combined effects on soil behaviors during undrained cyclic loading have remained less clear. Metrics to characterize each of the above individual mechanisms have yet to be agreed upon in past literature, however, it is hypothesized that: (1) $CaCO_3$ bonding between soil particles may be best assessed using small-strain stiffness measurements (e.g. shear wave velocity changes), (2) improvements in large-strain behaviors resulting from precipitated $CaCO_3$ solids may be best described using soil dry density, $CaCO_3$ content measurements, and mechanical testing, and (3) increases in soil particle surface roughnesses may be characterized using direct imaging of soil specimens and large-strain mechanical testing.

Numerous studies have examined the effect of $CaCO_3$ biocementation on the undrained cyclic behavior of sands. Studies have overwhelmingly concluded that the addition of biocementation increases soil cyclic resistances, with magnitudes of improvement generally correlating to cementation levels quantified by $CaCO_3$ contents and/or shear wave velocity (V_s) increases (Montoya et al. 2013 and others). More recent studies have significantly furthered our understanding of how biocemented materials may behave under a range of different conditions including various cementation levels, applied loadings, confining stresses, and fines contents. For example, Simatupang et al. (2018) performed undrained cyclic triaxial tests on lightly biocemented Toyoura and Keisha No.4 sand specimens improved using enzymatically-induced carbonate precipitation (EICP) with $CaCO_3$ contents of less than 0.8%. Although pre-triggering behaviors appeared to be primarily governed by interparticle $CaCO_3$ bonding as described by shear wave velocity increases (ΔV_s), improvements in post-triggering strain accumulation behaviors appeared

to primarily reflect $CaCO_3$-induced increases in soil dry densities. Zamani and Montoya (2019) performed undrained cyclic direct simple shear (DSS) tests on biocemented silty sand specimens and found that when ΔV_s increases were near 300 m/s, significant improvements in liquefaction triggering were achieved; with observed improvements also significantly influenced by soil fines contents. Xiao et al. (2019b) conducted a series of undrained cyclic triaxial tests on biocemented calcareous sands prepared to different initial relative densities (D_r) and concluded that the effect of biocementation on liquefaction triggering was more beneficial than that which could be attributed to cementation-induced dry density changes alone, with large benefits afforded by the presence of cohesive bonds. Darby et al. (2019) performed a series of centrifuge tests on untreated and biocemented loose ($D_r \approx 38\%$) Ottawa F-65 sand specimens subjected to multiple shaking events and found that when ΔV_s increases were near and above 60 m/s, significant increases in peak base accelerations were required to trigger liquefaction. Following the initial triggering event, these biocemented specimens also maintained greater resistances to triggering during subsequent loading events when compared to similar uncemented specimens, suggesting that cementation-induced improvements persisted following triggering. Riveros and Sadrekarimi (2020b) performed undrained cyclic DSS tests on biocemented Fraser River sand specimens with ΔV_s increases near 90 m/s and observed significant changes in pre-triggering excess pore pressure generation, which transitioned from rapid increases in uncemented specimens to more gradual and steady development with cycles in biocemented materials.

Although prior studies have provided significant insights regarding the potential of biocementation for liquefaction mitigation applications, to-date the spectrum of pre-triggering and post-triggering behaviors of sands near the transition from uncemented to lightly-cemented conditions has

remained poorly characterized. An improved understanding of the effect of low levels of biocementation may not only improve our understanding of MICP soil improvement, but may also provide a unique opportunity to better understand the behavior of naturally cemented soils, many of which involve weak bonding between particles resulting from cold-welding and light mineral coatings (Mitchell 2008). The importance of even small amounts of cementation on the behavior of natural geomaterials has long been recognized (Saxena and Lastrico 1978; Clough et al. 1981, 1989; Rad and Clough 1982; Saxena et al. 1988), however, a systematic study of its effects has remained challenging due to sample disturbance limitations (Frydman et al. 1980, Bachus et al. 1981; Clough and Bachus 1981; and others) and the limited sensitivity of traditional large-strain *in situ* testing instruments to light cementation levels (Rad and Tumay 1986; Akili and Al-Joulani 1988; Puppala et al. 1993; and others). Even when high-quality naturally cemented sand samples can be identified, researchers are unable to control specimen initial conditions (e.g. cementation magnitudes, initial D_r, curing stresses, etc.) and cementation heterogeneity and disturbances resulting from stress relief are unavoidable. Acknowledging these limitations, researchers have turned towards artificial cementation agents, such as portland cement, to recreate "natural" cementation in the laboratory. While potentially representative of some ground improvement processes, many of these cementation agents exhibit increased ductility when compared to naturally cemented geomaterials. Biocementation may afford significant advantages with respect to these aspects through the transformative ability to recreate "perfectly" cemented soil specimens in the laboratory using $CaCO_3$ mineral bonds that are likely more mineralogically- and mechanically-representative of natural cementation (Ismail et al. 2002; DeJong et al. 2006; Gomez et al. 2018a; El Kortbawi et al. 2021).

In this study, a DSS testing program was performed to further our understanding of the effect of light levels of biocementation on the undrained monotonic and cyclic behavior of loose poorly-graded sands. Although various definitions have been proposed to describe light, moderate, and heavy biocementation levels (Montoya and DeJong 2015; Nafisi et al. 2020, and others), in this study we refer to the achieved specimens which had cementation-induced ΔV_s increases of 100 m/s or less as being "lightly cemented." Twenty-eight undrained cyclic DSS tests were performed on biocemented Ottawa F-65 sand specimens prepared to loose initial relative densities ($D_r \approx 30\%$) and treated to varying cementation levels corresponding to ΔV_s increases ranging from 0 to 100 m/s and $CaCO_3$ contents from 0 to 0.9% with applied CSRs ranging from 0.1 to 0.3 ($\sigma'_{v\ initial} = 100$ kPa). In addition, thirty-four undrained cyclic DSS tests were performed on uncemented specimens prepared to loose ($D_r \approx 30\%$), medium-dense ($D_r \approx 55\%$), and dense ($D_r \approx 75\%$) initial relative densities with identical applied CSRs, in order to compare the behavior of biocemented specimens to similar uncemented specimens and to benchmark improvements resulting from biocementation through comparisons with improvements achievable via soil densification. In all cyclic tests the shearing phase was followed by drained reconsolidation to the initial overburden stress. Following the cyclic testing program, seven undrained monotonic tests were performed on loose biocemented specimens treated to similarly light biocementation levels ($\Delta V_s = 0$ to 93 m/s) to further explore the effect of light cementation on soil stress-strain behaviors and compare monotonic behaviors to previous results from cyclic testing. For all specimens, V_s and D_r values were characterized prior to shearing events. For biocemented specimens, changes in D_r, $CaCO_3$ contents, and V_s values resulting from the biocementation process were also assessed. Following testing, relationships between specimen properties, including D_r and biocementation magnitudes, and observed behaviors, including pre-triggering excess pore pressure generation, post-triggering strain

accumulation, and post-shearing reconsolidation strains, and V_s changes were examined. The achieved results provide new understandings regarding the effect of light levels of biocementation on soil pre-triggering and post-triggering behaviors and offer new insights regarding how biocementation degrades during undrained cyclic loading and how its influence on soil behavior evolves during the shearing process.

4.2 Materials and Methods

4.2.1 *Sand Material*

All tests involved Ottawa F-65 sand (U.S. Silica, Ottawa, IL) following previous investigations by Ziotopoulou et al. (2018), Darby et al. (2019), Carey et al. (2020), Burdalski and Gomez (2020), El Ghoraiby et al. (2020) and others. The sand had a D_{10} of 0.13 mm, D_{30} of 0.18 mm, D_{50} of 0.21 mm, D_{60} of 0.23 mm, no fines (Carey et al. 2020), and a USCS classification of SP following ASTM D2487 (ASTM, 2017). The minimum and maximum void ratios for this sand were 0.51 and 0.78, respectively, following ASTM D4253 and D4254 (ASTM, 2016a; ASTM, 2016b) as reported in Carey et al. (2020). Although the effect of soil type was not considered in this study, Ottawa F-65 sand was selected for lab testing due to its chemically-inert quartz mineralogy, near-uniform grain size distribution, and low fines content. These attributes were expected to be advantageous for this particular study as it allowed for other potentially complicating factors related to changes in specimen fines contents, gradations, and other variables to be minimized and therefore the effect of light levels of biocementation on soil behaviors to be better isolated.

4.2.2 *Direct Simple Shear Apparatus*

Figure 4.1 provides images of the direct simple shear testing apparatus, shear and pressure wave monitoring system, treatment solution application system, and specimen configuration. An electromechanical dynamic cyclic simple shear apparatus (EMDCSS, GDS Instruments, Hook, U.K.) was used to perform all monotonic and cyclic tests. The apparatus included several load cells and linear variable differential transformers (LVDTs) to measure applied axial forces (5 kN range, 0.045% accuracy), shear forces (5 kN range, 0.045% accuracy), axial displacements (25 mm range, 0.1% accuracy), and shear displacements (15 mm range, 0.1% accuracy). All tests involved pinned porous stone discs (2 mm pin lengths) to limit potential shear localization at soil-top platen interfaces. A ring retainment system was used to limit potential "rocking" of DSS rings during shearing.

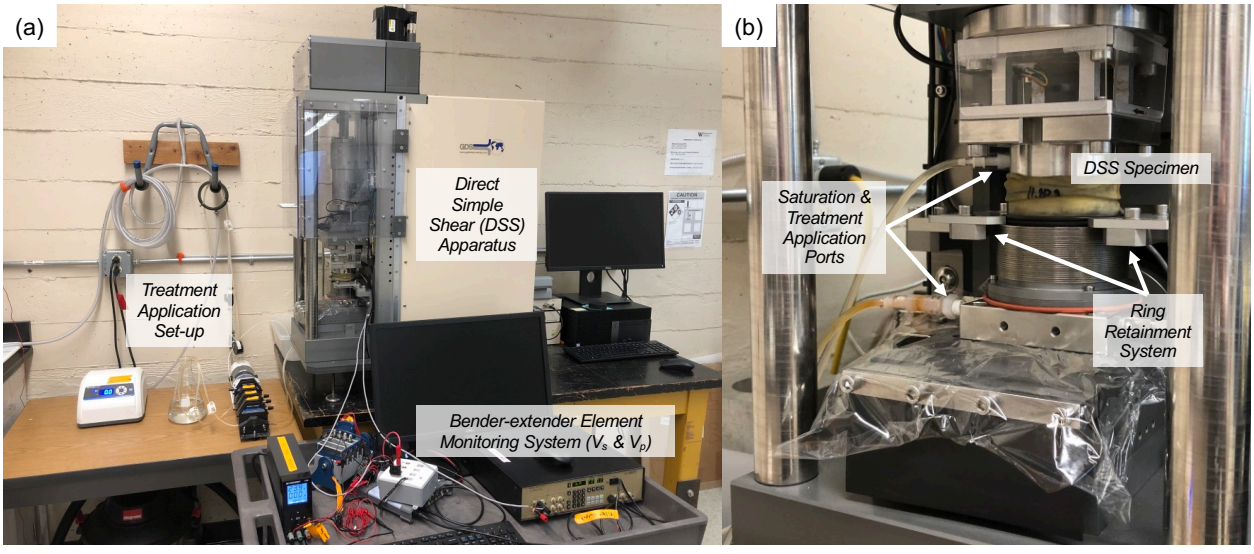

Figure 4.1. Images of the (a) direct simple shear (DSS) testing apparatus, treatment application set-up, bender-extender element monitoring system, and (b) DSS specimen configuration including saturation and treatment application ports and ring retainment system.

4.2.3 *Specimen Preparation*

DSS specimens were dry pluviated using a custom fabricated pluviation device and the pluviator aperture was adjusted, while maintaining a constant fall height, to achieve different targeted relative densities. Specimens were 70.22 mm in diameter and had heights near 22 mm. After pluviation, samples were placed within the DSS loading frame and a vertical effective stress of 100 kPa was applied to simulate stress conditions near 10 meters within a saturated soil deposit. Following stress application, a series of small amplitude strain-controlled drained cycles were applied to all specimens to ensure proper engagement of specimens at the porous disc and soil interface, as well as to establish K_0 conditions throughout specimens. A series of pre-conditioning protocol development tests were performed prior to this study to determine the appropriate number of drained cycles needed to properly engage specimens without resulting in densification (Humiere et al. 2021). A protocol was selected wherein 75 small-strain strain-controlled drained cycles (amplitude of 0.01 mm, 0.05% shear strain) were performed immediately following pluviation and before saturation and biocementation treatments. This protocol was identified by (1) analyzing changes in specimen relative densities and stiffnesses resulting from the application of varying numbers of small-strain drained cycles and (2) comparing the number of loading cycles required to trigger liquefaction for pre-conditioned specimens to past independent experimental data available for Ottawa F-65 sand (Ueda et al. 2018; Morales et al. 2020) to ensure consistency. In all cases, specimen D_r values changed by less than 2% following both initial saturation and small-strain drained cycling.

Following this “pre-conditioning” sequence, specimens were saturated with 450 mL (≈ 12 to 13 pore volumes) of de-ionized water that was boiled and de-aired using a Nold deaerator device to

eliminate the potential for partial saturation of specimens and matric suction effects. Saturation solutions were pumped slowly from the bottom cap to the top cap for at least 30 minutes until no bubbles were observed exiting the specimen over a period of 10 minutes. Saturation was verified using compressional wave velocity (V_p) measurements from bender-extender elements and V_p values exceeded 1400 m/s in specimens before shearing. For untreated specimens, shearing events proceeded immediately after saturation. For biocemented specimens, biocementation treatments were applied following saturation. All reported biocemented specimen total D_r values were calculated for conditions present immediately prior to undrained shearing events at a vertical effective stress of 100 kPa by oven-drying and weighing specimens after testing. Total D_r values therefore account for both dry sand masses as well as additional masses resulting from generated $CaCO_3$ biocementation. While the concept of relative density may not hold strictly true for biocemented sands, due to potential soil gradation changes and corresponding changes in e_{min} and e_{max} values, it is unlikely that such effects were significant given the low cementation magnitudes considered herein (< 0.9% $CaCO_3$ by mass). The use of total D_r values allowed for the response of biocemented specimens to be compared to other uncemented specimens on the basis of dry density alone. For biocemented specimens, estimates of initial relative densities prior to biocementation ($D_{r\ initial}$), were also further determined from total D_r measurements while removing precipitated $CaCO_3$ masses as informed by measured soil $CaCO_3$ contents. $D_{r\ initial}$ values were identical to total D_r values for uncemented specimens due to the lack of $CaCO_3$ precipitates. ΔD_r values were also determined and reflect the difference between $D_{r\ initial}$ and total D_r values and therefore reflect the impact of precipitated $CaCO_3$ masses on D_r. All DSS specimens had pore volumes (PV) between 32 and 35 mL (porosity ≈ 40%).

4.2.4 *Biocementation Treatments*

Biocemented specimens were augmented prior to cementation using *Sporosarcina pasteurii* (*S. pasteurii*, ATCC 11859) cells at cell densities between 10^7 to 10^8 cells/mL to enable urea hydrolysis and the biocementation process. *S. pasteurii* cells were cultured in sterile ATCC 11859 growth media (0.13M Tris Base, 20 g/L yeast extract, 10 g/L $(NH_4)_2SO_4$, pH-adjusted to 9.0, autoclaved at 121°C) by inoculating with a frozen stock culture stored at -80°C. Inoculated growth media was incubated for at least 24 hours at 30°C using a double-orbital shaker (150 rpm). During the pelleting process, cultured growth media (50 mL) was transferred to a sterile conical tube, centrifuged at 4150 g for 10 minutes to pellet cells, and the remaining clear supernatant was discarded. Sterile isotonic saline (9 g/L NaCl) was added to rinse pelleted cells, and again the tube was centrifuged and the resulting supernatant was discarded. Sterile saline was then added to obtain a total volume of 10 mL and the optical density of this cell suspension was measured at a wavelength of 600 nm (OD_{600}) with a microplate spectrophotometer. Cell densities were estimated from OD_{600} measurements using a lab-specific cell density to OD_{600} calibration curve generated using total direct cell counts (Burdalski 2020). Cell suspensions were added to solutions containing 100 mM urea and pH and conductivity measurements in time were used to verify ureolytic activity.

Augmentation solution volumes (250 mL, 8.3 PV) were prepared by adding rinsed cell suspensions to de-ionized water-based solutions containing 100 mM NH_4Cl, 10 mM urea, and 0.2 g/L yeast extract. In order to obtain uniform cell distributions throughout DSS specimens, augmentation solutions were applied in four different injection phases. First, 75 mL (2.5 PV) of augmentation solution was injected from the bottom cap to the top cap at a flow rate of 10 mL/min and all produced effluent was discarded. Next, 75 mL of the augmentation solution was injected from top

to bottom and all generated effluent was collected and mixed with the remaining 100 mL of fresh augmentation solution. Lastly, 75 mL of this mixture was injected again from bottom to top and then injected again from top to bottom, each time collecting and homogenizing effluent solutions. After injections, augmentation solutions resided within specimens for at least 1 hour to encourage cell attachment to soil surfaces prior to cementation injections. During the start of cementation injections, augmentation solution samples were collected to verify that active urea hydrolysis had occurred during augmentation treatments via measured solution pH increases. Although the efficacy of the selected augmentation procedure was not investigated extensively in this study, the procedure was similar to that presented in Gomez et al. (2019) and solution OD_{600} measurements performed before and after augmentation suggested that between 90% and 95% of the injected cells were retained within specimens.

After augmentation, calcium-containing cementation solutions were applied to specimens to initiate biocementation. Cementation solution volumes (250 mL, 8.3 PV) contained 100 mM NH_4Cl and urea and $CaCl_2$ concentrations at a ratio of 1.5-to-1.0. Although urea to calcium concentration ratios were constant, applied $CaCl_2$ concentrations were altered to achieve varying degrees of light cementation as reflected by varying ΔV_s increases. To achieve targeted ΔV_s values between 15 and 100 m/s, $CaCl_2$ concentrations between 50 and 250 mM were applied. Although the authors acknowledge that varying chemical concentrations could have impacted the properties of the achieved $CaCO_3$ precipitation, more extensive investigations by the authors have shown that when applied chemical concentrations are varied between 50 mM and 500 mM no significant differences in reaction kinetics, $CaCO_3$ mineralogy, or $CaCO_3$ morphology are observed (Burdalski and Gomez 2020). During cementation injections, 150 mL (5 PV) cementation solution

volumes were injected from the bottom to the top of specimens at a flow rate of 10 mL/min. Cementation solution injections resided within specimens for a minimum of 18 hours to ensure reaction completion. For all tests, only a single cementation solution injection was applied. For select tests, fluid samples were collected during saturation injections (which displaced residing cementation solutions) and urea and solution pH measurements were performed and indicated near full hydrolysis of the injected urea concentrations with post-treatment pH values near 8.4 (Gomez et al. 2018b). After cementation, specimens were re-saturated using 450 mL of de-aired de-ionized water that was pH-adjusted to 7.0 using sodium hydroxide to limit potential $CaCO_3$ dissolution. Saturation was again verified using compressional wave velocity (V_p) measurements from bender-extender elements and V_p values exceeded 1400 m/s in specimens before shearing. Measurements of axial strains during treatments suggested that all performed injections had no detectable effects on specimen dry densities.

Several preventative measures were incorporated into the testing program to ensure that specimen porous discs remained pervious following biocementation treatments including: (1) applying only low concentrations of urea (10 mM) during augmentation to limit the potential for abiotic precipitation upon the introduction of calcium during cementation (Gomez et al. 2019), (2) cleaning porous discs with 0.8 M acetic acid and sonication prior to all tests to remove $CaCO_3$ which may have accumulated within discs, and (3) applying cementation solutions at a relatively fast injection rate to limit reactions during solution transport. Observations of injection flow rates during initial saturation, cementation treatment, and post-treatment saturation injections as well as measured specimen axial strains and applied total stresses during injections suggested that no detectable clogging of porous stones occurred.

4.2.5 *Shear and Compression Wave Velocity Measurements*

Shear wave velocity (V_s) measurements were performed for specimens at various points in time using bender-extender elements (Lings and Greening 2001) to verify similar initial conditions between specimens, non-destructively track changes in biocementation magnitudes, and assess post-shearing V_s changes related to specimen densification and cementation damage. Bender-extender elements were installed within specimen top and bottom end platens and were excited using a 24-volt 100 Hz square wave generated by a signal generator. All received signals were measured and recorded with an oscilloscope using a sampling frequency of 1 MHz. V_s values were determined from known sensor spacings and measurements of shear wave transmission and arrival times. V_s measurements were performed for biocemented specimens: (1) before and immediately after augmentation, (2) before, immediately after, and ≈ 18 hours after cementation injections, (3) immediately prior to shearing, and (4) after shearing and reconsolidation events. V_s measurements were performed for uncemented specimens: (1) immediately before shearing and (2) after shearing and reconsolidation events. As described previously, bender-extender elements were also used to transmit and receive compression waves to assess specimen saturation before shearing events using V_p. Compression waves were transmitted, received, and interpreted using a similar process as shear waves, however, elements were excited differently by adjusting sensor wiring.

4.2.6 *Undrained Cyclic Shearing*

Undrained cyclic shearing events were performed under equivalent undrained (constant volume) conditions with no pore pressure measurements. Cycles were stress-controlled and involved application of cyclic stress ratios ($CSR = \tau/\sigma'_{v\ initial}$) of 0.1, 0.15, 0.2, 0.25, and 0.3. The loading

was applied at a frequency of 0.05 Hz for all tests with the exception of select uncemented loose specimens, wherein a lower frequency of 0.01 Hz was used to improve the ability of the DSS apparatus to achieve the intended loading. Displacement and stress measurements were recorded at a sampling frequency of 200 data points per cycle for all tests (either 2 or 10 Hz depending on applied loading frequency). All cyclic shearing events were terminated once specimens experienced a double amplitude shear strain (DASS) of 24%. Following the undrained cyclic shearing event, specimens were slowly re-centered to back to their initial position (shear deformation ≈ 0%) while maintaining the current vertical stress after failure (≈ 0 kPa). Reconsolidation was completed by reapplying the initial vertical stress of 100 kPa. Vertical displacements were allowed to stabilize for 5 minutes before final V_s measurements were completed following shearing and reconsolidation events. While it is acknowledged that actual post-liquefaction reconsolidation behaviors cannot be fully captured in equivalent-undrained DSS tests, the reapplication of the vertical total stress in this testing program following cyclic loading was intended to interpret the potential for volume change in these materials following liquefaction.

4.2.7 *Undrained Monotonic Shearing*

All monotonic tests were completed under equivalent undrained (constant volume) conditions with a shearing rate of 0.022 mm/min (approx. 0.1% shear strain per minute). Shearing proceeded until all specimens achieved single amplitude shear strains (SASS) of 24% intended to induce a similar magnitude of damage to cemented specimens as undrained cyclic shearing events. For all tests, displacement and stress measurements were recorded at a sampling frequency of 0.5 Hz. Following monotonic shearing events, vertical effective stresses were unloaded (≈ 0 kPa) and specimens were

slowly re-centered to back to their initial positions (shear displacement ≈ 0%). Reconsolidation was completed by reapplying the initial vertical stress of 100 kPa. Vertical displacements were again allowed to stabilize for 5 minutes prior to V_s measurements following shearing and reconsolidation events.

4.2.8 *$CaCO_3$ Content Measurements*

Following DSS testing, soil specimens were oven-dried for at least 18 hours and subsampled for $CaCO_3$ content measurements. $CaCO_3$ contents were quantified using a pressure chamber method in accordance with ASTM D4373 by reacting $CaCO_3$ minerals within soil subsamples of 10 to 15 grams with 1M hydrochloric acid to generate CO_2 gas and a corresponding increase in test chamber pressure (ASTM, 2014). Calibration relationships between generated chamber pressures and $CaCO_3$ masses were used to determine soil $CaCO_3$ contents from observed pressures. A minimum of three measurements were completed for each DSS specimen with the average $CaCO_3$ content reported. Individual measurements for the same specimen differed by no more than 0.1% by mass and coefficients of variation (COV) for the subsample measurements were generally less than 15%.

4.2.9 *SEM Imaging*

Scanning electron microscope (SEM) images were completed with a FEI XL830 Dual-Beam Focused Ion Beam Scanning Electron Microscope using an acceleration voltage of 1 kV and magnifications of 200x and 500x. Prior to imaging, soil specimens were oven-dried for an

additional 2 days, mounted to imaging pedestals using carbon tape, and sputter-coated using a 60%/40% Au/Pd alloy.

Table 4.1. Summary of Uncemented Undrained Cyclic Test Results

Specimen Initial Properties [1]			*Loading*	*Pre-triggering Results*			*Post-triggering Results*				
Packing[2]	D_r initial (%)	V_s initial (m/s)[3]	CSR	Cycles to r_u = 0.475	Cycles to r_u = 0.95	Cycles to 3% SASS	Cycles to 5% SASS	Cycles to 9% SASS[4]	Cycles to 24% DASS[4]	Reconsolidation Strain (%)[5]	ΔV_s after shearing and reconsol. (m/s)
L	27.1	152	0.1	14.27	17.01	16.77	17.13	17.66	19.16	1.74	1
L	28.1	150	0.1	18.95	23.51	23.19	23.62	24.22	25.61	2.54	14
L	30.8	153	0.1	16.22	20.51	20.59	20.67	21.66	23.17	2.59	12
M	50.1	162	0.1	32.02	45.01	45.60	46.61	48.72	52.75	2.08	-
M	55.1	155	0.1	15.08	20.02	20.59	21.60	24.65	29.28	1.86	-13
D	73.4	167	0.1	21.93	33.01	35.72	41.71	62.21	115.73	1.83	-3
D	73.9	173	0.1	37.16	58.02	63.18	71.20	107.22	N/A	1.94	-26
D	82.1	-	0.1	64.02	96.53	104.23	119.24	204.21	N/A	1.60	-
L	28.4	137	0.15	0.76	0.99	0.77	0.80	0.80	1.14	2.30	3
L	29.9	139	0.15	0.46	1.02	0.65	0.66	1.22	2.21	2.37	-3
L	33.5	-	0.15	0.74	0.99	0.75	0.76	0.78	1.60	2.64	-
M	56.1	143	0.15	1.73	3.01	2.69	3.64	6.66	N/A	1.78	-5
M	58.4	157	0.15	2.09	3.51	3.66	5.62	10.74	18.27	1.80	-11
D	75.4	163	0.15	2.86	5.03	7.68	22.23	80.20	174.25	1.43	-12
D	79.4	-	0.15	3.96	6.52	10.21	35.24	N/A	N/A	1.28	-
L	25.5	151	0.2	0.17	0.51	0.19	0.19	0.19	0.63	2.44	-4
L	32.8	-	0.2	0.17	0.50	0.18	0.18	0.17	1.06	2.61	-
L	34.7	139	0.2	0.25	0.50	0.26	0.26	0.57	1.06	2.44	7
M	43.8	142	0.2	0.21	0.52	0.25	0.60	1.58	2.18	2.31	18
M	48.0	-	0.2	0.60	1.01	0.65	0.69	1.62	3.12	2.22	-
D	70.0	-	0.2	0.65	2.02	2.65	6.21	29.24	N/A	1.74	-
D	77.1	167	0.2	0.69	2.01	3.14	6.21	18.20	49.24	1.70	-5
L	29.7	142	0.25	0.15	0.51	0.15	0.15	0.16	0.61	2.20	3
L	29.0	133	0.25	0.15	0.50	0.15	0.16	0.17	0.58	2.42	13
M	52.5	164	0.25	0.18	0.53	0.20	0.64	1.65	3.16	2.03	-12
M	63.8	162	0.25	0.38	1.01	0.56	1.58	3.67	7.68	1.57	-18
D	78.2	171	0.25	0.38	1.02	1.69	6.22	43.25	N/A	1.50	-33
D	78.8	167	0.25	0.46	1.02	1.61	3.74	46.25	N/A	1.33	-25
L	27.2	141	0.3	0.12	0.49	0.12	0.12	0.13	0.55	2.75	32
L	35.5	139	0.3	0.12	0.49	0.12	0.12	0.13	0.54	3.01	18
M	52.0	147	0.3	0.42	0.53	0.21	0.62	1.64	3.63	1.72	-7
M	56.2	153	0.3	0.43	1.02	0.23	0.62	1.65	3.64	1.60	-16
D	69.8	164	0.3	0.42	1.02	0.72	3.20	18.24	34.73	1.36	-15
D	76.5	160	0.3	0.47	1.52	1.71	5.70	32.22	N/A	1.70	-11

[1]All specimens were initially consolidated to σ'_v = 100 kPa

[2]L= loose, M= medium-dense, D= dense

[3]V_s values are reported when bender element measurements were available.

[4]"N/A" denotes when 9%SASS or 24% DASS was not achievable (dense samples).

[5]All specimens were re-consolidated back to σ'_v = 100 kPa

4.3 Results

4.3.1 *Summary of Undrained Cyclic Tests*

Undrained cyclic tests were performed on loose biocemented specimens as well as uncemented specimens prepared to different initial D_r values. **Table 4.1** summarizes the results of all uncemented undrained cyclic tests including specimen initial properties (e.g. packing, initial D_r,

initial V_s), applied loading (cyclic stress ratio, CSR = $\tau/\sigma'_{v\ initial}$), pre-triggering results (e.g. cycles to excess pore water pressure ratios [$r_u = \Delta u/\sigma'_{v\ initial}$] of 0.475 and 0.95, and cycles to 3% single-amplitude shear strains [SASS]), and post-triggering results (e.g. cycles to 5% SASS, 9% SASS, and 24% double-amplitude shear strains [DASS], reconsolidation vertical strains, and ΔV_s changes after shearing and reconsolidation events). Uncemented "loose" specimens had average D_r values of 30.2% (standard deviation of 3.1%) and average initial V_s values of 143 m/s (standard deviation of 7 m/s). Uncemented "medium-dense" specimens had average D_r values of 53.6% (standard deviation of 5.6%) and average initial V_s values of 154 m/s (standard deviation of 8 m/s).

Uncemented "dense" specimens had average D_r values of 75.9% (standard deviation of 3.8%) and average initial V_s values of 166 m/s (standard deviation of 4 m/s). **Table 4.2** summarizes the results of all biocemented undrained cyclic tests including specimen initial properties (e.g. packing, initial D_r, initial V_s), post-cementation specimen properties (e.g. ΔV_s from cementation, $CaCO_3$ content by mass, coefficients of variation (COV) for $CaCO_3$ content measurements, total D_r values before shearing [including cementation contributions], and increases in total D_r values [ΔD_r] from cementation), pre-triggering results (e.g. cycles to r_u of 0.475 and 0.95, and cycles to 3% SASS), and post-triggering results (e.g. cycles to 5% SASS, 9% SASS, and 24% DASS, reconsolidation vertical strains, and ΔV_s changes after shearing and reconsolidation events). All biocemented tests were completed on initially loose specimens with average initial D_r values of 31.0% (standard deviation of 3.3%) and average initial V_s values of 147 m/s (standard deviation of 8 m/s), which were similar to other uncemented loose tests. Biocemented specimens achieved total D_r increases up to 5.8% and ΔV_s increases up to 100 m/s.

Table 4.2. Summary of Results from Biocemented Undrained Cyclic Tests

Specimen Initial Properties [1]			*Post-cementation Specimen Properties*				*Loading*	*Pre-triggering Results*			*Post-triggering Results*				
Packing[2]	D_r initial (%)	V_s initial (m/s)	ΔV_s from cementation (m/s)	$CaCO_3$ by mass (%)	Total D_r (%)	ΔD_r (%)	CSR	Cycles to r_u = 0.475	Cycles to r_u = 0.95	Cycles to 3% SASS	Cycles to 5% SASS	Cycles to 9% SASS	Cycles to 24% DASS	Reconsolidation Strain (%)[3]	ΔV_s after shearing and reconsol. (m/s)
L	34.0	158	6	0.17	35.0	1.1	0.1	26.99	36.49	36.62	36.73	37.63	38.59	3.25	-6
L	37.1	167	14	0.13	37.9	0.8	0.1	66.09	85.02	85.57	85.65	86.66	87.65	2.46	-22
L	31.0	150	14	0.13	31.8	0.8	0.1	78.01	93.50	93.27	93.59	94.12	94.60	3.11	6
L	31.0	161	19	0.11	31.7	0.7	0.1	109.05	125.54	125.64	126.09	126.59	127.10	3.16	-20
L	27.3	159	35	0.46	30.2	2.9	0.1	1162.16	1236.03	1236.67	1237.17	1237.74	1238.61	2.51	-26
L	36.1	146	55	0.49	39.2	3.1	0.1	3022.12	3115.01	3115.62	3116.14	3116.66	3117.57	3.18	-64
L	34.9	140	3	0.14	35.8	0.9	0.15	1.15	1.49	1.21	1.22	1.23	1.56	3.02	0
L	31.2	142	10	0.20	32.4	1.2	0.15	5.83	7.00	6.66	6.72	7.58	8.07	2.66	1
L	29.2	148	15	0.03	29.4	0.2	0.15	2.71	3.01	3.06	3.08	3.18	3.72	2.57	-6
L	31.4	144	20	0.19	32.6	1.2	0.15	21.06	24.00	23.66	23.73	24.14	24.61	2.96	-11
L	34.3	141	50	0.44	37.0	2.8	0.15	38.99	44.54	44.62	44.73	45.59	46.08	3.25	-52
L	26.2	140	51	0.34	28.4	2.1	0.15	23.04	26.02	25.76	26.13	26.58	27.06	3.00	-37
L	27.6	151	64	0.61	31.5	3.8	0.15	555.05	594.52	595.73	596.74	598.60	599.62	2.44	-63
L	34.5	144	82	0.63	38.4	4.0	0.15	1413.12	1452.53	1453.64	1454.62	1455.75	1457.13	2.32	-72
L	26.8	137	92	0.72	31.4	4.5	0.15	1552.09	1575.02	1575.60	1576.13	1576.68	1577.60	2.44	-80
L	31.8	159	16	0.14	32.7	0.9	0.2	0.65	1.01	0.68	0.68	1.11	1.56	2.51	-18
L	29.8	146	36	0.43	32.5	2.7	0.2	5.89	8.02	7.21	7.66	8.65	9.61	2.30	-38
L	28.6	158	54	0.41	31.1	2.6	0.2	8.97	11.51	11.17	11.64	12.60	13.19	2.36	-57
L	31.2	157	77	0.51	34.4	3.2	0.2	41.99	47.01	47.14	47.62	48.17	49.08	2.73	-77
L	30.3	146	95	0.93	36.1	5.8	0.2	627.03	648.02	649.14	650.14	651.73	653.62	2.25	-87
L	30.9	135	9	0.19	32.1	1.2	0.25	0.17	0.51	0.19	0.20	0.21	0.55	3.34	-4
L	30.6	146	36	0.30	32.5	1.9	0.25	1.43	2.01	1.64	1.68	2.15	2.58	2.58	-29
L	29.1	143	70	0.38	31.5	2.4	0.25	2.67	3.01	2.71	2.71	3.12	3.55	2.57	-73
L	28.4	142	100	0.66	32.6	4.2	0.25	43.04	47.52	47.59	47.70	48.61	49.15	2.52	-92
L	37.0	144	14	0.17	38.1	1.1	0.3	0.24	0.51	0.26	0.27	0.28	0.56	2.93	-14
L	25.1	139	32	0.38	27.6	2.4	0.3	0.37	0.52	0.29	0.29	0.58	1.04	2.69	-24
L	27.9	139	64	0.45	30.7	2.8	0.3	2.06	3.01	2.64	2.68	3.13	3.56	2.62	-47
L	35.5	142	93	0.69	39.8	4.3	0.3	3.00	4.03	3.72	4.21	4.65	5.55	2.47	-94

[1]All specimens were initially consolidated to σ'_v = 100 kPa

[2]L= loose, M= medium-dense, D= dense

[3]All specimens were re-consolidated back to σ'_v = 100 kPa

4.3.2 *Biocementation-induced Changes in V_s, D_r, and Soil Microstructure*

For all specimens, increases in biocementation were expected to result in consistent increases in soil V_s values attributed to the formation of $CaCO_3$-based cementitious bonds between soil particles. **Figure 4.2** presents relationships between measured ΔV_s increases, soil $CaCO_3$ contents, and cementation-induced total D_r increases for all DSS specimens (data provided in **Tables 4.1 and 4.2**). As shown, light levels of cementation were achieved for all biocemented sand specimens with $CaCO_3$ contents up to 0.9%, which corresponded to maximum ΔV_s increases of 100 m/s and increases in soil relative densities (total D_r) up to 5.8%. The near linear relationship observed between $CaCO_3$ contents and V_s increases was consistent with observations from past studies (Gomez and DeJong 2017; Gomez et al. 2018a; Darby et al. 2019; and others). The limited scatter in the relationship shown in **Figure 4.2** ($\approx \pm 20$ m/s ΔV_s for similar $CaCO_3$ contents) suggests that the employed biocementation processes produced similar and relatively uniform distributions of cementation on soil particle contacts and surfaces for all cementation levels considered. As expected, cementation-induced increases in soil total D_r values were relatively small, with most biocemented specimens achieving total D_r values that were within the scatter of D_r variations observed for similar uncemented loose specimens (data provided in **Table 4.1**).

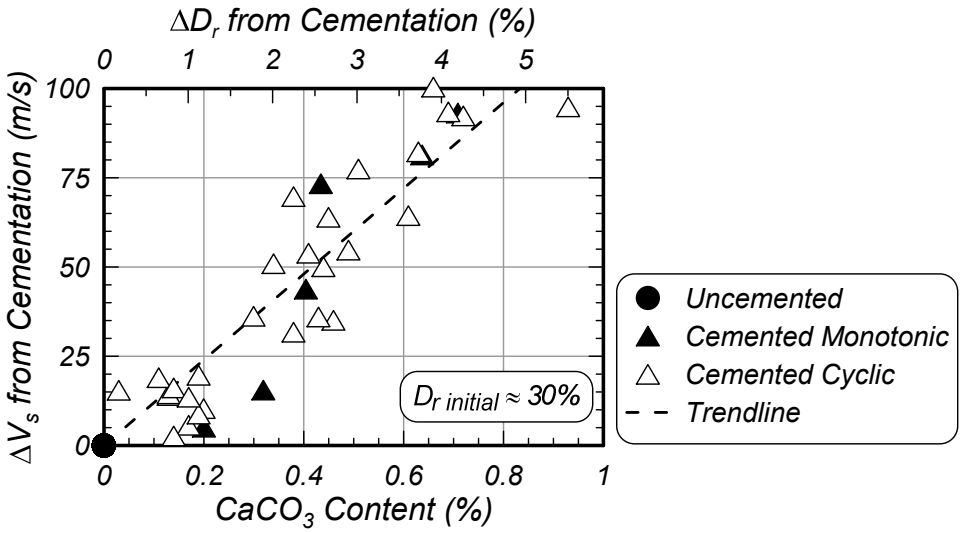

Figure 4.2. Relationships between cementation-induced shear wave velocity increases (ΔV_s), soil $CaCO_3$ contents, and changes in soil total relative densities (ΔD_r) for all biocemented and uncemented loose ($D_{r\ initial} \approx 30\%$) Ottawa F-65 specimens subjected to undrained cyclic and monotonic loading.

Figure 4.3 presents SEM images of select uncemented and biocemented sand specimens. Biocemented specimens had ΔV_s increases of 36 m/s and 77 m/s corresponding to $CaCO_3$ contents of 0.30% and 0.51%, by mass, respectively. As shown, uncemented specimens had sub-rounded and rounded particles with no evidence of $CaCO_3$ crystals on soil particle surfaces (**Figure 4.3a, 4.3b**). In contrast, rhombohedral $CaCO_3$ crystals were visible on sand particle surfaces in biocemented specimens with corresponding increases in crystal frequencies observed with increases in cementation (**Figure 4.3c to 4.3e**). Unlike more heavily biocemented materials observed in many past studies (DeJong et al. 2006; Montoya and DeJong 2015; Feng and Montoya 2015; Gomez et al. 2018a; and others), these light levels of cementation did not noticeably coat soil particle surfaces with $CaCO_3$ precipitates, suggesting that particle surface roughnesses were not likely significantly altered. Collectively, these results along with those presented in **Figure 4.2**,

which showed limited densification, suggested that the dominant improvement mechanism present in the lightly biocemented specimens was $CaCO_3$ bonding between soil particles.

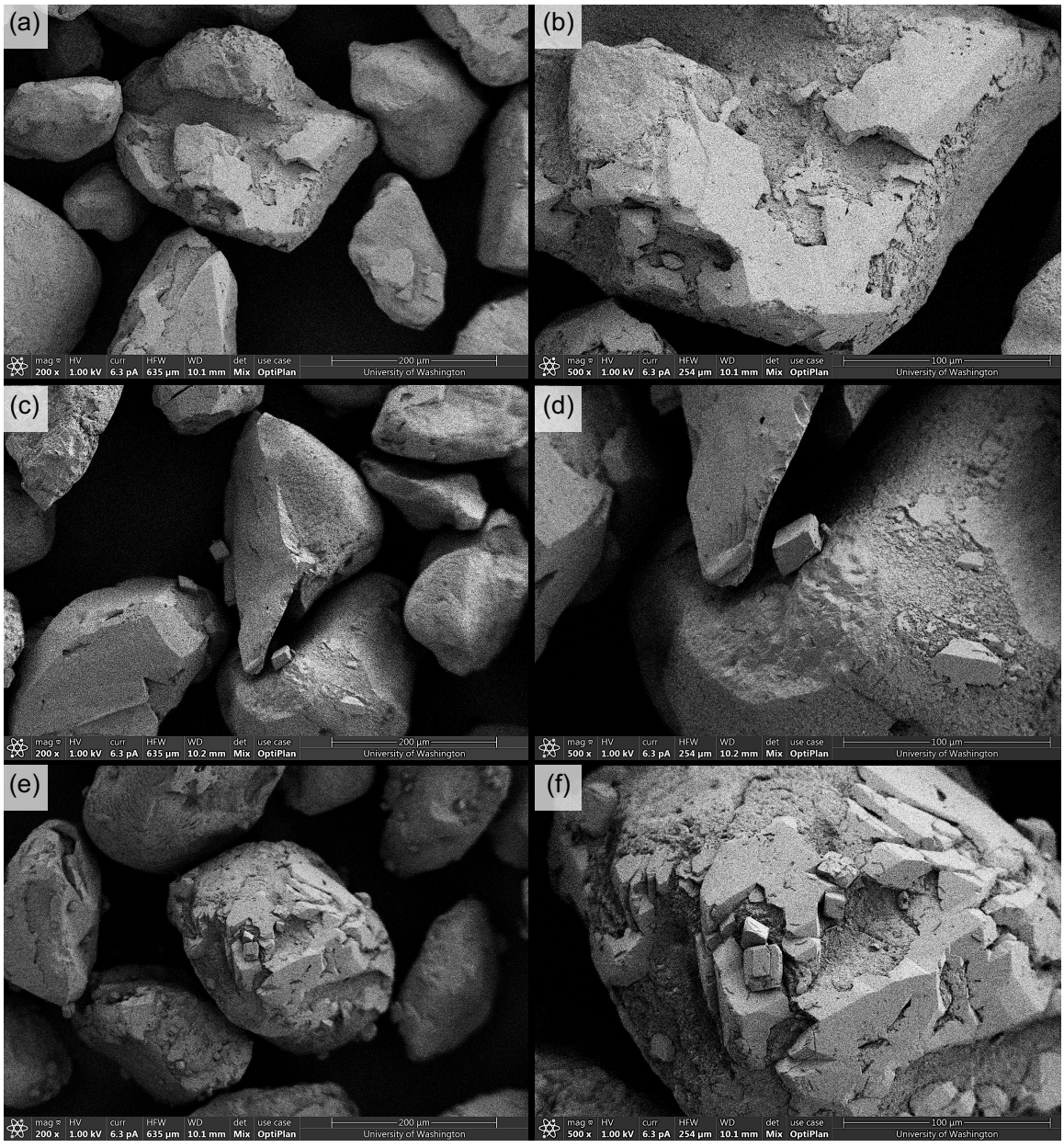

Figure 4.3. Scanning electron microscope (SEM) images of (a, b) untreated Ottawa F-65 sand, and biocemented Ottawa F-65 sand specimens with ΔV_s increases of (c, d) 36 m/s and (e, f) 77 m/s.

4.3.3 *Effect of Biocementation on Pre-Triggering Behaviors*

Figure 4.4 presents representative undrained cyclic responses for loose specimens with varying levels of biocementation (ΔV_s = 0, 16, 36, 54, 77, and 95 m/s) subjected to an applied CSR of 0.2. **Figures 4.4a through 4.4f** present responses in order of increasing cementation magnitude where column (i) presents shear stress versus vertical effective stress, column (ii) presents shear stress versus shear strain, column (iii) presents shear stress versus cycle number, and column (iv) presents r_u versus cycle number. As specimens achieved higher magnitudes of cementation, as indicated by larger ΔV_s increases, dramatic increases in the number of cycles required to trigger liquefaction (criteria of either 3% SASS or r_u = 0.95) were observed. For example, while the uncemented specimen (**Figure 4.4a**) achieved a SASS of 3% after 0.2 cycles and a r_u of 0.95 after 0.5 cycles, the most significantly biocemented specimen with a ΔV_s of 95 m/s (**Figure 4.4f)** required 649 and 648 cycles to achieve a SASS of 3% and a r_u of 0.95, respectively. For biocemented specimens with ΔV_s values exceeding 77 m/s, some initial dilation was also observed upon initiation of shearing (**Figure 4.4e and 4.4f**), in contrast to the immediate contractive behaviors exhibited by more weakly cemented and uncemented loose specimens. Despite these significant improvements in liquefaction triggering resistances, all lightly biocemented specimens exhibited post-triggering behaviors that were much more similar to uncemented specimens; only 0.4 cycles were required to accumulate strains from 3% SASS to 24% DASS in the uncemented specimen, while, in even the most significantly biocemented specimen (ΔV_s = 95 m/s) only 4.5 cycles were required to accumulate similar strains. Furthermore, no significant changes in specimen failure envelopes were observed with increases in cementation (see column i). For example, while the failure envelope for the uncemented specimen appeared to have a friction angle near 29.1^o, friction angles for biocemented specimens ranged from 29.2^o to 31.9^o with no

consistent trends observed with cementation level.

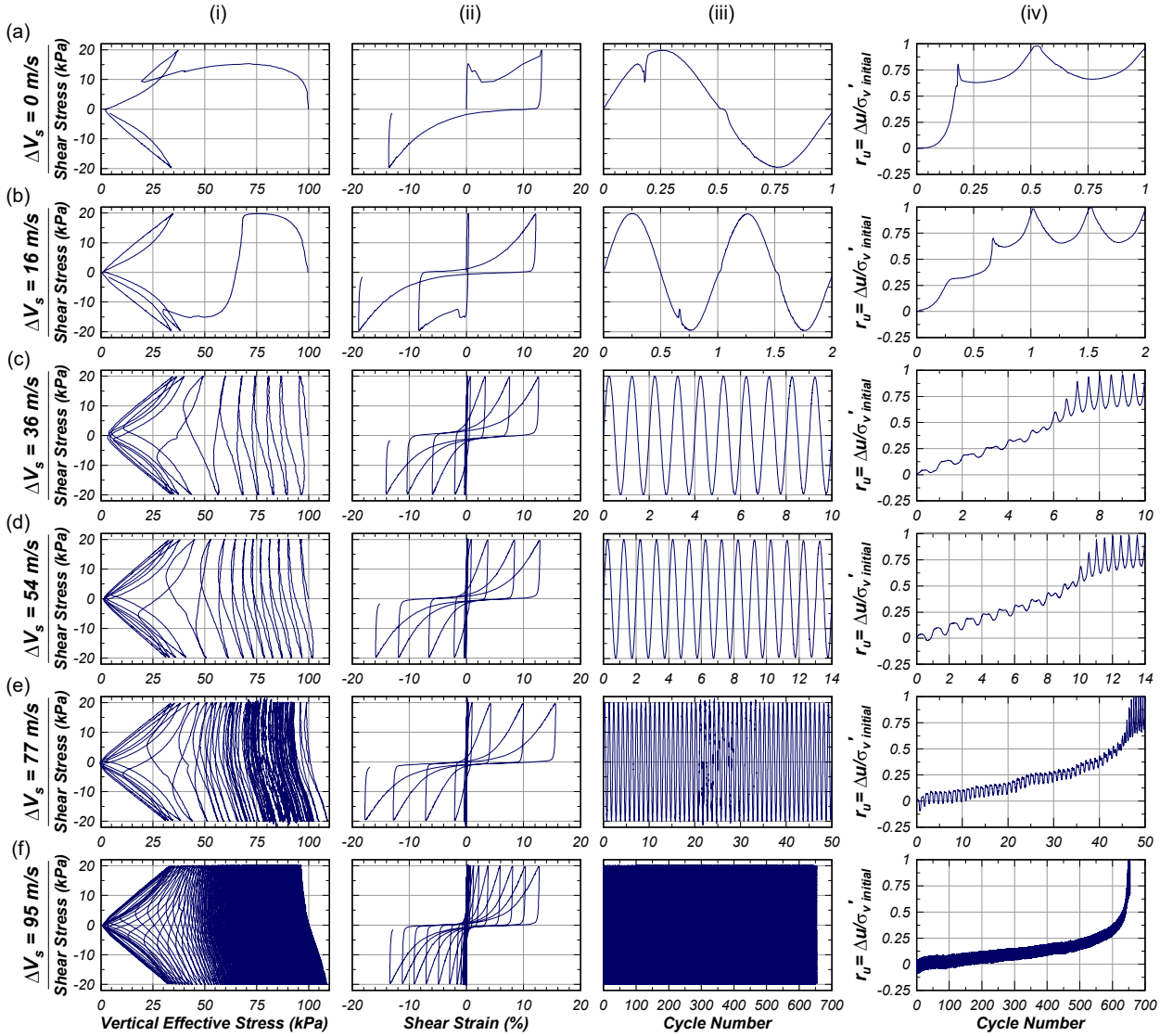

Figure 4.4. Results from undrained cyclic DSS tests performed on loose ($D_{r\ initial} \approx 30\%$) Ottawa F-65 specimens of varying cementation levels (assessed by ΔV_s) subjected to a CSR of 0.2. Plots in each column show: (i) shear stress versus vertical effective stress, (ii) shear stress versus shear strain, (iii) shear stress versus cycle number, and (iv) r_u ($=\Delta u/\sigma'_{v\ initial}$) versus cycle number.

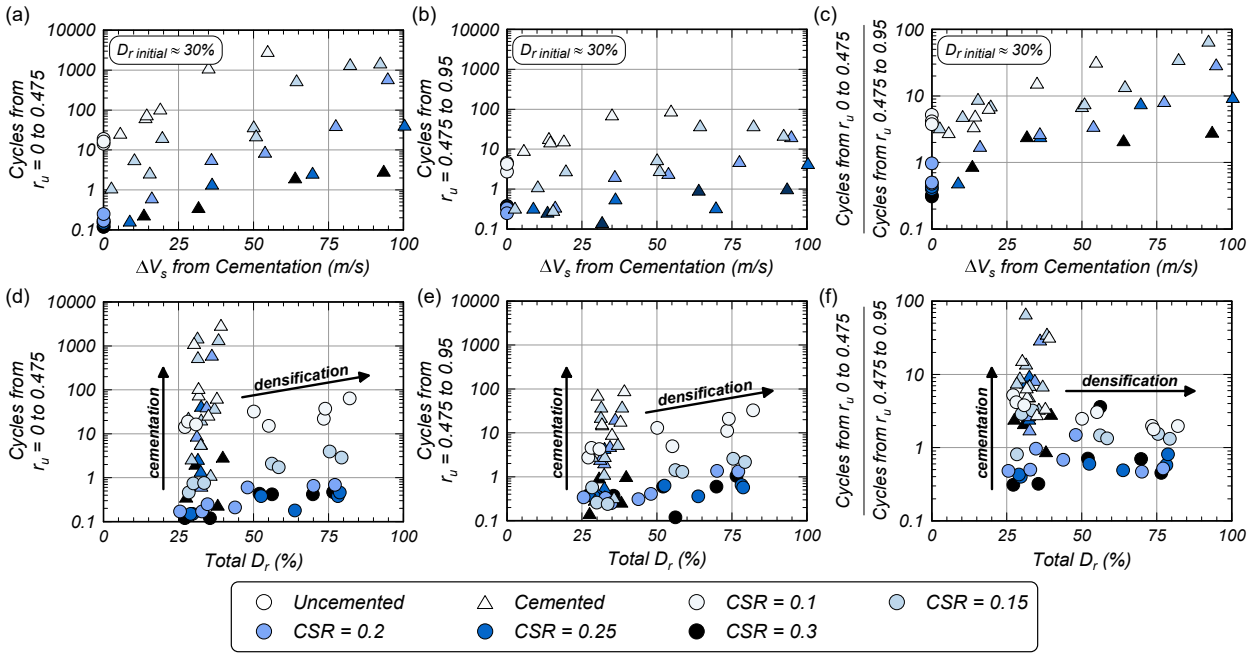

Figure 4.5. Number of cycles from (a) r_u = 0 to 0.475 and (b) r_u = 0.475 to 0.95, and (c) the ratio [cycles from r_u = 0 to 0.475 / cycles from r_u = 0.475 to 0.95] versus ΔV_s from cementation for loose (D_r initial ≈ 30%) biocemented specimens. Number of cycles (d) from r_u = 0 to 0.475 and (e) from r_u = 0.475 to 0.95, and (f) the ratio [cycles from r_u = 0 to 0.475 / cycles from r_u = 0.475 to 0.95] versus total D_r for all biocemented and uncemented specimens with varying relative densities.

Figure 4.5 presents cycles to different r_u thresholds as a function of ΔV_s increases (top row: **Figures 4.5a, b, and c**) and total D_r values (bottom row: **Figures 4.5d, e, and f**) to explore the effect of biocementation magnitudes and relative density differences on excess pore pressure generation prior to liquefaction triggering (e.g. r_u = 0.95). **Figures 4.5a through 4.5c** present the number of cycles needed to generate a r_u of 0.475, the number of cycles needed to increase r_u from 0.475 to 0.95, and the ratio between these two values versus ΔV_s increases for all loose specimens of varying biocementation levels. **Figures 4.5d through 4.5f** present similar plots versus total D_r for all biocemented specimens and uncemented specimens prepared to different initial D_r values. As shown, pre-triggering excess pore pressure generation was evaluated in two equal increments, wherein the number of cycles needed to generate a r_u of 0.475 and increase r_u from 0.475 to 0.95

represented the first and second half of excess pore pressure generation prior to triggering, respectively. As shown, significant increases in both the number of cycles required to generate a r_u of 0.475 and to increase r_u from 0.475 to 0.95 were observed with increases in biocementation (**Figure 4.5a and 4.5b**). In addition, for almost all specimens, more cycles were required to generate a r_u of 0.475 than to increase r_u from 0.475 to 0.95, with more significant differences observed for specimens subjected to lower applied CSRs (**Figure 4.5c**). While this trend was expected due to the presence of lower effective stresses and thus lower soil shear stiffnesses at higher excess pore pressures near triggering, more significant differences between the cycles required to generate a r_u of 0.475 and the cycles required to increase r_u from 0.475 to 0.95 were observed with increases in biocementation when compared to similar uncemented specimens. For example, while ratios between these cycle values were less than 5 for all uncemented specimens, these ratios appeared to consistently increase with biocementation magnitudes, reaching values near 70 at ΔV_s increases near 100 m/s (**Figure 4.5c**). This suggested that while uncemented specimens required fewer cycles to trigger liquefaction, pore pressures generated per cycle of loading were relatively similar for most cycles prior to triggering (i.e. cycles up to r_u of 0.95). In contrast, biocemented specimens appeared to require significantly more cycles during the first half of pre-triggering excess pore pressure generation (r_u of 0.475) when compared to the second half (r_u from 0.475 to 0.95). This behavior likely results from the presence of lightly-cemented bonds which hold particles together and inhibit the generation of excess pore pressure at small strains during the start of cyclic loading, but become less effective at inhibiting excess pore pressure generation as they gradually degrade with increases in strain magnitudes during later cycles. While biocementation appeared to significantly influence pre-triggering excess pore pressure generation, the same conclusion cannot be drawn when examining D_r changes for uncemented specimens

where the effects observed were more limited. While modest increases in both the number of cycles needed to generate a r_u of 0.475 and to increase r_u from 0.475 to 0.95 were observed with increases in D_r for uncemented specimens (**Figure 4.5d and 4.5e**), the ratios between these cycle values were again less than 5 for all uncemented tests regardless of total D_r (**Figure 4.5f**), suggesting that D_r changes alone had relatively insignificant effects on pre-triggering excess pore pressure generation.

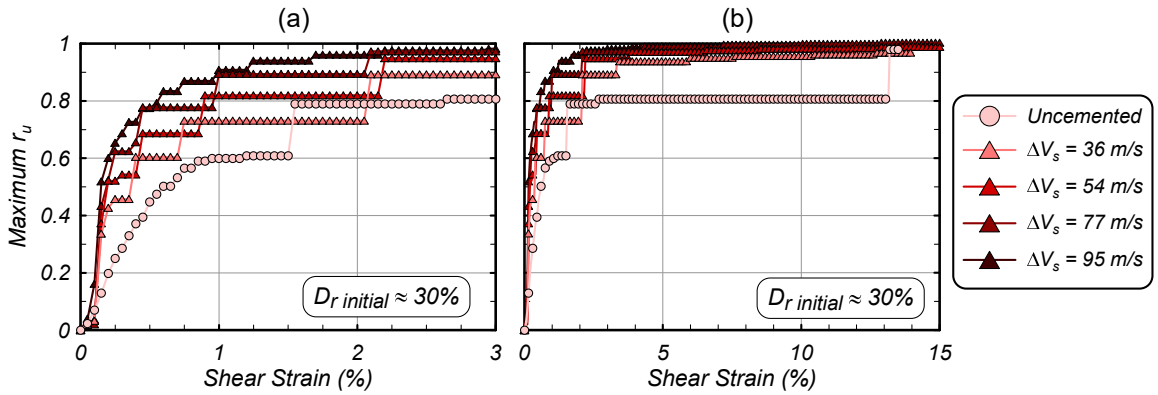

Figure 4.6. Evolution of maximum excess pore pressure ratios ($r_u = \Delta u/\sigma'_{v\ initial}$) with shear strain for loose specimens of varying-cementation levels subjected to a CSR of 0.2, wherein the maximum excess pore pressure ratio (r_u) is the largest r_u value that a specimen has experienced prior to achieving different shear strains. Plots present similar data for shear strains from 0% to (a) 3% and (b) 15%. Data points were evaluated at discrete increments of 0.05% shear strain.

Relationships between excess pore pressure generation and developed shear strains were explored in order to further examine the effect of biocementation on soil pre-triggering response as well as the associated progressive de-structuration of bonds during shearing. **Figure 4.6** presents maximum excess pore water pressure ratios (r_u) that specimens experienced prior to first achieving a given shear strain magnitude for loose specimens of varying biocementation levels subjected to a CSR of 0.2. All shear strains are presented as absolute values, thus information about cycle

numbers and stress reversals is not shown. The provided data are representative of similar trends observed for other biocemented specimens at different applied CSRs. As shown in **Figure 4.6a**, prior to triggering, biocemented specimens developed significantly smaller shear strains than uncemented specimens at similar maximum r_u values. For example, once specimens experienced a maximum r_u value near 0.6, the uncemented specimen developed shear strains near 1.5%, while the biocemented specimen with the largest increase in V_s (ΔV_s = 95 m/s) experienced shear strains of only 0.25%. In addition, while the uncemented specimen appeared to exhibit measurable shear strains once r_u values increased above ≈ 0.05, biocemented specimens appeared to require significantly larger maximum r_u values exceeding ≈ 0.4 before shear strains greater than 0.15% were observed. Threshold r_u values, or r_u values after which further increases in r_u resulted in large increases in shear strains, also appeared to systematically track with increases in biocementation levels. For example, while the ΔV_s = 36 m/s specimen had a threshold r_u near 0.4, the ΔV_s = 95 m/s specimen had a larger threshold r_u closer to 0.55. Interestingly, at larger shear strains post-triggering (> 5%), biocemented specimens appeared to experience larger r_u values than uncemented specimens for similar shear strains (**Figure 4.6b**). It is hypothesized, however, that this result may be simply an artifact of the more rapid shear strain development that occurred in uncemented specimens, in contrast to biocemented specimens, wherein many more cycles were required to generate such strains, which allowed for accompanying r_u increases to more fully develop. Collectively, these trends suggest that biocemented specimens can tolerate higher maximum excess pore water pressure ratios (i.e. lower vertical effective stresses) than uncemented specimens before significant shear strains develop, with threshold r_u values proportional to cementation level. This behavior likely results from the presence of cemented bonds in biocemented specimens, which provide tensile strength and allow for higher soil shear stiffnesses

to be maintained with increases in r_u, thus preventing shear strain development. However, it appears as though once biocemented specimens experience vertical effective stresses below some critical value (at some threshold r_u), the gradual breakage of cemented bonds intensifies and bonds become insufficient towards preventing shear deformations, resulting in abrupt increases in shear strains and further mobilization of soil contractive volumetric tendencies, thus increasing r_u.

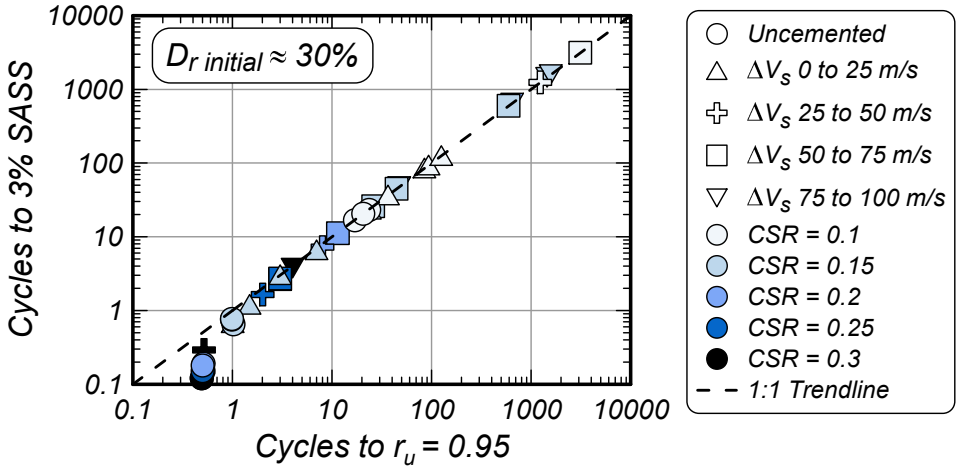

Figure 4.7. Number of cycles to 3% SASS versus number of cycles to $r_u = 0.95$ for specimens of varying biocementation (as indicated by ΔV_s) subjected to different applied CSRs. A 1:1 trendline is provided to compare criteria.

Established liquefaction triggering criteria were employed in order to examine changes in soil liquefaction triggering resistances with changes in biocementation levels, D_r, and applied loading magnitudes. The two liquefaction triggering criteria considered were: (1) number of loading cycles required to achieve a SASS of 3% (Ishihara 1993), and (2) number of loading cycles required to achieve a r_u of 0.95 (Ishihara 1993; Wu et al. 2004). A criterion of $r_u = 0.95$ was used instead of $r_u = 1.0$ to account for potential variations in laboratory measurements, as recommended by Wu et al. (2004). **Figure 4.7** presents relationships between the number of loading cycles required to achieve a SASS of 3% and the number of loading cycles required to achieve a r_u of 0.95 for all

loose specimens of varying biocementation levels subjected to different applied loading magnitudes. As shown, both liquefaction triggering criteria yielded nearly identical results with almost all specimens following a 1:1 trend. Results between criteria diverged only slightly for specimens subjected to higher CSR values (> 0.2) when triggering occurred within less than 1 cycle for both approaches. Since no significant differences were observed between criteria and all tests were completed under equivalent-undrained conditions with no direct pore pressure measurements, the number of loading cycles to 3% SASS was used to evaluate liquefaction triggering for all further results presented in this study.

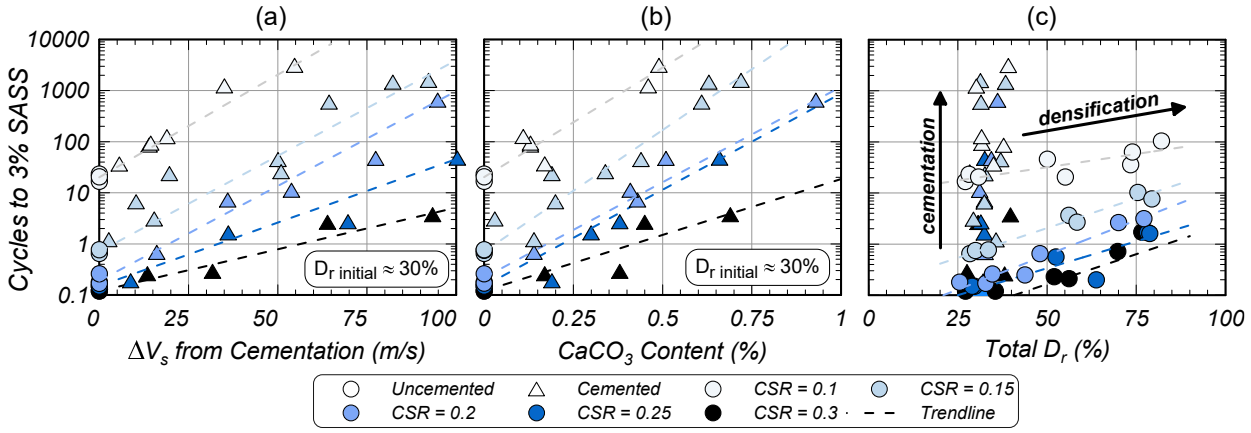

Figure 4.8. Number of cycles to 3% SASS versus (a) ΔV_s from biocementation and (b) $CaCO_3$ contents for loose ($D_{r\ initial} \approx 30\%$) specimens of varying biocementation. (c) Number of cycles to 3% SASS versus total relative densities (D_r) for all biocemented and uncemented specimens of varying D_r.

Figure 4.8 presents relationships between number of cycles to 3% SASS versus ΔV_s from cementation (**Figure 4.8a**), soil $CaCO_3$ contents (**Figure 4.8b**), and total D_r values (**Figure 4.8c**). As mentioned previously, all biocemented specimens shown in **Figure 4.8a** and **Figure 4.8b** had similar initial D_r values near 30%. For all CSR magnitudes, increases in biocementation, as

indicated by V_s and $CaCO_3$ content increases, resulted in log-linear increases in the number of cycles required to trigger liquefaction with the most pronounced effects at low CSR values (**Figure 4.8a, 4.8b**). For example, as ΔV_s values increased from 0 m/s (uncemented) to 50 m/s, cycles to trigger liquefaction increased by nearly 2 orders of magnitude for CSR of 0.1, 0.15, and 0.2 specimens, respectively, however, cycles to trigger liquefaction increased by a significant but smaller 1 to 1.5 orders of magnitude for specimens at CSRs exceeding 0.25. At higher levels of biocementation near a ΔV_s of 100 m/s, tests could only be performed at CSR values exceeding 0.15, and results suggested improvements in the cycles to trigger liquefaction between 1.5 and 3 orders of magnitude when compared to similar uncemented specimens. When comparing ΔV_s-based (**Figure 4.8a**) and $CaCO_3$ content-based (**Figure 4.8b**) relationships, similar trends were observed, however, noticeably larger scatter was observed in the $CaCO_3$ content-based relationship. As discussed earlier, even when identical cementation treatment techniques are used, variations in ΔV_s increases can occur at the same $CaCO_3$ content (**Figure 4.2**) as a result of small differences in the distribution of biocementation on particle surfaces and contacts. The better correlation between the number of cycles to liquefaction triggering and ΔV_s suggests that V_s measurements may offer improved assessment of triggering behaviors when compared to mass-based quantification of biocementation. **Figure 4.8c** provides the relationship between number of cycles to trigger liquefaction (3% SASS) and total D_r for all biocemented loose specimens as well as uncemented specimens prepared to different initial D_r values (≈30% to 75%). It should be mentioned that total D_r variations for cemented specimens are again indicative of both small differences in initial preparation and small dry density increases resulting from biocementation. As shown for uncemented specimens, when soil D_r values increased, increases in the number of cycles to trigger liquefaction were also observed, however, improvements were not as significant as those obtained

with increases in biocementation. For example, when D_r values increased from ≈ 30% to 75% for uncemented specimens subjected to a CSR of 0.1, increases in the number of cycles to trigger liquefaction of less than one order of magnitude was observed. When compared to loose biocemented specimens (under the same applied CSR of 0.1), however, a ΔV_s increase of only 19 m/s would be needed to achieve similar improvement. These results may have significant practical implications, as densification of loose soils via various ground improvement techniques (e.g. deep dynamic compaction) is oftentimes considered for liquefaction mitigation. While soil densification did yield modest improvements in liquefaction triggering resistances, for the loading magnitudes considered in this study, the presence of light levels of biocementation resulted in more dramatic improvements in liquefaction triggering behaviors.

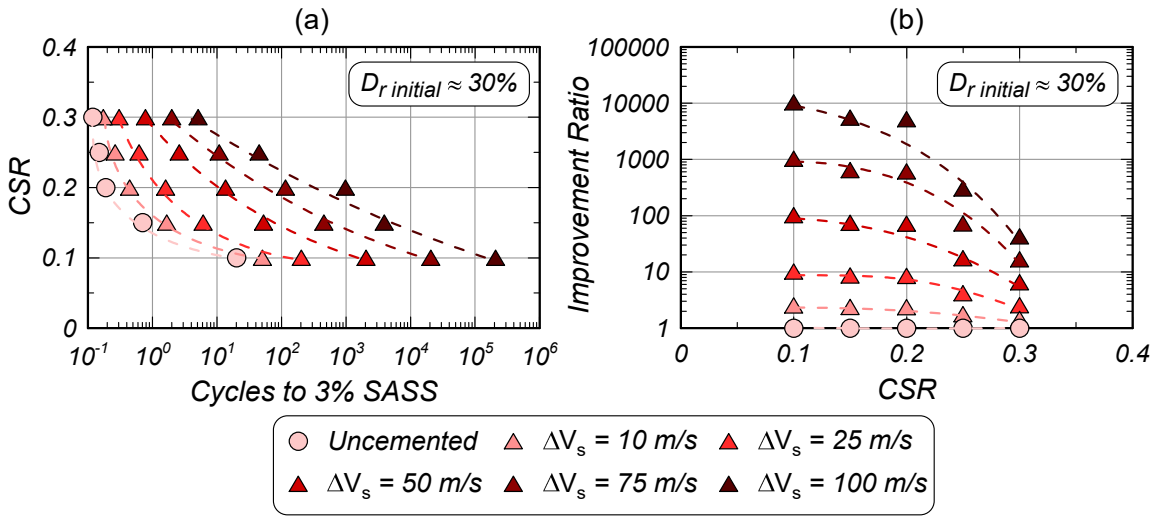

Figure 4.9. Relationships between (a) applied CSRs versus number of cycles to 3% SASS and (b) improvement ratios ($N_{3\%\ SASS\ Cemented}$ / $N_{3\%\ SASS\ Uncemented}$) versus applied CSRs for loose ($D_{r\ initial}$ ≈ 30%) specimens of varying biocementation levels (ΔV_s = 0, 10, 25, 50, 75, 100 m/s).

Figure 4.9 presents relationships between applied CSRs versus number of cycles to trigger liquefaction (3% SASS) (**Figure 4.9a**) and improvement ratios versus applied CSRs (**Figure 4.9b**)

for varying biocementation levels. Improvement ratios were determined by dividing the number of cycles needed to achieve 3% SASS in biocemented specimens by that required for identical uncemented specimens. Since biocemented specimens with identical ΔV_s values were not tested at different CSR values, and the number of cycles to liquefaction triggering was shown to change dramatically with even small increases in ΔV_s, trendline relationships between ΔV_s values and number of cycles to 3% SASS presented in **Figure 4.8a** were used to develop curves by estimating cycles to 3% SASS for consistent ΔV_s increments. As shown in **Figure 4.9a**, developed curves allow for changes in liquefaction resistances with changes in applied CSRs to be understood for a single cementation level (i.e. ΔV_s increase). Several main trends are observed from these liquefaction triggering curves: (1) with increases in biocementation magnitudes, increases in the number of cycles to 3% SASS occur for all applied CSRs, and (2) the effect of biocementation on soil liquefaction triggering resistances was more pronounced at lower applied CSRs than at higher CSRs. Similar trends can be observed in **Figure 4.9b**, where improvement ratios are largest with increasing biocementation at lower applied CSRs. For example, the highest cementation level considered (ΔV_s = 100 m/s) had an improvement ratio of 10,363 at a CSR of 0.1, however, this same cementation level corresponded to an improvement ratio of only 43 at a CSR of 0.3. While changes in cyclic resistances with applied loading magnitudes are expected for even uncemented soils (Idriss and Boulanger 2008), these resistances appeared to be more significantly influenced by applied loading magnitudes with increases in biocementation. It is hypothesized that the greater improvement ratios observed at lower CSRs are related to the mode of cemented bond de-structuration which involves more gradual fatigue-like deterioration at smaller applied CSRs, in comparison to more abrupt damage of cemented bonds at higher applied CSRs. A power law function is commonly used to describe the functional form of liquefaction triggering curves (e.g.

$CSR = a*N_L^b$, wherein N_L is number of cycles to 3% SASS, and "a" and "b" values are empirically fit parameters that capture the vertical position and slope of curves, respectively). However, this functional form did not appear to reasonably capture observed trends for biocemented specimens in this study. Significant discrepancies have also been reported between past studies, wherein the slopes of liquefaction triggering curves (i.e. "b" values) have been suggested to decrease (Hernandez 2018; Xiao et al. 2018, 2019b), remain constant, or even increase (Riveros and Sadrekarimi 2020b) with increasing biocementation (El Kortbawi et al. 2021), suggesting that further investigation of this aspect is needed.

4.3.4 *Effect of Biocementation on Post-Triggering Behaviors*

Numbers of cycles to different strain thresholds following triggering were examined in order to explore changes in post-triggering behaviors with changes in biocementation magnitudes and relative densities. **Figure 4.10** presents the number of cycles from 3% to 9% SASS versus ΔV_s from cementation (**Figure 4.10a**), the number of cycles from 3% to 9% SASS versus total D_r (**Figure 4.10b**), and the number of cycles from 3% SASS to 24% DASS versus ΔV_s from cementation (**Figure 4.10c**). As shown in **Figure 4.10a** and **Figure 4.10c,** for all biocementation levels and applied CSRs almost no detectable changes in post-triggering strain accumulation behaviors were observed when compared to the behavior of the uncemented specimens. For example, a maximum of only 3 additional cycles were required for biocemented specimens relative to uncemented specimens to progress from 3% to 9% SASS (**Figure 4.10a**), with a maximum of only 4 additional cycles required to progress from 3% SASS to 24% DASS (**Figure 4.10c**). The limited improvements in post-triggering strain accumulation behaviors with increases in biocementation, suggest that biocemented bonds may be already significantly damaged prior to

triggering, with the effect of light cementation diminished at larger strains due to the absence of cohesive bonds and the limited densification of specimens ($\Delta D_r < 5.8\%$). In contrast, when the post-triggering behavior of uncemented specimens prepared to different D_r values was compared to that of biocemented loose specimens, significant differences were observed (**Figure 4.10b**). For example, when the D_r of uncemented specimens was increased from ≈ 30% to 75%, the number of cycles from 3% to 9% SASS increased by over two orders of magnitude for all applied CSRs (**Figure 4.10b**). Large improvements in post-triggering strain accumulation behaviors with increases in soil D_r were in stark contrast to the minimal effects of light biocementation and resulted from increasingly dilative volumetric behaviors (Bolton 1986). Interestingly, when compared on the basis of total D_r, results from biocemented and uncemented specimens were relatively consistent (**Figure 4.10b**), further suggesting that light biocementation may have minimal effects on soil post-triggering shearing behaviors beyond those afforded by small dry density increases.

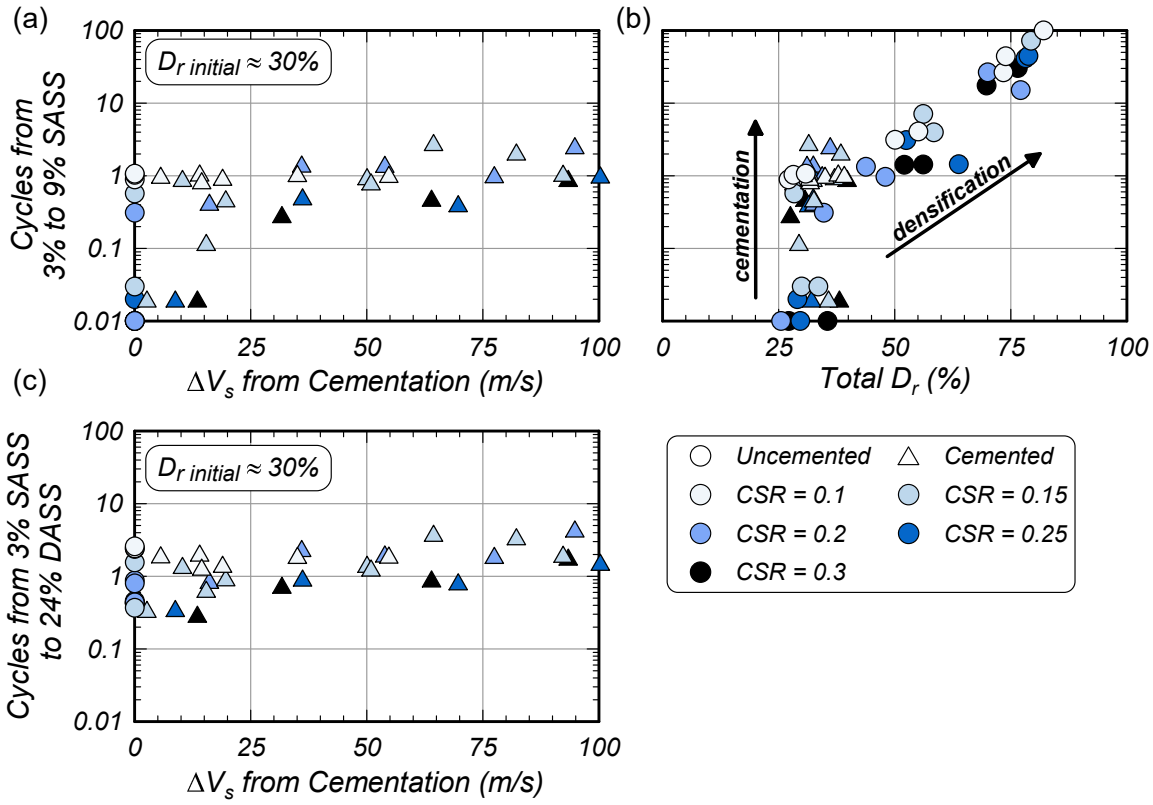

Figure 4.10. Number of cycles from 3% to 9% SASS versus (a) ΔV_s from cementation for loose ($D_{r\ initial} \approx 30\%$) specimens of varying biocementation and (b) D_r for all biocemented specimens and uncemented specimens prepared at varying D_r. (c) Number of cycles from 3% SASS to 24% DASS versus ΔV_s from cementation for loose ($D_{r\ initial} \approx 30\%$) specimens of varying biocementation.

In addition to strain accumulation, changes in reconsolidation behaviors following shearing events were also examined with changes in soil biocementation levels and D_r. **Figure 4.11** presents reconsolidation strains versus ΔV_s from cementation for all biocemented loose specimens (**Figure 4.11a**) as well as D_r for all biocemented loose specimens and uncemented specimens prepared to varying initial D_r values (**Figure 4.11b**). Reconsolidation vertical strains were measured during the reapplication of the 100 kPa vertical effective stress following the accumulation of 24% DASS for all samples. As shown in **Figure 4.11a,** as biocementation magnitudes increased, almost no

effects on reconsolidation strains were observed. For example, for biocemented specimens with ΔV_s values near 100 m/s, average reconsolidation strains were reduced by only 1.65% (0.04% strain) when compared to uncemented specimens. In several instances, reconsolidation strains for biocemented specimens with ΔV_s increases of less than 50 m/s even exceeded those for similar uncemented specimens. In contrast, soil D_r increases were observed to have much more dramatic effects on reconsolidation behaviors, with average reconsolidation strains decreasing by nearly 36% (0.88% strain) for uncemented specimens when D_r was increased from ≈ 30% to 75% (**Figure 4.11b**). Reconsolidation trends were consistent with previous post-triggering strain accumulation behaviors and again suggested that light levels of biocementation (ΔV_s < 100 m/s) may afford almost no improvements in large-strain soil behaviors.

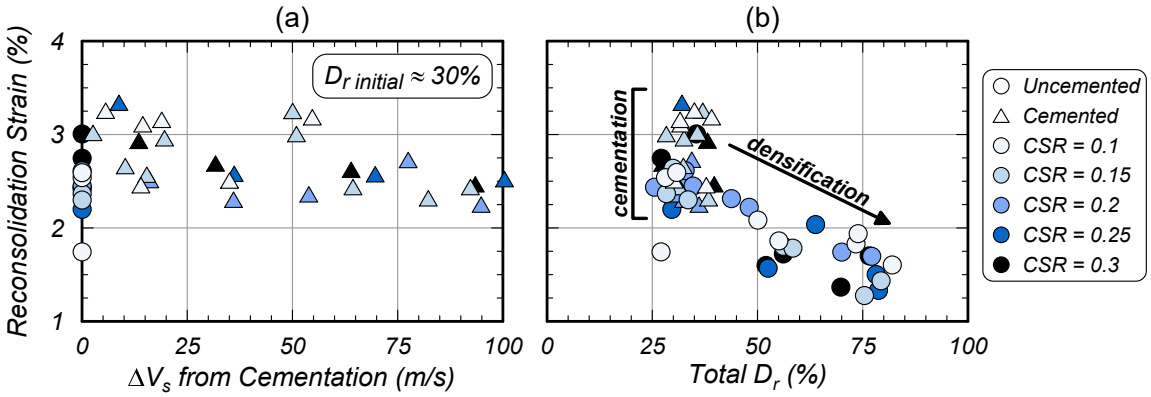

Figure 4.11. Reconsolidation strains versus (a) ΔV_s from cementation for loose ($D_{r\ initial}$ ≈ 30%) specimens of varying biocementation levels and (b) total D_r for all biocemented loose specimens and uncemented specimens prepared at varying initial D_r.

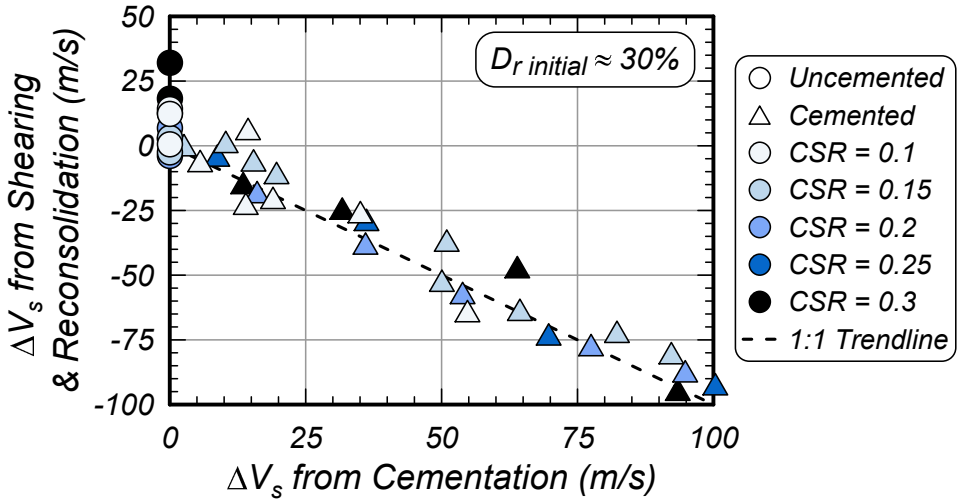

Figure 4.12. Shear wave velocity changes (ΔV_s) following shearing and reconsolidation events versus shear wave velocity increases (ΔV_s) from cementation for loose ($D_{r\ initial} \approx 30\%$) specimens of varying cementation with different applied CSRs. Data points plotting near the 1:1 trendline suggest that increases in V_s from cementation were eliminated following shearing and reconsolidation events.

Figure 4.12 presents relationships between ΔV_s changes measured following shearing and reconsolidation events and ΔV_s increases resulting from biocementation. ΔV_s changes measured following shearing and reconsolidation were indicative of both V_s decreases resulting from biocementation damage during shearing events as well as potential V_s increases resulting from soil densification during reconsolidation. It should be noted that for all biocemented specimens, shearing events were stopped following the accumulation of 24% DASS, thus all specimens experienced similar shear strain magnitudes prior to reconsolidation. For all uncemented specimens, ΔV_s increases from biocementation were non-existent, however, following shearing and reconsolidation events small increases in V_s values of less than 25 m/s were observed resulting from some densification. For biocemented specimens, ΔV_s increases from cementation had similar magnitudes as ΔV_s decreases following shearing and reconsolidation events suggesting that small-strain stiffness improvements resulting from light biocementation were largely erased following

shearing events, irrespective of applied CSRs or cementation levels. It should be noted that some biocemented specimens plotted above the 1:1 trendline by less than 25 m/s and may be suggestive of small V_s increases due to specimen densification and/or some retention of cementation integrity (i.e. bonding). The absence of significant ΔV_s increases from biocementation remaining following shearing events was consistent with other post-triggering observations, which suggested that light biocementation had limited effects at larger strains.

4.3.5 *Summary of Undrained Monotonic Tests*

Undrained monotonic tests were performed on loose specimens of varying biocementation levels to examine changes in stress-strain behaviors and volumetric tendencies with changes in cementation and to relate observed monotonic responses to previous cyclic results. **Table 4.3** summarizes the results of all undrained monotonic tests including specimen initial properties (e.g. packing, initial D_r, initial V_s), post-cementation specimen properties (e.g. ΔV_s from cementation, $CaCO_3$ content by mass, coefficients of variation (COV) for $CaCO_3$ content measurements, total D_r values before shearing [including cementation contributions], and increases in total D_r values [ΔD_r] from cementation), and test results (e.g. peak shear stress from 0 to 3% SASS, corresponding CSR to achieve 3% SASS in 0.25 cycles, reconsolidation vertical strains, and ΔV_s changes after shearing and reconsolidation events). All specimens had initial D_r values between 26.4% and 33.3% and initial V_s values between 136 m/s and 152 m/s. Biocemented specimens achieved D_r increases up to 4.5% and V_s increases up to 93 m/s, which were consistent with the light biocementation levels investigated in cyclic tests (**Figure 4.2**).

Table 4.3. Summary of Results from Undrained Monotonic Tests

Specimen Initial Properties [1]			*Post-cementation Specimen Properties*				*Results*			
Packing[2]	D_r initial (%)	V_s initial (m/s)	ΔV_s from cementation (m/s)	$CaCO_3$ by mass (%)	Total D_r (%)	ΔD_r (%)	Peak τ from 0 to 3% SASS (kPa)	$CSR_{3\%\ SASS}$ in 0.25 cycles	Reconsolidation Strain (%)[3]	ΔV_s after shearing and reconsol. (m/s)
L	30.3	138	0	0.00	30.3	-	17.7	0.18	2.95	-2
L	33.3	139	5	0.20	34.6	1.3	20.0	0.20	2.82	-9
L	32.6	141	16	0.32	34.6	2.0	24.0	0.24	2.78	-20
L	27.5	140	44	0.40	30.0	2.6	30.8	0.31	2.80	-48
L	26.4	136	73	0.43	29.2	2.8	32.9	0.33	2.85	-74
L	28.3	152	81	0.64	32.3	4.0	49.1	0.49	1.41	-86
L	31.2	138	93	0.71	35.6	4.5	72.0	0.72	2.44	-99

[1]All specimens were initially consolidated to σ'_v = 100 kPa

[2]L= loose, M= medium-dense, D= dense

[3]All specimens were re-consolidated back to σ'_v = 100 kPa

4.3.6 *Effect of Biocementation on Undrained Monotonic Behaviors*

Figure 4.13 presents results from undrained monotonic tests including shear stresses versus shear strains (**Figure 4.13a**), shear stresses versus vertical effective stresses (**Figure 4.13b**), and excess pore water pressures versus shear strains (**Figure 4.13c**) for loose specimens of varying biocementation levels (ΔV_s = 0, 16, 44, 81, and 93 m/s). As shown, all specimens exhibited initially contractive tendencies at strains less than 0.25%, with increasingly dilative behaviors observed at larger strains with increases in biocementation. Biocemented specimens with ΔV_s increases less than or equal to 44 m/s exhibited strong contractive volumetric tendencies, with positive excess pore water pressures observed at all shear strains. In more significantly biocemented specimens (ΔV_s values of 81 m/s and 93 m/s), however, dilative volumetric behaviors were observed with negative excess pore water pressures generated at higher shear strains. Corresponding increases in vertical effective stresses in more significantly biocemented specimens resulted in increases in shear strengths and stiffnesses with increases in biocementation. While some of these improvements may have also resulted from increases in soil cohesion and interparticle friction, only small differences in failure envelopes were observed with increases in biocementation, suggesting that observed improvements were primarily related to changes in volumetric behaviors. When comparing behaviors at shear strains of less than 3%, representative of strain magnitudes

experienced in cyclic specimens prior to triggering, significant differences in peak shear strengths and stiffnesses were observed. For example, from 0 to 3% shear strain, the peak shear strength of the uncemented specimen was only 17.7 kPa, while the most significantly biocemented specimen (ΔV_s of 93 m/s) achieved a peak shear strength of 72 kPa, an increase of over 300%.

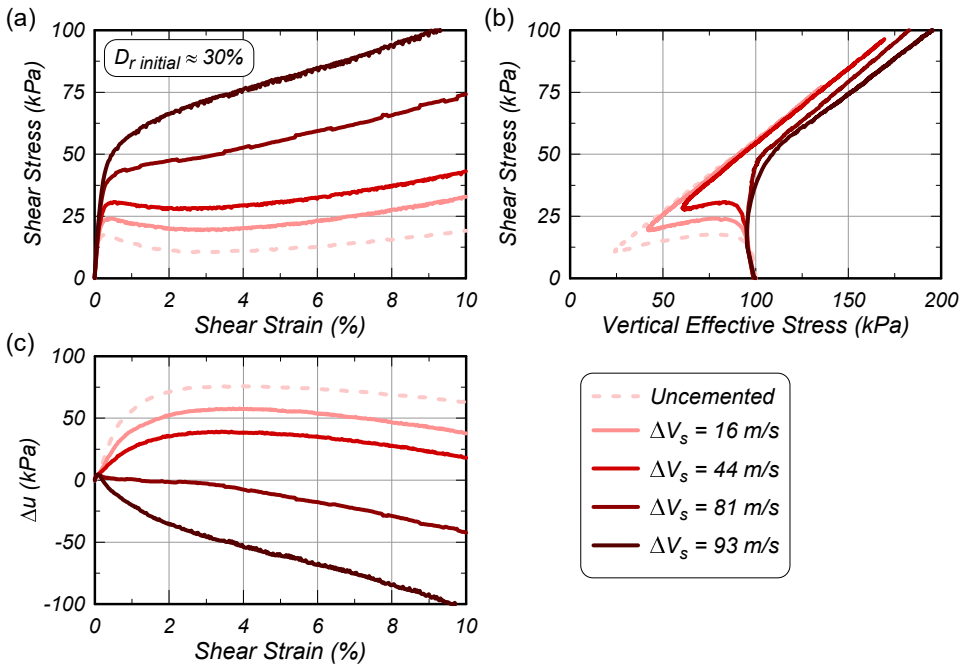

Figure 4.13. Results from undrained monotonic tests on loose ($D_{r\ initial} \approx 30\%$) specimens of varying biocementation levels including plots of (a) shear stresses versus shear strains, (b) shear stresses versus vertical effective stresses, and (c) excess pore water pressures (Δu) versus shear strains.

In order to compare observed undrained monotonic responses to pre-triggering behaviors observed in undrained cyclic tests, the CSR required to achieve 3% SASS in 0.25 cycles (equivalent to "triggering" during undrained monotonic shearing) was determined by taking the peak shear stress observed from 0 to 3% SASS in monotonic tests (**Figure 4.13**) and normalizing this value by the

initial vertical effective stress of 100 kPa. ΔV_s magnitudes resulting in triggering in 0.25 cycles for CSRs applied during cyclic testing were also determined from results presented in **Figure 4.9a**.

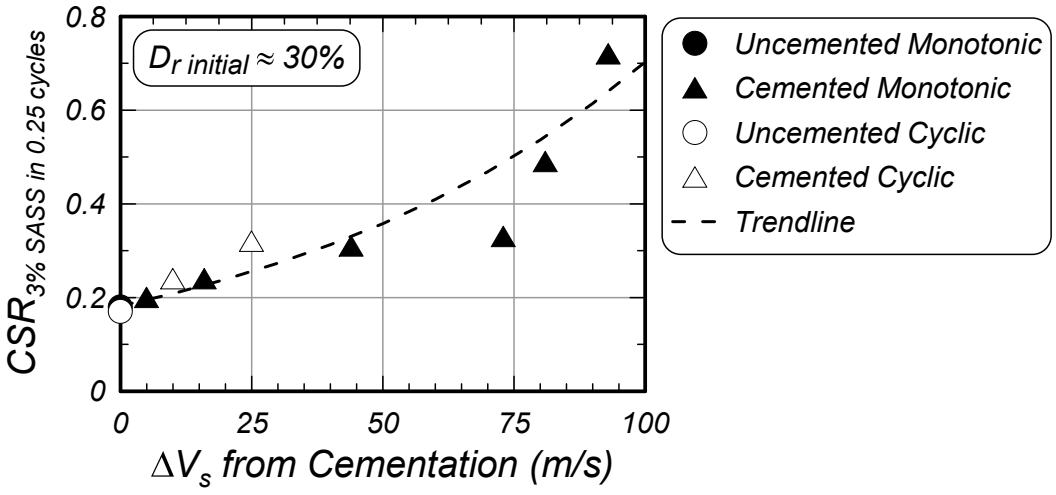

Figure 4.14. Relationships between applied CSRs required to achieve 3% SASS in 0.25 cycles and ΔV_s from cementation for loose ($D_{r\ initial} \approx 30\%$) specimens of varying cementation as determined from both undrained monotonic and cyclic DSS tests.

Figure 4.14 presents CSRs required to achieve 3% SASS in 0.25 cycles determined from both undrained monotonic and cyclic tests versus ΔV_s from cementation for loose specimens of varying biocementation levels. As expected, CSRs required to trigger liquefaction in 0.25 cycles agreed well between both cyclic and monotonic tests, with CSR values increasing from near 0.2 for uncemented loose specimens to near 0.7 for biocemented loose specimens with ΔV_s values near 100 m/s. It should be noted that biocemented cyclic results were only plotted up to a ΔV_s increase of 25 m/s, as applied CSR values exceeding 0.3 were not investigated during cyclic tests. The observed consistency between test results suggests that the liquefaction triggering behavior of

biocemented soils may be further characterized through the strategic combination of monotonic and cyclic undrained tests in future studies.

4.4 Conclusions

A study was completed to evaluate the liquefaction triggering and post-triggering behaviors of lightly biocemented loose sands. Twenty-eight undrained cyclic DSS tests were performed on biocemented Ottawa F-65 sand specimens prepared to loose relative densities, treated to varying light biocementation levels (ΔV_s = 0 to 100 m/s, $CaCO_3$ contents = 0 to 0.93%), and subjected to different loading magnitudes (CSR = 0.1 to 0.3). Thirty-four similar undrained cyclic DSS tests were also performed on uncemented specimens prepared to loose ($D_r \approx 30\%$), medium-dense ($D_r \approx 55\%$), and dense ($D_r \approx 75\%$) relative densities to compare the response of biocemented soils to behavioral improvements achievable through densification. Seven undrained monotonic tests were also performed on biocemented loose specimens to further investigate stress-strain behaviors and observations from cyclic testing. From the results of this study, the following conclusions can be made: (1) the presence of light levels of biocementation can significantly improve the pre-triggering behaviors of loose sands with more limited shear strains observed with increasing r_u and significantly more cycles required to generate excess pore water pressures initially during undrained cyclic loading, (2) light levels of biocementation can dramatically improve the liquefaction resistance of loose sands with the number of cycles required to trigger liquefaction increasing by over 3 orders of magnitude at smaller applied CSRs and higher biocementation levels ($\Delta V_s \approx 100$ m/s), (3) pre-triggering improvements afforded by light biocementation ($\Delta V_s \approx 100$ m/s) exceeded those achievable through soil densification ($D_r \approx 30\%$ to 75%) for all loading

magnitudes considered (CSR = 0.1 to 0.3), (4) pre-triggering behaviors observed for biocemented specimens correlated best with increases in soil V_s rather than $CaCO_3$ contents or increases in D_r from precipitated $CaCO_3$ masses, (5) in stark contrast to pre-triggering behaviors, post-triggering strain accumulation and reconsolidation behaviors were not significantly improved by the presence of light levels of biocementation, with V_s measurements suggesting that small-strain stiffness improvements afforded by light biocementation were largely erased following shearing and reconsolidation events, and (6) undrained monotonic tests demonstrated that light levels of biocementation can result in large increases in shear strengths and stiffnesses through increasingly dilative volumetric tendencies with interpreted cyclic strengths that were consistent with those obtained from undrained cyclic testing. While the obtained results suggest that light levels of biocementation can dramatically improve soil liquefaction triggering resistances, further investigations are needed to provide a more comprehensive understanding of these materials including potential improvements in post-triggering behaviors obtainable at higher cementation levels and the effect of various practical loading scenarios, treatment techniques, and initial soil conditions.

Chapter 5. IMPROVING THE SPATIAL CONTROL OF SOIL BIOCEMENTATION USING INDIGENOUS MICROORGANISMS: COLUMN EXPERIMENTS AND REACTIVE TRANSPORT MODELING

This chapter has been submitted as a journal paper entitled, "Improving the Spatial Control of Soil Biocementation Using Indigenous Microorganisms: Column Experiments and Reactive Transport Modeling" to *Engineering Geology*. The paper was authored by (in-order) Minyong Lee, Michael G. Gomez, Charles M.R. Graddy, Alexandra C.M. San Pablo, Jason T. DeJong, and Douglas C. Nelson.

ABSTRACT

Conventional ground improvement technologies rely heavily on energy-intensive materials and high mechanical energy to improve problematic soils. Microbially-Induced Calcite Precipitation (MICP), or biocementation, instead uses microbial ureolytic activity to mediate $CaCO_3$ precipitation and improve soil engineering properties with the potential for environmental impact reductions. As the technology has matured, challenges have persisted with respect to controlling the distribution of $CaCO_3$ precipitation. Approaches that can modulate the spatial uniformity of biocementation and maximize treatment extent at meter-scale will be critical towards reducing implementation costs and impacts. Although recent experiments have shown that modifications to microbial reaction rates can be used to alter improvement distributions under specific injection conditions, the development of rate controlling treatment strategies and their efficacy across a broader range of reactive transport conditions has not yet been systematically investigated. A study was performed to identify treatment strategies capable of reliably enriching indigenous microorganisms at controlled ureolytic activities and to assess the ability of these techniques to control improvement distributions. Twelve soil column experiments received treatment solutions

containing different nutrient concentrations thereby enriching indigenous ureolytic microorganisms at different activities but with minimal differences in engineering improvements. Reactive transport simulations subsequently investigated relationships between the experimentally achieved ureolytic rates and improvement distributions in 3.67-meter-long columns subjected to varying injection rates, thereby extending the implications of the developed techniques and allowing for comparisons with outcomes from recent meter-scale experiments. Finally, two parameters were proposed to quantitatively capture differences in reactive transport conditions and treatment uniformity and provide new metrics by which treatment outcomes can be compared and field treatment strategies can be designed.

5.1 Introduction

Geotechnical ground improvement is a 6 billion dollar per year industry in the U.S. (DeJong et al. 2010) that has relied almost exclusively on energy-intensive materials and high mechanical energy to improve problematic soils (Karol 2003). Over the past two decades, researchers have shown the transformative potential of bio-mediated processes to improve soil engineering behaviors while reducing environmental impacts relative to conventional soil improvement methods (Seagren & Aydilek 2010; DeJong et al. 2013, 2022; DeJong & Kavazanjian 2019; Sharma et al. 2021). One such process, Microbially-induced Calcite Precipitation (MICP), uses microbial urea hydrolysis (ureolysis) to induce the precipitation of calcium carbonate ($CaCO_3$) minerals on soil particle surfaces and contacts (Ferris et al. 1997; Stocks-Fischer et al. 1999; DeJong et al. 2006). The biocementation process can improve the strength and stiffness of soils while also reducing soil porosity and hydraulic conductivity (Montoya & DeJong 2015; Feng & Montoya 2016; Gomez et al. 2018a). Potential applications include the modification of subsurface groundwater flow

(Cuthbert et al. 2013; Tobler et al. 2014; Minto et al. 2016), erosion and scour prevention (Jiang & Soga 2017; Montoya et al. 2018; Clarà Saracho et al. 2020), repair of damaged concrete, marble, and limestone materials (Ramakrishnan et al. 2005; Tziviloglou et al. 2006; Minto et al. 2018), immobilization of divalent groundwater contaminants (Fujita et al. 2008; Kumari et al. 2016; Jiang et al. 2019), improved petroleum extraction and recovery (Ferris et al. 1997; Phillips et al. 2018), and mitigation of earthquake-induced soil liquefaction (Montoya et al. 2013; Xiao et al. 2018; Darby et al. 2019; Zamani & Montoya 2019; Riveros & Sadrekarimi 2020a; Lee et al. 2022). Soil improvement applications for biocementation have been increasingly explored in recent years through field demonstrations (Gomez et al. 2015; Phillips et al. 2016; Saneiyan et al. 2019; Terzis et al. 2020; Ghasemi & Montoya 2020) with notable advances in the characterization of the engineering response of biocemented materials (Darby et al. 2019; Nafisi et al. 2020; Riveros & Sadrekarimi 2020b; Lee et al. 2022), process reactive transport numerical modeling (Nassar et al. 2018; Minto et al. 2019), and the use of indigenous soil microorganisms (Fujita et al. 2000; Burbank et al. 2011; Gomez et al. 2016; San Pablo et al. 2020). The process holds significant promise for practical applications; however, challenges have persisted with respect to controlling the spatial distribution and uniformity of MICP at meter-scale (Mujah et al. 2017; DeJong et al. 2022). Treatment extent limitations can be overcome by installing wells at shorter well-to-well spacings, however, such constraints will significantly increase economic and environmental impacts and undermine process advantages. Identification of reliable techniques that can improve the spatial control of the biocementation process may yield transformative benefits once applied at field-scale.

Urea hydrolysis during MICP is most commonly mediated by nonnative ureolytic bacteria such as *Sporosarcina pasteurii* (*S. pasteurii*), which can be introduced into soils at high cell densities prior to cementation injections. Recently, researchers have shown that the biocementation process can be mediated by indigenous ureolytic microorganisms existing in natural geomaterials, including alluvial and marine sands, clays, and groundwater samples, thereby eliminating the need for *ex situ* cell culturing and injection (Fujita et al. 2000, 2008; Burbank et al. 2011, 2013; Tobler et al. 2011; Gat et al. 2014, 2016; Gomez et al. 2014, 2016, 2018b; Lee et al. 2019; Graddy et al. 2018, 2021; Cardoso et al. 2020; Islam et al. 2020; San Pablo et al. 2020; Wang et al. 2020; Safdar et al. 2021). These studies developed stimulation solutions that impose selective environmental conditions, including alkaline solution pH and high ammonium concentrations, to promote enrichment of ureolytic microorganisms over other non-ureolytic microorganisms which may compete for supplied nutrients (Gomez et al. 2018b). In many of these studies, the rapid accumulation of high bulk ureolytic activity was paramount in stimulation solution design and taken to be indicative of more successful ureolytic enrichment. Although high ureolytic activities may be characteristic of enriched soils that can more rapidly generate biocementation, high urea hydrolysis rates can also dramatically reduce biocementation spatial uniformity when treatment injections are transported at relatively slow velocities (Zambare et al. 2019, Montoya et al. 2021). Such conditions can increase urea hydrolysis and related precipitation reactions during injections and promote greater $CaCO_3$ precipitation near injection sources with more limited transport of reactants to further distances (Gomez et al. 2019; San Pablo et al. 2020). Given the importance of microbial urea hydrolysis rates on reactive transport conditions present during MICP, it is clear that treatment strategies that can reliably control achieved urea hydrolysis rates may provide new

opportunities to control the spatial distribution of biocementation for different field-scale treatment scenarios.

Few studies have considered the interplay between ureolytic reaction rates and solution transport rates and their combined impacts on biocementation spatial uniformity (Zambare et al. 2019). In addition, almost all past studies have relied on the mediation of the MICP process using augmented *S. pasteurii* cells. Recent meter-scale experiments suggest that achieving uniform distributions of augmented cell densities may be exceedingly difficult over large injection distances, even in controlled laboratory experiments, due to cell attachment and filtration by porous media, which act to concentrate augmented cells near injection sources (Ginn et al. 2002; Gomez et al. 2016, 2019; San Pablo et al. 2020). In contrast, the stimulation of indigenous ureolytic microorganisms may eliminate these cell transport limitations by enriching microorganisms already distributed throughout soil pore spaces (Graddy et al. 2018) with the potential for significant economic and environmental benefits relative to augmentation (Gomez et al. 2016; Raymond et al. 2022). Despite these practical advantages, the ability to regulate achieved stimulated urea hydrolysis rates through treatment solution design has remained poorly understood (San Pablo et al. 2020). Control of bulk ureolytic activity may be difficult in stimulated soils as such materials contain diverse microbial communities where even small changes in solution composition can shift microbial populations dramatically (Graddy et al. 2018, 2021). San Pablo et al. (2020) first demonstrated that changes in applied yeast extract (YE) concentrations could be used to alter reactive transport conditions thereby controlling the spatial distribution of biocementation realized in two 3.67-meter-long column experiments treated using identical flow rates. In these experiments, lower supplied YE concentrations reduced stimulated urea hydrolysis rates and enabled improved

cementation uniformity. While promising, the ability of ureolytic rates to be reliably and systematically controlled through variations in supplied nutrient concentrations, the potential consequences of such changes on achieved engineering improvements, and the collective impacts of simultaneous changes in ureolytic reaction rates and injection rates on improvement distributions expected at meter-scale remained unexplored.

In this study, twelve centimeter-scale soil column experiments were employed to systematically investigate the ability of novel treatment strategies to enrich natural soils for a broad spectrum of ureolytic rates capable of improving the spatial control of ureolytic biocementation under different field-scale transport conditions. In all experiments, applied stimulation and cementation solutions were modified to contain varying YE concentrations between 0 and 0.2 g/L and resulting effects on stimulated ureolytic rates, soil shear wave velocities (V_s), and soil $CaCO_3$ contents were investigated. Leveraging these experimental insights, a one-dimensional reactive transport model was used to further explore the implications of the achieved ureolytic rates on the distribution of biocementation expected in 3.67-meter-long soil column models similar to those physically tested by San Pablo et al. (2020) but subjected to different injection conditions. Relationships between stimulated ureolytic rates, injection rates, and biocementation spatial uniformity and extent were investigated and compared to previous observations by San Pablo et al. (2020) to provide a more comprehensive understanding of the ability of the investigated enrichment techniques to address practical field treatment challenges. Two new parameters were also explored which may allow for improved comparisons of reactive transport conditions and treatment uniformity between studies.

5.2 Materials and Methods

5.2.1 *Soil Materials*

All soil column experiments contained a poorly-graded Concrete Sand material characterized extensively in past biocementation experiments (Gomez et al. 2014, 2016, 2018b; Lee et al. 2019). The soil was obtained from an alluvial deposit in Woodland, CA and had a D_{10} of 0.23 mm, D_{30} of 0.54 mm, D_{60} of 1.54 mm, fines content of 1.1% by mass, and an e_{min} and e_{max} of 0.35 and 0.60, respectively. The USCS classification for this soil was SP following ASTM D2487-10 (ASTM, 2017). Previous microbiological characterizations of Concrete Sand (Graddy et al. 2018, 2021) have indicated that significant microbial diversity exists in this parent soil, with nearly 20 different strains of *Sporosarcina* identified following sequential enrichment injections.

5.2.2 *Centimeter-scale Soil Column Specimens*

Centimeter-scale soil column specimens were prepared in 15.2 cm high, 7.6 cm inner diameter acrylic cylinders that included fittings for bender element V_s sensors and aqueous sampling ports at mid-height (**Supplemental Figure 1** in Appendix A). Soil materials were placed in columns in six lifts using moist tamping to obtain a relative density around 55%. All columns had initial porosities of 35% ± 1% and the pore volume (PV) of each column was approximately 250 mL. Spring-loaded reaction frames were used to apply a total vertical stress of 100 kPa to all columns that was maintained throughout the treatment process. Following preparation, all columns were saturated with deionized water and remained untreated for 24 hours. Four soil columns were tested in experiment set A and eight soil columns were tested in experiment set B.

5.2.3 *Treatment Injections*

Centimeter-scale soil columns received treatments in three phases: (i) stimulation, (ii) carbonate flushing, and (iii) cementation. For all treatments, injection volumes of 375 mL (≈ 1.5 PV) were applied at a flow rate of 2.4 PV/hr (10 mL/min for a total injection time of 37.5 minutes). All columns received stimulation solutions once daily for the first 6 days. Stimulation solution compositions followed previous techniques shown to effectively select for ureolytic microorganisms (Gomez et al. 2018b) but included large reductions in supplied urea (350 mM to 50 mM) shown to have no significant effects on stimulation efficacy (San Pablo et al. 2020). All stimulation solutions were pH-adjusted to 9.0 prior to injection and contained 50 mM urea, 42.5 mM sodium acetate, 100 mM ammonium chloride, and varying YE concentrations intended to alter obtained stimulated ureolytic activities. In experiment set A, three columns received daily stimulation treatments with either 0.01, 0.07, or 0.2 g/L YE. A fourth column received alternating daily injections with either 0.07 g/L YE (odd treatments) or 0 g/L YE (even treatments) to explore the effect of alternating nutritionally complete and incomplete treatments on ureolytic activity. In experiment set B, four columns received daily injections with either 0.02, 0.04, 0.08, or 0.2 g/L YE and four columns received alternating daily injections with identical YE concentrations and no YE applied on alternating days. Following six stimulation treatments and immediately before the first cementation injection, all columns received a carbonate "flush" solution that was identical to the stimulation solution but was not pH-adjusted. This injection was intended to remove high aqueous carbonate concentrations existing within soil columns following stimulation thereby preventing immediate $CaCO_3$ precipitation from occurring during the introduction of high calcium concentrations in the first cementation injection (Gomez et al. 2019).

Subsequently, all columns in experiment set A received 10 cementation treatments and all columns in experiment set B received 9 cementation treatments intended to obtain post-treatment soil $CaCO_3$ contents near 5% by mass (Gomez & DeJong 2017). Cementation solutions were similar in composition to stimulation solutions but contained calcium chloride and higher urea concentrations as well as reduced initial pH and ammonium concentrations. In experiment set A, cementation solutions were applied once daily and contained 350 mM urea and 250 mM calcium chloride. In experiment set B, cementation solutions were applied once every 48 hours to allow for reaction completion to occur in all columns including those with slower ureolytic rates. Experiment set B solutions contained 250 mM urea and calcium chloride, based on recent experiments that showed urea concentrations could be reduced to be equimolar with calcium chloride without affecting precipitation efficiency (San Pablo et al. 2022). In both experiment sets, the YE additions during cementation treatments were identical to those applied during stimulation treatments and continued to alternate in columns receiving nutritive and non-nutritive treatments. Following cementation, rinse solutions that were pH-adjusted to 9.0 and contained 500 mM calcium chloride were applied to all columns to remove soluble treatment by-products (Lee et al. 2019). A summary of all stimulation and cementation solutions for both sets of experiments is provided in **Supplemental Table 5.1** (in Appendix A).

5.2.4 *Aqueous Sampling*

Solution samples (≈ 2 mL) were collected from column mid-height sampling ports using sterile syringes and needles before and after each treatment injection and for select injections at various times during solution retention periods to monitor ureolytic rates. In experiment set A, all columns were sampled 2, 4, 8, and 24 hours after applying the 2^{nd}, 4^{th}, and 6^{th} stimulation treatment and the

3rd, 6th, 8th, and 10th cementation treatment. In experiment set B, all columns were sampled 2, 4, 8, 24, and 48 hours after applying the 2nd and 6th stimulation treatment and the 1st, 5th, and 9th cementation treatment. All samples were stored at -20°C immediately following collection and remained frozen until analysis.

5.2.5 *Aqueous Measurements*

Solution pH measurements were completed using a semi-micro pH electrode and meter system (Fisher Scientific, Waltham, MA) that was calibrated daily using a three-point buffer sequence (4.01, 7.00, 10.01) and had ± 0.01 pH unit accuracy. Solution urea measurements were completed using a colorimetric urea assay similar to Knorst et al. (1997) wherein a colorimetric reagent consisting of 4% (w/v) p-Dimethylaminobenzaldehyde and 4% (v/v) HCl in 96% ethanol was added to dilute sample volumes. Absorbance values were measured at 422 nm using a microplate spectrophotometer.

5.2.6 *Shear Wave Velocity Measurements*

Shear wave velocity measurements were obtained for experiment set B soil columns using piezo-ceramic bender element sensor pairs oriented perpendicular to columns at mid-height. Bender elements were assembled following procedures similar to Montoya et al. (2012) and were isolated from the highly conductive aqueous environment using a multi-step Hysol E-90FL epoxy (Henkel Corp., Düsseldorf, Germany) and electronics wax coating process (Gomez et al. 2016). All transmitting bender elements were excited using a 24-volt 100 Hz square wave generated by a signal generator system (National Instruments, Austin, TX) and all received signals were measured

and recorded with an oscilloscope (Pico Technology, Tyler, TX) at a sampling frequency of 1 MHz. Shear wave velocity measurements were completed once daily before injections and values were determined from visual interpretation of S-wave arrivals and known sensor spacings.

5.2.7 *Soil Sampling and $CaCO_3$ Content Measurements*

Following all rinse injections, soil columns were drained, extruded using a hydraulic jack, and oven-dried at 110°C for at least 48 hours. Soil columns were subsampled into four discrete sections at varying distances from the injection port (0 to 38 mm, 38 to 76 mm, 76 to 114 mm, and 114 to 152 mm) that were homogenized to yield representative subsamples for $CaCO_3$ content measurements. $CaCO_3$ contents were quantified in accordance with ASTM D4373 (ASTM, 2014) by reacting $CaCO_3$ in soil samples with 1 M hydrochloric acid to generate CO_2 gas and a corresponding increase in test chamber pressure. Relationships between chamber pressure and known reagent-grade $CaCO_3$ masses were used to determine sample $CaCO_3$ contents. A minimum of three $CaCO_3$ content measurements were completed per column section and all section values were averaged to determine average $CaCO_3$ contents for columns.

5.2.8 *Previous Meter-scale Soil Column Experiments*

Results from past meter-scale experiments by San Pablo et al. (2020) are discussed to compare results obtained from reactive transport simulations performed in this study to past observations from physical experiments. Although more details regarding these experiments can be found in San Pablo et al. (2020), a brief summary of relevant details is provided here. Two 3.67-meter-long soil column experiments containing Concrete Sand were treated to achieve relatively low and high

ureolytic reaction rates to examine the effect of microbial activity on achieved cementation magnitudes and uniformity. All columns received 6 stimulation and 9 cementation injections that were 1.5 PV in volume and were applied at a constant injection rate (0.48 PV/hr). Prior to all injections, passive tracer tests were performed to determine column advective-dispersive transport properties. Passive tracer testing involved the injection of 76 L (1.5 PV) of a 15 mM NaBr solution followed by 76 L (1.5 PV) of deionized water with samples collected at the column outlet. Bromide ion (Br^-) concentrations in samples were assessed using solution conductivity measurements and breakthrough curves were determined. Ureolytic rates were monitored during the 9^{th} cementation treatment using samples obtained from four ports along the length of the columns. Soil $CaCO_3$ contents were also quantified along column lengths after treatments.

5.2.9 *PHREEQC Modeling*

A one-dimensional advective-dispersive soil column transport model was developed using the geochemical software PHREEQC (Parkhurst & Appelo 2013) to further explore the implications of the ureolytic rates achieved in the centimeter-scale soil columns on biocementation magnitudes and distributions expected at meter-scale. Simulations allowed for changes in urea hydrolysis rates, injection rates, and their collective impacts on biocementation spatial distributions to be subsequently explored in the context of meter-scale experiments to expand understandings beyond the specific conditions investigated by San Pablo et al. (2020). Simulations investigated treatment injections applied to a column model that was identical to that tested by San Pablo et al. (2020) and was 3.67 meters in length, had a square cross-sectional area of 0.04 m^2, and consisted of 163 cells (length of 0.022 meters each). A passive tracer injection sequence identical to the physical experiments was simulated using the PHREEQC soil column model and the model's mobile

porosity (n) and longitudinal dispersivity (α_L) values were calibrated to match experimental passive tracer data. Although each column had a physical pore volume (PV) of 50 L, an apparent PV of 37.5 L was used in the model to match passive tracer data due to the presence of air bubbles. All models had a hydraulic conductivity of 2.2 x 10^{-4} m/s following experimental measurements.

In all PHREEQC simulations, ureolysis was modeled as a kinetic reaction using the Michaelis-Menten ureolytic kinetic expression presented in **Equation (5.1)** wherein K_m is the half-saturation coefficient in [mM urea] and bulk V_{max} is the maximal velocity of bulk solution in [mM urea hour^{-1}]. Although actual K_m values vary between stimulated ureolytic strains, the value reported by Graddy et al. (2018) for *Sporosarcina pasteurii* (ATCC 11859) (K_m = 305 mM urea) well approximated experimentally observed urea degradation trends and was used in all simulations. By varying the bulk V_{max}, the ureolytic kinetic model was calibrated to match experimentally observed urea degradation trends from centimeter-scale soil columns. In all models, $CaCO_3$ precipitation was treated as an equilibrium reaction (**Equation (5.2)**) following recent experiments that demonstrated that $CaCO_3$ precipitation occurs exceedingly fast once CO_3^{2-} ions are produced from microbial ureolysis (Burdalski & Gomez 2020). In all simulations, columns received a single 76 L (1.5 PV) injection of a cementation solution that was identical to that used in both experiment set B and the physical experiments by San Pablo et al. 2020 (250 mM calcium chloride, 250 mM urea, 12.5 mM NH_4Cl, and 42.5 mM sodium acetate). In order to examine changes in reactive transport conditions, injections were applied at varying injection rates ranging from 0.06 PV/hr to 1.8 PV/hr (50 to 1500 mL/min) and different ureolytic rates were considered, which encompassed variations observed in centimeter-scale experiments. Models were calibrated to capture three different ureolytic rates representative of the 0.01 g/L YE daily, 0.07 g/L YE alternating, and 0.2

g/L YE daily columns from experiment set A during the 8th cementation injection. In all simulations, urea hydrolysis activities were assumed to be spatially uniform along columns with length following data from San Pablo et al. (2020) which indicated that relatively similar stimulated ureolytic activities could be obtained along meter-scale injection pathways with no consistent bias in activities towards the injection or production locations.

$$\frac{d[Urea]}{dt} = \left(\frac{Bulk\ V_{\max cell}[Urea]}{K_m + [Urea]}\right) \qquad \textbf{[Equation 5.1]}$$

$$Ca^{2+} + CO_3^{2-} \rightarrow CaCO_{3_{solid}}\ (K_{sp} = 10^{-8.48}) \qquad \textbf{[Equation 5.2]}$$

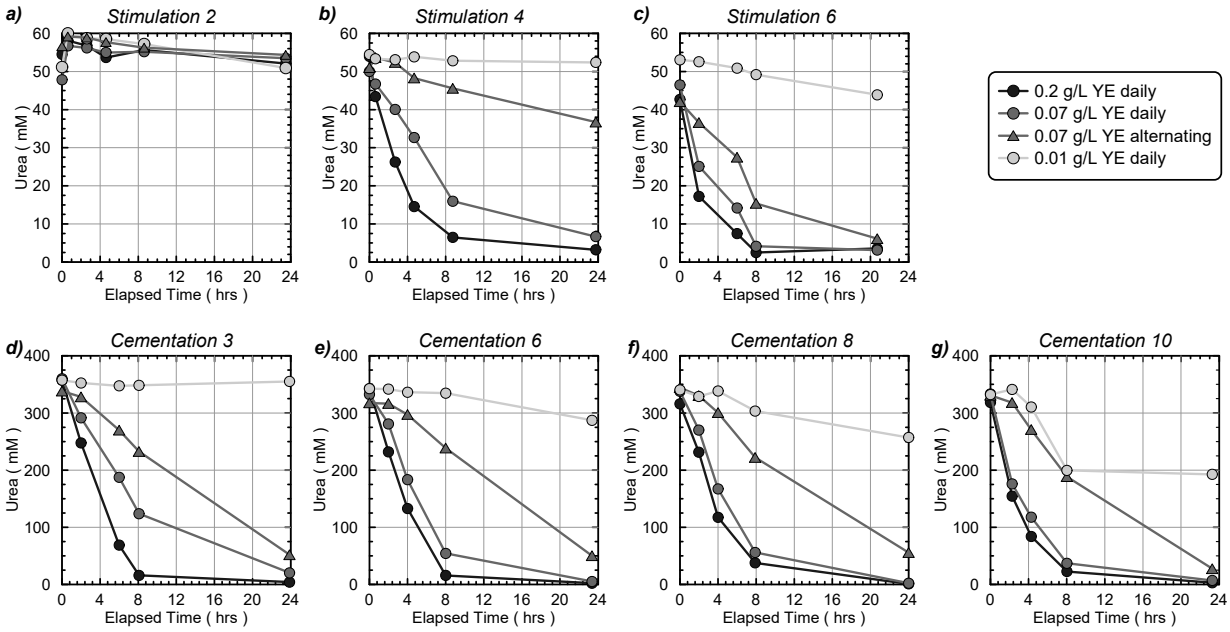

Figure 5.1. Solution urea concentrations (mM) in time during the **(a)** 2nd, **(b)** 4th, and **(c)** 6th stimulation injection and the **(d)** 3rd, **(e)** 6th, **(f)** 8th, and **(g)** 10th cementation injection for all set A columns. Urea concentrations supplied in injected solutions were 50 mM during stimulation and 350 mM during cementation.

5.3 Results and Discussion

5.3.1 *Set A Centimeter-scale Soil Column Experiments*

Figure 5.1 presents measurements of solution urea concentrations in time for all centimeter-scale soil columns during experiment set A for three stimulation injections and four cementation injections. No significant urea hydrolysis activity was observed in any column during the second stimulation injection (**Figure 5.1a**). As stimulation injections proceeded, however, increases in urea hydrolysis activity were observed with all columns except the 0.01 g/L YE daily column degrading more than ≈ 20 mM and ≈ 40 mM urea during stimulation injections 4 and 6, respectively (**Figures 5.1b, 5.1c**). Increasing ureolytic rates were expected during successive injections of a selective growth medium, which stimulated the growth of ureolytic bacteria and progressively biased microbial communities towards increased ureolytic activity. During the cementation phase, solution urea concentrations increased from 50 mM to 350 mM and more significant differences in rates were observed. During cementation injection 3, the 0.2 g/L YE daily, 0.07 g/L YE daily, and the 0.07 g/L YE alternating columns hydrolyzed approximately 341 mM, 236 mM, and 106 mM urea, respectively, after only 8 hours. However, no detectable urea degradation was observed in the 0.01 g/L YE daily column after the full 24-hour retention period (**Figure 5.1d**). After cementation injection 6, pseudo-steady urea hydrolysis rates were observed in all columns except the 0.01 g/L YE daily column (**Figures 5.1e, 5.1f, 5.1g)**, where urea hydrolysis rates continued to increase with further injections but remained significantly lower than other columns. When comparing urea hydrolysis rates, increases in ureolytic activity consistently corresponded to increases in applied YE concentrations (**Figure 5.1b to 5.1g**) with the alternating 0.07 g/L YE column also achieving notable rate reductions when compared to the similar 0.07 g/L YE daily column.

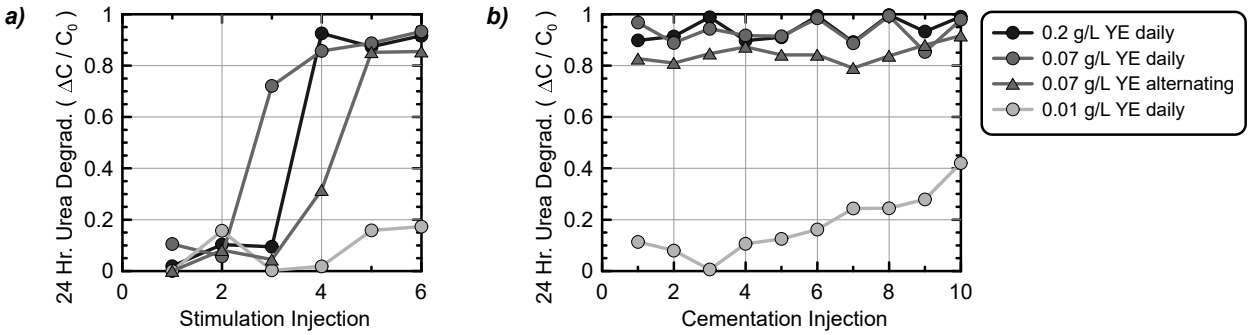

Figure 5.2. Normalized urea degradation ($\Delta C/C_o$) observed after 24-hour injection and retention periods during all **(a)** stimulation and **(b)** cementation injections in set A columns.

Figure 5.2 presents normalized urea degradation ($\Delta C/C_0$) observed in all set A columns during the 24-hour injection and retention periods for all treatment injections. Normalized urea degradation was calculated by dividing the concentration of urea hydrolyzed during treatment periods (ΔC) by the initial urea concentration (C_0). Limited urea degradation was observed in all columns until stimulation injection 3, during which 75% of the injected urea concentration was hydrolyzed in the 0.07 g/L YE daily column (**Figure 5.2a)**. The appearance of significant urea hydrolysis in this column before the 0.2 g/L YE daily column was unexpected and suggested that either higher YE transiently favored certain non-ureolytic subgroups (i.e., protein-degrading clostridia) or that there was some variability in initial microbial populations between columns. During stimulation injection 4, urea degradation magnitudes corresponded to applied YE concentrations with approximately 95%, 85%, 30%, and 2% of the injected urea concentration hydrolyzed after 24 hours in the 0.2 g/L YE daily, 0.07 g/L YE daily, 0.07 g/L YE alternating, and 0.01 g/L YE daily columns, respectively. After 5 stimulation treatments, between 85% and 90% of the injected urea was hydrolyzed after 24 hours in all columns except the 0.01 g/L YE daily column which achieved only 17% degradation. Urea hydrolysis activity continued to increase in the 0.01 g/L YE daily column with additional cementation injections with nearly 45% of the injected urea concentration

hydrolyzed during the last cementation injection (**Figure 5.2b**). Bulk V_{max} values were determined by fitting the Michaelis-Menten ureolytic kinetic expression (**Equation (5.1)**) to observed urea degradation trends (**Supplemental Figure S5.2**). Bulk V_{max} values varied between 3 and 89 mM/hr during stimulation and increased to values between 3 and 134 mM/hr during cementation. Despite similar 24-hour cumulative urea degradation in the 0.2 g/L and 0.07 g/L YE daily columns during all cementation injections (**Figure 5.2b**), bulk V_{max} values continued to increase during cementation suggesting ongoing enrichment for ureolysis. In the 0.07 g/L YE alternating column, bulk V_{max} values instead remained relatively constant during cementation likely due to the absence of nutrients included in alternate injections, which are speculated to maintain near constant ureolytic cell densities. In the 0.01 g/L YE daily column, detectable increases in bulk V_{max} values occurred after cementation injection 3; however, all bulk V_{max} values remained less than 12.5 mM/hr.

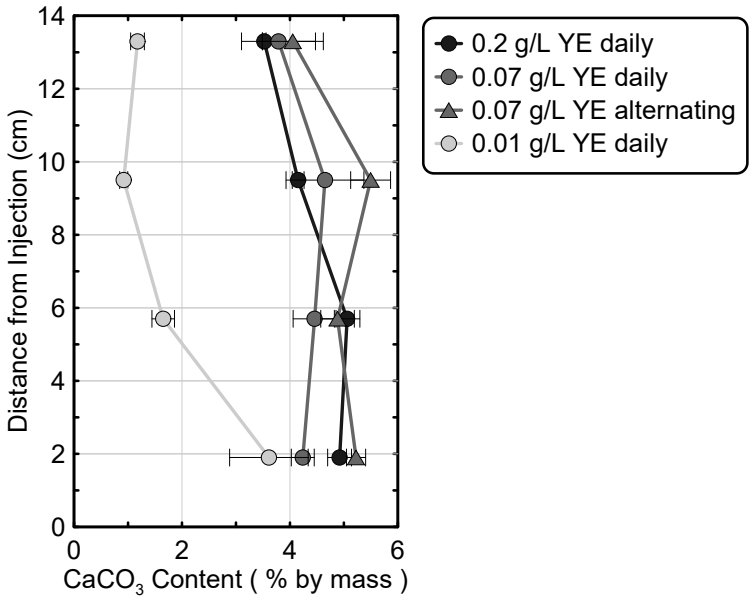

Figure 5.3. Soil $CaCO_3$ contents versus distance from injection location for all experiment set A columns. Provided error bars indicate ± one standard deviation for all measurements.

Following cementation, $CaCO_3$ content measurements were performed for all columns. **Figure 5.3** presents measured soil $CaCO_3$ contents along column lengths and **Supplemental Table 5.2** provides all $CaCO_3$ content measurements for sections as well as average $CaCO_3$ contents for entire columns. As shown, the 0.2 g/L YE daily column and both 0.07 g/L YE columns achieved similar $CaCO_3$ content distributions and average $CaCO_3$ contents between 4.3% and 4.9% by mass. Similar $CaCO_3$ contents between these columns were consistent with the comparable urea degradation observed during retention periods (**Figure 5.2b**). All three columns had small reductions in $CaCO_3$ contents with distance from the injection location, however, attributed to minor precipitation reactions occurring during injections at the solution mixing interface. In the 0.01 g/L YE daily column, significantly lower $CaCO_3$ contents were observed (average $CaCO_3$ = 1.8% by mass) due to more limited urea degradation during cementation injections. The $CaCO_3$ content gradient along the length of the 0.01 g/L YE daily column was also more pronounced than in other columns, suggesting that higher ureolytic activity may have localized near the injection source. Although a significant cementation gradient was observed in the column with the lowest ureolytic rate, it was hypothesized that $CaCO_3$ content magnitudes comparable to other columns could have been achieved if residence periods had been extended to allow for full utilization of the supplied urea and calcium concentrations. Moving forward, if lower ureolytic rates were to be employed to achieve greater cementation uniformity, it was anticipated that post-injection retention periods would need to be extended accordingly.

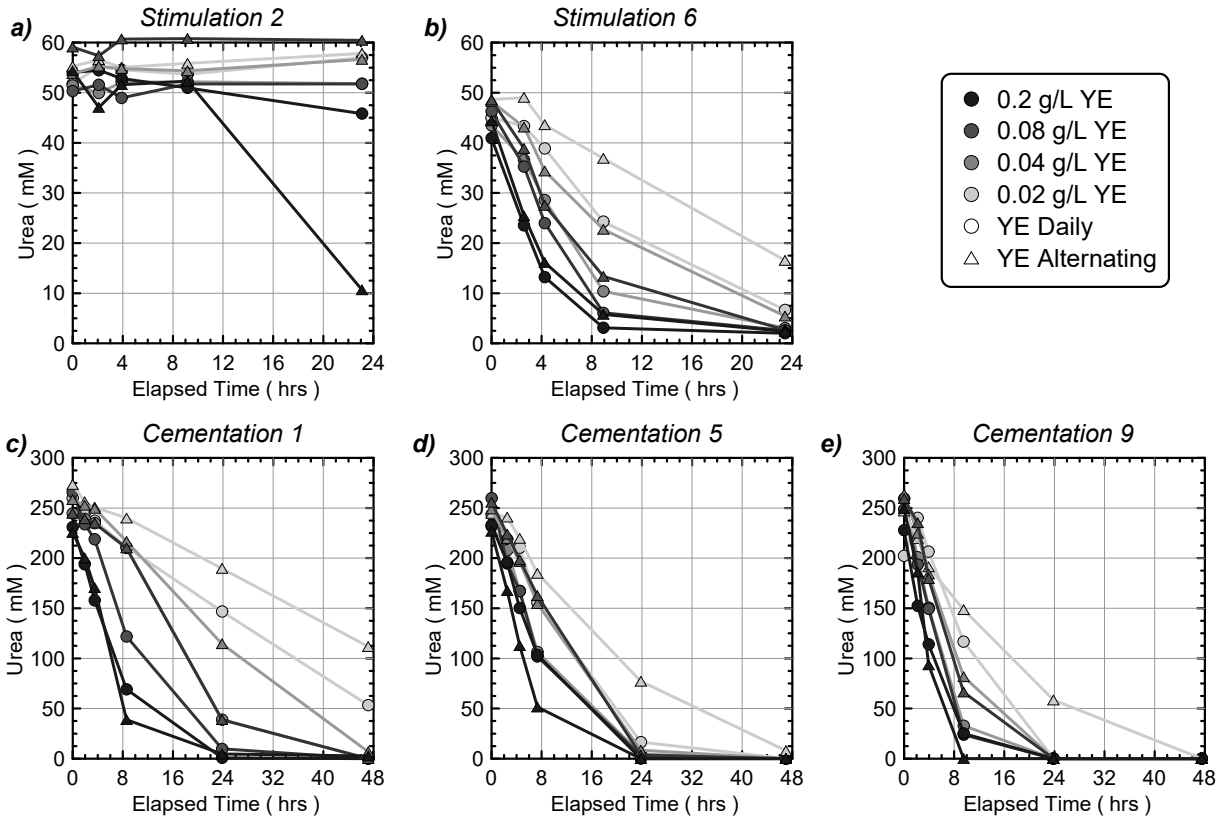

Figure 5.4. Solution urea concentrations (mM) in time during the **(a)** 2nd and **(b)** 6th stimulation injection and the **(c)** 1st, **(d)** 5th, and **(e)** 9th cementation injection for all set B columns. Urea concentrations provided in injected solutions were 50 mM during stimulation and 250 mM during cementation.

5.3.2 *Set B Centimeter-scale Soil Column Experiments*

Figure 5.4 presents measurements of solution urea concentrations in time for all centimeter-scale soil columns during experiment set B for two stimulation injections and three cementation injections. In order to allow columns with lower ureolytic rates to achieve greater reaction completion during residence periods, cementation injection retention periods were extended from 24 hours (as was used in set A) to 48 hours; however, stimulation injections were still applied once every 24 hours. During stimulation injection 2, almost no urea degradation was observed with the

exception of the 0.2 g/L YE daily and alternating columns, which hydrolyzed approximately 8 and 44 mM urea, respectively (**Figure 5.4a**). Significant urea hydrolysis activity was observed in all columns during stimulation injection 6, however, with increases in ureolytic rates reliably consistently corresponding to increases in supplied YE concentrations and YE treatment frequencies. At the end of stimulation, both 0.2 g/L YE columns achieved similar ureolytic activities with almost all urea hydrolyzed within 9 hours (**Figure 5.4b**). In columns receiving lower YE concentrations, a broader range of ureolytic rates were achieved with significant differences in rates observed between columns receiving alternating and daily YE injections. During cementation injections, ureolytic rates continued to accelerate in all columns (**Figure 5.4c to 5.4e)** with rates becoming more similar in all higher YE columns (YE $\geq$ 0.04 g/L) during and after cementation injections 5. Interestingly, when comparing columns that received similar total masses of YE on a differing schedule (i.e., 0.04 g/L YE daily vs. 0.08 g/L YE alternating, 0.02 g/L YE daily vs. 0.04 g/L YE alternating), nearly identical ureolytic rates were observed with slightly higher rates generally observed in the column receiving alternating higher YE injections.

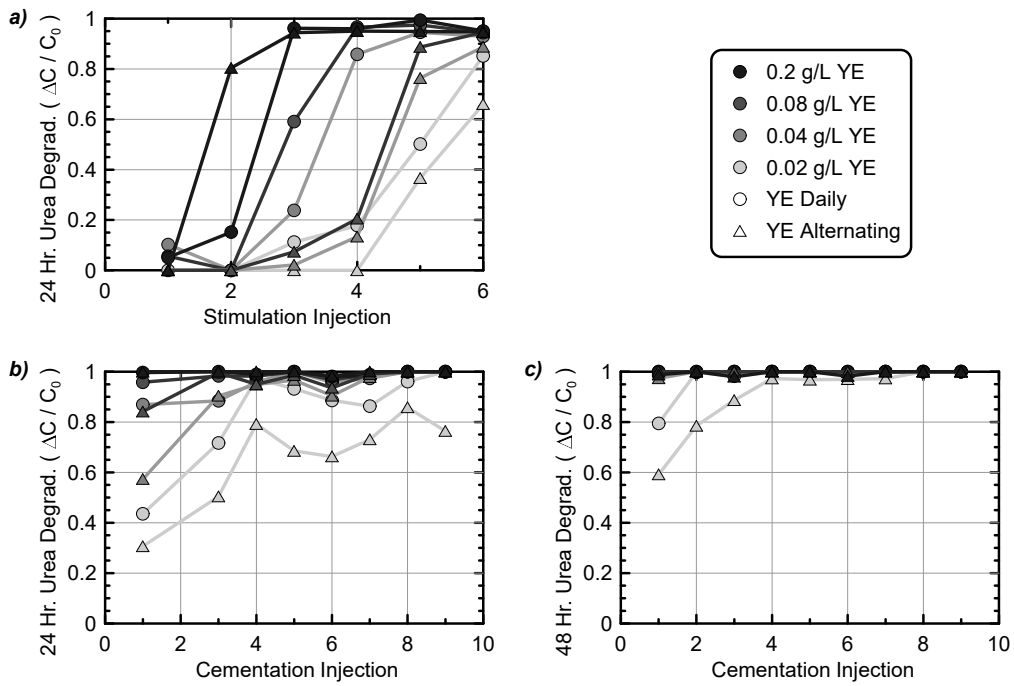

Figure 5.5. Normalized urea degradation ($\Delta C/C_o$) observed 24-hours after all **(a)** stimulation and **(b)** cementation injections and 48-hours after all **(c)** cementation injections in set B columns.

Figure 5.5 presents normalized urea degradation ($\Delta C/C_o$) observed 24-hours after stimulation and cementation injections and 48-hours after cementation injections. No significant urea degradation was detected in any column until stimulation injection 2, wherein both 0.2 g/L YE columns had measurable urea degradation (**Figure 5.5a**). By stimulation injection 5, significant urea degradation was detected in all columns. Immediately following the transition to cementation, similar 24-hour degradation was maintained in all higher YE columns (YE ≥ 0.08 g/L); however, in lower YE columns (0.04 g/L YE and 0.02 g/L YE), significant reductions in 24-hour normalized urea degradation were observed (**Figure 5.5b**). In all columns receiving at least 0.08 g/L YE, near full urea degradation was achieved 24 hours after all cementation injections; however, in the 0.02 and 0.04 g/L YE columns, 24-hour urea degradation varied between 30% and 100% but increased with further injections. Despite large differences in 24-hour degradation, almost all columns

achieved full degradation of the supplied urea after the longer 48-hour retention period, with the exception of the 0.02 g/L YE daily and alternating columns, which achieved near full degradation only for treatments after cementation injection 2 and 4, respectively (**Figure 5.5c**). Bulk V_{max} values were determined for all columns from urea degradation trends (**Supplemental Figure 5.3**) and increased from between 0 and 20 mM/hr during stimulation injection 2 to values ranging between 13 and 76 mM/hr during stimulation injection 6. Immediately following the transition to cementation, bulk V_{max} values decreased in almost all columns, however, with values then progressively increasing with further cementation injections to between 25 and 89 mM/hr during cementation injection 10. The reduction in bulk V_{max} values immediately after the transition to cementation was unexpected due to the presence of higher urea concentrations, which would be expected to increase ureolytic rates following Michaelis-Menten kinetics. This outcome was similar to observations from previous studies (Gomez et al. 2018b), however, and may have resulted from a variety of differences including (1) cell elution from the additional flush injection applied immediately prior to cementation, (2) large changes in solution composition and ionic strength which may have increased cell osmotic stress, and (3) the initiation of $CaCO_3$ precipitation which may have acted to encapsulate cells and reduce bulk ureolytic activity (van Paassen 2009; Cuthbert et al. 2012).

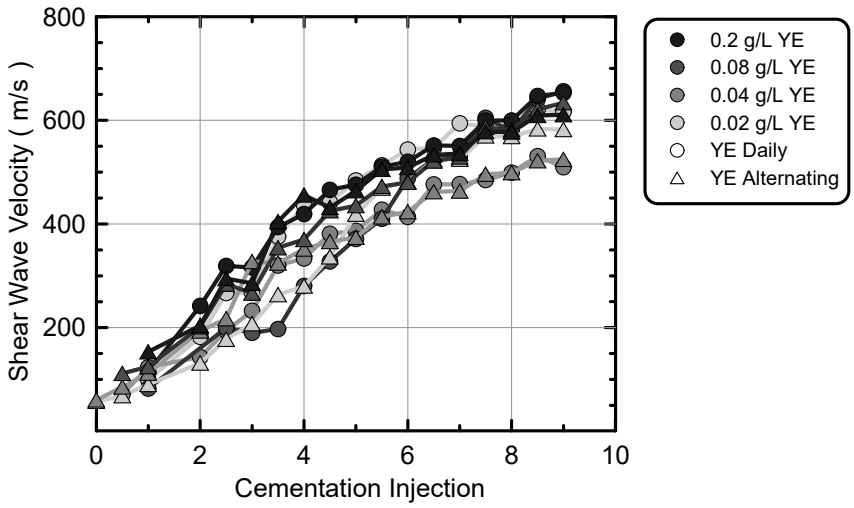

Figure 5.6. Soil column shear wave velocities (V_s) measured immediately before all injections during experiment set B at the mid-height of columns.

Figure 5.6 presents soil shear wave velocities measured at mid-depth within soil columns during cementation injections. As shown, all V_s values were near 80 m/s immediately prior to cementation and increased in a near-linear manner to final V_s values between 500 and 650 m/s after 9 cementation injections. Similar V_s trends for all columns in time suggested that similar engineering improvements and $CaCO_3$ magnitudes were achieved between columns at mid-depth. **Figure 5.7** presents measured soil $CaCO_3$ contents along column lengths and **Supplemental Table 5.3** summarizes final shear wave velocity increases (ΔV_s) and $CaCO_3$ content measurements for all columns including section and average $CaCO_3$ content values. As shown, all columns had similar soil $CaCO_3$ content distributions with small decreases in $CaCO_3$ contents again observed with increasing distance from the injection source. For all columns, average $CaCO_3$ contents were between 3.5% and 4.4% by mass and ΔV_s increases were between 448 and 595 m/s consistent with past column studies (Gomez & DeJong 2017). No significant differences in post-treatment improvements were observed between columns as a function of supplied YE concentrations or YE treatment frequencies, which was consistent with the similar 48-hour urea degradation observed

between all columns during cementation injections (**Figure 5.5c**).

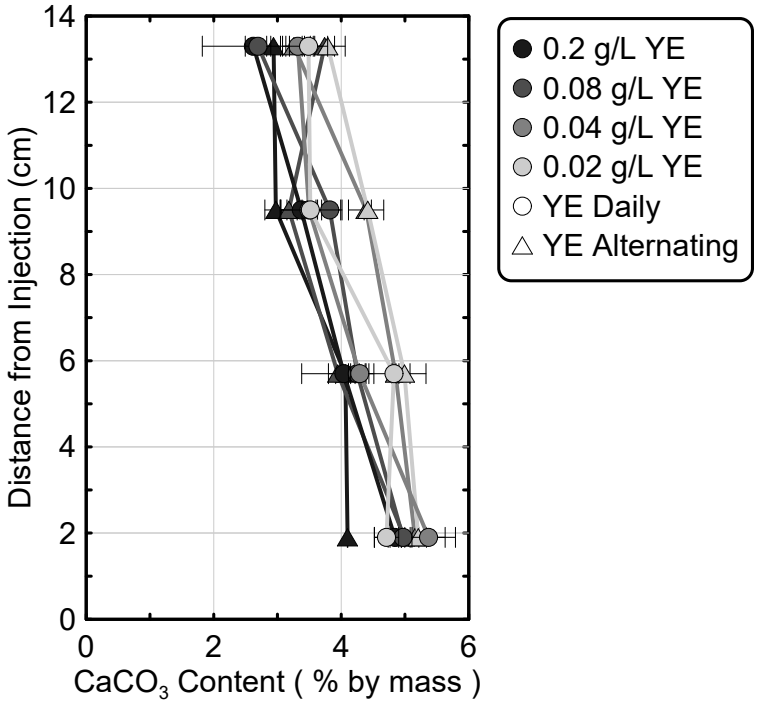

Figure 5.7. Soil column $CaCO_3$ contents versus distance from injection location for all experiment set B columns. Provided error bars indicate ± one standard deviation for all measurements.

5.3.3 *Summary of Ureolytic Rates Obtained in Centimeter-scale Soil Column Experiments*

Figure 5.8 summarizes bulk V_{max} values versus supplied YE concentrations for all columns from both experimental sets. As shown, variations in supplied YE concentrations and YE treatment frequencies produced a wide spectrum of bulk V_{max} values (i.e., urea hydrolysis rates) between 3 and 89 mM/hr at the end of stimulation (stimulation injection 6) which increased to between 16 and 134 mM/hr during the final cementation injections. In both experiments, greater YE concentrations and YE treatment frequencies consistently resulted in higher ureolytic rates; however, YE concentrations exhibited non-linear relationships with achieved microbial activities,

indicating that increases in ureolytic cell densities were not linear with increases in supplied YE. This non-linearity suggested that while components within YE strongly limited ureolytic cell growth at the community level, other factors such as limited dissolved oxygen, metabolic waste generation, and/or other trace nutrient requirements may have limited growth at high YE concentrations. Furthermore, large differences in stimulated ureolytic activity as a function of supplied YE concentrations were noteworthy given the excess of acetate organic carbon in all treatment solutions (85 mM C) relative to the ≈ 0.8 to ≈ 17 mM C provided by YE for the range of concentrations examined (0.01 to 0.2 g/L). One interpretation is that the growth of enriched ureolytic bacteria, primarily using acetate, was limited by specific growth factors provided by YE, such as trace elements or essential vitamins, and not total organic carbon. Another potential explanation could be that while acetate supports biosynthesis, it is not a sufficient sole energy source for ureolytic bacteria, with some components of YE, such as amino acids, being essential, thus rendering it the limiting nutrient. Interestingly, when comparing achieved ureolytic rates between experiment sets A and B at similar YE concentrations, experiment set B columns consistently exhibited lower bulk V_{max} values during cementation. This outcome likely resulted from the lower urea concentrations included in cementation solutions applied in experiment set B (250 mM) in comparison to experiment A (350 mM). Lower urea concentrations included in set B resulted in lower post-treatment pH values (≈ 7.3 to 7.7) when compared to experiment set A (≈ 8.5) wherein urea was supplied in excess of calcium. Lower post-treatment pH values and total ammonium concentrations could have reduced selective pressure for ureolytic bacteria, thereby resulting in lower bulk V_{max} values at similar YE concentrations. Despite rate differences between sets, almost all columns exhibited considerable ureolytic rate increases during the cementation phase. Interestingly, columns receiving alternating YE additions

also appeared to exhibit a more linear relationship between supplied YE and achieved rates when compared to similar daily YE columns during similar treatment injections. This outcome suggests that employing an alternating YE treatment strategy may allow for a desired ureolytic rate to be more easily achieved, as variations in YE provided greater latitude with respect to altering achieved rates. Alternating nutritive/non-nutritive injections also appeared to minimize rate changes throughout the treatment process when compared to similar columns with daily YE additions and may be preferred for applications where near constant rates are desired. Although large differences in ureolytic rates were achieved between columns, similar post-treatment $CaCO_3$ content distributions and engineering improvements were observed for nearly all columns in both sets. This suggested that when retention periods were sufficient to enable full reaction completion, lower ureolytic rates could be used to minimize reactions during injections without sacrificing process efficacy.

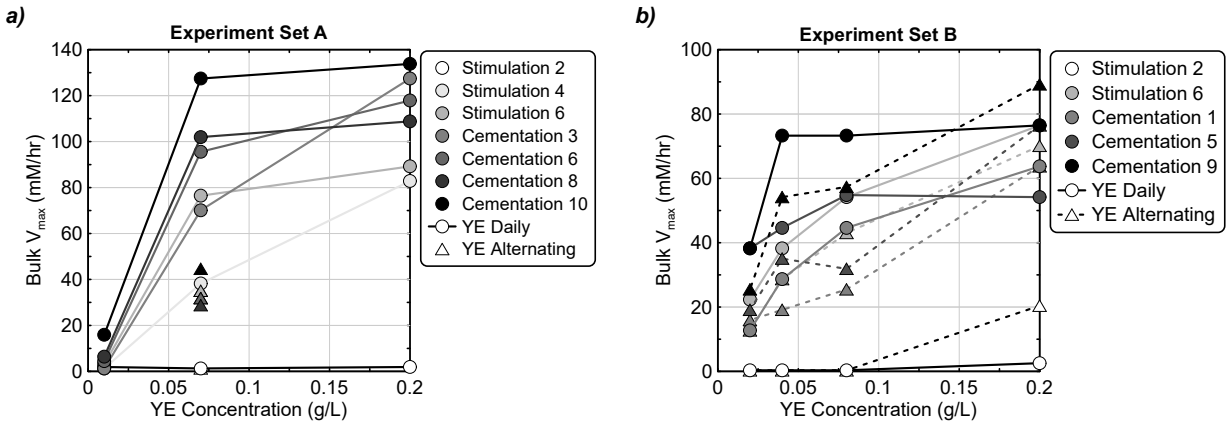

Figure 5.8. Bulk V_{max} values versus supplied YE concentrations obtained during select stimulation and cementation injections for all soil columns from experiment set **(a)** A and **(b)** B.

5.3.4 *Reactive Transport Simulations*

Informed by previous results from the centimeter-scale soil column experiments, twenty-seven different reactive transport simulations were performed to investigate relationships between ureolytic rates, solution transport conditions, and biocementation distributions realized in 3.67-meter-long soil column numerical models similar to that physically tested by San Pablo et al. (2020). In order to calibrate the PHREEQC advective-dispersive soil column numerical models to passive tracer data from the actual meter-scale experiments, simulated normalized bromide concentrations (C/C_0) were compared to experimental measurements (**Supplemental Figure 5.4**). A mobile porosity (n) of 0.234 and longitudinal dispersivity (α_L) of 0.3 meters was assumed in the model and was able to well capture normalized bromide concentrations during the entire passive tracer injection sequence. The numerical model allowed for the implications of the treatment techniques identified in the previous centimeter-scale soil column experiments to be applied at meter-scale under varying injection rates and outcomes from these simulations to be compared for different reactive transport conditions.

In order to explore the full spectrum of ureolytic rates realized in the previous centimeter-scale soil column experiments, the Michaelis-Menten kinetic (**Equation (5.1)**) was calibrated to urea degradation trends from experiment set A for the 0.01 g/L YE daily, 0.07 g/L YE alternating, and 0.2 g/L YE daily columns during cementation injection 8. **Figure 5.9** presents normalized urea concentrations (C/C_0) in time from the centimeter-scale columns and the calibrated PHREEQC models which assumed bulk V_{max} values of 6.4, 28.8, and 108.8 mM urea/hr for the 0.01 g/L YE daily, 0.07 g/L YE alternating, and 0.2 g/L YE daily columns, respectively. After calibrating the soil column models to capture both advective-dispersive transport properties and ureolytic reaction

rates from the centimeter-scale column experiments, simulations were performed considering nine different injection flow rates (0.06 PV/hr to 1.8 PV/hr) and the three different ureolytic reactions rates. In all simulations, a single 1.5 PV cementation solution injection was applied similar to that employed in San Pablo et al. (2020) and $CaCO_3$ distributions were determined along column lengths both immediately after injections as well as following a retention period that was varied to allow for complete ureolysis and cementation reactions. **Table 5.1** presents a summary of all PHREEQC soil column simulations including injection rates, injection volumes, injection durations, ureolytic reaction rates, post-injection reaction durations, total model durations, and reaction-to-injection duration ratios (described later).

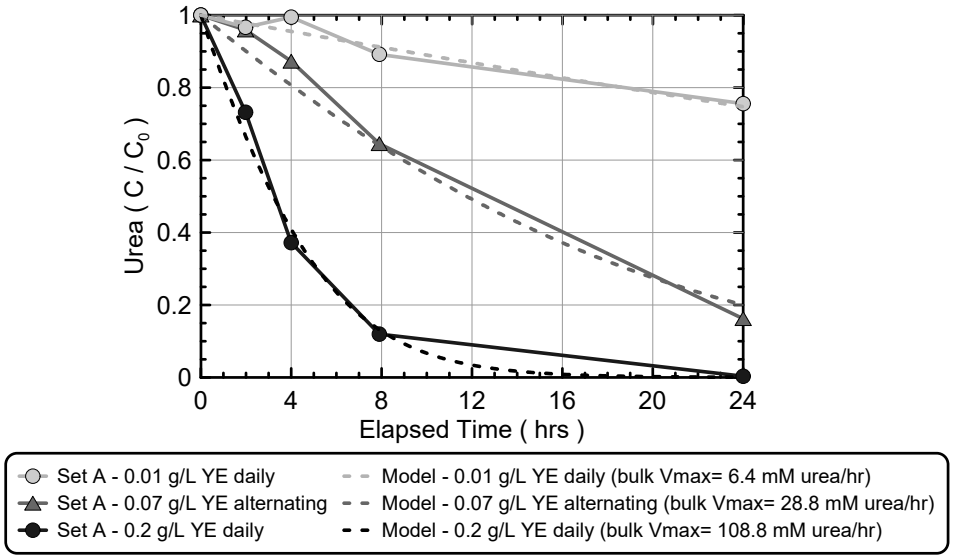

Figure 5.9. Comparison of normalized urea concentrations (C/C_0) in time from the 0.01 g/L YE daily, 0.07 g/L YE alternating, and 0.2 g/L YE daily columns from set A during cementation injection 8 with simulated trends from PHREEQC models assuming bulk V_{max} values of 6.4, 28.8, or 108.8 mM urea/hr.

Table 5.1. Summary of PHREEQC 3.67-meter Soil Column Simulations

Injection Rate (PV/hr)[1]	Injection Rate (mL/min)	Injection Volume (PV)[1]	Injection Duration (hr)	Ureolysis Reaction Rate (from experiment A) -	Post-injection Reaction Duration (C/C0 <5%) (hr)	Total Model Duration (hr)	Reaction-to-Injection Duration Ratio (RTIDR) -
0.06	50	1.5	25.3	0.2 g/L YE daily	10.7	36.0	0.4
				0.07 g/L YE alternating	38.9	64.2	1.5
				0.01 g/L YE daily	174.6	199.9	6.9
0.09	75	1.5	16.9	0.2 g/L YE daily	10.7	27.6	0.6
				0.07 g/L YE alternating	38.9	55.8	2.3
				0.01 g/L YE daily	174.6	191.5	10.3
0.12	100	1.5	12.7	0.2 g/L YE daily	10.7	23.4	0.8
				0.07 g/L YE alternating	38.9	51.6	3.1
				0.01 g/L YE daily	174.6	187.3	13.8
0.30	250	1.5	5.1	0.2 g/L YE daily	10.7	15.8	2.1
				0.07 g/L YE alternating	38.9	44.0	7.7
				0.01 g/L YE daily	174.6	179.7	34.5
0.60	500	1.5	2.5	0.2 g/L YE daily	10.7	13.2	4.2
				0.07 g/L YE alternating	38.9	41.4	15.4
				0.01 g/L YE daily	174.6	177.1	68.9
0.90	750	1.5	1.7	0.2 g/L YE daily	10.7	12.4	6.3
				0.07 g/L YE alternating	38.9	40.6	23.0
				0.01 g/L YE daily	174.6	176.3	103.4
1.20	1000	1.5	1.3	0.2 g/L YE daily	10.7	12.0	8.4
				0.07 g/L YE alternating	38.9	40.2	30.7
				0.01 g/L YE daily	174.6	175.9	137.8
1.50	1250	1.5	1.0	0.2 g/L YE daily	10.7	11.7	10.6
				0.07 g/L YE alternating	38.9	39.9	38.4
				0.01 g/L YE daily	174.6	175.6	172.3
1.80	1500	1.5	0.8	0.2 g/L YE daily	10.7	11.5	12.7
				0.07 g/L YE alternating	38.9	39.7	46.1
				0.01 g/L YE daily	174.6	175.4	206.8

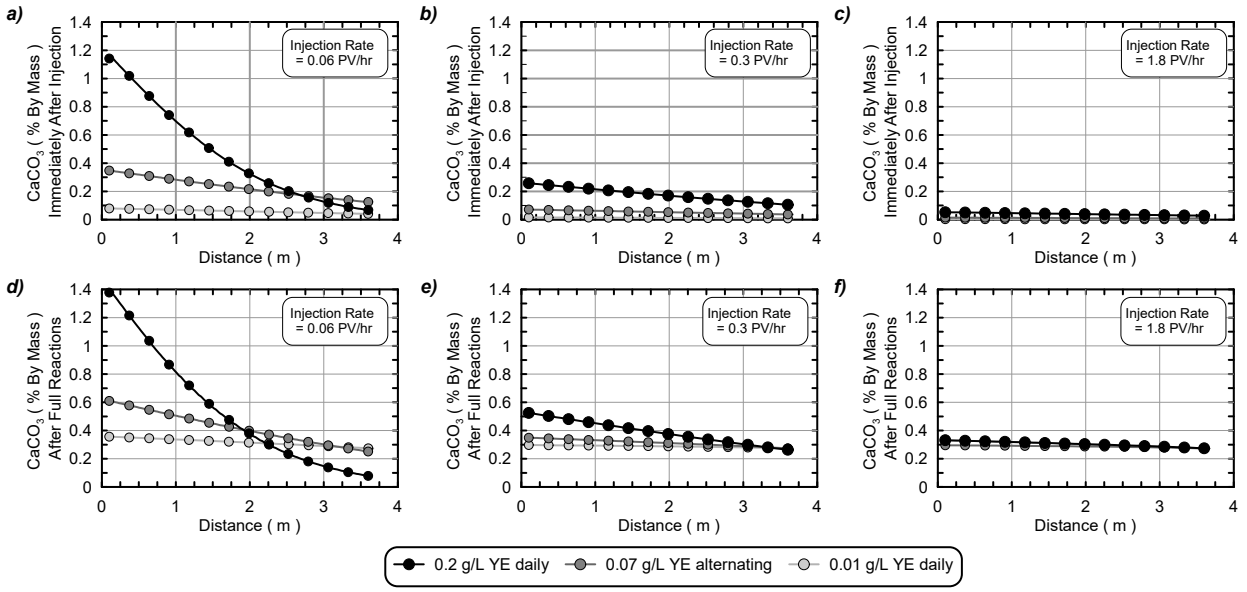

Figure 5.10. Simulated soil column $CaCO_3$ distributions **(a, b, c)** immediately after injections and **(d, e, f)** following reaction completion for select injection rates including **(a, d)** 0.06 PV/hr (50 mL/min), **(b, e)** 0.3 PV/hr (250 mL/min) and **(c, f)** 1.8 PV/hr (1500 mL/min) for the three different ureolytic reaction rates (as described by YE additions).

Figure 5.10 presents simulated soil column $CaCO_3$ distributions immediately after injections, representing the reactions during transport, (**Figures 5.10a, 5.10b, 5.10c**) and after reaction completion (**Figures 5.10d, 5.10e, 5.10f**) for three select injection rates (0.06 PV/hr, 0.3 PV/hr, and 1.8 PV/hr) as well as the three different ureolytic rates shown in **Figure 5.9** (0.2 g/L YE daily, 0.07 g/L YE alternating, 0.01 g/L YE daily). At the slowest flow rate (0.06 PV/hr), significantly larger $CaCO_3$ contents were observed near the injection location (distance = 0 m) both immediately after injections (**Figure 5.10a**) and after reaction completion (**Figure 5.10d**) when compared to the end of the column (distance = 3.67 m). Localization of biocementation near the injection source became more pronounced with both decreases in flow rates and increases in ureolytic activities, which resulted in greater urea hydrolysis and precipitation reactions during injections thereby limiting the transport of reactants (i.e., urea, Ca^{+2}) to farther distances within columns. In contrast, as injection rates increased, more limited reactions occurred during solution transport (**Figures**

5.10b, 5.10c) resulting in more uniform $CaCO_3$ contents along column lengths after reaction completion (**Figures 5.10e, 5.10f**), albeit with smaller $CaCO_3$ magnitudes than those observed for the slowest flow rate (**Figure 5.10d**). Although the greatest localization of $CaCO_3$ near the injection source occurred in the column with the highest ureolytic rate and slowest injection rate (0.2 g/L YE daily rate, 0.06 PV/hr), at this same slow injection rate, the two lower ureolytic rates (0.01 g/L YE daily, 0.07 g/L YE daily) achieved substantially improved uniformity as well as greater $CaCO_3$ contents near the end of the column (distances > 2 m) (**Figure 5.10d**). Collectively, these results demonstrated that when reactions during injections were minimized either through decreases in ureolytic rates or increases in injection rates, supplied reactants were distributed both more uniformly and over greater injection distances. When deployed at field-scale, such conditions may provide significant practical advantages by allowing injection and extraction wells to be installed at greater well-to-well spacings.

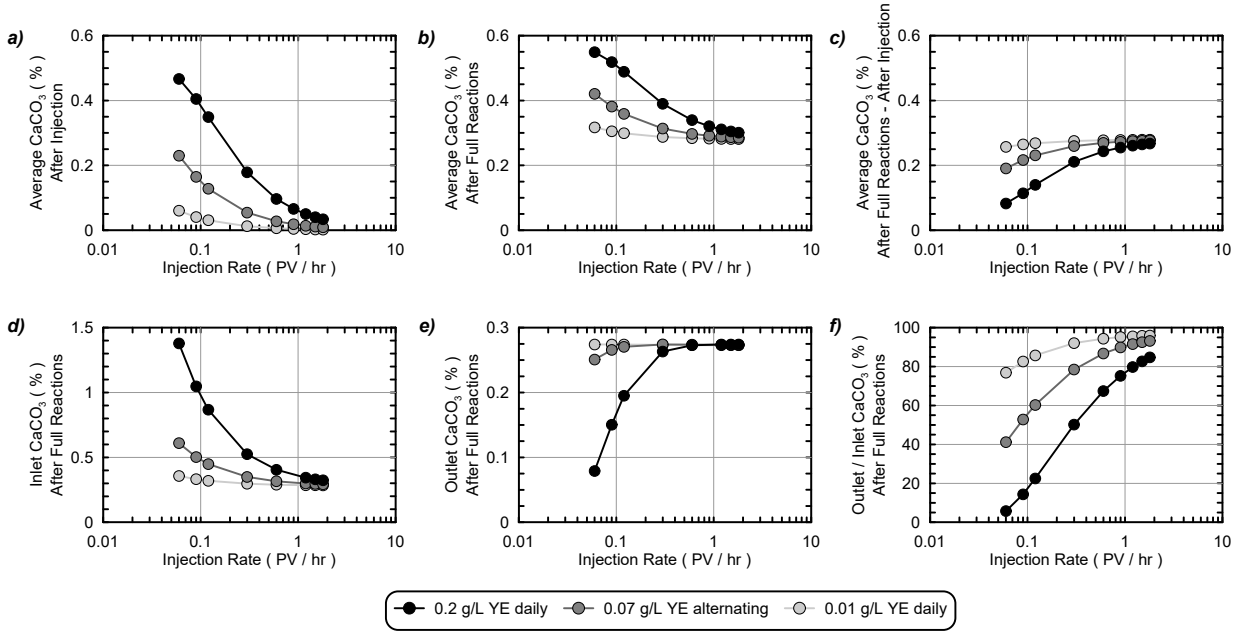

Figure 5.11. Results from soil column simulations for different injection rates and ureolytic reaction rates (as described by YE additions) including: average $CaCO_3$ contents in columns **(a)** immediately after injections and **(b)** after reaction completion, **(c)** differences between column average $CaCO_3$ contents after injections and after reaction completion, $CaCO_3$ contents after reaction completion at the column **(d)** inlet and **(e)** outlet, and (**f)** outlet-to-inlet $CaCO_3$ content ratios after reaction completion versus injection rates.

Differences in treatment uniformity and extent as a function of differences in ureolytic rates and injections rates were examined using various metrics. **Figure 5.11** presents results from all soil column simulations including relationships between average $CaCO_3$ contents over column lengths immediately after injections (**Figure 5.11a**) and after reaction completion (**Figure 5.11b**), average $CaCO_3$ content increases that occurred during the residence period (calculated by taking the difference between the previous two values) (**Figure 5.11c**), $CaCO_3$ contents observed after reaction completion at column inlets (**Figure 5.11d)** and outlets (**Figure 5.11e**), and the ratio between $CaCO_3$ contents at column outlets and inlets (**Figure 5.11f)** versus injection rates. When injection rates were reduced and ureolytic rates were increased, significant increases in column

average $CaCO_3$ contents were observed both immediately after injections and after reaction completion (**Figures 5.11a, 5.11b**). This resulted from greater precipitation reactions occurring during solution transport and therefore greater utilization of the Ca^{2+} available in the provided 1.5 PV injection. As injection rates were increased above 1 PV per hour, average $CaCO_3$ contents in columns immediately after injections were nearly 0% for all ureolytic rates (**Figure 5.11a**) with almost all $CaCO_3$ content increases occurring during retention periods (**Figure 5.11c**). At both lower injection rates and higher reaction rates, greater precipitation was observed near the column inlet (**Figure 5.11d**) with less precipitation near the column outlet (**Figure 5.11e**) due to greater Ca^{+2} consumption near the injection source. Again, once injection rates exceeded 1 PV per hour, the effect of ureolytic rate on inlet and outlet $CaCO_3$ contents was minimized (**Figures 5.11d, 5.11e**) as reactions occurring during solution injections were negligible. While changes in injection rates had significant effects on $CaCO_3$ uniformity for columns with high ureolytic rates (0.2 g/L YE daily), interestingly when lower ureolytic rates were present, the effect of injection rate on $CaCO_3$ uniformity was diminished (**Figures 5.11a to 5.11f**). Moving forward, the use of lower ureolytic rates during field applications may afford reduced sensitivity of realized cementation spatial distributions to changes in solution transport rates, in addition to improvements in uniformity and extent.

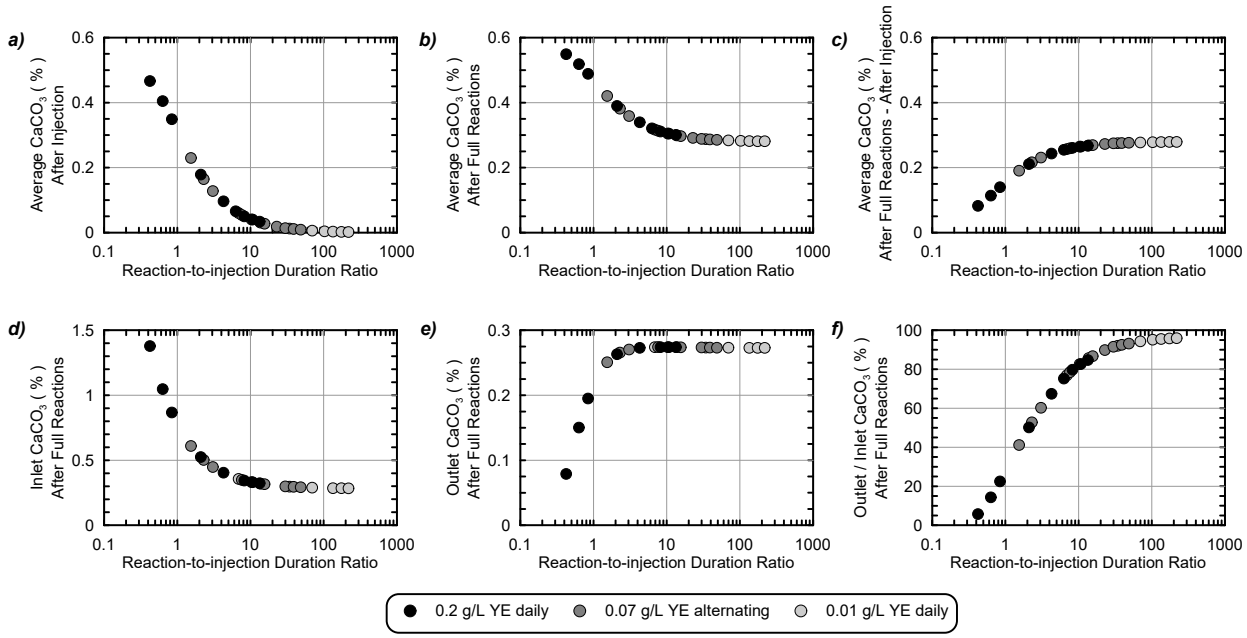

Figure 5.12. Results from soil column simulation's for different injection rates and ureolytic reaction rates (as described by YE additions) including: average $CaCO_3$ contents in columns **(a)** immediately after injections and **(b)** after reaction completion, **(c)** differences between average $CaCO_3$ contents in columns after injections and after reaction completion, $CaCO_3$ contents after reaction completion at the column **(d)** inlet and **(e)** outlet, and (**f)** outlet-to-inlet $CaCO_3$ content ratios after reaction completion versus dimensionless reaction-to-injection duration ratios.

$$Reaction - to - injection\ Duration\ Ratio\ (RTIDR) = \frac{Time\ to\ \frac{[Urea]}{[Urea]_{initial}} = 5\%}{Injection\ Duration} \qquad \text{Equation (5.4)}$$

5.3.5 *Characterizing Biocementation Treatment Conditions and Outcomes*

Results from column simulations demonstrated the combined effects of changes in injection and ureolytic rates on $CaCO_3$ precipitation magnitudes and distributions. However, in order to better characterize differences in reactive transport conditions between simulations, a dimensionless reaction-to-injection duration ratio (RTIDR) parameter was proposed which related the rate of

reactions to solution transport rates. The RTIDR parameter is similar to a Damköhler number and was calculated by dividing the time required to achieve 95% hydrolysis of the supplied urea by the injection duration (**Equation (5.4)**). At low RTIDRs and high Damköhler number transport the time required to complete ureolysis and $CaCO_3$ precipitation reactions is small relative to the overall injection time, thus reactions occurring during injections are more significant and greater nonuniformity in produced $CaCO_3$ can be expected. In contrast, at high RTIDRs and low Damköhler number transport the reaction time is large relative to the injection time, reactions during transport are minimized, and greater uniformity in produced $CaCO_3$ can be achieved. **Figure 5.12** presents similar parameters as **Figure 5.11** plotted versus the dimensionless RTIDR parameter. As shown, results from all 27 simulations were unified when plotted versus the RTIDR parameter, which reflected changes in reactive transport conditions. At RTIDR values greater than ≈10, all average, inlet, and outlet $CaCO_3$ contents were similar between simulations due to minimal reactions occurring during solution transport. At lower RTIDRs, higher average $CaCO_3$ contents were achieved (**Figure 5.12a and 5.12b**) but at the cost of substantial nonuniformity (**Figure 5.12d, 5.12e, and 5.12f**). Despite large differences in reaction conditions, the dimensionless RTIDR provided a unified framework for understanding the combined effects of both changes in injection and ureolytic reaction rates on biocementation distributions and magnitudes. During field-scale applications, RTIDR values may provide a valuable metric by which treatment injections can be designed to achieve desired reaction conditions and cementation distributions.

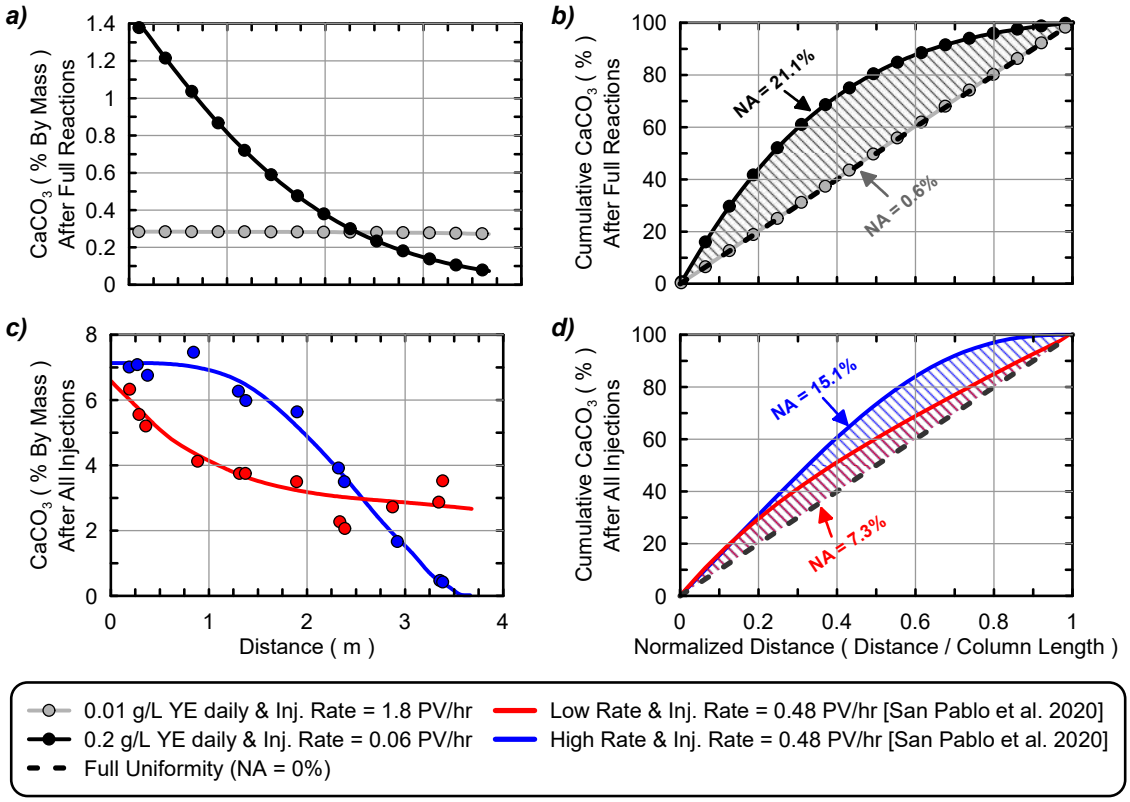

Figure 5.13. (a, c) Soil column $CaCO_3$ content distributions versus distance and **(b, d)** cumulative $CaCO_3$ content distributions versus normalized distance for **(a, b)** simulations with the highest (0.01 g/L YE daily, injection rate = 1.8 PV/hr) and lowest (0.2 g/L YE daily, injection rate = 0.06 PV/hr) reaction-to-injection duration ratios and **(c, d)** low and high ureolytic rate physical meter-scale experiments by San Pablo et al. (2020) involving a constant flow rate (0.48 PV/hr). Nonuniformity area (NA) values are indicated as shaded areas between respective cumulative $CaCO_3$ content distributions and dashed line trends expected for full uniformity (NA = 0%).

Although outlet-to-inlet $CaCO_3$ content ratios reasonably described biocementation uniformity in 1D column simulations, such ratios will not likely be suitable for assessment of treatment uniformity under field relevant flow regimes which may be complicated by the presence of three-dimensional flow, alternating injection patterns, and soil stratigraphic differences, among other factors. In order to quantitatively assess cementation uniformity and potential biases in cementation distributions towards injection or production locations, cumulative distributions of

$CaCO_3$ were analyzed which describe the accumulation of cementation along an injection pathway. **Figure 5.13** presents soil $CaCO_3$ content distributions (**Figure 5.13a**) and cumulative soil $CaCO_3$ content distributions (**Figure 5.13b**) for column simulations with the highest (0.01 g/L YE daily, 1.8 PV/hr, RTIDR = 206.8) and lowest (0.2 g/L YE daily, 0.06 PV/hr, RTIDR = 0.4) reaction-to-injection duration ratios versus injection distance (**Figure 5.13a**) and normalized injection distance (**Figure 5.13b**). For cumulative distributions, normalized distances were computed as the distance from the injection source divided by the overall length of the columns to remove the influence of pathway length and generalize the approach. Similar soil $CaCO_3$ distributions are also presented for the high and low ureolytic rate meter-scale column experiments by San Pablo et al. (2020) (**Figure 5.13c**) along with computed cumulative soil $CaCO_3$ distributions (**Figure 5.13d**) in order to compare simulation outcomes to actual distributions realized in physical experiments. As shown, the highest RTIDR simulation (0.01 g/L YE daily, 1.8 PV/hr) minimized reactions during transport and achieved a cumulative soil $CaCO_3$ content distribution with a near-constant linear slope (**Figure 5.13b**) indicative of near complete uniformity in $CaCO_3$ along the column length (**Figure 5.13a**). In contrast, the lowest RTIDR simulation (0.2 g/L YE daily, 0.06 PV/hr) realized $CaCO_3$ contents that were much larger near the injection source resulting in a cumulative $CaCO_3$ content distribution with a concave down parabolic slope reflective of greater $CaCO_3$ masses localizing near the injection source. Results from the meter-scale column experiments by San Pablo et al. (2020) involved higher cementation magnitudes due to repeated injections, with greater cementation uniformity achieved in the low ureolytic rate column when compared to the high ureolytic rate column, despite identical flow rates (**Figure 5.13c**). In both columns, however, greater cementation was achieved near the injection source with concave down cumulative $CaCO_3$ content distributions observed (**Figure 5.13d**).

$$Nonuniformity\ Area = \int_{x=0}^{x=1} Cumulative\ CaCO_3\ Dist.(\%) - \int_{x=0}^{x=1} Uniform\ Cumulative\ CaCO_3\ Dist.(\%)$$

$$= \int_{x=0}^{x=1} Cumulative\ CaCO_3\ Dist.(\%) - 50\% \quad \text{Equation (5.5)}$$

In order to quantitatively compare $CaCO_3$ content gradients between simulations and experiments, irrespective of cementation magnitudes and length scales, a nonuniformity area (NA) parameter was proposed. Nonuniformity area (NA) was calculated as the area between a given cumulative soil $CaCO_3$ distribution and the cumulative soil $CaCO_3$ distribution that would be obtained for a completely uniform pathway (**Equation (5.5)**). NA values are illustrated in **Figures 5.13b and 5.13d** along with linear dashed lines, which represent the cumulative soil $CaCO_3$ content distributions expected for a fully uniform cemented column. NA values describe both the degree to which soil $CaCO_3$ content distributions deviate from perfect uniformity as well as the bias of the $CaCO_3$ content distributions towards the injection or production location. A positive nonuniformity area suggests that the $CaCO_3$ distribution is weighted towards the injection source and a negative nonuniformity area suggests that the $CaCO_3$ content distribution is biased towards the production location. As shown in **Figure 5.13**, NA values were positive for both simulations indicating biases in cementation toward the injections source, with near perfect uniformity achieved in the lowest RTIDR simulation (NA = 0.6%) and more significant nonuniformity in the highest RTIDR simulation (NA = 21.1%). In the physical experiments, a similar bias in cementation was observed towards the injection source, with the low ureolytic rate column achieving a significantly lower NA (NA = 7.3%) than the high ureolytic rate column (NA = 15.1%), indicating that greater uniformity was again achieved through reductions in ureolytic rates. The ability of the NA parameter to quantify uniformity differences between the meter-scale

experiments was particularly noteworthy given the more irregular changes in measured soil $CaCO_3$ contents with length.

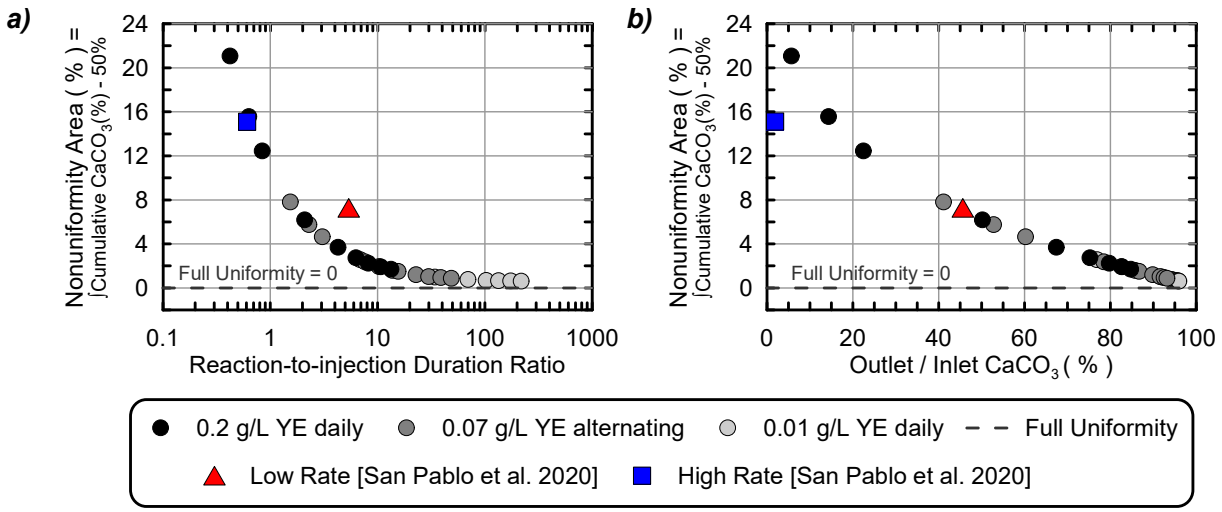

Figure 5.14. Nonuniformity area parameters determined from cumulative $CaCO_3$ distributions for all soil column simulations and low and high ureolytic rate physical meter-scale experiments by San Pablo et al. (2020) versus **(a)** reaction-to-injection duration ratios and **(b)** outlet-to-inlet $CaCO_3$ ratios.

Figure 5.14 presents calculated NA parameters for all column simulations as well as the low and high ureolytic rate meter-scale experiments versus RTIDRs (**Figure 5.14a**) and outlet-to-inlet $CaCO_3$ content ratios (**Figure 5.14b**). RTIDR values for the meter-scale experiments were determined by fitting the ureolytic kinetic (**Equation (5.1)**) to urea degradation trends observed from 4 sampling port locations along the length of columns during the last cementation injection and determining an average time to 95% completion of urea hydrolysis. As shown, at lower RTIDRs and outlet-to-inlet $CaCO_3$ content ratios, large positive NA values were computed for all simulations suggesting a more significant bias of $CaCO_3$ masses towards the injection source. At higher RTIDRs and outlet-to-inlet $CaCO_3$ content ratios approaching 1, NA values decreased and

approached 0%, indicative of near perfect uniformity in achieved cementation. NA values from both meter-scale column experiments were consistent with trends from the numerical models, suggesting that the RTIDR parameter could successfully account for differences in reaction conditions and anticipate changes in cementation nonuniformity independent of differences in injection numbers, $CaCO_3$ content magnitudes, injection rates, and ureolytic rates. As expected, outlet-to-inlet $CaCO_3$ content ratios were also well correlated with NA values for both simulations and experiments due to the application of injections in a single direction, however, the presence of more complicated injection conditions relevant to field applications (e.g., reversed injections, radial flow) may make these ratios less useful for practical applications. Moving forward, the proposed NA and RTIDR parameters may allow for improved comparisons and unification of experimental observations between studies as well as allow for treatment strategies to be more effectively designed to meet site-specific engineering performance objectives (e.g., localization of cementation vs. cementation uniformity).

5.3.6 *Practical Implications of Reduced Reaction Rates*

Although all simulations considered a finite soil column length of 3.67 meters, under free-field conditions more representative of field-scale applications, the applied 1.5 PV injection would have transported reagents to more distal locations beyond the column length. In order to explore anticipated effects at greater treatment distances, models were extended to 15 meters in length while still applying 1.5 PV cementation solution injections under identical flow rates and reaction rates as those considered earlier. **Figure 5.15** presents results from 15-meter-long column simulations including the percentage of supplied calcium that was precipitated within the 3.67-

meter length previously considered (**Figure 5.15a**) and the maximum injection distances over which soil $CaCO_3$ content exceeded 0.25% (**Figure 5.15b**) and 0.1% (**Figure 5.15c**) by mass versus RTIDR. At RTIDRs of less than 1, over 80% of the injected calcium was precipitated within the 3.67-meter column length (**Figure 5.15a**). As RTIDRs increased to values above 10, however, the percentage of supplied calcium that was precipitated within the column length approached 50%, which was reflective of the minimal reactions that occurred during injections. While low RTIDRs achieved greater $CaCO_3$ contents near the injection source, such conditions also resulted in a more limited extent of improvement. For example, while high RTIDR simulations (RTIDR > 10) achieved $CaCO_3$ contents exceeding 0.1% at distances up to 8 meters, the lowest RTIDR simulation (RTIDR = 0.4) achieved this same $CaCO_3$ content only up to 3.5 meters. High RTIDR conditions may permit significant increases in treatment extent when applied under free-field conditions, with the potential to realize large reductions in process impacts and implementation costs through increased well-to-well spacings.

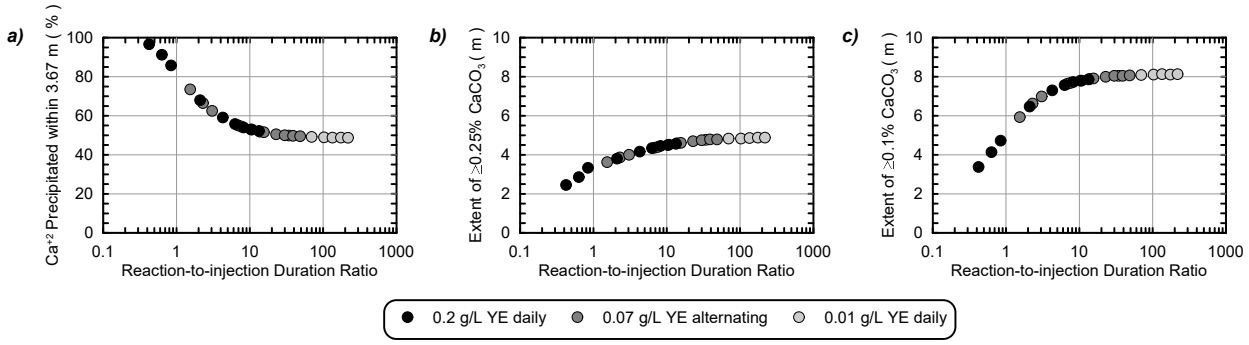

Figure 5.15. Results from extended 15-meter-long soil column simulations including: **(a)** the percentage of supplied Ca^{2+} that was precipitated within the 3.67-meter-long column previously considered, and the treatment distances over which $CaCO_3$ contents exceeded **(b)** 0.25% and **(c)** 0.1% by mass versus reaction-to-injection duration ratios.

5.4 Conclusions

A study was completed to identify treatment approaches which could reliably enrich indigenous ureolytic microorganisms at controlled ureolytic rates to improve the spatial control of biocementation soil improvement. Twelve centimeter-scale soil column experiments were performed wherein columns received treatment solutions with varying YE concentrations intended to control enriched ureolytic cell densities and ureolytic rates. Following centimeter-scale soil column experiments, a one-dimensional reactive transport model was used to further investigate the implications of the experimentally observed ureolytic rates on the uniformity and distribution of biocementation expected in a 3.67-meter-long soil column, thereby extending our understanding of changes in reactive transport conditions beyond those experimentally examined by San Pablo et al. (2020). Results from simulations were compared to those obtained from the physical meter-scale experiments and parameters to assess reactive transport conditions and cementation uniformity were explored. From the results of this study, the following conclusions can be made:

- YE concentrations supplied in MICP treatment solutions can be used to reliably control stimulated indigenous ureolytic microorganisms and achieve a wide spectrum of ureolytic rates. Ureolytic rates can be used to control reactive transport conditions during MICP and can be tailored to specific engineering applications through changes in treatment solution design.
- The ability of applied YE concentrations to reliably control stimulated ureolytic activity in the presence of significant acetate suggests that either: (1) enriched ureolytic bacteria were able to utilize the total organic carbon provided by acetate but were limited by specific growth factors provided by YE or (2) acetate was not a favorable energy source and only components of YE, such as amino acids, were utilized by ureolytic bacteria for this purpose.

Applied YE concentrations had a non-linear relationship with achieved microbial activities over the range of concentrations studied suggesting that while YE strongly influenced ureolytic cell activity, other factors were limiting at high YE concentrations.

- When injection retention periods were extended to allow for full hydrolysis of the supplied urea concentrations, all centimeter-scale soil column experiments achieved similar post-treatment engineering improvements independent of differences in ureolytic activities.
- Reactive transport simulations investigated relationships between the ureolytic rates achieved in the centimeter-scale soil columns and improvement distributions expected in 3.67-meter-long columns subjected to varying flow rates. Simulations demonstrated that lower ureolytic rates could achieve more uniform transport of reactants, reduced sensitivity to changes in solution injection velocities, and greater improvement extent. A reaction-to-injection duration ratio (RTIDR) parameter was shown to capture the collective impacts of changes in injection rates and ureolytic reaction rates on reactive transport conditions thereby unifying results between simulations.
- In simulations involving low reaction-to-injection duration ratios (high Damköhler number conditions), significant reactions occurred during injections, resulting in localization of cementation near injection sources, a more limited extent of improvement, and greater spatial nonuniformity. At higher reaction-to-injection duration ratios (low Damköhler number conditions), reactions occurring during transport were minimized, resulting in more uniform $CaCO_3$ distributions and a greater extent of improvement.
- A nonuniformity area (NA) parameter was introduced to quantitatively characterize changes in biocementation uniformity independent of column length and $CaCO_3$ content magnitudes for all simulations and two recent meter-scale experiments. NA provides a

metric by which cementation uniformity can be quantitively assessed and compared between studies.

- Results from recent meter-scale soil column experiments by San Pablo et al. (2020) were consistent with simulated trends when both differences in injection rates and reaction rates were accounted for. Outcomes from this study further demonstrated the utility of changes in stimulated ureolytic activities to control the spatial uniformity and extent of biocementation over meter-scale treatment distances for conditions which had not yet been experimentally examined.

Although not exhaustive, the treatment techniques and reactive transport metrics identified in this study are anticipated to have important implications towards informing future MICP treatment designs and controlling the spatial distributions of ureolytic MICP for practical field-scale applications.

Chapter 6. INVESTIGATING AMMONIUM BY-PRODUCT REMOVAL FOLLOWING STIMULATED UREOLYTIC MICROBIALLY-INDUCED CALCITE PRECIPITATION

This paper has been published as a conference paper in the Proceedings of ASCE Geo-Congress 2019. The paper is presented herein, with slight modifications.

Citation:

Lee, M., Kolbus, C.M., Yepez, A.D., & Gomez, M.G. Investigating Ammonium By-Product Removal following Stimulated Ureolytic Microbially-Induced Calcite Precipitation. *In Geo-Congress 2019: Soil Improvement (pp. 260–272)*. Reston, VA: American Society of Civil Engineers (2019).

ABSTRACT

Microbially induced calcite precipitation (MICP), or biocementation, has advanced rapidly in the past decade as a promising environmentally-conscious ground improvement alternative. In the ureolytic biocementation process, microorganisms containing urease enzymes are used to mediate the degradation of urea, thereby producing total ammonium, dissolved inorganic carbon, and hydroxide ions. Despite recent advances, concerns regarding the fate of produced ammonium by-products have persisted. Methods to manage and remove ammonium following biocementation will likely be needed as the technology transitions toward industrial field-scale application. In this study, a preliminary investigation of the removal of ammonium from a bio- cemented poorly-graded sand was performed using soil column experiments to improve our understanding of the effect of rinse solution chemistry on ammonium removal efficiency, bio- cementation integrity, and potential for long-term attenuation. Four soil columns received identical treatments for 14 days targeting a final calcite content near 4 to 5% and daily rinse injections were subsequently applied to investigate post-treatment ammonium removal. Results suggest that the injection of 5 pore

volumes of a high pH, high ionic strength solution may offer the ability to remove near 99.1% of post-treatment pore fluid ammonium concentrations with minimal biocementation degradation.

6.1 Introduction

Microbially Induced Calcite Precipitation (MICP), or biocementation, has shown significant promise as an environmentally-conscious alternative to traditional geotechnical ground improvement technologies, which oftentimes rely on hazardous grouting chemicals, high mechanical energy, and energy-intensive materials to improve the engineering properties of soils (Seagren and Aydilek 2010; DeJong et al. 2013). In the urea hydrolysis driven process, microorganisms containing urease enzymes are used to catalyze a hydrolysis reaction that degrades urea, yielding total ammonium, dissolved inorganic carbon, and hydroxide ions (Stocks-Fisher et al. 1999). In the presence of soluble calcium from treatment solutions or groundwater, the process can supersaturate solutions with respect to calcium carbonate and initiate mineral precipitation on soil particle surfaces and contacts. The resulting biocementation can transform the engineering properties of granular soils through large increases in shear stiffness and strength, with reductions in hydraulic conductivity and porosity (DeJong et al. 2006; Montoya & DeJong 2015; Gomez & DeJong 2017; Gomez et al. 2018b). The technology has a variety of applications in geotechnical and geoenvironmental engineering including liquefaction mitigation, slope stability improvement, subsurface flow manipulation, and contaminant immobilization among other potential uses (Fujita et al. 2004; Montoya et al. 2013; Minto et al. 2016).

Despite significant advances in MICP treatment techniques (O'Donnell et al. 2017; Gomez et al. 2018a), up-scaling of the process to meter-scale (van Paassen et al. 2011, Smith et al. 2012; Gomez

et al. 2015; 2017), and improved characterization of biocemented materials (Montoya and DeJong 2015; Zamani & Montoya 2018), environmental concerns regarding the fate of produced ammonium by-products during MICP have remained largely unaddressed. Although ammonium is a commonly encountered source of inorganic nitrogen in soil systems, high aqueous ammonium concentrations produced following MICP may present serious environmental and human health concerns if left untreated in near surface and subsurface soils and groundwater. For example, the presence of high ammonium levels in surface waters can encourage the growth of toxic algal blooms, which can decrease aquatic dissolved oxygen availability, produce high levels of toxins, and encourage bacterial growth, therefore threatening fish, humans, and other flora and fauna (Paerl et al. 1997). While no maximum contaminant levels have been established by the U.S. EPA for total ammonium in drinking water, water quality criteria for aquatic life of 17 mg/L (≈ 1 mM) and 1.9 mg/L (≈ 0.1 mM) total ammonium for acute and chronic exposure, respectively, have been recommended (EPA, 2013). During field-scale MICP applications, aqueous ammonium concentrations remaining in treated subsurface locations may be required to meet or exceed such recommendations or maintain similar water quality as that observed prior to MICP treatments. This may present a significant challenge, as ammonium concentrations are expected to be near twice the concentration of applied urea by reaction stoichiometry as shown in many previous experiments (**Figure 6.1**). In order for MICP to achieve widespread industrial acceptance as a truly environmentally-conscious technology, it is clear that scalable methods to manage, remediate, and/or remove nitrogen by-products following biocementation are needed.

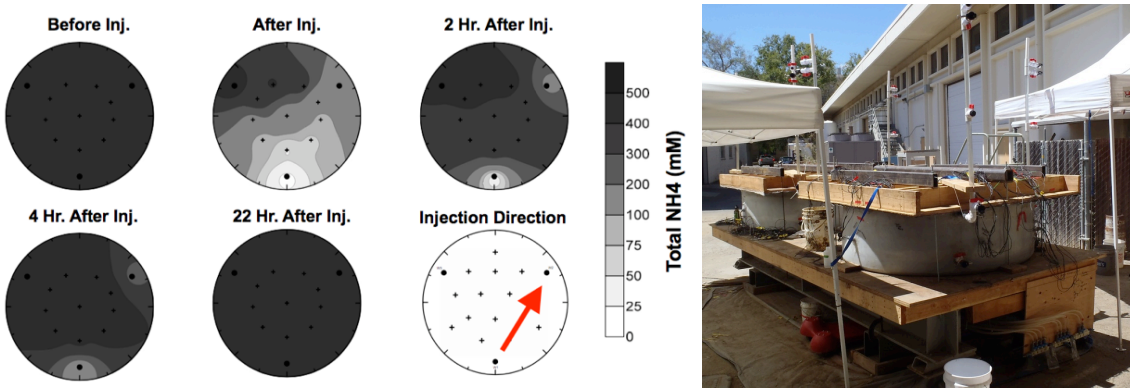

Figure 6.1. Spatial contours of total NH_4^+ concentrations during and after treatment injections in a meter-scale experiment involving stimulated ureolytic MICP indicated NH_4^+ concentrations exceeding 500 mM when urea concentrations of 350 mM were applied (Gomez et al. 2017).

In this study, a soil column experiment was performed to investigate the production, transport, and removal of ammonium by-products following MICP in a relatively clean poorly-graded sand material. Prior to all treatments, columns were saturated with de-ionized water and an ammonium bromide tracer solution was applied to examine the transport of ammonium ions (NH_4^+) relative to non-reactive (passive) bromide ions (Br^-) through columns. Following tracer testing, all columns received identical treatment injections for 14 days intended to uniformly biocement soil specimens. Stimulation treatments were applied for the first 4 days to enrich soil specimens for indigenous ureolytic soil microorganisms capable of completing urea hydrolysis and the biocementation process. Following successful enrichment, soil columns then received identical cementation treatment injections over 10 days targeting final post-treatment calcite contents between 4 and 5% by mass. During all treatments, shear wave (V_s) velocity measurements were completed to non-destructively monitor changes in soil shear stiffness resulting from biocementation and aqueous samples were obtained in time to examine temporal changes in solution chemistry related to microbial urea hydrolysis, calcite precipitation, and ammonium sorption and transport. Following all cementation treatments, soil columns received daily rinse injections with solutions of differing

ionic strength and pH to investigate the effect of rinse solution chemistry on by-product removal and the potential for ammonium attenuation during an extended retention period. It was hypothesized that rinse solution ionic strength and pH would significantly influence ammonium transport and removal efficiency through cation exchange with ammonium on negatively-charged soil particle surfaces. Following all rinse injections, the effect of ammonium by-product removal on biocementation integrity was assessed through V_s, unconfined compressive strength, and calcite content measurements.

6.2 Materials and Methods

6.2.1 *Soil Column Specimens*

Four soil column specimens were prepared using 15.2 cm high, 7.6 cm inner diameter hollow acrylic cylinders, which included fittings for bender element sensors and aqueous sampling ports at mid-height (**Figure 6.2**). Top and bottom column caps with solution ports were used to confine soil specimens, exchange treatment solutions, and maintain soil saturation throughout the treatment process. In order to mitigate soil particulate losses during injections, Porex plastic filter material with pore sizes between 125 and 175 μm were placed between column caps and soils. All columns contained a poorly-graded Concrete Sand material (D_{10} = 0.18 mm, D_{30} = 0.45 mm, D_{60} = 1.81 mm, fines content of 2.7%) obtained from an alluvial deposit in Woodland, CA. Columns were prepared in three lifts using moist tamping to achieve initial relative densities near 53%. The initial porosity of all columns was 35% ± 1%, which corresponded to a single pore volume (PV) for each column of approximately 250 mL. Following soil preparation, a total stress of 100 kPa was applied to all soil columns using a reaction frame system and was maintained during the MICP

treatment process. The applied stress was intended to replicate conditions encountered within a saturated soil deposit at a depth near 10 meters. Prior to all injections, columns were saturated with de-ionized water and remained untreated for one day.

6.2.2 *Treatment Injections*

Treatment solution injections were performed for all soil columns in a series of three treatment phases. During the first treatment phase, all columns received identical stimulation injections to enrich soils for indigenous ureolytic soil microorganisms needed to complete the MICP process. Stimulation solutions contained 0.2 g/L yeast extract, 42.5 mM sodium acetate, 350 mM urea, 100 mM NH_4Cl, and were pH adjusted to an initial value of 9.0 following techniques shown to effectively select for ureolytic microorganisms (Gomez et al. 2018a). The first stimulation solution injection was retained within columns for 48 hours, following previous observations of limited cell growth and ureolytic activity during the first treatment residence period (Gomez et al. 2018a). After this first extended retention period, all subsequent stimulation injections were applied once daily. After three stimulation injections, sufficient ureolytic activity was detected and columns were transitioned to the cementation treatment phase during which soluble calcium was included in applied treatment solutions to initiate calcite precipitation and cement soil materials. Immediately before the first cementation injection, a “flush” solution containing 0.1 g/L yeast extract, 42.5 mM sodium acetate, 350 mM urea, and 100 mM NH_4Cl was applied to reduce carbonate concentrations in soil columns and prevent immediate calcite precipitation at the high calcium and high carbonate mixing front (Gomez et al. 2017). A total of 10 cementation treatments were applied to all columns targeting a final calcite content between 4 to 5% by mass. Cementation

solutions contained 0.1 g/L yeast extract, 42.5 mM sodium acetate, 350 mM urea, 12.5 mM NH_4Cl, and 250 mM calcium chloride following previous employed techniques (Gomez et al. 2017; 2018a). All treatment volumes for stimulation and cementation injections were 375 mL (1.5 PV), which were intended to fully replace solutions within columns after each injection.

Figure 6.2. Soil columns received solutions using a peristaltic pump and included sampling ports and bender elements at mid-height for monitoring of V_s and pore fluid chemistry during treatments.

Following the last cementation injection, columns were transitioned to the ammonium removal rinse treatment phase. During this phase, columns received four different rinse solutions to investigate the effect of rinse solution ionic strength and solution pH on ammonium removal. Column 1 and 2 received rinse solutions with a low ionic strength of 0.06 M obtained from the addition of 10 mM calcium chloride and were pH adjusted to an initial pH of 5.0 and 9.0, respectively. Column 3 and 4 received rinse solutions with a high ionic strength of 2.5 M obtained from the addition of 500 mM calcium chloride and were also pH adjusted to an initial pH of 5.0 and 9.0, respectively. All rinse solutions were pH adjusted following the addition of calcium chloride through the addition of either sodium hydroxide or hydrochloric acid immediately prior to injection. The selection of calcium for rinse solutions was intended to examine the effect of a

high charge density cation (52 C mm^{-3}), which would be preferred for sorption on soil particle surfaces relative to ammonium (charge density of 11 C mm^{-3}). Rinse solution injections were applied once daily in volumes of 250 mL (1 PV). Following the application of 5 rinse injections, all solutions resided in soil columns for an additional 103 days during which no further rinse treatments were performed.

6.2.3 *Shear Wave Velocity Measurements*

Shear wave velocity (V_s) measurements were completed using piezo-ceramic bender element sensor pairs oriented perpendicular to columns at mid-height. Bender elements were assembled following procedures outlined in Montoya et al. (2012), but were isolated from the highly conductive aqueous environment using a multi-step Hysol epoxy and electronics wax coating process. All transmitting bender elements were excited using a 24V 100 Hz square wave generated by a signal generator and all received signals were measured and recorded with an oscilloscope using a sampling frequency of 1 MHz. V_s values were determined from visual interpretation of S-wave arrivals and known sensor spacings.

6.2.4 *Aqueous Chemical Measurements*

Solution samples of approximately 2 mL were collected from soil column sampling ports using sterile syringes and needles before and after each injection during stimulation, cementation, and rinse treatment phases. Following collection, solution samples were stored frozen until chemical measurements were completed. Solution pH measurements were completed using a semi-micro pH electrode and meter system that was calibrated daily using a three-point buffer sequence (4.01,

7.00, 10.00) and had ± 0.01 pH unit accuracy. Urea measurements were completed using a colorimetric urea assay modified from Knorst et al. (1997) wherein a colorimetric reagent consisting of 4% (weight/volume) p-Dimethylaminobenzadehyde, and 4% (volume/volume) HCl in 99.8% ethanol was added to dilute sample volumes and absorbance values were measured at 422 nm using a microplate spectrophotometer. Total ammonium measurements were completed using a salicylate reaction method, wherein two reagents (Reagent A & B) were added to dilute sample volumes and absorbance values were measured at 650 nm using a microplate spectrophotometer. Reagent A consisted of 0.05% (weight/volume) sodium nitroprusside, 13% (weight/volume) sodium salicylate, 10% (weight/volume) sodium citrate, and 10% (weight/volume) sodium tartrate in water. Reagent B consisted of 5% sodium hypochlorite (volume/volume) and 6% sodium hydroxide (weight/volume) in water. Bromide measurements were completed using a calibrated bromide Orion ion-selective probe and meter.

6.2.5 *Ammonium Bromide Tracer Testing*

Ammonium bromide tracer testing was performed prior to all stimulation and cementation treatments. During tracer testing, a 59 mM ammonium bromide solution was first injected into soil columns at a constant rate of 10 mL per minute using a peristaltic pump for a total volume of 750 mL (≈ 3 PV). Following this ammonium bromide injection, de-ionized water was then subsequently applied for a total volume of 750 mL (≈ 3 PV) at the same flow rate. During both injection periods, solution samples of at least 5 mL were collected from the column effluent port every 2.5 minutes for subsequent ammonium and bromide breakthrough curve analysis.

6.2.6 *Unconfined Compressive Strength Measurements*

Unconfined compressive strength (UCS) testing was completed on biocemented soil columns after all rinse treatments following ASTM D2166. Prior to UCS testing, soil columns were drained, oven-dried, and extrusion was completed using a hydraulic jack and frame. During loading, a constant axial strain rate of 1% per minute was maintained and measurements were electronically recorded using a GDS load frame data acquisition system.

6.2.7 *Calcite Content Measurements*

Following UCS testing, soil columns were partitioned along their length into four discrete sections at varying distances from the injection port (0 to 38 mm, 38 to 76 mm, 76 to 114 mm, 114 to 152 mm). Soil sections were then oven-dried and homogenized to yield subsamples for calcite content measurements. Calcite content was quantified in accordance with ASTM D4373 by reacting calcite in soil samples with 1M hydrochloric acid to generate CO_2 gas and a corresponding increase in test chamber pressure. Relationships between chamber pressure and calcite masses were used to determine sample calcite contents from observed pressures. A minimum of three measurements were completed for each soil section.

6.3 Results and Discussion

6.3.1 *Ammonium Bromide Tracer Testing*

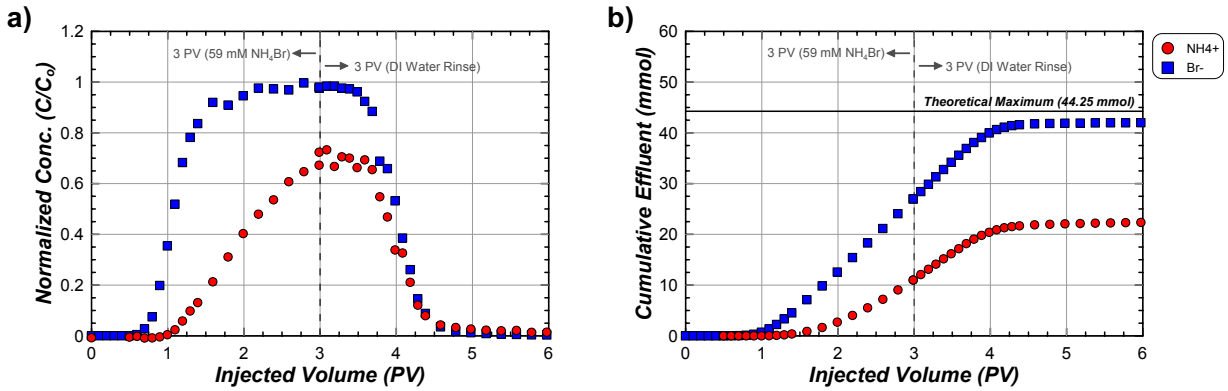

Figure 6.3. (a) Normalized concentrations of bromide (Br^-) and total ammonium (NH_4^+) measured during 59 mM NH_4Br tracer testing, (b) cumulative mmol of bromide and ammonium determined from measured effluent concentrations and injected volumes.

Figure 6.3a presents normalized concentrations of bromide (Br^-) and total ammonium (NH_4^+) measured during ammonium bromide tracer testing from soil column effluent. All measurements were completed before MICP treatments and were intended to examine the transport of ammonium ions in a relatively clean sand relative to non-reactive (passive) bromide ions. As shown, non-zero concentrations of bromide were first detected in soil column effluent after injecting 0.75 PV of the ammonium bromide solution. In contrast, non-zero concentrations of ammonium were observed only after the injection of more than 1 PV of ammonium bromide solution. The significant delay or retardation of the arrival of ammonium ions at the column effluent location in comparison to the bromide passive tracer suggested that the injected ammonium ions experienced significant reactivity (sorption) during transport through soil columns. Following the injection of 2.0 PV of the ammonium bromide solution, normalized bromide concentrations achieved values near 0.97

and remained constant during the remaining 1 PV of pumping. At these same times, much lower normalized concentrations of ammonium near 0.40 and 0.67 were observed after 2 and 3 PV of ammonium bromide solution, respectively. After transitioning to the injection of de-ionized water after 3 PV, the passive bromide tracer exhibited similar behaviors as that seen during initial injections. Reductions in bromide ion concentrations were first detected after injection of 0.60 PV of de-ionized water and normalized concentrations below 0.05 were observed after injection of approximately 1.6 PV. Similar behaviors for normalized ammonium concentrations were also observed, with concentrations dropping from 0.67 to near 0.04 after 1.6 PV of de-ionized water.

While these results suggested significant sorption of ammonium on soil particles surfaces had occurred, the mass of ammonium retained on soil surfaces remained unclear. In order to examine this further, cumulative moles of ammonium and bromide ions from soil column effluent measurements were determined by integrating measured effluent concentrations over the injected volume and plotted versus injected solution volume in **Figure 6.3b**. The theoretical maximum moles of bromide and ammonium obtainable from the injected solutions are shown as 44.25 mmol and were determined by multiplying 0.75 L (3 PV) by the injected ammonium bromide concentration of 59 mM. For bromide ions, the cumulative mmol of measurements approached a value near 41.9 mmol suggesting that almost all injected bromide could be accounted for through integration of the breakthrough curves shown in **Figure 6.3a**. In contrast, the cumulative mmol of ammonium ions approached much smaller values near 22.3 mmol suggesting that only ≈ 53% of injected ammonium could be accounted for through effluent concentrations and therefore ≈ 47% (19.7 mmol) was retained within the soil column. These results suggest that the transport of ammonium in soils during MICP may not only be strongly retarded when compared to passive

ions, but some produced ammonium may also remain sorbed to soil surfaces resulting in a fraction of ammonium, which may remain unavailable for removal through advective-dispersive transport alone.

6.3.2 *Aqueous Solution Chemistry*

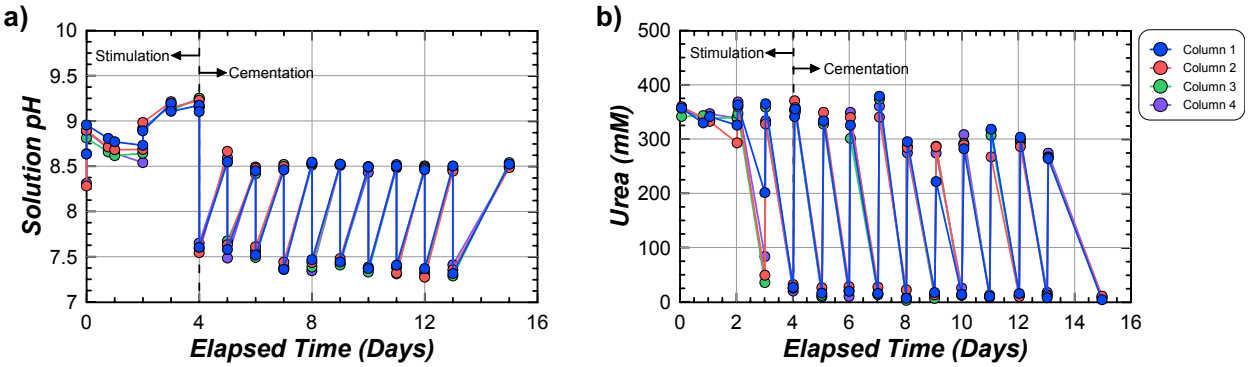

Figure 6.4. (a) Solution pH and (b) urea measurements during stimulation and cementation phases.

Aqueous chemical measurements of solution pH (**Figure 6.4a**) and urea (**Figure 6.4b**) were completed before and after all injections during the stimulation and cementation treatment phases to monitor changes in ureolytic activity and calcite precipitation occurring during the treatment process. As shown in **Figure 6.4a**, solution pH values increased from 8.4 to near 9.0 following application of the enhanced stimulation solution. During the first retention period (Day 0 to 2), pH values in all columns decreased from near 9.0 to near 8.5 over 48 hours likely resulting from soil solution equilibration. During this same time, almost no urea degradation was detected with the exception of Column 2 wherein 60 mM degradation was observed. After the second stimulation injection from Day 2 to 3, solution pH again reached 9.0 and increased over the residence period to values near 9.2. During this time, urea degradation of ≈ 150 mM was detected in Column 1 and

urea degradation between 270 mM and 315 mM was observed in Columns 2, 3, and 4. From Day 3 to 4, pH values remained near 9.2 and near full urea degradation (≈ 350 mM) was detected in all columns. On Day 5, all columns received a "flush" treatment to remove excess carbonate immediately prior to cementation and a cementation solution injection was applied. Immediately after the first cementation solution injection, pH values in all columns decreased to near 7.6 due to the presence of calcite precipitation, which yields protons (H^+) during carbonate consumption. During the first cementation treatment from Day 4 to 5, pH values increased from 7.6 to 8.6 and full urea degradation was again observed. Similar sequences of decreases in pH and increases in urea after injections followed by increases in pH and decreases in urea were observed for all subsequent cementation treatments suggesting continued hydrolysis of injected urea concentrations and full utilization of injected calcium concentrations (Gomez et al. 2018a). No significant differences were observed between columns during the cementation process suggesting that columns were nearly identical prior to all rinse treatments.

6.3.3 *Shear Wave Velocity*

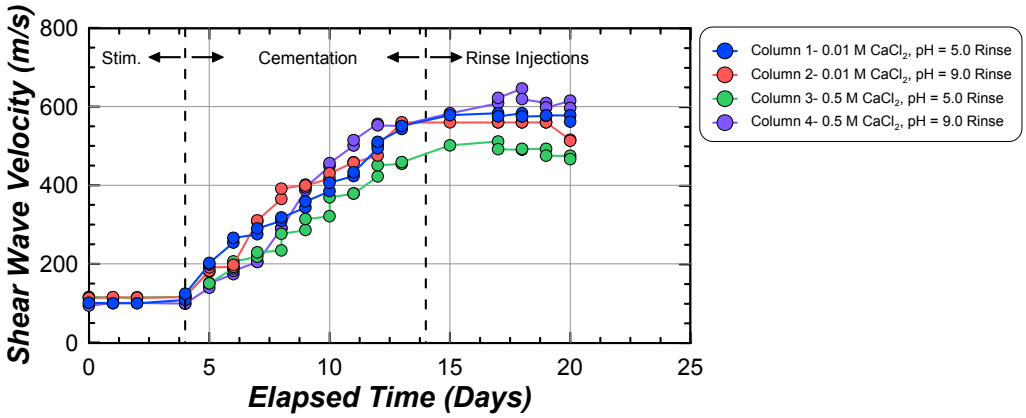

Figure 6.5. Shear wave velocities (V_s) measured in all soil columns during stimulation, cementation, and ammonium removal rinse phases.

Figure 6.5 presents soil shear wave velocity measurements completed for all columns immediately before stimulation, cementation, and ammonium rinse treatment injections. As shown, immediately prior to treatments (Day 0), V_s values for all columns were between 100 and 115 m/s. During stimulation (Day 0 to 4), no noticeable increases in shear wave velocities were detected due to the absence of soluble calcium in treatment solutions and therefore lack of calcite precipitation. Following the introduction of calcium and the initiation of calcite precipitation on Day 4, shear wave velocity values in all columns increased almost linearly to values between 510 and 640 m/s after 10 cementation injections. These values were slightly lower than previous soil column experiments wherein increases to values near 750 m/s have been observed over similar treatment intervals (Gomez and DeJong 2017). Following the start of ammonium rinse treatments, V_s values in all columns remained relatively constant despite differences in rinse solution chemistry. For Columns 1 and 3, which received the most acidic solutions (pH = 5.0), only slight reductions in V_s values between 30 and 40 m/s over five injections were observed. In Columns 2 and 4, which received the most alkaline solutions (pH = 9.0), similar V_s reductions of 20 to 50 m/s were observed. These reductions in soil V_s during rinsing may be related to the dissolution of more soluble carbonate precipitates and salts that may have precipitated during the treatment process as well as dissolution of produced calcite. Only modest reductions in V_s values suggested that rinse solution chemistry did not appear to significantly influence biocementation integrity at column mid-depth locations during ammonium removal rinse injections. It remained unknown, however, if rinse solution injections resulted in more significant dissolution of calcite at other locations outside of the zone of soil primarily influencing V_s measurements.

6.3.4 *Ammonium Removal*

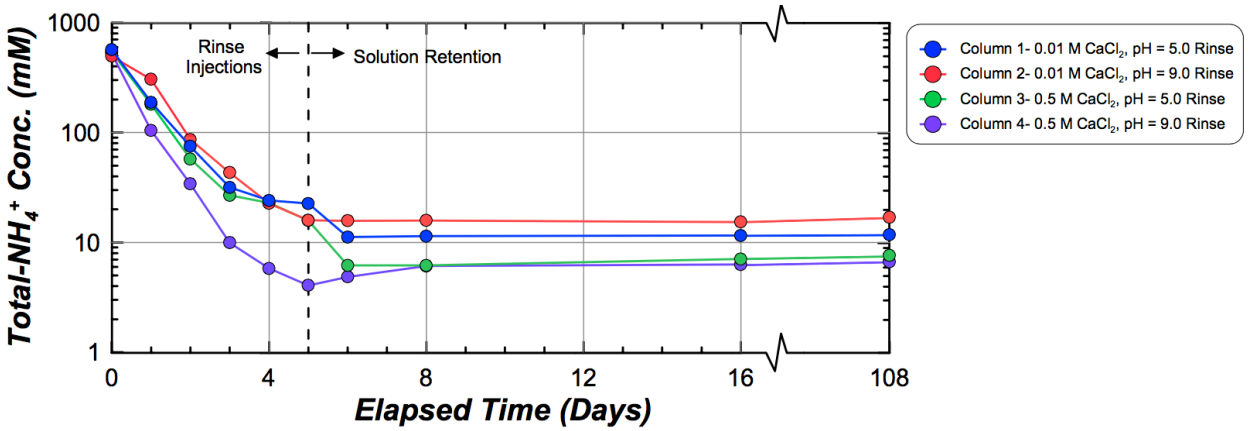

Figure 6.6. Aqueous total ammonium (NH_4^+/NH_3) concentrations at mid-height in soil columns during ammonium removal rinse injections and the 103-day solution retention period.

Aqueous total ammonium concentrations were measured in all soil columns at mid-height before ammonium removal rinse injections and at various points in time during the 103-day solution retention period. Figure 6.6 presents total ammonium concentrations versus time after cementation for all four columns over the 108-day rinse and monitoring period. As shown, in all columns immediately after the last cementation treatment, total ammonium concentrations were between 494 and 567 mM. These values were considerably less than the 700 mM expected to result from 350 mM urea by reaction stoichiometry. Following the first rinse injection, total ammonium concentrations were reduced to 33%, 62%, 33%, and 20% of the initial NH_4^+ concentration in columns 1 through 4, respectively. After 3 rinse injections, total NH_4^+ concentrations were further reduced to 5.6%, 8.7%, 4.9%, and 1.9% of the initial concentration in columns 1 through 4, respectively. Following the completion of all five rinse injections, total NH_4^+ concentrations were further reduced to 2.0%, 3.2%, 1.1%, and 0.9% of the initial NH_4^+ concentration in columns 1 through 4, respectively. This corresponded to NH_4^+ concentrations ranging from 15.7 to 4.8 mM

in all columns. After 5 rinse injections, continued injections were not performed and solutions were allowed to reside in columns for an extended period of time to examine the potential for ammonium attenuation through either nitrification/denitrification or nitrogen mineralization during a 103-day retention period. During this time, no significant changes in aqueous ammonium concentrations were detected in any of the columns, suggesting that NH_4^+ concentrations observed after rinsing may persist for long periods of time following MICP treatments unless additional efforts are made to actively remediate NH_4^+ *in situ* or further remove NH_4^+ through rinse injections. The highest NH_4^+ removal observed in column 4, which received high pH and high ionic strength solutions, may be related to several factors. First, it is hypothesized that higher Ca^{2+} concentrations improved NH_4^+ removal efficiency through increased cation exchange with NH_4^+ on soil particle surfaces. Second, the use of high solution pH may have driven the speciation of total NH_4^+ to the uncharged species NH_3 which may be more readily removed from soil columns. At later times during the residence period it appears that both high ionic strength columns (Column 3 and 4) achieved similar NH_4^+ removal, suggesting that ionic strength may be a primary variable governing ammonium removal efficiency with pH having only a secondary influence.

In order to further understand the effect of solution pH during NH_4^+ removal, solution pH values were measured in all columns during the rinse treatment period. As shown in Figure 6.7, in both high pH columns (Column 2 and 4), pH values between 8.2 and 8.75 were present during rinsing. In the high ionic strength Column 4, slightly higher pH values around 8.4 were observed likely resulting from increased buffering capacity from calcium hydroxide. In the low pH columns (Column 1 and 3), much lower pH values were obtained in the higher ionic strength Column 3 wherein pH values were generally between 6.3 and 6.8. In contrast in the low ionic strength

Column 1, pH gradually decreased from 8.6 to near 7.1 over 5 days and remained relatively constant during the retention period. Despite injecting solutions at pH=5.0, all pH values measured in Columns 1 and 3 were significantly higher (pH = 6.3 to 7.5), suggesting that acidic solutions were made more alkaline during transport within soil columns. It is hypothesized that pH increases were not the result of residual ammonium buffering, which is a poor buffer at low pH values, but rather due to alkalinity generated from the dissolution of calcite. The lack of significant differences in NH_4^+ removal efficiency between Column 3 and 4 at late time, suggests that changes in pH may not significantly influence NH_4^+ removal and therefore higher pH solutions may be preferred to limit calcite dissolution during rinsing.

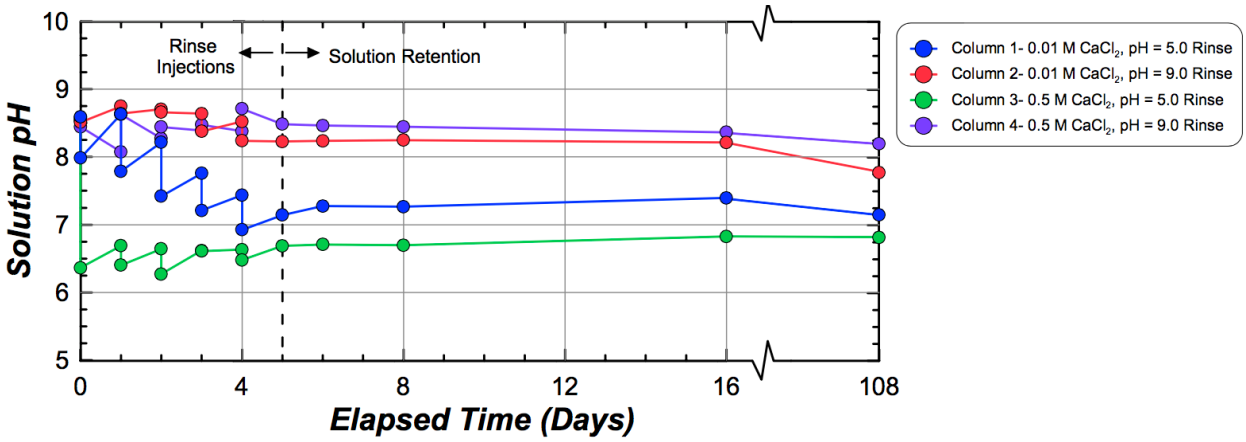

Figure 6.7. Solution pH values at mid-height in soil columns during ammonium removal rinse injections and the 103-day solution retention period.

6.3.5 *Unconfined Compressive Strength*

During unconfined compressive strength (UCS) testing, all columns experienced brittle failures at axial strains ranging between 0.2% and 1.8%. In Columns 1 and 3, which received acidic (pH= 5.0) rinse solutions, UCS values of 256 and 140 kPa were measured, respectively. In Columns 2

and 4, which received alkaline (pH= 9.0) rinse solutions, similar UCS values of 358 and 166 kPa were observed, respectively. These observed UCS values were significantly lower than expected for the V_s values measured and may have been influenced by column damage observed during the soil column extrusion process. In the most acidic rinse solution columns, localized cracking and crushing was observed near injection port locations suggesting that materials may have been weakened near the injection site from calcite dissolution.

6.3.6 *Calcite Content*

Figure 6.8 presents calcite contents measurements completed for discrete soil sections with mid-depths located at four distances from the injection port. Error bars shown indicate one standard deviation from average values for each section and were generally between 0.3% and 0.6%, with slightly more variability observed in acidic rinse solution columns (Column 1 and 3). Overall average calcite contents for entire columns were 5.0%, 4.4%, 4.6%, and 5.2% by mass for columns 1 through 4, respectively. Despite similar average calcite content values between columns, significant differences in calcite content trends along columns lengths were observed between acidic and alkaline rinse solution columns. Near the injection port location (19 mm), alkaline rinse solution columns (Column 2 and 4) had the highest calcite contents of 5.5% and 5.8%, respectively, however, calcite contents decreased to values between 3.0% and 4.2% near the column effluent port location (133 mm). In acidic solution columns (Column 1 and 3), the lowest calcite contents of 4.7% and 3.8%, respectively, were observed near the injection port location, however, calcite contents increased to values near 5.2% at the column effluent port. Significant differences in calcite content trends along column lengths are believed to result from additional precipitation near the injection port in alkaline columns (Column 2 and 4) and dissolution at the injection port and re-

precipitation of calcite near the effluent port resulting from carbonate buffering in acidic columns (Column 1 and 3). Despite these differences, at column mid-depths, where bender element sensors were located (76 mm), average calcite contents were similar values of 5.0%, 4.5%, 4.6%, and 5.4% for columns 1 through 4, respectively.

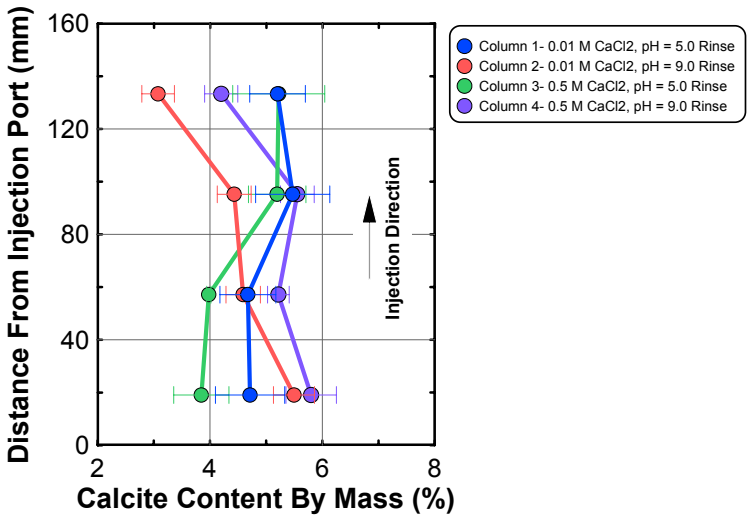

Figure 6.8. Average calcite contents for column sections versus distance from injection port (error bars represent one standard deviation from average values).

6.4 Conclusions

A preliminary investigation of the removal of total ammonium from a biocemented poorly graded sand was performed to understand the effect of rinse solution chemistry on ammonium removal efficiency, biocementation integrity, and potential for long-term attenuation. The results of this study suggest that ammonium transport may be significantly retarded in clean sands (fines content of less than 3%) when compared to a passive tracer, likely resulting from NH_4^+ sorption on negatively-charged soil surfaces. Following the injection of a 59 mM ammonium bromide solution, ≈ 47% of injected NH_4^+ was retained within soil columns and could not be accounted for through

effluent chemical measurements. During MICP treatments, similar reaction chemistry and cementation was verified in all columns through urea, solution pH, and shear wave velocity measurements. During post-treatment rinse injections, results suggested that removal of NH_4^+ may be primarily governed by rinse solution ionic strength with rinse solution pH having a much smaller effect. After five 1 PV rinse injections, columns receiving 2.5 M ionic strength solutions achieved reductions in NH_4^+ concentrations from post-treatment values near 540 mM to values between 5 and 6 mM (98.9% to 99.1% removal) and columns receiving lower 0.06 M ionic strength solutions achieved reductions to higher values between 11 and 16 mM over five injections (96.8% to 98.0% removal). During the 103-day retention period, NH_4^+ concentrations remained relatively constant in all columns suggesting limited potential for natural attenuation without further modification of column conditions. In all cases, post-rinsing NH_4^+ concentrations exceeded recommended concentrations of ammonium for aquatic life suggesting that more than 5 PV of rinse injections may be required to remove NH_4^+ at sufficient levels following MICP in 1D flow. Although calcite content measurements indicated significant differences in biocementation distributions between columns treated with acidic and alkaline rinse solutions, mid-depth V_s and UCS measurements suggested no consistent differences following rinsing. Further investigation is needed to fully understand the effect of NH_4^+ removal on biocementation engineering properties.

Chapter 7. EXAMINATION OF RINSE INJECTION STRATEGIES FOR REMOVAL OF AMMONIUM BY-PRODUCTS FOLLOWING BIOCEMENATATION SOIL IMPROVEMENT

This chapter has been submitted as a journal paper entitled, “Examination of Rinse Injection Strategies for Removal of Ammonium By-products Following Biocementation Soil Improvement” to *Engineering Geology*. This paper was authored by Minyong Lee and Michael G. Gomez.

ABSTRACT

Bio-mediated soil improvement technologies leverage microbial enzymatic and metabolic processes to generate minerals, gases, and biopolymers that can improve soil engineering behaviors with the potential to reduce detrimental environmental impacts when compared to conventional methods. Ureolytic biocementation is perhaps the most widely researched of these processes and relies on urea hydrolysis in the presence of soluble calcium to initiate the precipitation of calcium carbonate minerals on soil particle surfaces and contacts, thereby improving soil mechanical behaviors. Although effective, urea hydrolysis generates aqueous ammonium by-products that may result in undesirable environmental and human health impacts, if left unaddressed. Recent studies have shown the potential of rinse solution injections to effectively remove generated ammonium following biocementation, however, critical gaps remain in our understanding of the effect of rinse solution composition and injection strategies. In this study, sixteen soil column experiments were performed to investigate the effect of rinse solution cation types, cation concentrations, applied injection sequences, and biocementation treatment variations on the removal of ammonium from a biocemented poorly-graded sand. All columns receiving cation-enriched rinse solutions achieved greater than 98% aqueous, 65% sorbed, and 95%

total ammonium removal after injecting 12 pore volumes (PV), with no detectable impacts on cementation integrity. Cation-enriched solutions specifically enhanced sorbed ammonium removal and achieved sorbed ammonium concentrations up to 2 orders of magnitude less than those observed in columns rinsed with deionized water alone. Columns receiving K^+-based rinse solutions and twelve daily 1 PV rinse injections also achieved greater total ammonium removal when compared to comparable columns receiving rinse solutions containing other cations and continuous 12 PV rinse injections.

7.1 Introduction

Bio-mediated soil improvement technologies have advanced rapidly in the past two decades, motivated in part by the need to address unprecedented natural hazards within the context of emerging societal and environmental constraints related to population growth, urbanization, and climate change (DeJong et al. 2013; DeJong & Kavazanjian 2019). Bio-mediated methods leverage the capabilities of microorganisms already present in the geotechnical subsurface to generate a diverse range of products, including inorganic mineral precipitates, gas phases, and biopolymers, which can dramatically improve soil engineering behaviors (DeJong et al. 2010, 2013). Such processes offer the exciting potential to reduce detrimental environmental impacts when compared to other more traditional ground improvement methods by eliminating the need for high-energy (e.g., portland cement) and potentially environmentally hazardous chemicals (e.g., polyurethane) (Seagren and Aydilek 2010; DeJong et al. 2010). Biocementation is perhaps the most well-researched bio-mediated process and uses enzymatic and microbial processes to generate calcium carbonate ($CaCO_3$) minerals that can coat and cement soil particles together, altering interparticle cohesion, particle surface roughnesses, and bulk dry densities (Ferris et al.

1996; Stocks-Fischer et al. 1999; DeJong et al. 2006, 2022). Biocementation methods, including Enzymatically-Induced Calcium Carbonate Precipitation (EICP) (Hamdan and Kavazanjian 2016) and Microbially-Induced Calcium Carbonate Precipitation (MICP) (DeJong et al. 2006), rely on the biologically-mediated hydrolysis of urea to generate aqueous carbonate species, which in the presence of sufficient soluble calcium can supersaturate soil pore fluids and enable $CaCO_3$ precipitation (Mobley et al. 1995; Stocks-Fischer et al. 1999; Ferris et al. 2004; Gomez et al. 2019). Although not strictly integral to the formation of $CaCO_3$ minerals, the use of urea hydrolysis also results in the production of aqueous ammonium (NH_4^+) by-products, which allow carbonate molecules needed for $CaCO_3$ precipitation to become increasingly availabile through hydroxide generation.

Despite being initially developed for oil recovery and extraction purposes (Ferris et al. 1996), MICP has received significant attention for a variety of different geotechnical applications, owing to its ability to achieve dramatic enhancements in soil shear strength and stiffness, while largely preserving porous soil structure and initial hydraulic conductivities (DeJong et al. 2006, 2022; Montoya and DeJong 2015; Gomez et al. 2018a; Nafisi et al. 2020). Recent studies have highlighted the potential of MICP to address an expanding range of geotechnical and geoenvironmental applications including general ground improvement (Martinez and DeJong 2009; van Paassen et al. 2010b; Montoya & DeJong 2015; Feng and Montoya 2016; Gomez et al. 2017; Lin et al. 2016; Gao et al. 2019), liquefaction mitigation (Montoya et al. 2013; Simatupang and Okamura 2017; Simatupang 2018; Darby et al. 2019; Zamani and Montoya 2019; Riveros and Sadrekarimi 2020a; Lee et al. 2022), rock fracture sealing (Cuthbert et al. 2013; Phillips et al. 2016; Minto et al. 2016), concrete remediation (Ramakrishnan et al. 2001; Ramachandran et al. 2001;

De Muynck et al. 2008), soil scour and erosion prevention (Gomez et al. 2015; Montoya et al. 2018; Tao et al. 2018; Ghasemi and Montoya 2020), divalent contaminant immobilization (Fujita et al. 2004; Bhattacharya et al. 2018; He et al. 2019; Jiang et al. 2019), and the development of sustainable construction materials (Bernardi et al. 2014; Fang et al. 2021).

In stark contrast to these continuous advances in ureolytic biocementation, the management and removal of generated NH_4^+ by-products has remained a persistent and largely unresolved challenge that has limited practical demonstration and adoption of the technology (DeJong et al. 2013; Gat et al. 2017; Lee et al. 2019a; 2019b). Although the magnitudes of generated NH_4^+ concentrations can be controlled through modification of supplied urea concentrations, the molar ratio of NH_4^+ generated per $CaCO_3$ molecule remains fixed near 2:1 due to reaction stoichiometry (van Paassen 2009; El Mountassir et al. 2018; Gomez et al. 2019) with no clear opportunities for NH_4^+ reductions without simultaneous decreases in biocementation magnitudes. If left unaddressed in treated soils and surrounding groundwater, generated NH_4^+ concentrations may result in detrimental human health and environmental impacts including those related to increased eutrophication of surface waters (Paerl et al. 1997). Although no maximum contaminant levels have been established by the U.S. EPA for total NH_4^+ in drinking water, maximum total NH_4^+ concentrations for aquatic life of 17 mg/L (≈ 1 mM) and 1.9 mg/L (≈ 0.1 mM) at a pH of 7.0 for acute (1 hour) and chronic (30 day) exposure, respectively, have been recommended (U.S. EPA, 2013). Limits for total NH_4^+ in surface water bodies are location specific; but these limits generally range between 0.25 mg/L (≈ 0.01 mM) and 32.5 mg/L (≈ 1.8 mM) across the U.S. (ODHS, 2020). More broadly, the European Union has set a maximum total NH_4^+ concentration for drinking water at 0.5 mg/L (≈ 0.03 mM) (European Union, 2020). While acceptable post-treatment total NH_4^+

concentrations will likely be site-specific, aqueous NH_4^+ concentrations produced during biocementation will likely exceed such recommendations by several orders of magnitude, therefore necessitating removal and/or *in situ* remediation in order to meet site water quality requirements.

Few studies have investigated the post-treatment management and removal of generated NH_4^+ from biocemented soils and groundwater (Cuthbert et al. 2013; van Paassen 2011; Gat et al. 2017; Lee et al. 2019a, 2019b; Yu et al. 2021), however, three primary management strategies have been proposed, namely: (1) *in situ* biogeochemical transformations of produced NH_4^+ into more benign end-products, (2) removal of NH_4^+ from treated soils with subsequent remediation of generated effluent *ex situ*, and (3) avoidance of NH_4^+ generation altogether through the use of alternative microbial pathways (i.e., denitrification, carbonic anhydrase) to generate the aqueous carbonate species required for biocementation (van Paassen et al. 2010a; Dhami et al. 2016; Hamdan et al. 2017; Wang et al. 2020). While microbial transformations of produced NH_4^+ to nitrite (NO_2^-) and nitrate (NO_3^-) via nitrification and subsequent denitrification of intermediate products to dinitrogen gas (N_2) may be a possible pathway for *in situ* treatment (Gat et al. 2017), the required fluctuations in subsurface dissolved oxygen concentrations may present significant implementation challenges. In addition, although alternative microbial pathways for biocementation, such as microbial denitrification, have proven to be successful, clear drawbacks include the need for substantially longer treatment times, lower magnitudes of biocementation generated per treatment, and limited understanding of the fate of supplied reactants (e.g., NO_3^{2-}) (van Paassen et al. 2010a; Moug et al. 2020), all of which suggest that alternative processes will not likely fully supplant the continued interest in and need for ureolytic biocementation.

Albeit limited, almost all previous investigations have examined the removal of NH_4^+ from treated soils using post-treatment rinse injections, which act to remove generated NH_4^+ from both soil solutions and surfaces with further remediation occurring *ex situ* via wastewater treatment systems, if desired (Lee et al. 2019a, 2019b; Gowthaman et al. 2021; Mohsenzadeh et al. 2021). These studies have both improved our understanding of NH_4^+ transport in biocemented soils and demonstrated the effectiveness of such processes. For example, Lee et al. (2019b) found that the transport of NH_4^+ in soils was retarded due to interactions with negatively-charged soil particles with NH_4^+ removal improved when alkaline and high ionic strength rinse injections were provided, which promoted cation exchange and speciation of NH_4^+ as charge-neutral ammonia (NH_3). Lee et al. (2019a) leveraged the previously identified rinsing techniques and examined NH_4^+ by-product removal in meter-scale soil column experiments involving five different poorly-graded sands wherein Ca^{2+}-based solutions were applied in a single 12 PV continuous injection after biocementation and achieved over 98% aqueous NH_4^+ removal in all columns. Gowthaman et al. (2021) examined NH_4^+ removal and recovery in poorly-graded sands that were initially saturated using NH_4Cl solutions intended to simulate MICP treatments with subsequent investigation of aqueous NH_4^+ removal via rinsing and NH_4^+ recovery as struvite ($NH_4MgPO_4 \cdot 6H_2O$) minerals using *ex situ* additions of phosphate (PO_4^{2-}) and magnesium (Mg^{2+}). Yu et al. (2021) examined the ability of phosphate-rich solutions to immobilize ammonia gases generated during the biocementation process through struvite precipitation. Collectively, these studies have demonstrated that rinse injections can be used to effectively remove generated NH_4^+ following ureolytic biocementation, however, such methods also necessitate both significant cation additions and injected solution volumes in order to reduce NH_4^+ concentrations to levels likely needed for

field-scale applications. An opportunity exists to improve the material-efficiency of rinse injection strategies in order to minimize the financial and environmental impacts of post-treatment NH_4^+ removal. Specifically, the effect of variations in MICP treatment designs and rinse strategy characteristics including rinse injection sequencing, supplied cation types, and supplied cation concentrations have remained largely unexplored. An improved understanding of such effects remains critical towards further optimizing post-treatment rinsing strategies and ensuring the continued development of ureolytic biocementation towards practical adoption.

In this study, sixteen soil column experiments were performed to investigate the efficacy of various rinsing strategies towards removing generated NH_4^+ following ureolytic biocementation. All columns contained the same poorly-graded sand and received daily stimulation and cementation injections over 6 and 10 days, respectively, intended to enrich native ureolytic microorganisms and achieve similar post-treatment NH_4^+ concentrations and average $CaCO_3$ contents near 3.5% by mass. Although the majority of columns received identical biocementation treatments, three columns received modified treatments intended to evaluate the effect of alternative NH_4^+ management strategies including (i) "pre-treatment" of soil particles with KCl rinse solutions intended to limit NH_4^+ sorption on soil surfaces during MICP, (ii) augmentation of MICP treatment solutions with KCl intended to encourage NH_4^+ removal during MICP, and (iii) reductions in applied MICP reagent concentrations intended to reduce generated NH_4^+ concentrations. Following cementation, all but one column received alkaline rinse solution injections containing one of three different cations (Ca^{2+}, Na^+, K^+) at varying concentrations or deionized water. Rinse injections were applied in either a single 12 PV injection (continuous injections) or twelve 1 PV daily injections (staged injections), which maintained an identical injection volume between all

columns. A single column also received no rinse injections intended to quantify baseline NH_4^+ concentrations prior to rinsing. During treatments, aqueous samples were collected at various times to monitor changes in solution chemistry indicative of ureolysis, $CaCO_3$ precipitation, and NH_4^+ removal and soil shear wave velocities (V_s) were monitored to track both cementation progression and the potential impact of rinsing. Following all rinse injections, soil and fluid samples were obtained to quantify soil $CaCO_3$ contents and sorbed and aqueous NH_4^+ concentrations. The results of this study significantly improve our understanding of the effect of solution composition and injection sequencing on NH_4^+ removal following ureolytic biocementation using rinse injections.

7.2 Materials and Methods

7.2.1 *Soil Materials*

All soil columns contained a poorly-graded Concrete Sand material used extensively in past biocementation experiments involving stimulated indigenous ureolytic soil microorganisms (Gomez et al. 2014, 2017, 2018b, 2019; Graddy et al. 2018; Lee et al. 2019a, 2019b; San Pablo et al. 2020). Concrete Sand has a D_{10} of 0.23 mm, D_{30} of 0.54 mm, D_{60} of 1.54 mm, fines content of 1.1% by mass, and an e_{min} and e_{max} of 0.35 and 0.60, respectively (Gomez et al. 2014). The USCS classification for this soil was SP following ASTM D2487-10 (ASTM, 2017). Concrete Sand was quarried from a natural alluvial deposit in Woodland, CA and then commercially processed to remove fines. Previous sterile sampling and testing at this quarry location confirmed the presence of indigenous ureolytic microorganisms in these materials in the *in situ* condition (Gomez et al. 2018b). The cation exchange capacity (CEC) of Concrete Sand was determined to be 2.58 milliequivalents per 100 grams of soil following methods similar to those described in U.S. EPA

Method 9080 (U.S. EPA, 1986) and Lee et al. (2019a).

7.2.2 *Soil Columns Specimens*

S soil column specimens were prepared using hollow acrylic cylinders (15.2 cm height, 7.6 cm inner diameter) that included bender element sensors and aqueous sampling ports at mid-height to track changes in soil small-strain shear stiffnesses and aqueous chemical changes during treatments. Sand materials were contained within columns using custom-fabricated polytetrafluoroethylene (PFTE) top and bottom caps that had treatment ports which allowed for solution exchange while maintaining specimen saturation. Plastic filters (Porex Inc.) with pore sizes between 125 and 175 μm were placed between column caps and soil surfaces to minimize soil particulate losses during treatment injections. Sand materials were placed within columns in six lifts using moist tamping and achieved average porosities near 35% and pore volumes near 250 mL ± 13 mL. Spring-loaded reaction frames were used to apply a total vertical stress of 100 kPa to all specimens through column top caps, which was maintained throughout the treatment process. **Figure 7.1** presents images of soil column specimens including the treatment application system, shear wave velocity monitoring system and bender element sensors, column loading frames, injection and effluent treatment ports, and mid-height sampling ports.

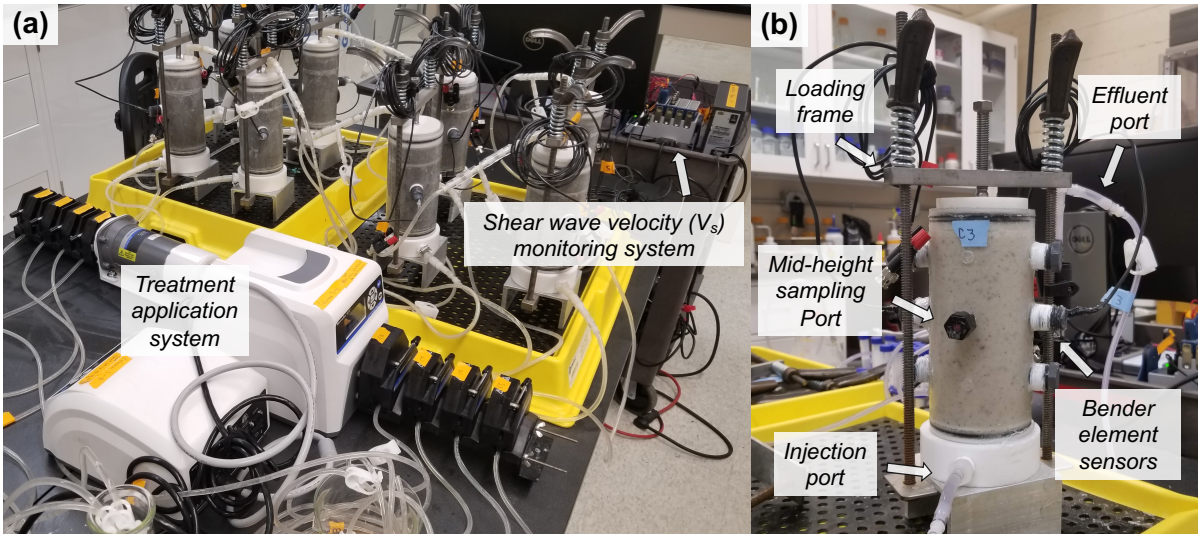

Figure 7.1. Images of (a) soil column experiments with treatment application and shear wave velocity monitoring system and (b) a single soil column with loading frame, sampling and treatment ports, and bender element sensors.

7.2.3 *Treatment Injections*

All treatment injections were applied to columns using flexible polyvinyl chloride tubing and peristaltic pumps that were connected to treatment ports on column caps via polypropylene barbed fittings. Treatments were applied from the bottom upwards to maintain saturation of columns and limit the potential influence of fluid density differences. Applied treatment solution volumes were 375 mL (≈ 1.5 PV) for all biocementation treatment injections (i.e., saturation/pretreatment, stimulation, cementation, carbonate reduction) and were designed to fully replace pore fluids residing within columns. Injection volumes only differed during passive tracer testing and rinse injections, as described later. All injections were applied at a constant flow rate of 10 mL/min (≈ 0.04 PV/min).

7.2.4 *Passive Tracer Testing*

Passive tracer testing was performed to verify that all columns achieved similar advective-dispersive transport conditions prior to biocementation treatments. All columns were first saturated using deionized water, which was allowed to reside within columns for 2 days prior to tracer testing. During passive tracer testing, each column received a 3 PV (750 mL) injection of a 50 mM NaBr solution followed by a 3 PV injection of deionized water at a flow rate of 10 mL/min. During both injections, aqueous samples were collected from the effluent port once every 3 to 5 minutes (≈0.12 to 0.2 PV) to monitor solution Br^- concentration changes. The conductivity of effluent samples was measured using a calibrated 4-cell conductivity probe (range = 1 µS/cm to 200 mS/cm) and meter (Fisher Scientific, Waltham, MA) and all values were normalized by the initial conductivity of the 50 mM NaBr solution (C_0) (5.33 mS/cm) to determine normalized Br^- concentrations (C/C_0) and breakthrough curves.

7.2.5 *Treatment Schemes*

All column specimens were named according to the following convention: (i) the first letter describes whether or not columns received either one continuous 12 PV injection (C) or twelve daily staged 1 PV injections (S); (ii) the second term describes the cation salts included within applied rinse solutions including either NaCl (Na), $CaCl_2$ (Ca), KCl (K), or deionized water (DI) which had no added salts; (iii) the third term describes the concentration of applied cation salts in mM (50, 200, or 500); and (iv) the fourth term, when provided, describes other treatment variations including the use of lower cementation reagent concentrations (L), pre-treatment of soil columns with KCl solutions prior to MICP treatments (P), or augmentation of treatment solutions with KCl

during the MICP process (T). Two columns received identical 12 PV continuous 200 mM $CaCl_2$ rinse injections, which were similar to that used by Lee et al. (2019a) and were repeated to assess the repeatability of experiments. The replicate number for these repeated experiments (C-Ca-200) is noted in the fourth term as either E1 or E2.

All columns received treatments in a series of five different treatment phases: (i) saturation/pre-treatment, (ii) stimulation, (iii) carbonate reduction, (iv) cementation, and (v) NH_4^+ rinsing. First, all columns were initially saturated with deionized water and remained saturated for 3 days prior to stimulation with the exception of a single column, which received a 1.5 PV 500 mM KCl solution injection 2 days after initial saturation and 1 day prior to stimulation (C-K-200-P). The KCl injection applied to C-K-200-P was intended to pre-treat soil surfaces with K^+ ions prior to ureolytic activity in order to limit subsequent sorption of NH_4^+ generated during MICP. K^+ ion additions were specifically investigated in our experimental program due to the frequent use of K^+ in soil NH_4^+ extraction protocols and the ability of K^+ to encourage desorption of NH_4^+ from soil surface sites (Keeney & Nelson 1982; Dorich & Nelson 1983; Lee et al. 2019a). Following saturation/pre-treatment, all columns received six daily 1.5 PV stimulation solution injections intended to enrich soils for indigenous ureolytic microorganisms. All but one column received standard stimulation solution injections containing 50 mM urea, 100 mM NH_4Cl, 42.5 mM sodium acetate, and 0.2 g/L yeast extract which were pH-adjusted using sodium hydroxide (NaOH) to an initial value of 9.0 following techniques similar to previous studies (Gomez et al. 2018b; San Pablo et al. 2020). A single column (C-K-200-T), however, received similar stimulation solutions that were instead augmented with 200 mM KCl, intended to encourage the removal of produced NH_4^+ during the treatment process.

Following stimulation, all columns received a single carbonate reduction solution injection that was identical to the standard stimulation solution but was not pH-adjusted. This solution was intended to remove high aqueous carbonate present within columns after stimulation to limit spontaneous chemically induced precipitation of $CaCO_3$ during the introduction of Ca^{2+} in subsequent cementation injections (Gomez et al. 2019). Immediately after the carbonate reduction injection, all columns received cementation solution injections containing soluble Ca^{2+} to initiate the bi-cementation process. Cementation injections were 1.5 PV and were applied once daily over 10 days, targeting final average $CaCO_3$ contents in columns near 5% by mass. All but two columns received standard cementation solutions containing 250 mM $CaCl_2$, 250 mM urea, 12.5 mM NH_4Cl, 42.5 mM sodium acetate, and 0.2 g/L yeast extract. The column receiving KCl-augmented stimulation injections (C-Ca-200-T), however, also received KCl-augmented cementation solutions that were identical to standard cementation solution but contained 200 mM KCl. An additional column received similar cementation solutions with lower 50 mM equimolar concentrations of urea and Ca^{2+} (C-Ca-200-L) intended to examine the impact of reductions in produced NH_4^+ concentrations. **Table 7.1** provides a summary of all MICP treatment solution compositions.

Table 7.1. Summary of MICP Treatment Solution Compositions for All Columns

			Solution Composition						
	Solution Type	**Column**	**KCl (mM)**	**$CaCl_2$ (mM)**	**Urea (mM)**	**NH_4Cl (mM)**	**Sodium Acetate (mM)**	**Yeast Extract (g/L)**	**Solution pH**
Saturation/ Pre-treatment	DI-water	All Other Columns	-	-	-	-	-	-	≈ 6.0
	KCl Pre-treatment	C-K-200-P	500	-	-	-	-	-	≈ 7.5
Stimulation	Standard Stimulation	All Other Columns	-	-	50	100	42.5	0.2	9.0 (adjusted)
	KCl-augmented Stimulation	C-K-200-T	200	-	50	100	42.5	0.2	9.0 (adjusted)
Carbonate Reduction	Carbonate Reduction	All Columns	-	-	50	100	42.5	0.2	≈ 7.1
Cementation	Standard Cementation	All Other Columns	-	250	250	12.5	42.5	0.2	≈ 8.3
	Low Conc. Cementation	C-Ca-200-L	-	50	50	12.5	42.5	0.2	≈ 7.7
	KCl-augmented Cementation	C-K-200-T	200	250	250	12.5	42.5	0.2	≈ 8.3

After completing all cementation injections, columns were transitioned to the NH_4^+ rinsing phase, during which alkaline rinse solutions of varying chemical compositions were applied in either a single 12 PV (3 L) continuous injection or twelve daily 1 PV (250 mL) injections. Injections were designed to maintain an identical rinse solution volume between all columns (12 PV) but allowed for investigation of the effect of rinse injection sequencing, which was expected to result in NH_4^+ removal differences due to the presence or absence of prolonged retention and equilibration periods. All but one column received rinse solution injections containing either $CaCl_2$, NaCl, or KCl at one of three different concentrations (50 mM, 200 mM, or 500 mM) or deionized water.

The inclusion of Ca^{2+}, Na^{+}, and K^{+} cations in applied rinse solutions was specifically considered to: (i) examine cations commonly found in natural soils that would be of minimal environmental concern, (ii) examine the impact of cation valence and charge densities on NH_4^{+} removal, and (iii) examine the performance of rinse solutions containing other cations than Ca^{2+} used in previous studies (Lee et al. 2019a; 2019b) with the potential to enable material cost and environmental impact reductions. All rinse solutions were pH-adjusted using NaOH to an initial pH of 9.0 following past studies, which suggested that alkaline solutions can improve NH_4^{+} removal due to increased speciation of NH_4^{+} as charge-neutral NH_3 (Lee et al. 2019a; 2019b). A single column received no rinse injections (No Rinse) and was used to quantify baseline NH_4^{+} concentrations present after biocementation in the absence of rinsing. Applied rinse injections extended upon past studies investigating the influence of ionic strength and initial pH on NH_4^{+} removal (Lee et al. 2019b) and were specifically designed to further examine the influence of cation type, cation concertation, rinse injection sequencing, and other biocementation treatment variations described previously. **Table 7.2** summarizes rinse solution compositions and injections for all columns.

Table 7.2. Summary of Rinse Injections for All Columns Including Solution Constituents and Injection Sequences

Rinse Solution Type	Column(s)	Injection Sequence	Rinse Solution Constituents			
			KCl (mM)	$CaCl_2$ (mM)	NaCl (mM)	Solution pH
500 mM Ca^{2+}	C-Ca-500	12 PV Continuous	-	500	-	9.0
200 mM Ca^{2+}	C-Ca-200-E1	12 PV Continuous	-	200	-	9.0
	C-Ca-200-E2	12 PV Continuous				
	S-Ca-200	1 PV Staged (12x)				
	C-Ca-200-L	12 PV Continuous				
50 mM Ca^{2+}	C-Ca-50	12 PV Continuous	-	50	-	9.0
500 mM Na^{+}	C-Na-500	12 PV Continuous	-	-	500	9.0
200 mM Na^{+}	C-Na-200	12 PV Continuous	-	-	200	9.0
50 mM Na^{+}	C-Na-50	12 PV Continuous	-	-	50	9.0
200 mM K^{+}	C-K-200	12 PV Continuous	200	-	-	9.0
	S-K-200	1 PV Staged (12x)				
	C-K-200-P	12 PV Continuous				
	C-K-200-T	12 PV Continuous				
DI-water	C-DI	12 PV Continuous	-	-	-	9.0
	S-DI	1 PV Staged (12x)				
None	No Rinse	N/A	N/A	N/A	N/A	N/A

7.2.6 *Aqueous Samples*

Aqueous samples were collected from column mid-height sampling ports and effluent locations at various times in order to examine changes in ureolytic activity, $CaCO_3$ precipitation, and NH_4^+ removal. During stimulation and cementation, aqueous samples (≈ 2 mL) were collected from all mid-height column sampling ports before and after treatment injections. During rinsing, sampling protocols varied depending on whether or not columns received continuous or staged injections. For columns receiving 12 PV continuous rinse injections (C), aqueous samples (≈ 2 mL) were obtained from effluent locations at least once every 0.5 PV and from mid-height sampling ports at least seven times during injections. When collecting effluent samples, a minimum volume of 2 mL

was purged from effluent tubing and discarded before collecting samples. For columns receiving staged 1 PV rinse injections (S), aqueous samples (≈ 2 mL) were only obtained from mid-height sampling ports before and after rinse injections. All aqueous samples were frozen immediately after collection and stored at -4ºC until subsequent chemical measurements were performed.

7.2.7 *Aqueous Chemical Measurements*

Solution pH measurements were completed using a semi-micro pH electrode and meter system that was calibrated daily using a three-point buffer sequence (4.01, 7.00, 10.00) and had ± 0.01 pH unit accuracy. Aqueous NH_4^+ measurements were completed using a salicylate reaction method similar to Krom (1980), wherein two reagents (Reagent 1 & 2) were added to dilute sample volumes and absorbance values were measured at 650 nm using a microplate spectrophotometer (Biotek Inc, Winooski, VT). Reagent 1 was composed of 1.9 mM sodium nitroprusside, 811 mM sodium salicylate, 387 mM sodium citrate, and 515 mM sodium tartrate in water. Reagent 2 was composed of 1.32 mM sodium hypochlorite and 1.5 M sodium hydroxide in water. Urea measurements were completed using an assay similar to Knorst et al. (1997) wherein a colorimetric reagent consisting of 216 mM p-dimethylaminobenzaldehyde, 2.32 M hydrochloric acid, and 13.83 M ethanol in water was added to dilute samples and absorbance values were measured at 422 nm using a microplate spectrophotometer. Aqueous Ca^{2+} measurements were completed using a QuantiChrom Ca^{2+} assay kit (BioAssay Systems, Hayward, CA) wherein samples were mixed with a colorimetric reagent, allowed to react for 10 minutes, and absorbance values were measured at 612 nm using a microplate spectrophotometer.

7.2.8 *Shear Wave Velocity Measurements*

Bender element sensor pairs were located at column mid-heights and were oriented perpendicularly in order to monitor changes in soil shear wave velocities (V_s). Bender elements were constructed from piezoelectric sheets (Piezo Inc., Woburn, MA) following procedures outlined in Montoya et al. (2012). Sensors were sealed using Hysol E-90FL epoxy (Henkel Corp., Düsseldorf, Germany) and electronics wax (Vishay Inc., Malvern, PA) following previous studies (Gomez et al. 2017). Transmitting bender elements were excited using a 100 Hz square wave generated by a CompactDAQ chassis data acquisition system (National Instruments Inc., Austin, TX) and 24-volt voltage supply (B&K Precision, Yorba Linda, CA). Received S-waves were measured and recorded using a Picoscope 5443D digital oscilloscope (Picoscope Inc., Cambridgeshire, UK) at 1 MHz. V_s values were determined from visual interpretations of S-wave arrivals and known sensor spacings. Shear wave velocity (V_s) measurements were completed for all columns once daily prior to all treatment injections. For columns receiving 12 PV continuous rinse injections, V_s measurements were performed after injecting 3, 6, 9, and 12 PVs of rinse solutions. For columns receiving staged 1 PV rinse injections, V_s measurements were performed before and after each rinse injection.

7.2.9 *Post-treatment Soil Sampling*

After completing all rinse injections, soil columns were freely drained, extruded using a hydraulic jack, and subsampled into four discrete sections located at varying distances from the injection location (0 to 38 mm, 38 to 76 mm, 76 to 114 mm, 114 to 152 mm). Section samples were homogenized and then partitioned into two equal masses for either NH_4^+ extraction or $CaCO_3$

content measurements. Samples for NH_4^+ extraction were frozen immediately at their residual water content. Samples for $CaCO_3$ content measurements were oven-dried at 100°C for at least 48 hours and then stored dry.

7.2.10 *Soil NH_4^+ Extractions*

In order to quantify sorbed NH_4^+ concentrations remaining within soil columns, NH_4^+ extraction was performed using moist soil samples following procedures similar to past studies (Lee et al. 2019a). During the NH_4^+ extraction process, free soil solution was first removed from thawed and homogenized soil samples by adding 30 grams of moist soil to conical centrifuge tubes with 0.45-micron nylon filter baskets (Thermo Scientific, Waltham, MA) and centrifuging at 800 g for 60 minutes. A minimum volume of 2 mL of this free soil solution was collected, stored, and frozen for subsequent aqueous NH_4^+ measurements. Next, in order to quantify sorbed NH_4^+ masses, a KCl extraction procedure similar to that by Keeney & Nelson (1982) was used. In this process, 10 grams of moist soil was mixed with 20 mL of a 2 M KCl solution and was allowed to equilibrate for one hour to facilitate removal of NH_4^+ ions from soil surfaces. KCl-equilibrated samples were then similarly placed in 0.45-micron nylon filter baskets and centrifuged at 800 g for 60 minutes to extract solutions. During the extraction process, soil sample water contents were determined at various points to determine total fluid volumes within samples. KCl-extracted solution samples contained both the free NH_4^+ present within pore fluids as well as the extracted sorbed NH_4^+ masses. All extracted samples were frozen until subsequent aqueous NH_4^+ measurements. Measurements of both aqueous NH_4^+ from free soil solutions and KCl-extracted samples were used to determine

sorbed NH_4^+ masses for all soil column section samples and these values were normalized per gram of dry soil.

7.2.11 *Soil $CaCO_3$ Content Measurements*

Soil $CaCO_3$ content measurements were completed for all soil column section samples using a pressurized chamber measurement process in accordance with ASTM D4373 (ASTM, 2014). Dry biocemented soil samples were first homogenized, added to a sealed acrylic chamber, and reacted with 1M hydrochloric acid, generating CO_2 gas and a corresponding increase in test chamber pressure. Chamber pressures were measured using a 15-psi pressure transducer (Omega Inc., Norwalk, CT). Relationships between measured chamber pressures and known reagent-grade $CaCO_3$ masses were used to determine sample $CaCO_3$ contents. A minimum of three $CaCO_3$ content measurements were completed for each soil section and section measurements were averaged to determine average $CaCO_3$ contents for entire soil columns.

7.3 Results

7.3.1 *Passive Tracer Testing*

In order to evaluate potential differences in advective-dispersive transport between columns prior to biocementation and rinse injections, passive tracer testing was performed for select soil columns. **Figure 7.2** presents measurements of normalized conductivity (C/C_0) from effluent solution samples versus injected volume for twelve select soil columns. As shown, all columns exhibited nearly identical breakthrough behaviors reflective of similar advective-dispersive transport.

During the initial 3 PV 50 mM NaBr injection, C/C_0 values gradually increased to values near 50% after injecting 1 PV with larger values between 85% and 95% observed after injecting 1.5 PV. Similar behaviors were observed during the subsequent 3 PV deionized water injection with C/C_0 values decreasing to near 40% after 1 PV and further decreases in values to below 10% after injecting 1.5 PV. Collectively, these breakthrough curves suggested that no significant differences in advective-dispersive transport existed between columns. Furthermore, breakthrough responses also confirmed that the 1.5 PV treatment injection volumes applied during MICP treatments resulted in near full replacement of soil column pore fluids and therefore spatially uniform distributions of injected urea and generated NH_4^+ by-product concentrations were expected.

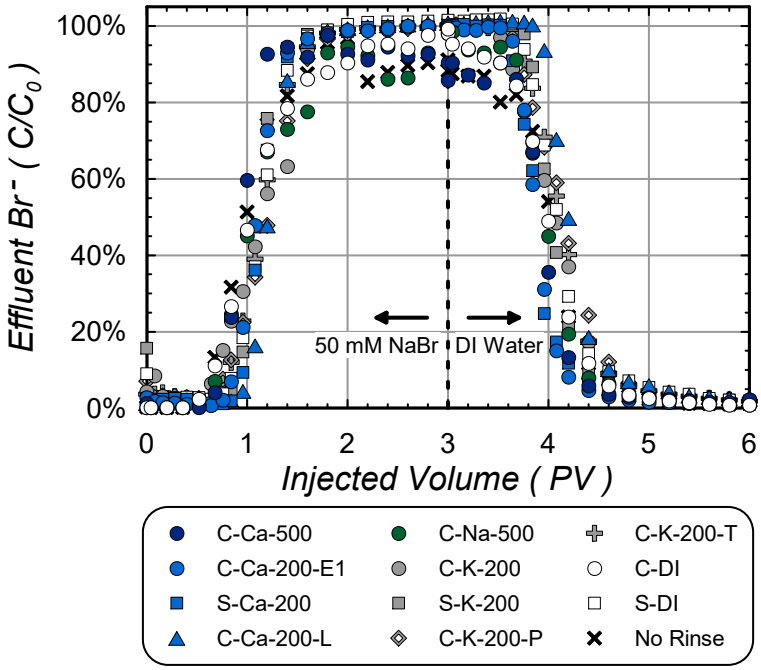

Figure 7.2. Measurements of normalized effluent Br^- concentrations (C/C_0) versus injected volume obtained during passive tracer testing for twelve select soil column specimens.

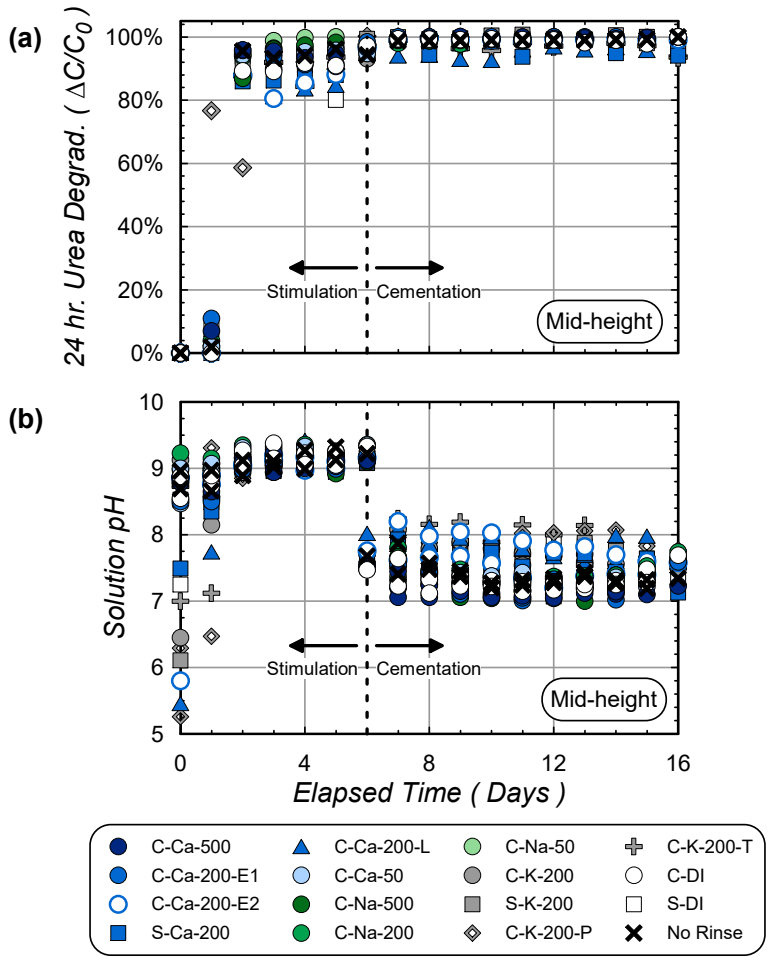

Figure 7.3. Measurements of **(a)** normalized 24 hour urea degradation ($\Delta C/C_0$) and **(b)** pre-treatment solution pH obtained from mid-height column sampling ports for all stimulation and cementation treatments.

7.3.2 *Biogeochemical & Mechanical Changes During Biocementation*

Variations in ureolytic activity were assessed between columns during biocementation in order to ensure that all columns generated similar post-treatment aqueous NH_4^+ concentrations. **Figure 7.3** presents measurements of both 24-hour normalized urea degradation (**Figure 7.3a**) and solution pH measured prior to injections (**Figure 7.3b**) at column mid-height sampling ports during both stimulation and cementation treatments. 24-hour normalized urea degradation ($\Delta C/C_0$) was the

percentage of the injected urea concentration (C_0) that was degraded during the 24-hour treatment residence periods (ΔC), with values of 100% reflective of full urea degradation. As shown, during the first 2 stimulation injections, no detectable urea degradation was observed in almost all columns with the exception of the single column that received the 500 mM KCl pre-treatment solution prior stimulation (C-K-200-P), which exhibited near 80% urea degradation during the second treatment. While this outcome may have resulted from minor biological variability between columns, it also remains possible that the 500 mM KCl solution may have enabled more effective selection for halotolerant microorganisms prior to stimulation injections, thereby promoting faster ureolytic cell growth. During the first 2 stimulation injections, a broad range of pH values was also observed between 5 and 9, which were likely reflective of the equilibration of injected alkaline rinse solutions ($pH_{initial}$ = 9.0) with existing soil minerals. Between the second and fourth stimulation injections, ureolytic activity increased dramatically with greater than 80% normalized urea degradation and pH values increasing to between 9 and 9.5 in all columns. High ureolytic activities were maintained through the end of stimulation treatments and following the transition to cementation during the seventh treatment injection, all columns continued to maintain between 95% and 100% normalized urea degradation. Solution pH values decreased to between 7 and 8 after the first cementation injection, however, reflective of near full urea degradation in the presence of $CaCO_3$ precipitation (Gomez et al. 2018b). Similar pH values and urea degradation magnitudes were maintained throughout the cementation phase.

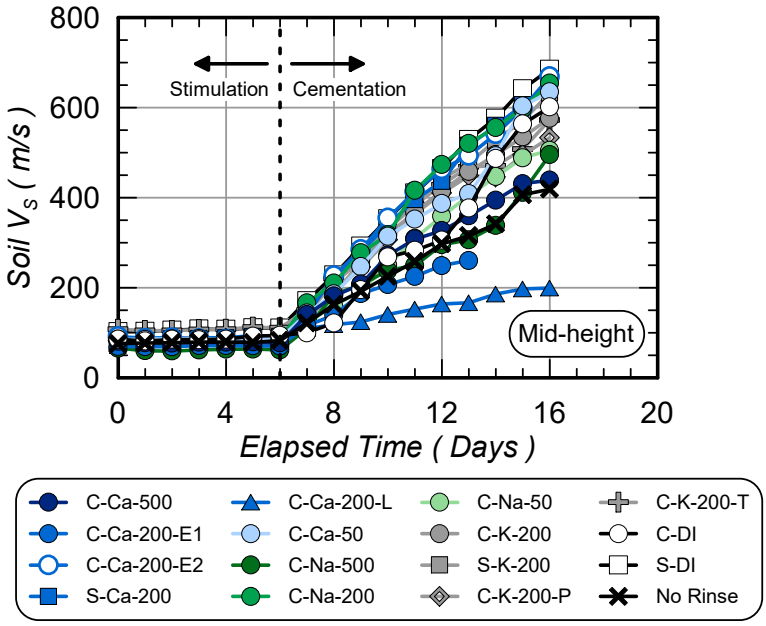

Figure 7.4. Shear wave velocities (V_s) measured at column mid-heights during all stimulation and cementation treatments. V_s measurements for C-Ca-200-E1 were not obtained beyond the 7th cementation injection due to sensor failure.

During cementation treatments, changes in soil column shear wave velocities were also monitored to track cementation progression. **Figure 7.4** presents soil V_s values measured at column mid-heights prior to all stimulation and cementation treatments. As shown, initial V_s values in all columns were near 85 m/s ± 25 m/s with no detectable changes during stimulation due to the lack of $CaCO_3$ precipitation. Following the introduction of soluble Ca^{2+}, most columns exhibited V_s increases near 50 m/s after each cementation treatment with final V_s values ranging between 418 and 685 m/s. The single column receiving 80% lower concentrations of calcium and urea (C-Ca-200-L), however, achieved a significantly lower final V_s of 199 m/s, as expected. This was nearly 20% of the improvement observed in all other columns, which was consistent with the 80% lower urea and calcium concentrations applied in this column during cementation (50 mM) in comparison to all other columns (250 mM). Collectively, passive tracer tests, aqueous urea and

pH measurements, and soil V_s monitoring suggested that all columns achieved similar conditions following biocementation treatments and immediately prior to rinsing, apart from the single column achieving an intended reduction in MICP improvement (e.g., C-Ca-200-L).

7.3.3 *NH_4^+ Removal During Rinse Injections*

Figure 7.5 presents aqueous NH_4^+ concentrations measured in column effluent for all continuously rinsed columns (**Figure 7.5a**) with columns receiving Ca^{2+}-based rinse solutions (**Figure 7.5b**), Na^+-based rinse solutions (**Figure 7.5c**), and rinse solutions with varying cations at 200 mM (**Figure 7.5d**) plotted separately. As shown during the first 1 PV of rinsing, all columns maintained concentrations of effluent NH_4^+ near twice that of the injected urea concentration, reflective of the displacement of fully reacted cementation solutions, which had resided within the columns. As expected, lower initial NH_4^+ concentrations near 100 mM were observed in effluent from C-Ca-200-L with all other columns having effluent NH_4^+ concentrations near 500 mM. As rinsing proceeded, all columns exhibited large effluent NH_4^+ reductions to values between 17 and 54 mM NH_4^+ after injecting 2 PV and between 2 and 6 mM NH_4^+ after 6 PV. With further increases in injected volumes, more minimal reductions were observed with effluent NH_4^+ concentrations between 0.4 and 2.4 mM NH_4^+ observed after injecting 12 PV. Reductions in NH_4^+ removal efficiency at large injection volumes were similarly observed in previous studies (Lee et al. 2019a; 2019b) and were reflective of sorption and exchange of NH_4^+ with soil surfaces, which limits the ability of NH_4^+ to be efficiently removed using advection at low concentrations (i.e., $< \approx 10$ mM NH_4^+).

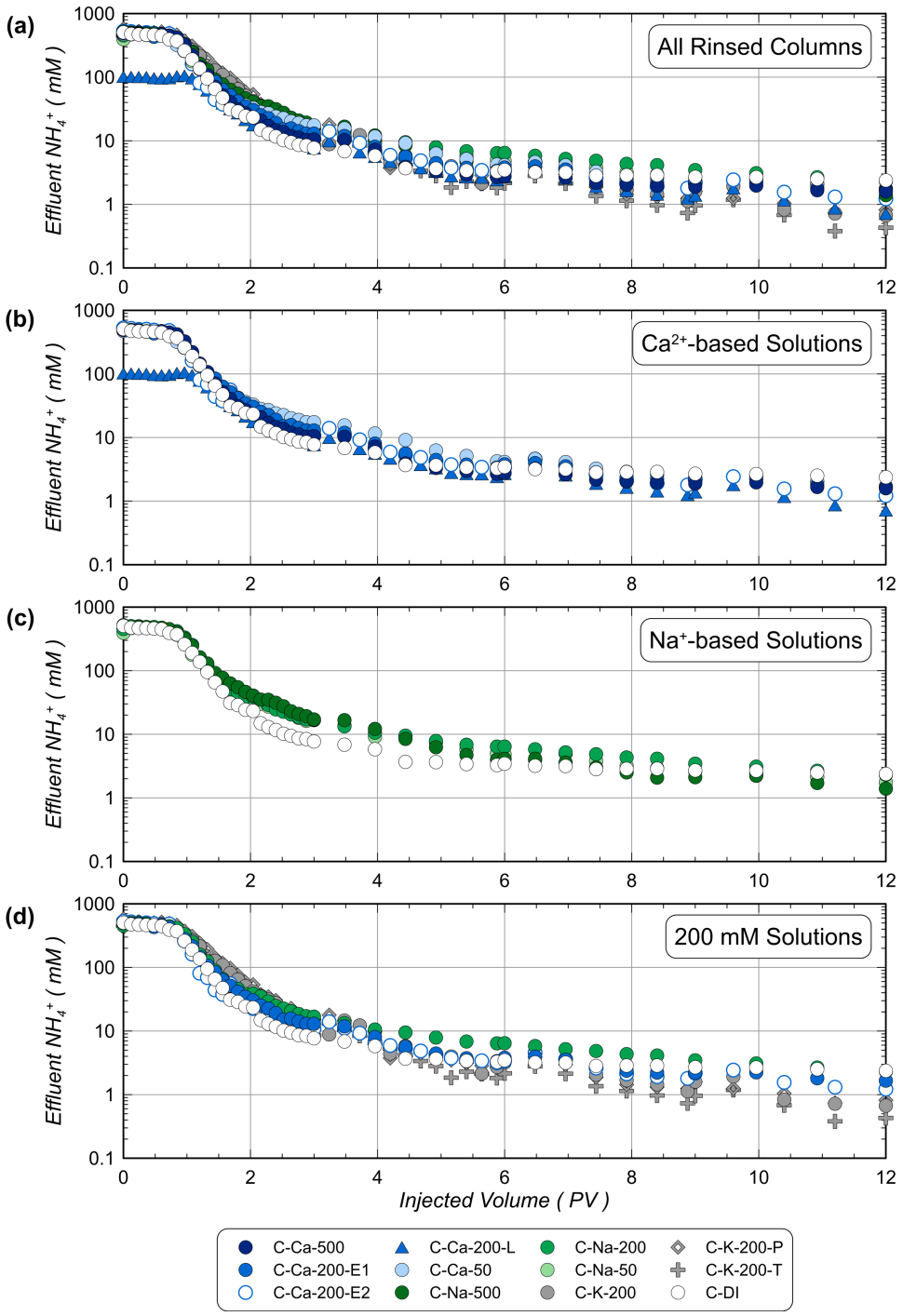

Figure 7.5. Measurements of aqueous NH_4^+ concentrations in column effluent solutions during continuous-rinse injections for **(a)** all continuous columns, **(b)** continuous columns receiving Ca^{2+}-based rinse solutions, **(c)** continuous columns receiving Na^+-based rinse solutions, and **(d)** continuous columns receiving rinse solutions with 200 mM of various cations. Effluent concentrations were not measured for columns with staged injections.

When examining the effect of changes in rinse solution composition, several trends were observed. First, when comparing columns receiving cation-enriched rinse solutions to the column receiving only deionized water (C-DI), consistently lower effluent NH_4^+ concentrations were observed exiting C-DI early on during rinse injections (≈ 1 PV to 7 PV) with instead the highest effluent NH_4^+ concentrations near 2.4 mM persisting in this column at the end of the 12 PV injection (**Figure 7.5a**). Both observations suggested that less NH_4^+ was removed from C-DI, when compared to other columns which received solutions with supplied cations and that these supplied cations likely promoted exchange with NH_4^+ on soil surfaces and enabled more effective removal during continuous injections. When considering the impact of reduced MICP reagent concentrations, interestingly, C-Ca-200-L exhibited only minimal differences when compared to other columns receiving more highly concentrated cementation solutions but similar rinse solutions (i.e., C-Ca-200-E1, C-Ca-200-E2). Although rinse solution cation concentrations were expected to significantly impact NH_4^+ removal, only minimal differences were observed for columns receiving rinse solutions with variations in supplied Ca^{2+} (**Figure 7.5b**) and Na^+ (**Figure 7.5c**) concentrations. However, comparable effluent NH_4^+ concentrations between 1.2 mM and 2.3 mM were observed near the end of rinsing in all Ca^{2+} and Na^+-rinsed columns and were consistently lower than the 2.4 mM NH_4^+ observed at the end of rinsing in the deionized water control column (C-DI).

When comparing all continuously-rinsed columns receiving 200 mM rinse solutions (**Figure 7.5d**), effluent NH_4^+ concentrations were consistently higher early on during rinse injections (1 PV to 3 PV) in columns receiving K^+-based solutions, indicative of improved NH_4^+ removal when

compared to other cations. However, columns receiving 200 mM Na^+- and Ca^{2+}-based solutions also achieved greater effluent NH_4^+ concentrations at the start of rinsing when compared to the deionized water control column (C-DI). At large injection volumes near the end of rinsing (12 PV), columns receiving Na^+- and Ca^{2+}-based solutions achieved comparable removal with effluent NH_4^+ concentrations near 1.2 mM. Lower NH_4^+ concentrations between 0.4 mM and 1 mM were measured at the end of rinsing in columns receiving K^+-based solutions, however, consistent with the greater removal observed initially during rinsing. When comparing the response of the column pre-treated with 500 mM KCl before MICP treatments (C-K-200-P) and the column receiving MICP treatments amended with 200 mM KCl (C-K-200-T) to the comparable column which did not receive these variations (C-K-200), pre-treatment was shown to exhibit no clear benefits with respect to reducing post-rinsing effluent NH_4^+ concentrations, however, slightly lower effluent NH_4^+ concentrations were observed in C-K-200-T, which received amended MICP treatments and achieved the lowest post-rinsing effluent NH_4^+ concentration of any continuously-rinsed column near 0.4 mM. Finally, when comparing the two column replicates (C-Ca-200-E1, C-Ca-200-E2), nearly identical trends in effluent NH_4^+ concentrations were observed, suggesting that experiments were repeatable.

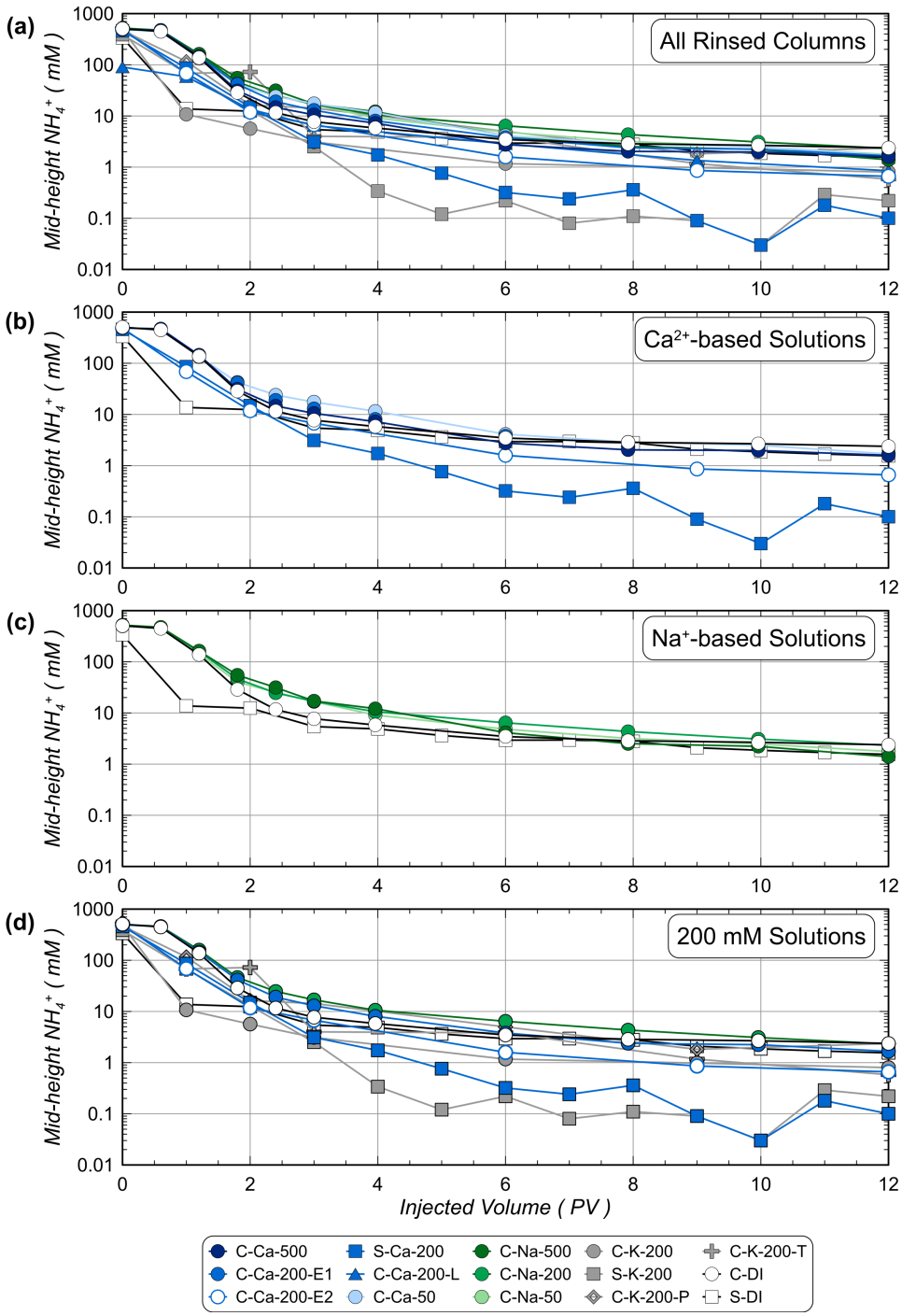

Figure 7.6. Measurements of mid-height aqueous NH_4^+ concentrations versus rinse injection volume for **(a)** all continuous and staged injection columns, **(b)** all columns receiving Ca^{2+}-based rinse solutions, **(c)** all columns receiving Na^+-based rinse solutions, and **(d)** all columns receiving rinse solutions with 200 mM concentrations of various cations.

Figure 7.6 aqueous NH_4^+ concentrations measured in column mid-height solution samples obtained during rinsing for all sixteen continuously-rinsed and staged-rinsed columns (**Figure 7.6a**) including columns receiving Ca^{2+}-based rinse solutions (**Figure 7.6b**), Na^+-based rinse solutions (**Figure 7.6c**), and rinse solutions with varying cations at 200 mM (**Figure 7.6d**), which were plotted separately. Similar relative trends observed for effluent NH_4^+ concentrations were also observed for mid-height NH_4^+ concentrations, with generally less pronounced differences between columns receiving variations in rinse solution composition. All continuously-rinsed columns achieved similar mid-height NH_4^+ concentration reductions at injection volumes exceeding ≈1 PV with mid-height aqueous NH_4^+ concentrations between 0.6 mM and 2.4 mM observed after injecting 12 PV and no consistent trends related to cation concentrations or cation type. In contrast, the two columns receiving cation-enriched staged injections (S-Ca-200, S-K-200) exhibited significantly lower mid-height aqueous NH_4^+ concentrations throughout much of the rinsing process, when compared to all other continuously-rinsed columns including those receiving similar solutions (i.e., C-Ca-200-E1, C-Ca-200-E2, C-K-200). After injecting 12 PV, mid-height aqueous NH_4^+ concentrations were between 0.1 and 0.3 mM in staged rinsed columns; nearly an order of magnitude less than was observed in many of the continuously rinsed columns. Although differences between staged and continuous rinse injections had a significant impact on mid-height NH_4^+ removal when cations were present, interestingly, variations in injection sequences had minimal impacts on mid-height NH_4^+ removal for columns rinsed with deionized water (C-DI, S-DI). Improved mid-height NH_4^+ removal in staged columns receiving cation-enriched rinse solutions likely resulted from both enhanced cation exchange between supplied cations and sorbed NH_4^+ and increased diffusion and equilibration of NH_4^+ concentrations during the 24-hour retention periods. Conversely, increases in retention time appeared to have little impact on

deionized water rinsed columns likely due to the absence of supplied cations and related cation exchange reactions. Again, mid-height NH_4^+ concentrations were also similar between the repeated experiments (C-Ca-200-E1, C-Ca-200-E2), with slightly greater viability observed than earlier effluent concentrations.

Figure 7.7 presents mid-height solution pH measurements during rinsing for all continuously-rinsed and staged-rinsed columns. All rinse solutions were pH-adjusted to 9.0 prior to injection, however, during the rinsing process, injected solutions equilibrated with existing soil solutions, generated $CaCO_3$, and parent soil minerals. As shown, all columns had initial pH values between 7.25 and 8 prior to rinse injections, with gradual pH increases observed in most columns until approximately 3 PVs were injected. pH changes with increases in injected volumes appeared to associate strongly with solution type, with deionized water rinsed columns exhibiting the most rapid pH increases followed by columns receiving K^+-, Na^+-, and Ca^{2+}-based rinse solutions. Although most columns exhibited similar gradual pH increases likely reflective of small differences in solution buffering capacities with differences in supplied cations, interestingly, columns receiving Ca^{2+}-based rinse solutions exhibited small pH reductions early on during rinsing with significantly lower final pH values near 8 observed at the end of rinsing. Although unexpected, lower pH values in the columns receiving Ca^{2+}-based rinse solutions may have been reflective of some additional $CaCO_3$ precipitation occurring during the introduction of high Ca^{2+} due to the mixing of rinse solutions with column pore fluids, which contained residual carbonate species following MICP treatments. Lower pH values present in columns rinsed with Ca^{2+}-based rinse solutions may have also resulted in increased speciation of total NH_4^+ towards positively-charged NH_4^+ rather than charge-neutral NH_3 (63.5% NH_4^+ & 36.5% NH_3 at pH = 9.0 versus 94.5%

NH_4^+ & 5.5% NH_3 at pH = 8.0), which could have slightly inhibited NH_4^+ removal in these columns due to increased interactions with negatively-charged soil minerals. Despite this significant pH difference, earlier results suggest that pH variations experienced in columns receiving Ca^{2+}-based rinse solutions likely had only minor effects on aqueous NH_4^+ removal, when compared to the other rinse variations considered.

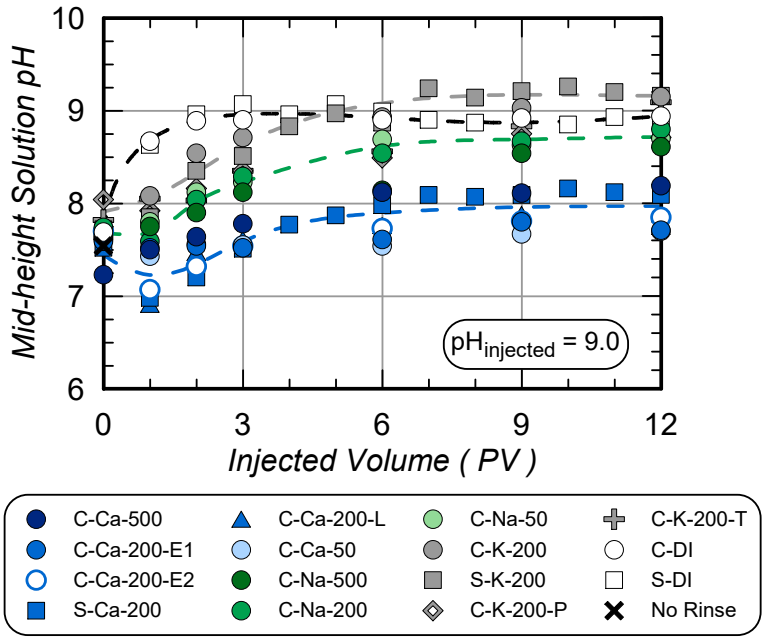

Figure 7.7. Measurements of solution pH obtained from mid-height column sampling ports during rinse injections versus injected volume.

7.3.4 *NH_4^+ Removal Achieved Following Rinsing*

Following all rinse injections, soil columns were sampled into four discrete sections and section samples were extracted to determine final aqueous and sorbed NH_4^+ concentrations and assess removal efficacy following rinsing. **Table 7.3** provides a summary of NH_4^+ measurements obtained following rinsing for all columns including aqueous and sorbed NH_4^+ concentrations

measured for all sections. **Figure 7.8** presents post-rinsing aqueous NH_4^+ concentrations (**Figure 7.8a**) and sorbed NH_4^+ concentrations (**Figure 7.8c**) versus soil column length as well as sorbed NH_4^+ concentrations versus aqueous NH_4^+ concentrations presented for two different aqueous NH_4^+ ranges (**Figure 7.8b, 7.8d**). As shown in **Figure 7.8a**, aqueous NH_4^+ concentrations were relatively uniform within all columns following rinsing with small NH_4^+ concentration increases observed with increasing distance from the injection location, which was similar to trends observed in previous meter-scale experiments (Lee et al. 2019a). In the column receiving no rinse injections (No Rinse), aqueous NH_4^+ concentrations remained near 500 mM, however, following the application of different rinsing strategies, a range of aqueous NH_4^+ concentrations between ≈1 and 12 mM were observed. Aqueous NH_4^+ concentrations extracted from soil samples were slightly larger than those measured at mid-height sampling ports for similar columns, likely due to the removal of more concentrated pore fluids near soil particle surfaces, which remained in columns following free draining. While no consistent trends were observed as a function of cation type and concentration, the two columns receiving cation-based staged injections again exhibited the lowest aqueous NH_4^+ concentrations of all columns between ≈ 1 and 1.5 mM with comparable concentrations also measured in the 50 mM Na^+ continuously-rinsed column (C-Na-50). Interestingly, post-rinsing aqueous NH_4^+ concentrations were again similar between both deionized water rinsed columns (C-DI, S-DI) as well as other columns that received cation-enriched continuous rinse injections. This outcome suggested that added cations may have only minimal impacts on aqueous NH_4^+ removal when continuous rinse injections are used, however, clear benefits can be realized when staged injections are employed.

Table 7.3. Summary of Post-rinsing Aqueous and Sorbed NH_4^+ Concentrations for All Columns

			Section Measurements							
			Aqueous NH_4^+ (mM)				Sorbed NH_4^+ (10^{-3} mol/kg soil)			
Rinse Solution Type	**Column(s)**	**Injection Sequence**	**0 to 4 cm from injection**	**4 to 8 cm from injection**	**8 to 12 cm from injection**	**12 to 16 cm from injection**	**0 to 4 cm from injection**	**4 to 8 cm from injection**	**8 to 12 cm from injection**	**12 to 16 cm from injection**
500 mM Ca^{2+}	C-Ca-500	12 PV Continuous	12.3	12.3	9.9	9.9	2.3	2.2	2.4	2.0
200 mM Ca^{2+}	C-Ca-200-E1	12 PV Continuous	11.4	11.5	11.7	11.8	1.9	1.8	2.0	1.8
	C-Ca-200_E2	12 PV Continuous	8.9	9.8	10.3	10.3	1.6	1.4	1.7	1.6
	S-Ca-200	1 PV Staged (12x)	1.1	1.1	1.0	1.2	0.2	0.2	0.3	0.3
	C-Ca-200-L	12 PV Continuous	7.6	7.2	7.9	7.1	1.4	1.3	1.5	1.3
50 mM Ca^{2+}	C-Ca-50	12 PV Continuous	9.1	9.8	9.2	9.3	2.1	2.2	2.3	2.5
500 mM Na^+	C-Na-500	12 PV Continuous	5.8	5.6	5.6	5.9	1.1	1.5	1.6	1.3
200 mM Na^+	C-Na-200	12 PV Continuous	3.1	3.3	3.5	4.1	3.8	4.2	5.1	5.5
50 mM Na^+	C-Na-50	12 PV Continuous	1.2	1.4	1.2	1.4	2.3	2.6	2.4	1.9
200 mM K^+	C-K-200	12 PV Continuous	7.6	7.7	8.0	8.8	0.7	0.7	0.7	0.7
	S-K-200	1 PV Staged (12x)	1.0	1.2	1.3	1.6	0.1	0.1	0.2	0.2
	C-K-200-P	12 PV Continuous	6.9	7.2	7.7	8.0	0.7	0.4	0.6	0.5
	C-K-200-T	12 PV Continuous	5.3	5.2	5.3	5.4	0.5	0.3	0.5	0.4
DI-water	C-DI	12 PV Continuous	4.6	5.2	6.1	9.4	7.0	9.0	12.3	12.8
	S-DI	1 PV Staged (12x)	2.5	3.2	4.1	5.1	2.8	6.0	9.9	11.7
None	No Rinse	N/A	533	499	497	499	14.9	16.9	16.1	15.2

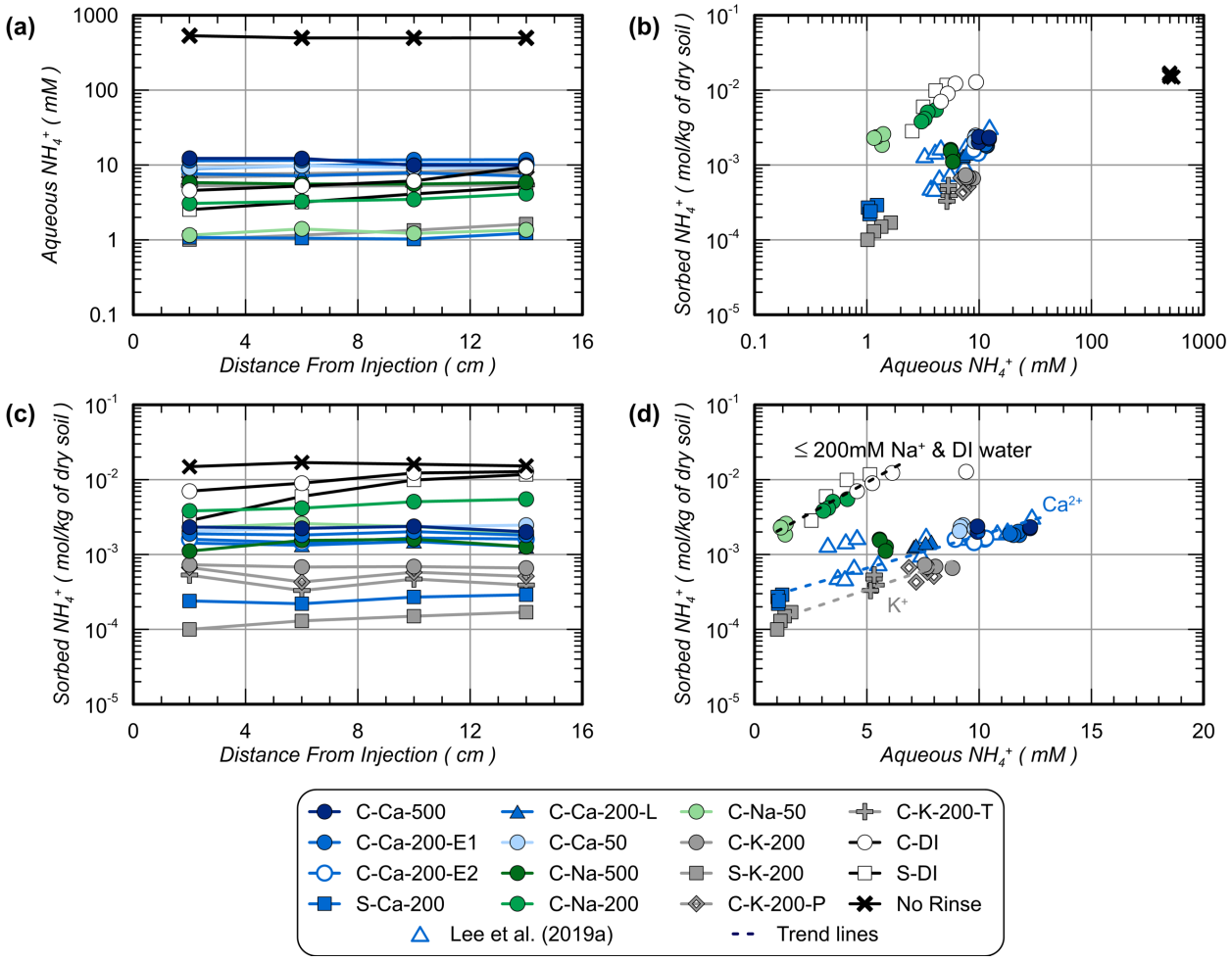

Figure 7.8. Measurements of **(a)** aqueous NH_4^+ concentrations versus column lengths, **(b)** sorbed NH_4^+ versus aqueous NH_4^+ concentrations (log-scale), **(c)** sorbed NH_4^+ concentrations versus column lengths, and **(d)** sorbed NH_4^+ masses versus aqueous NH_4^+ concentrations (linear-scale). Data included from recent meter-scale experiments (Lee et al. 2019b) involved the same Concrete Sand material and was obtained following continuous rinse injections of 200 mM $CaCl_2$ solutions.

When examining sorbed NH_4^+ concentrations as a function of column length (**Figure 7.8c**), more significant differences were observed between rinsing strategies. As expected, the column receiving no rinse injections (No Rinse) had the highest sorbed NH_4^+ concentrations between 1.5 and 1.7 x 10^{-2} mol per kg of soil, which was near 61% of the total cation exchange capacity of the Concrete Sand material (CEC = 2.58*10^{-2} mol per kg of soil as NH_4^+). In contrast, the lowest sorbed NH_4^+ concentrations between 1 and 3 x 10^{-4} mol per kg of soil were measured in columns

receiving staged injections with cation-enriched solutions (S-Ca-200, S-K-200). Both deionized water rinsed columns (C-DI, S-DI) had sorbed NH_4^+ concentrations near 1 x 10^{-2} mol per kg of soil that were similar to the non-rinsed column (No Rinse); thereby suggesting that while deionized water rinses were able to effectively remove aqueous NH_4^+, these injections achieved almost no removal of sorbed NH_4^+. When examining other continuously-rinsed columns, those receiving both Na^+- and Ca^{2+}-based solutions generally achieved reductions in sorbed NH_4^+ concentrations near 0.5 to 1 order of magnitude below values observed in the non-rinsed column (No Rinse), with supplied cation concentrations exhibiting no consistent effects. All continuously-rinsed columns receiving K^+-based solutions, however, achieved significantly lower sorbed NH_4^+ concentrations than all other continuously-rinsed columns, with the single column receiving KCl-amended MICP treatment solutions (C-K-200-T) achieving the lowest sorbed NH_4^+ concentrations of all continuously-rinsed columns (3 to 5 x 10^{-4} mol per kg of soil). Similar to aqueous NH_4^+ concentrations, sorbed NH_4^+ masses also appeared to increase with distance from the injection source. This reduction in NH_4^+ removal with injection distance likely resulted from solution dispersion and retardation of NH_4^+ transport.

Past studies examining NH_4^+ sorption kinetics in soils (Huang et al. 2010; Uğurlu et al. 2011; Sieczka & Koda 2016) have shown that aqueous and sorbed NH_4^+ concentrations are correlated at low concentrations due to equilibration between NH_4^+ present in free solution and sorbed on soil surfaces. In an effort to better understand this relationship, sorbed NH_4^+ concentrations were compared to corresponding aqueous NH_4^+ concentrations at all soil column section locations (**Figure 7.8b, 7.8d**). Similar measurements of both aqueous and sorbed NH_4^+ obtained from recent meter-scale biocementation experiments receiving continuous 12 PV alkaline 200 mM $CaCl_2$ rinse

injections (Lee et al. 2019b) were also provided for comparison. As shown, columns receiving staged rinse injections exhibited both the lowest sorbed NH_4^+ and aqueous NH_4^+ concentrations with the non-rinsed column (No Rinse) achieving the highest values for both (**Figure 7.8b**). In all rinsed columns, aqueous NH_4^+ concentrations were below ≈ 12.5 mM and sorbed NH_4^+ concentrations exhibited a log-linear relationship with aqueous NH_4^+ concentrations, with data points from columns receiving the same cation type clustered closely together (**Figure 7.8d**). For the same aqueous NH_4^+ concentration, sorbed NH_4^+ concentrations appeared to follow a consistent order based upon cation type with K^+-based solutions achieving the lowest sorbed NH_4^+ concentrations, followed by Ca^{2+}-based and high concentration (500 mM) Na^+-based solutions, and deionized water and low concentration (≤ 200 mM) Na^+-based solutions. Similar aqueous and sorbed NH_4^+ trends between columns rinsed with deionized water and low concentration (≤ 200 mM) Na^+-based solutions was unexpected and suggesting that low concentration Na^+-based rinses were less effective at removing sorbed NH_4^+ concentrations. One exception was the column receiving the 500 mM Na^+-based solution (C-Na-500), however, which had considerably lower sorbed NH_4^+ concentrations that were more consistent with trends for the Ca^{2+}-based rinses. Log-linear relationships between aqueous and sorbed NH_4^+ concentrations for all solutions were consistent with results from Lee et al. (2019a) and suggested that the equilibrium between aqueous and sorbed phases may be well described by a Freundlich adsorption isotherm (Goldberg 2005). In contrast, at higher aqueous NH_4^+ concentrations near 500 mM present in the non-rinsed soil column (No Rinse), soil surface sorption sites became saturated, and sorbed NH_4^+ concentrations closer to the CEC of the parent soil were observed. Measurements from Lee et al. (2019a) also compared well with measurements obtained from this study for columns which received similar continuous injections of 200 mM Ca^{2+}-based rinse solutions (C-Ca-200-E1, C-Ca-200-E2), further

demonstrating that relationships between aqueous and sorbed NH_4^+ concentrations may remain similar for a given rinse injection strategy and soil material type. This outcome may have important practical implications for post-rinsing assessment of NH_4^+ removal at field sites, wherein such relationships could be developed through soil column testing prior to field applications and measurements of either aqueous or sorbed NH_4^+ could be used to estimate expected NH_4^+ concentrations in the unmeasured phase.

In order to evaluate NH_4^+ removal in all columns, aqueous and sorbed NH_4^+ concentrations measured following rinsing were compared between all columns and the non-rinsed column (No Rinse), which was representative of conditions present immediately after biocementation treatments. **Figure 7.9** presents the percentages of aqueous NH_4^+ removal (**Figure 7.9a**), sorbed NH_4^+ removal (**Figure 7.9b**), and total NH_4^+ removal (**Figure 7.9c**) for all columns, of which the latter accounted for NH_4^+ removal from both aqueous and sorbed phases. As shown in **Figure 7.9a**, all columns achieved greater than 97% aqueous NH_4^+ removal, with achieved removal generally decreasing with distance from the injection location and varying only slightly with differences in rinse solution chemistry. However, when comparing sorbed NH_4^+ removal between columns (**Figure 7.9b)**, much more significant differences were observed. Although nearly all columns achieved greater than ≈80% sorbed NH_4^+ removal, both deionized water rinsed columns (C-DI, S-DI) and the 200 mM Na^+-rinsed column (C-Na-200) achieved significantly less removal. In the deionized water rinsed columns, sorbed NH_4^+ removal varied between ≈ 20% and 80% with a large gradient in removal observed along the length of columns and only slightly greater removal in the column receiving staged injections. Surprisingly, the 200 mM Na^+-rinsed column only achieved between ≈ 64% and 76% sorbed NH_4^+ removal, which was considerably lower than all other

columns rinsed with cation-enriched solutions including Na^+ at other concentrations. All columns receiving continuous K^+-based rinse injections consistently achieved greater sorbed NH_4^+ removal than all other continuously rinsed columns with removal exceeding 98% at all locations. As expected, columns receiving cation-enriched staged injections achieved greater sorbed NH_4^+ removal than all other columns.

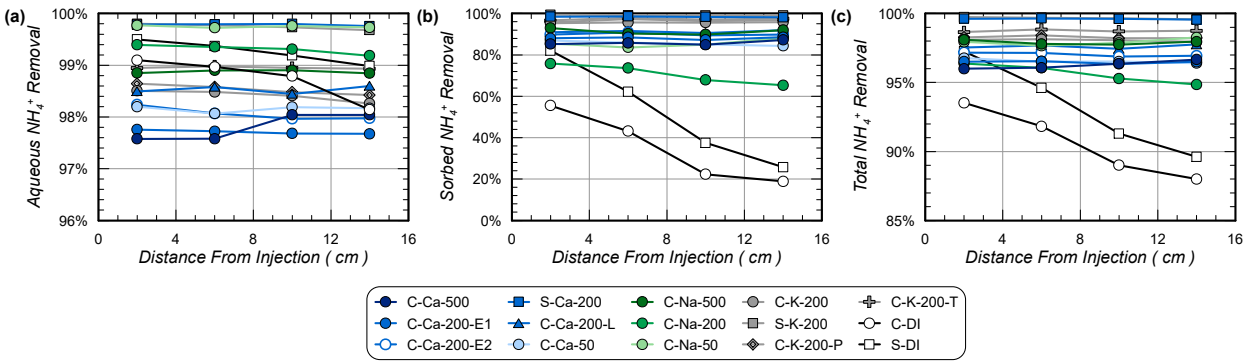

Figure 7.9. Comparisons of **(a)** aqueous NH_4^+ removal, **(b)** sorbed NH_4^+ removal, and **(c)** total NH_4^+ removal in all columns as a function of column length. Removal was determined by comparing aqueous and sorbed NH_4^+ concentrations in all columns following rinsing to values measured in the single column receiving no rinse injections (No Rinse).

Total NH_4^+ removal trends further demonstrated the collective impacts of aqueous and sorbed NH_4^+ removal on the total NH_4^+ present within columns following MICP (**Figure 7.9c**). At all column locations, the deionized water continuous column (C-DI) achieved the lowest total NH_4^+ removal between ≈ 88% and 93.5% with the deionized water staged column (S-DI) achieving the second lowest total NH_4^+ removal between ≈ 89.5% and 97%. In contrast, all other columns receiving cation-enriched solutions achieved between ≈ 94.9% and 99.7% total NH_4^+ removal at all sampled locations. Although more dramatic differences in sorbed NH_4^+ removal was previously observed between columns, minor differences in total NH_4^+ removal between all columns was

reflective of the greater contribution of aqueous NH_4^+ to the total NH_4^+ present within columns following biocementation, when compared to sorbed NH_4^+, and the more minimal differences in aqueous NH_4^+ removal observed between different rinsing strategies. While sorbed NH_4^+ masses may be a significantly smaller fraction of the total NH_4^+ residing within sandy soils following biocementation, sorbed NH_4^+ may have important implications for field-scale applications, as progressive desorption of sorbed NH_4^+ may result in higher sustained aqueous NH_4^+ concentrations following treatments and the potential for continued and prolonged regulatory challenges. From this perspective, the percentage of total NH_4^+ removal will likely be practically less important than the realized aqueous NH_4^+ concentrations achieved following rinsing and their relation to site-specific regulations. Although not investigated in this study, treated soils with higher fines contents may also have larger sorbed NH_4^+ concentrations due to increases in soil cation exchange capacities. For these soils, sorbed NH_4^+ may be a larger fraction of the total NH_4^+ present following biocementation and removing such concentrations may be critical. For these cases, both staged injections and K^+-based rinse solutions may provide important advantages with respect to the long-term management of generated NH_4^+ concentrations.

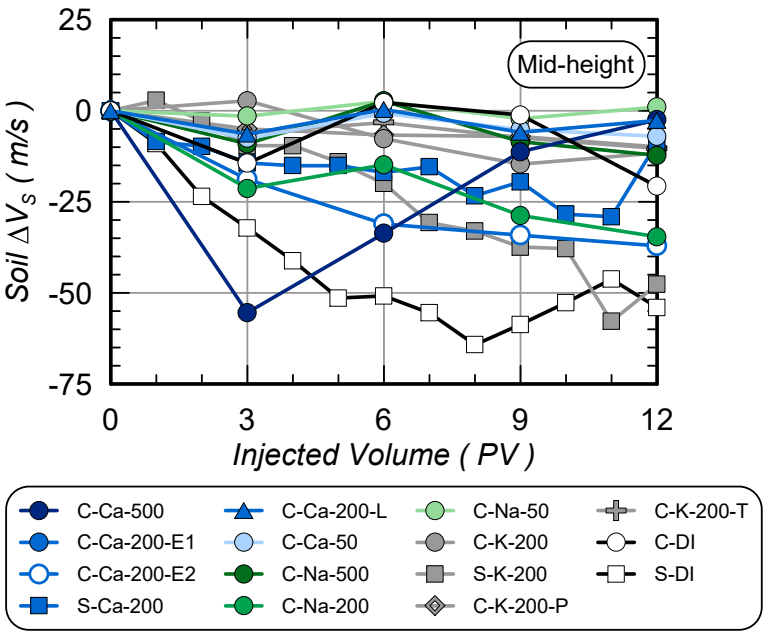

Figure 7.10. Shear wave velocity changes (ΔV_s) measured at column mid-heights during rinsing versus injected volume.

7.3.5 *Effect of Rinsing on Cementation Integrity*

Although rinse injections were shown to effectively remove NH_4^+ by-products following biocementation, it remained unclear if post-treatment cementation integrity would be affected by differences in rinse solution composition and injection sequencing. Alkaline rinse solutions were used in part to limit the potential for $CaCO_3$ dissolution, which is controlled by solution CO_3^{2-} and Ca^{2+} activities, the solubility of the $CaCO_3$ minerals present, mineral specific surface areas, and the exposure time of $CaCO_3$ minerals to undersaturated solutions (injection flow rates and residence times). Potential differences in cementation integrity during rinsing were therefore expected to be most apparent between (1) columns receiving Ca^{2+}-based rinse solutions versus other rinse solutions that lacked added soluble Ca^{2+} and (2) columns receiving staged versus continuous rinse injections, which altered exposure times. In order to evaluate changes in

cementation integrity, V_s measurements were obtained at various points during the rinsing process. **Figure 7.10** presents soil column mid-height V_s values versus injected rinse solution volume for all columns. As shown, all columns exhibited only minor V_s differences during rinsing with decreases of up to 55 m/s and increases of up to 10 m/s observed at the end of all rinse injections. While differences in V_s trends were expected between columns receiving continuous rinse injections of varying chemical compositions, surprisingly, columns receiving Ca^{2+}-based solutions exhibited similar behaviors as those rinsed with K^+- and Na^+-based solutions. However, when staged injections were used, which allowed for extended retention periods, both columns rinsed with solutions lacking Ca^{2+} (S-DI, S-K-200) exhibited the largest V_s reductions observed in all columns near 50 m/s (≈ 10% of post-treatment values) with more minimal V_s reductions observed in the column receiving staged Ca^{2+}-enriched solutions (S-Ca-200). In order to further resolve potential differences in $CaCO_3$ dissolution during rinsing, aqueous Ca^{2+} concentrations were measured in effluent solution samples from select columns during rinsing (**Supplemental Figure 7.1** in Appendix B). Greater aqueous Ca^{2+} concentrations observed exiting columns during rinsing were expected to be indicative of greater $CaCO_3$ dissolution. Although Ca^{2+} concentration differences from $CaCO_3$ dissolution could not be resolved for columns receiving Ca^{2+}-based rinse solutions due to high background Ca^{2+} concentrations, for all other tested columns (S-DI, C-DI, C-K-200, S-K-200, and C-Na-200), effluent Ca^{2+} concentrations were less than 1 mM after injection volumes exceeded 3 PV, suggesting that minimal dissolution of $CaCO_3$ occurred during the rinsing process. Although unexpected, measured Ca^{2+} concentrations during rinsing were highest for columns rinsed with K^+- and Na^+-based solutions with deionized water rinsed columns exhibiting the lowest Ca^{2+} concentrations. This may have resulted from the higher ionic strength

of the cation-enriched solutions, which would have reduced Ca^{2+} activities for the same Ca^{2+} concentration, therefore requiring greater $CaCO_3$ dissolution to reach equilibrium.

Following all rinse injections, columns were destructively sampled to determine soil $CaCO_3$ contents with distance from the injection location. **Figure 7.11** presents a summary of soil column $CaCO_3$ contents including soil $CaCO_3$ content measurements versus distance from the injection location (**Figure 7.11a**) and relationships between soil column average $CaCO_3$ contents and mid-height V_s values (**Figure 7.11b**). As shown, almost all columns achieved similar $CaCO_3$ content distributions with values between 4.0 and 5.5% by mass near the injection location and small reductions in values to between 2.5% and 4.0% by mass near column outlets (**Figure 7.11a**). Observed cementation gradients were consistent with other past experiments and were reflective of some $CaCO_3$ precipitation reactions occurring during cementation solution injections. Although no significant differences were observed as a function of rinse solution chemistry or injection sequencing, the single column receiving lower reagent concentrations (C-Ca-200-L) achieved significantly lower $CaCO_3$ contents between 0.5% and 1.0% by mass, consistent with the 80% reduction in applied urea and Ca^{2+} concentrations. $CaCO_3$ contents in the non-rinsed column (No Rinse) were also within the scatter of variations observed in the other rinsed columns, but generally had some of the highest measured values. When comparing average $CaCO_3$ contents and mid-height V_s values (**Figure 7.11b**), V_s values between 400 and 700 m/s were observed in most columns with average $CaCO_3$ contents between 3% and 4.25% by mass. Although variations in final V_s values were larger than expected for similar average $CaCO_3$ contents, values from this study compared well with past datasets from other studies involving biocemented Concrete Sand specimens that were both rinsed (Lee et al. 2019a; 2019b) and not rinsed (Gomez and DeJong

2017) following MICP. Although C-Ca-200-L had a significantly lower final V_s and average $CaCO_3$ content than other columns, its values remained consistent with the trends from other studies. Collectively, these results suggested that no significant differences in biocementation magnitudes or small-strain stiffness improvements were observed between columns as a function of differences in rinse injection strategies. **Table 7.4** provides a complete summary of final V_s values and soil $CaCO_3$ content measurements for all columns.

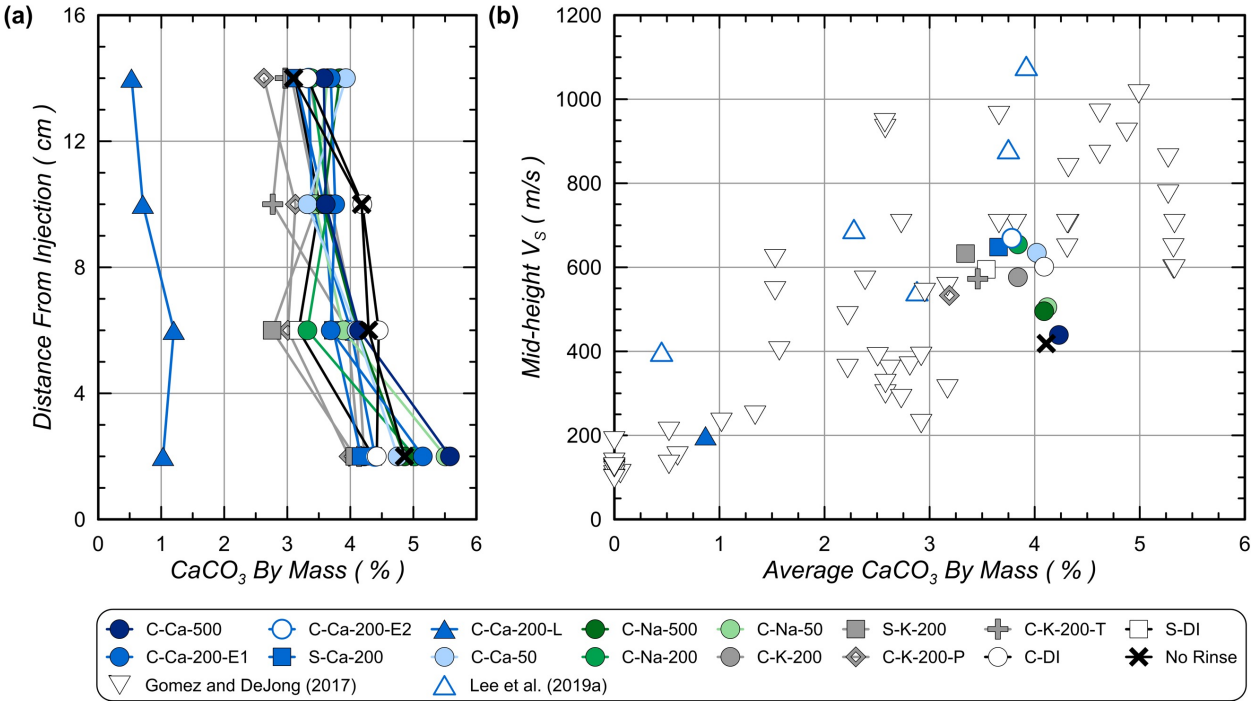

Figure 7.11. Summary of **(a)** soil column $CaCO_3$ contents by mass versus column length and **(b)** mid-height shear wave velocities (V_s) versus average soil column $CaCO_3$ contents by mass.

Table 7.4. Summary of Post-treatment Engineering Improvements for All Columns

Rinse Solution Type	Column(s)	Injection Sequence	Final V_s (m/s)	$CaCO_3$ Content (% By Mass)					
				Section Measurements					
				0 to 4 cm from injection	4 to 8 cm from injection	8 to 12 cm from injection	12 to 16 cm from injection	Average	Standard Deviation
500 mM Ca^{2+}	C-Ca-500	12 PV Continuous	496	4.86	4.11	3.57	3.83	4.09	0.56
200 mM Ca^{2+}	C-Ca-200-E1	12 PV Continuous	655	5.02	3.32	3.65	3.38	3.84	0.8
	C-Ca-200-E2	12 PV Continuous	669	4.39	4.01	3.39	3.34	3.78	0.51
	S-Ca-200	1 PV Staged (12x)	648	4.17	3.73	3.58	3.14	3.65	0.43
	C-Ca-200-L	12 PV Continuous	199	1.03	1.2	0.71	0.53	0.87	0.31
50 mM Ca^{2+}	C-Ca-50	12 PV Continuous	505	5.51	3.89	3.44	3.64	4.12	0.94
500 mM Na^{+}	C-Na-500	12 PV Continuous	439	5.58	4.14	3.61	3.58	4.23	0.94
200 mM Na^{+}	C-Na-200	12 PV Continuous	ND[1]	5.15	3.69	3.76	3.69	4.07	0.8
50 mM Na^{+}	C-Na-50	12 PV Continuous	635	4.75	4.1	3.32	3.93	4.02	0.59
200 mM K^{+}	C-K-200	12 PV Continuous	577	4.22	4.1	3.69	3.35	3.84	0.4
	S-K-200	1 PV Staged (12x)	633	4.07	2.76	3.47	3.07	3.34	0.56
	C-K-200-P	12 PV Continuous	533	3.98	3.01	3.13	2.63	3.19	0.57
	C-K-200-T	12 PV Continuous	573	4.14	3.96	2.77	2.97	3.46	0.69
DI-water	C-DI	12 PV Continuous	602	4.42	4.45	4.19	3.32	4.09	0.53
	S-DI	1 PV Staged (12x)	595	4.36	3.18	3.51	3.12	3.54	0.57
None	No Rinse	N/A	419	4.86	4.29	4.18	3.1	4.11	0.74

[1]*ND = V_s not determined due to sensor failure*

7.4 Conclusions

A study was performed to investigate the efficacy of different rinse injection strategies for the post-treatment removal of NH_4^+ by-products following ureolytic biocementation in poorly-graded clean sands. Sixteen soil column experiments were performed which received stimulation and cementation treatments over 16 days intended to enrich native ureolytic microorganisms and achieve similar post-treatment NH_4^+ concentrations and average $CaCO_3$ contents near 3.5% by mass. Three columns received modified biocementation treatments intended to evaluate several additional factors including the effect of K^+-based solutions applied prior to biocementation, amendment of treatment solutions with K^+ additions, and reductions in applied urea and calcium concentrations. Following biocementation, columns received alkaline rinse solution injections containing one of three different cations (Ca^{2+}, Na^+, K^+) at varying concentrations or deionized water. Rinse injections were applied in either a single continuous 12 PV injection or twelve 1 PV daily injections and a single column received no rinse injections to quantify baseline NH_4^+ concentrations existing prior to rinsing. During all treatments, aqueous samples were collected at various times to monitor changes in solution chemistry indicative of ureolysis, $CaCO_3$ precipitation, and NH_4^+ removal and soil shear wave velocities (V_s) were monitored to track cementation progression and changes in integrity during rinsing. Following all rinse injections, soil and fluid samples were used to quantify sorbed and aqueous NH_4^+ concentrations as well as soil $CaCO_3$ contents. From the results of this study, the following conclusions can be made:

- All columns rinsed with cation-enriched solutions achieved greater than 98%, 65%, and 95% aqueous, sorbed, and total NH_4^+ removal, respectively, at all sampled locations. In contrast, columns receiving solely deionized water injections achieved significantly less removal with greater than 98%, 19%, and 88% aqueous, sorbed, and total NH_4^+ removal observed,

respectively. Supplied cations in rinse solutions appeared to have more minimal impacts on aqueous NH_4^+ removal but enabled greater reductions in sorbed NH_4^+ concentrations likely due to exchange between supplied cations and sorbed NH_4^+ concentrations.

- While variations in supplied K^+ concentrations were not considered, results from columns rinsed with Ca^{2+}- and Na^+-based solutions suggested that differences in rinse solution cation concentrations had minimal effects for Ca^{2+}-based solutions with inconsistent effects observed for Na^+-based solutions. In particular, sorbed NH_4^+ removal comparable to Ca^{2+}-based solutions was observed at the 500 mM Na^+ concentration, however, lower Na^+ concentrations achieved significantly less sorbed NH_4^+ removal, which was more comparable to deionized water.
- Although differences between staged and continuous injections were minimal for columns rinsed with deionized water, when cation-enriched solutions were applied, staged injections resulted in significantly lower aqueous and sorbed NH_4^+ concentrations when compared to similar columns receiving continuous injections. Improvements in NH_4^+ removal with staged injections may be attributed to longer retention periods, which likely allowed for increased cation exchange and homogenization of NH_4^+ concentrations within columns during retention periods.
- Linear relationships were observed between sorbed and aqueous NH_4^+ concentrations in all rinsed columns with a maximum sorbed NH_4^+ concentration observed in the column receiving no rinse injections, which was near 61% of the CEC of Concrete Sand. Although not considered in this study, sandy soils containing greater clay and silt fractions with higher CECs may exhibit significantly higher sorbed NH_4^+ concentrations following biocementation. For these materials, sorbed NH_4^+ may constitute a larger fraction of the total NH_4^+ present

following biocementation and rinse strategies addressing these concentrations may be increasingly important.

- Although the selection of staged versus continuous injections had a greater impact on removal than rinse solution cation type, K^+-based rinse solutions enabled improved removal for similar injections due to its preference for exchange with sorbed NH_4^+ over other cations. Accordingly, the single column receiving K^+-based staged rinse injections (S-K-200) achieved the greatest NH_4^+ removal of all conditions examined.
- The use of both reduced MICP reagent concentrations and pre-treatment of soils with K^+-based solutions prior to biocementation resulted in minimal effects on NH_4^+ removal during rinsing. In contrast, the column receiving MICP treatment solutions amended with K^+ resulted in the lowest aqueous and sorbed NH_4^+ concentrations of all continuously-rinsed columns. Such additions during MICP treatments will necessitate significant increases in supplied cation masses, however, and should be carefully considered prior to use.
- Mechanical and geochemical data obtained during rinsing demonstrated that post-treatment NH_4^+ removal had minimal effects on biocementation integrity regardless of the particular rinsing strategy employed. V_s and soil $CaCO_3$ content relationships from this study were consistent with data from other past studies involving the same Concrete Sand material both with and without post-treatment rinsing.

Outcomes from this study significantly improve our understanding of NH_4^+ removal following ureolytic biocementation using rinse injections. However, further work remains needed to more fully understand the effect of rinse injection sequences, including combinations of staged and continuous rinse injections, as well as the potential of other remediation strategies such as those involving *in situ* nitrogen transformations.

Ultimately the determination of optimal rinse injection strategies will likely require site-specific analyses, which consider local material costs and associated environmental impacts, site-specific NH_4^+ removal requirements, existing groundwater chemistry and flow regimes, and other operational constraints.

Chapter 8. METER-SCALE BIOCEMENTATION EXPERIMENTS TO ADVANCE PROCESS CONTROL AND REDUCE IMPACTS: EXAMINING SPATIAL CONTROL, AMMONIUM BY-PRODUCT REMOVAL, AND CHEMICAL REDUCTIONS

This paper has been published in the ASCE *Journal of Geotechnical and Geoenvironmental Engineering*. Although Minyong Lee is the second author for this paper, Minyong had extensive involvement in the experimental design, performance, and writing of this publication. Therefore, this paper is presented herein, with slight modifications.

Citation:

San Pablo, A. C. M., Lee, M., Graddy, C. M. R., Kolbus, C. M., Khan, M., Zamani, A., Martin, N., Acuff, C., DeJong, J. T., Gomez, M. G., and Nelson, D. C. (2020). Meter-Scale Biocementation Experiments to Advance Process Control and Reduce Impacts: Examining Spatial Control, Ammonium By-Product Removal, and Chemical Reductions. *Journal of Geotechnical and Geoenvironmental Engineering*, 146(11), 04020125.

ABSTRACT

Microbially Induced Calcite Precipitation (MICP) is a ground improvement technique that uses ureolytic bacteria to biocement soils by precipitating calcium carbonate on soil contacts and surfaces. In this study, five 3.7-meter long horizontal columns, each containing 0.15 m^3 of natural sand, were treated to address current knowledge gaps regarding the application of MICP at field-scale including investigating treatment extent, improvement of spatial uniformity, stimulation strategies, and post-treatment removal of ammonium by-products. Two stimulated columns containing poorly-graded alluvial sand were treated to achieve high and low ureolytic rates to investigate differences in treatment uniformity and extent. An additional column with the same sand was augmented with *Sporosarcina pasteurii* targeting a high ureolytic rate similar to the high

rate stimulated column. Two additional stimulated columns, containing poorly-graded alluvial and marine sands, were treated to achieve a low ureolytic rate to evaluate the effect of soil mineralogy. Treatments were first applied to establish either indigenous or augmented microorganisms, after which all columns received 9 cementation treatments. Following cementation, produced ammonium by-products were removed using a rinse solution injection and soil samples were obtained and analyzed for calcite content. During all treatments, solution urea and ammonium concentrations as well as soil hydraulic conductivities and shear wave velocities were monitored. In all columns, insignificant changes in permeability were observed during treatments despite V_s increases up to 1325 m/s. Results also suggest that improvements in the spatial uniformity and extent of biocementation can be achieved through the use of lower ureolytic rates that minimize reactions during injections.

8.1 Introduction

Microbially Induced Calcite Precipitation (MICP) is a bio-mediated soil cementation process that uses ureolytic microorganisms capable of hydrolyzing urea to generate carbonate species and enable precipitation of calcium carbonate minerals (Stocks-Fisher et al. 1999). When precipitated on soil surfaces and contacts, produced calcium carbonate can bond soil particles, thereby increasing soil shear strength and shear stiffness with small reductions in hydraulic conductivity (Montoya et al. 2013; Montoya and DeJong 2015; Gomez and DeJong 2017; and others). MICP has been increasingly studied as a technology capable of addressing a diverse range of geotechnical and geoenvironmental problems, including mitigation of earthquake-induced liquefaction (DeJong et al. 2006; Montoya et al. 2013; Burbank et al. 2013; Han et al. 2016; Feng and Montoya 2017; Xiao et al. 2018; Darby et al. 2019), erosion prevention (Gomez et al. 2015), borehole stabilization

(van Paassen et al. 2010), fracture sealing (Cuthbert et al. 2013), bearing capacity improvement (Martinez and DeJong 2009), and soil strengthening (Gomez et al. 2016; Saneiyan et al. 2019). Additionally, MICP has been used for strengthening and repair of ornamental stone structures (Rodriguez-Navarro et al. 2003; De Muynck et al. 2010), concrete rehabilitation (Ramakrishnan et al. 1998, 2001; Ramachandran et al. 2001; De Muynck et al. 2008), fugitive dust control (Meyer et al. 2011), and immobilization of contaminants (Fujita et al. 2004, 2008; Dupraz et al. 2009). Despite recent advances in MICP and its implementation, knowledge gaps have remained regarding developing effective and economical strategies for stimulation of indigenous ureolytic microorganisms, improving biocementation spatial uniformity over large meter-scale distances, and managing ammonium by-products produced during urea hydrolysis.

Stimulation and augmentation are two approaches capable of establishing ureolytic activity in soils for MICP. During stimulation, selective media is applied to soils to enrich for indigenous ureolytic microorganisms. In the augmentation approach, *ex situ* culturing of ureolytic bacteria such as *Sporosarcina pasteurii (S. pasteurii)* is completed and the culture is amended to the soil, generally at high cell densities. Both approaches can be used to increase the capacity of the soil to hydrolyze urea for the MICP process through either increases in ureolytic cell densities and/or increased ureolytic microbial activity (DeJong et al. 2010). While most researchers have used the augmentation approach to generate ureolytic activity (Ferris et al. 1997, 2004; Ramachandran et al. 2001; Fujita et al. 2004; Mitchell and Ferris 2005; DeJong et al. 2006; Whiffin et al. 2007; Dupraz et al. 2009), concerns regarding permitting, financial costs, environmental impacts, and cell transport limitations in porous media remain. More recently, researchers have shown successful stimulation of indigenous ureolytic bacteria in a diverse range of environments

including the Snake River Plain Aquifer in Idaho, USA (Fujita et al. 2008; Burbank et al. 2010), the Israeli coastal plain (Gat et al. 2016), the Wildmoor Sandstone Formation aquifer in Birmingham, UK (Tobler et al. 2011), and various locations in Northern California, USA and British Columbia, Canada (Gomez et al. 2014, 2018; Gomez and DeJong 2017). In these enrichments, most researchers have provided urea, trace minerals, carbon sources such as molasses (Fujita et al. 2008; Burbank et al. 2010; Tobler et al. 2011; Gat et al. 2016) and yeast extract (Gomez et al. 2014, 2018; Gat et al. 2016), and other constituents. Although stimulation may require an extended timeframe for development of ureolytic activity relative to augmentation, the approach may provide significant advantages through the elimination of costs and environmental impacts associated with *ex situ* bacterial cultivation and the introduction of non-native bacterial species. The stimulation process may also improve the spatial uniformity of microbial activity by stimulating *in situ* ureolytic communities already distributed throughout soil pore space.

Several MICP experiments have been conducted at meter-scale using both augmentation and stimulation approaches. For example, Whiffin et al. (2007) augmented sands with *S. pasteurii* in a 5-meter column and observed detectable increases in strength, stiffness, and calcite. van Paassen et al. (2010) performed a large-scale experiment wherein 100 m^3 of poorly graded sand was biocemented at transport distances of 5 meters. van Paassen et al. (2011) performed a field-scale demonstration wherein 1,000 m^3 of gravel was augmented and cemented for horizontal directional drilling applications. Gomez et al. (2015) augmented and cemented loose sands to develop a cemented crust for mitigation of surficial soil erosion issues at a mine site. Smith et al. (2012) and Saneiyan et al. (2019) stimulated indigenous ureolytic bacteria in Rifle, CO for both co-precipitation of strontium carbonate during MICP and soil improvement, respectively. Lastly,

Gomez et al. (2016) performed a comparative study between *S. pasteurii* augmentation and stimulation using 1.7-m diameter tanks and showed comparable post-treatment engineering properties between approaches despite some reaction differences. Although these meter-scale demonstrations have significantly advanced this technology, challenges have remained with respect to field-scale deployment including the need for improved spatial uniformity at meter-scale, removal of ammonium by-products following treatments, and reductions in process financial costs and environmental impacts.

In this study, five 3.7-meter long horizontal columns received biocementation treatments over 26 days to investigate the effect of different biological approaches on biocementation spatial uniformity and extent, the effect of different natural soils on biocementation and stimulation processes, and the success of post-treatment ammonium by-product removal at meter-scale. Two columns containing poorly-graded alluvial sand were stimulated to achieve high and low ureolytic rates to investigate the effect of ureolytic rate on biocementation uniformity and extent. An additional column with the same sand was augmented with *S, pasteurii* targeting a high ureolytic rate, comparable to the high rate stimulated column, to examine differences between stimulation and augmentation processes. Lastly, two additional columns, which contained different poorly-graded alluvial and marine sands, were stimulated to achieve low ureolytic rates to evaluate the effect of soil type and mineralogy. Treatments were first applied to establish either indigenous or augmented microorganisms, after which all columns received nine cementation treatments. Following cementation, produced ammonium by-products were removed using a rinse solution injection and soil samples were obtained and analyzed for calcite content. During all treatments,

solution urea and ammonium concentrations as well as soil hydraulic conductivities and shear wave velocities were monitored.

8.2 Experimental Objectives and Development

8.2.1 *Experimental Development*

While further details are provided in related manuscripts, a summary of experimental design for stimulated ureolytic MICP are briefly summarized below.

8.2.2 *Control of Stimulated Ureolysis*

Centimeter-scale soil column experiments were performed to examine the control of stimulated ureolytic activity with the intention of improving the spatial control of biocementation over meter-scale distances. Tests examined the ability of changes in yeast extract concentrations applied during stimulation to control achieved total cell densities and thus control stimulated urea hydrolysis rates. Eight soil columns received daily stimulation treatments for six days containing yeast extract concentrations ranging from 0 g/L to 0.2 g/L. Four columns received yeast extract concentrations of 0.02, 0.04, 0.08, and 0.2 g/L every injection while the other four columns only received these same yeast extract concentrations on alternating days with 0 g/L applied on other days. After stimulation treatments, all columns received nine cementation treatments with similar alternating yeast extract additions once every 48 hours. Columns receiving the highest concentrations of 0.2 g/L yeast extract once daily achieved a high ureolysis rate corresponding to degradation of 250 mM urea in 24 hours, while columns receiving the lowest concentrations of

0.02 g/L yeast extract every other day achieved a low ureolysis rate corresponding to degradation of 250 mM urea in 48 hours. While further work is still needed to better characterize the effects of yeast extract additions, these preliminary experiments confirmed that a spectrum of stimulated bulk ureolytic rates could be obtained when the supplied yeast extract was varied.

8.2.3 *Ammonium By-product Removal*

Recent centimeter-scale soil column experiments examined ammonium by-product removal following stimulated ureolytic biocementation (Lee et al. 2019). Four columns contained the same Concrete Sand material and received identical stimulation and cementation injections. Following all biocementation treatments, rinse solution injections were applied once daily for five days to examine removal of produced ammonium concentrations from soil pore fluids. In these experiments, rinse solutions had initial pH values that varied from 5.0 to 9.0 and calcium chloride concentrations that ranged from 10 to 500 mM. A high pH (9.0) and high ionic strength (500 mM) rinse solution was found to increase ammonium removal following biocementation while limiting adverse effects on cementation integrity.

8.2.4 *Solution Optimization*

Centimeter-scale column experiments were performed to examine the effect of reductions in chemical concentrations used in stimulation and cementation treatments on post-treatment soil engineering properties. Stimulation and cementation solutions were formulated following the solutions used in Gomez et al. (2018), however, changes in applied urea concentrations were considered. In these experiments, urea concentrations used in stimulation solutions were varied

from 0 mM to 350 mM to investigate the effect of urea concentrations on stimulated ureolytic activity. Results suggested that urea concentrations used during stimulation could be reduced from 350 mM to 50 mM with no significant effects on stimulated bulk ureolysis rates. Although cementation solutions had contained urea-to-calcium ratios of 1.4:1 in past studies (Gomez et al. 2016; 2018), additional experiments were also performed to examine reductions in applied urea concentrations during cementation. Urea-to-calcium ratios varying from 1.4:1 to 1:1 were examined. Results suggested that urea-to-calcium ratios of 1:1 could be used during cementation treatments with no detectable loss in cementation or engineering performance (as evaluated by shear wave velocity and unconfined compressive strength measurements). In tandem, these results confirmed that a net reduction in urea consumption of 45% could be achieved.

8.2.5 *Reactive Transport Pre-modeling*

Numerical reactive transport pre-modeling was performed to examine the effect of changes in stimulated ureolytic rates on expected biocementation spatial uniformity in the meter-scale columns. A one-dimensional advective-dispersive soil column transport model was developed using the open-source geochemical code PHREEQC (Parkhurst and Appelo 2013) to explore the effect of changes in ureolytic rates ranging from the high rates measured in past experiments (Gomez et al. 2016; 2018) to lower rates observed in recent column experiments wherein applied yeast extract was reduced. From the meter-scale column geometries, soil properties, and anticipated flow rates, a ureolytic activity corresponding to ≈ 250 mM urea degradation within 48 hours was targeted to improve cementation uniformity across columns and was the basis for the development of the low ureolytic rate stimulation protocol discussed subsequently.

8.2.6 *Experiment Objectives*

Meter-scale horizontal soil column experiments were designed to address fundamental and practical barriers limiting the application of biocementation soil improvement at field-scale including: (1) to examine treatment uniformity and extent as a function of biocementation treatment strategies, (2) to investigate augmentation, stimulation, and cementation success at meter-scale distances in different natural sands, (3) to compare the relative efficacy of augmentation and stimulation biological strategies, and (4) to demonstrate and evaluate post-treatment removal of ammonium by-products. Techniques employed in these experiments built on recent advances in the control of stimulated ureolysis, ammonium by-product removal, optimization of MICP chemical constituents, and reactive transport pre-modeling.

8.2.7 *Experiment Rationale*

Five 3.7-meter long horizontal soil columns were prepared and treated using biocementation techniques to investigate the aforementioned knowledge gaps and factors at the meter-scale. For brevity, soil columns are referred to by their biological treatment type (L = low ureolytic rate stimulation, H = high ureolytic rate stimulation, A = augmentation with *S. pasteurii*) and sand (C = Concrete Sand, D = Delta Sand, R= Covelo River Sand). For example, LC, LD, and LR are low ureolytic rate stimulation columns that contained Concrete Sand, Delta Sand, and Covelo River Sand, respectively. HC is a high ureolytic rate stimulation column that contained Concrete Sand and AC is the augmentation column that contained Concrete Sand.

As mentioned previously, stimulation techniques capable of achieving low bulk ureolytic rates were identified through small column experiments. It was hypothesized that decreasing ureolytic activity would reduce ureolysis and related precipitation reactions during transport and therefore allow unconsumed calcium ions to be transported to further distances from the injection location. In this experiment, two stimulation strategies, high and low ureolytic rate stimulation treatments, were used on the same Concrete Sand to investigate this hypothesis (comparison of columns HC and LC). Additional experiments were completed using the low ureolytic rate stimulation strategy in the two other natural soils to better understand the effect of soil type on ureolytic stimulation (comparison of columns LC, LD, LR).

Previous meter-scale tank experiments investigated differences between MICP mediated by stimulated native microorganisms and augmented *S. pasteurii* (Gomez et al. 2016; 2019). While similar results were obtained between approaches, slightly more localized improvement was observed at early time in the augmented specimen. Results suggested that the inclusion of yeast extract in treatments applied to the augmentation tank led to a convergence of microbial communities near the end of both experiments (Graddy et al. 2018). Other augmentation experiments, however, have not included nutrients and instead relied on augmented cell densities alone to complete MICP (Whiffin et al. 2007; van Paassen et al. 2010). In order to investigate differences between native microbial stimulation and augmentation with non-nutritive media, a fifth column (column AC) was augmented with *S. pasteurii* using a non-nutritive solution to prevent simultaneous stimulation of indigenous ureolytic bacteria. The augmented cell density applied to AC was designed to match the high ureolytic rate of HC to enable comparison of

improvement using native and augmented microorganisms at similar ureolytic activities (comparison of columns HC and AC).

Lastly, the production of ammonium by-products associated with the degradation of urea during MICP is an environmental concern that must be addressed at field-scale. Following successful biocementation, all columns received high pH and high ionic strength rinse solutions to examine ammonium by-product removal at meter-scale as a function of biological treatment strategy and soil type. To evaluate removal success, concentrations of ammonium remaining in the pore fluid and on soil surfaces were monitored during and after rinse injections.

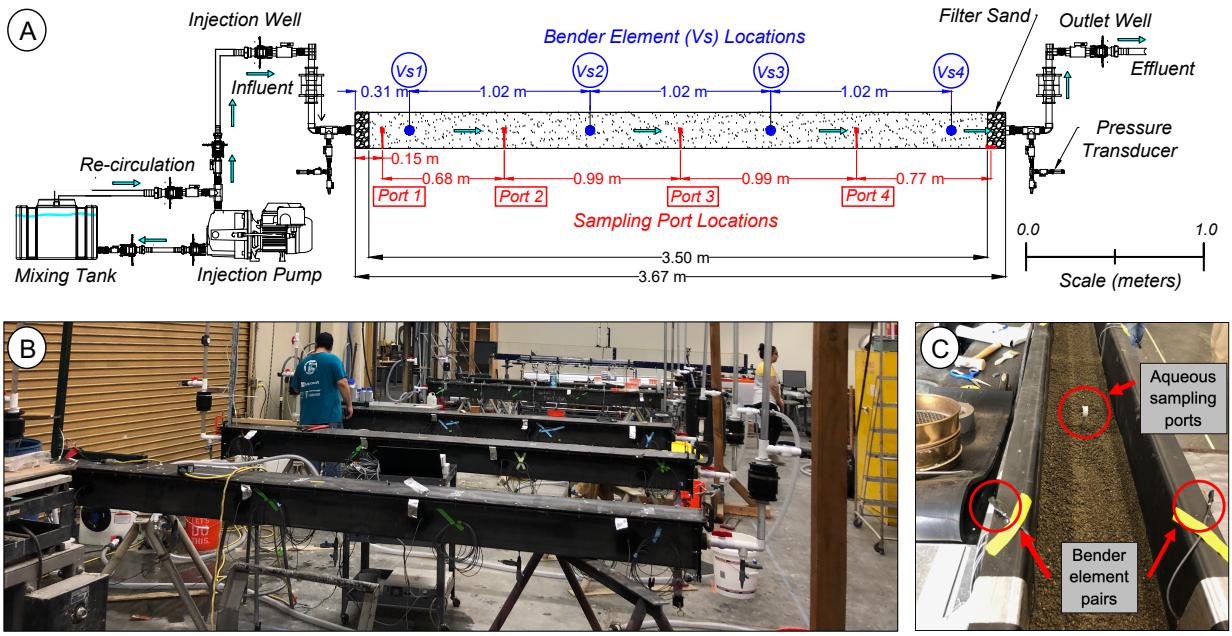

Figure 8.1. (a) Schematic of columns outlining locations of sampling ports and bender elements, treatment application systems, and the injected solution direction, (b) meter-scale column set-up, and (c) bender element pairs and sampling ports during soil placement.

8.3 Materials and Methods

8.3.1 *Meter-scale Soil Columns*

Five horizontal 3.7-meter long hollow steel columns with square cross-sections (0.2 m x 0.2 m) contained 0.15 m^3 of soil. Columns received solution injections in one direction to simulate a single stream tube within a well-to-well half-space. A rubber coating material was applied to the column surfaces to mitigate potential solution interactions. Clear PVC tubing (ID = 26.6 mm) and valves were located at column ends and allowed for pressurization of injected solutions and removal of effluent solutions. Soil materials were placed along the length of columns in three lifts, with lift thicknesses varying from 16 to 102 mm. Lifts allowed for bender element sensors to be installed at mid-height within columns. Following soil placement, lift surfaces were tamped using a 10-pound Modified Proctor compaction hammer. Between lifts, soil surfaces were scarified to limit density differences and preferential flow between layers. After soil placement, a 6.35 mm thick neoprene rubber sheet was placed on top of the soil and a steel cap was used to compress the rubber sheet against the soil surface (resulting in a modest level of confinement and prevention of any gaps that could provide preferential flow along the boundaries). Placed relative densities for sand materials varied between 56 and 67% and porosities varied between 0.3 and 0.4. Pore volumes (PV) were 50.7, 48.5, 50.6, 63.0, and 50.3 L for HC, LC, AC, LD, and LR columns, respectively. Monterey Sand was placed at the end of each column as a filter material with a thickness of 0.08 m near the injection well and 0.10 m near the outlet well. The total length of treated soil was 3.48 m. Columns were instrumented with 4 bender element pairs placed at 0.31 m, 1.33 m, 2.35 m, and 3.37 m away from the injection well and 4 aqueous sampling ports were located at 0.15 m, 0.83 m, 1.82 m, and 2.81 m away from the injection well. Aqueous sampling ports were designed to sample at mid-height within columns and were constructed with 0.15 m long steel tubes (ID = 3.35

mm) with 25.4 mm diameter circular plastic filters (125-195 μm). Sampling ports were equipped with valves for both solution sampling and pore pressure measurements. **Figure 8.1** provides a detailed schematic as well as images of soil columns during treatments and soil placement.

8.3.2 *Treatment Application System*

Small 0.1 HP pumps (Wayne Inc.) were used to inject treatment solutions. Injection pressures were monitored using pressure gauges between pumps and injection wells. A flow rate of 400 mL/min was used during saturation, stimulation, and cementation treatment phases and treatment volumes of ≈ 76 L were applied over ≈ 189 minutes. During the ammonium by-product rinsing phase, a flow rate of 750 mL/min was used to inject 525 L of rinse solutions in each column and rinsing treatments lasted ≈ 700 minutes. All solutions were mixed for at least 10 minutes before injection and were allowed to continuously recirculate during treatments through the injection pump and mixing tanks to ensure that injected solutions remained homogenized.

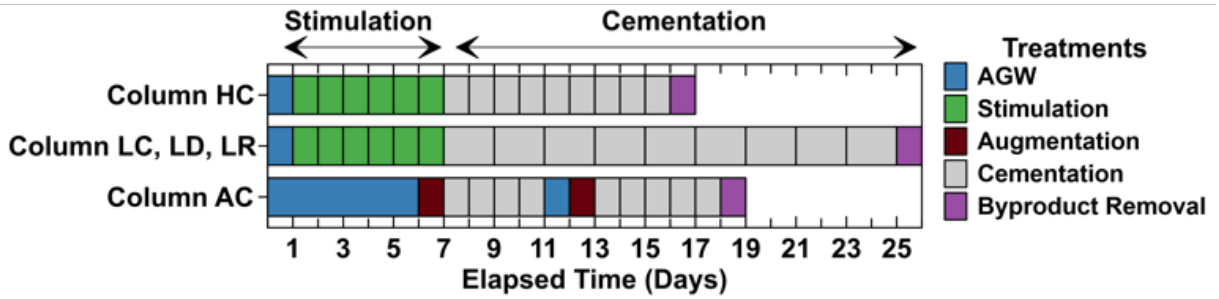

Figure 8.2. Schedule of soil column treatments including treatment durations and type of treatment for each respective column. Black horizontal lines indicate when treatments were injected.

8.3.3 *Treatment Schemes*

All columns were saturated with an artificial ground water (AGW) solution, which included 40 μM potassium nitrate, 40 μM sodium nitrate, 60 μM potassium bicarbonate, 450 μM magnesium sulfate, 1.1 mM sodium bicarbonate, and 1.75 mM calcium chloride as described in Ferris et al. (2004). Following saturation, all columns received passive tracer test injections consisting of 76 L of 15 mM NaBr followed by 76 L of de-ionized (DI) water to evaluate solution transport properties between columns. All columns were then subjected to three different treatment phases: (1) stimulation/augmentation, (2) cementation, and (3) ammonium by-product rinsing. **Figure 8.2** outlines the treatment schedule for all columns wherein horizontal bars indicate when a treatment injection was applied. During the first treatment phase, stimulation/augmentation, all four stimulation columns received different stimulation solutions once daily for 6 days to stimulate native ureolytic microorganisms, as shown by the green boxes in **Figure 8.2**. On the last day of stimulation treatments, Column AC received an inoculation treatment consisting of 76 L of *S. pasteurii* (ATCC strain 11859) at a cell density of 9.4 x 10^7 cells/mL in an isotonic 9 g/L NaCl saline solution, as shown by the maroon box in **Figure 8.2**. As mentioned previously, the cell density applied to AC was intended to match the higher ureolytic rate of the high rate stimulation column, HC. After augmentation and stimulation, all columns received nine cementation treatments (gray boxes in **Figure 8.2**). Columns HC and AC received cementation treatments once daily over 9 days, while columns LC, LD, and LR were treated once every other day over 18 days to allow complete hydrolysis of urea to occur. Due to lower than expected ureolytic activity in AC, a second augmentation treatment was applied after the 4^{th} cementation injection. An artificial ground water flush was injected in between the 4^{th} cementation injection and the second augmentation to rid the system of unconsumed chemicals from the 4^{th} cementation treatment. The

second augmentation injection consisted of 1.4 x 10^6 cells/mL in 456 L of the isotonic saline solution. The 456 L injected was intended to equal the total volume of stimulation solution that was received by the stimulated columns during the 6 stimulation treatments. This increased injected volume was designed to match the pumping effort of stimulation columns and enable more uniform distribution of *S. pasteurii* along the length of the column. These two augmentation injections are shown in **Figure 8.2** (maroon boxes). After completing all cementation treatments, ammonium by-product rinsing was performed, (purple boxes in **Figure 8.2**). During rinsing, all columns received 525 L of a high pH and high ionic strength rinse solution.

Table 8.1. Summary of Column Soil Properties

Soil Material	USCS	Source	Deposition	D_{10} (mm)	D_{30} (mm)	D_{60} (mm)	Fines Content (%)	Gravel Content (%)	Initial Calcite Content (%)
Concrete Sand (C)	SP	Woodland, CA	Alluvial	0.23	0.54	1.54	1.1	0.2	0.04
Delta Sand (D)	SP	Petaluma, CA	Marine	0.19	0.25	0.37	1.3	0.0	0.11
Covelo River Sand (R)	SP	Covelo, CA	Alluvial	0.23	0.52	1.55	1.6	2.5	1.64
Monterey Sand (Filter material)	SP	Pleasanton, CA	Alluvial	1.01	1.15	1.45	0.0	0.0	-*

*Not measured.

8.3.4 *Soil Materials*

Three different natural sands were used to prepare soil columns. Two sands were quarried from natural alluvial deposits (Concrete Sand and Covelo River Sand) and a third sand was obtained from a marine depositional environment (Delta Sand). Monterey Sand, a coarser sand, was used as filter material at column ends. Untreated soil calcite contents were measured for treatment sands and were 0.04%, 0.11%, and 1.64% by mass for Concrete Sand, Delta Sand, and Covelo River Sand, respectively. **Table 8.1** summarizes select soil properties.

Table 8.2. Summary of Solution Chemical Compositions and Treatment Injections

Constituent	Column HC		Column LC, LD, LR		Column AC		All Columns
	Stimul-ation	*Cement-ation*	*Stimul-ation*	*Cement-ation*	*Augment-ation*	*Cement-ation*	*NH_4^+ Rinsing*
Calcium Chloride (mM)	-	250	-	250	-	250	200
Urea (mM)	50	250	50	250	-	250	-
Ammonium Chloride (mM)	100	12.5	100	12.5	-	12.5	-
Sodium Acetate (mM)	42.5	42.5	42.5	42.5	-	42.5	-
Sodium Hydroxide* (g/L)	1.28	-	1.28	-	-	-	-
Yeast Extract (g/L)	0.2	0.2	0.04	0.02	-	-	-
Sodium Chloride (g/L)	-	-	-	-	9	-	-
S. pasteurii (cells/mL)	-	-	-	-	$9.4 \times 10^{7**}$ $1.4 \times 10^{6***}$	-	-
Initial solution pH	9.0	8.4	9.0	8.4	≈ 7.0	8.4	10.0
Number of treatments	6	9	6	9	2	9	1
Treatment volume (L)	76	76	76	76	76^{**} 456^{***}	76	525
Treatment time (min)	186	186	186	186	186^{**} $1{,}140^{***}$	186	700
Retention time (hours)	20.8	20.8	20.8	44.8	24.5	20.8	12.3

*Used to adjust pH to 9.0 for stimulation treatments.
**First augmentation treatment.
***Second augmentation treatment.

8.3.5 *Treatment Solutions*

Chemical constituents and concentrations for all applied treatment solutions are outlined in **Table 8.2**. All stimulation columns included 50 mM urea, with differences only in applied yeast extract. Stimulation solutions were pH-adjusted to 9.0 as described by Gomez et al. (2018) to increase selectivity for ureolytic microorganisms. Following successful stimulation, a flush solution that consisted of the same cementation treatment solution without urea, yeast extract, and calcium chloride was applied before the first cementation injection to reduce aqueous carbonate

concentrations (Gomez et al. 2019). All columns received cementation solutions with urea-to-calcium ratios of 1:1 with either 0 g/L, 0.02 g/L, or 0.2 g/L yeast extract. Ammonium by-product rinse solutions consisted of 200 mM calcium chloride with an initial pH near 10.

8.3.6 *Passive Tracer Measurements*

After saturation, passive tracer testing was completed for all columns. In these tests, 76 L of a 15 mM NaBr solution was applied to all columns followed by a 76 L de-ionized water injection. During tracer injections, solutions were pumped at a flow rate of 400 mL/min and 50 mL samples were collected at the outlet well every 5 minutes. Solution transport properties in all columns were examined by comparing the arrival and removal of passive Br^- ions at the outlet well. Solution conductivities were measured for each sample and were normalized by injected Br^- concentrations to calculate C/C_0 values.

8.3.7 *Aqueous Sampling*

Aqueous samples were collected from all sampling ports to monitor pH, urea, and aqueous ammonium concentrations. Samples were obtained from each sampling port before and after treatment injections. Additional samples were obtained 1, 2, 4, and 8 hours after the 2^{nd}, 4^{th}, and 6^{th} stimulation treatments for the stimulated columns and on the 1^{st}, 2^{nd}, 3^{rd}, 5^{th}, 7^{th}, and 9^{th} cementation treatments for all columns to monitor bulk ureolytic activity. For all low rate stimulation columns, a 24-hour sample was also collected. During ammonium by-product rinsing, ≈ 10 mL samples were collected every 20 minutes from the outlet well and every 60 minutes

samples were collected from all sampling ports including the injection and outlet well. Prior to collection of ≈ 10 mL samples, ≈ 30 mL of fluid was flushed from each sampling port. All samples were frozen after collection and stored at -20°C until subsequent analysis.

8.3.8 *Shear Wave Velocity Measurements*

Shear wave velocity (V_s) measurements were obtained using bender element sensor pairs placed at mid-height within columns and were oriented horizontally. Bender element sensors were fabricated and waterproofed using epoxy, electronics wax, and an insulating coating (Montoya et al. 2012; Gomez et al. 2016). Transmitting bender elements were excited with a 24V 100 Hz square wave and signals were received by the bender element pair using an oscilloscope with a sampling frequency of 1 MHz. V_s measurements were taken before treatment injections and were visually interpreted based on the arrival of the shear wave and measured sensor spacings. On select days, additional V_s measurements were taken 4 and 8 hours after injections for all columns and 24 hours after injections for all low rate stimulation columns. During ammonium by-product rinsing, V_s measurements were completed before injections and 2, 4, 8, 11.6, and 24 hours after the start of injections to assess potential effects on cementation integrity in time.

8.3.9 *Hydraulic Conductivity Measurements*

Hydraulic conductivities were calculated for soil column sections located between sampling ports using pressure head and flow rate measurements obtained during injections. Six pressure transducers (Omega Inc., 0 to 200 kPa range) were located at all sampling port locations and at the

injection and outlet wells. Pressure transducers were excited with 5V DC and pressures were recorded using a data acquisition system. Prior to all treatments, hydrostatic conditions were measured to ensure consistent reference conditions. During injections, flow rates were stabilized at 400 mL/min for 30 minutes and pressure measurements were recorded for at least 10 minutes after flow stabilization. Hydraulic gradients ($\Delta h/L$) for all columns were calculated from head differences between sampling ports and the injection and outlet wells. Hydraulic conductivities were then calculated between ports from the measured flow rates, hydraulic gradients, and the cross-sectional area of columns.

8.3.10 *Biological Measurements*

Aqueous solution and soil samples were collected from all columns for subsequent biological measurements. After ≈ 30 mL of fluid was discarded from each sampling port, aqueous samples of 10 to 50 mL were obtained at various points in time for total direct counts, dissolved oxygen measurements, and future 16S rDNA sequencing. Prior to ammonium by-product rinsing, soil samples were collected from select columns for future 16S rDNA extraction and sequencing. Total direct counts of suspended bacteria were measured using epifluorescene microscopy as described by Hobbie et al. (1977).

8.3.11 *Soil Sample Measurements*

After ammonium by-product rinsing, column caps were removed, and soil samples were collected at mid-height within columns at various locations. An oscillating saw was used in heavily-

cemented regions to extract samples. Soil samples were oven-dried at 60 ºC for at least 72 hours following sampling. Calcite content measurements (by mass) were then obtained for soil samples following ASTM D4373-14 (ASTM 2014) wherein oven-dried soil was reacted with 2 M hydrochloric acid to produce carbon dioxide gas in a sealed chamber. Increases in chamber pressures were measured and correlated to calcite masses from developed calibration relationships. For each soil sample, at least three calcite content measurements were performed and then averaged.

8.3.12 *Chemical Measurements*

Urea and ammonium concentrations were measured in aqueous samples to assess ureolytic activity and ammonium by-product removal spatially and temporally. Urea measurements were completed using a colorimetric assay similar to Knorst et al. (1997). Aqueous samples were diluted and reacted with a colorimetric reagent, consisting of absolute ethanol with 4% (w/v) p-dimethyaminobenzaldehyde and 4% (v/v) 12 M hydrochloric acid. Sample absorbances were measured at 422 nm using a microplate spectrophotometer. Sample ammonium concentrations were measured using a salicylate reaction similar to Krom (1980), wherein two reagents (Reagent A and B) were added to dilute samples and a microplate spectrophotometer was used to measure absorbance at 650 nm. Reagent A consisted of 0.05% (w/v) sodium nitroprusside, 13% (w/v) sodium salicylate, 10% (w/v) sodium citrate, and 10% (w/v) sodium tartrate in water. Reagent B consisted of 5% sodium hypochlorite (v/v) and 6% sodium hydroxide (w/v) in water.

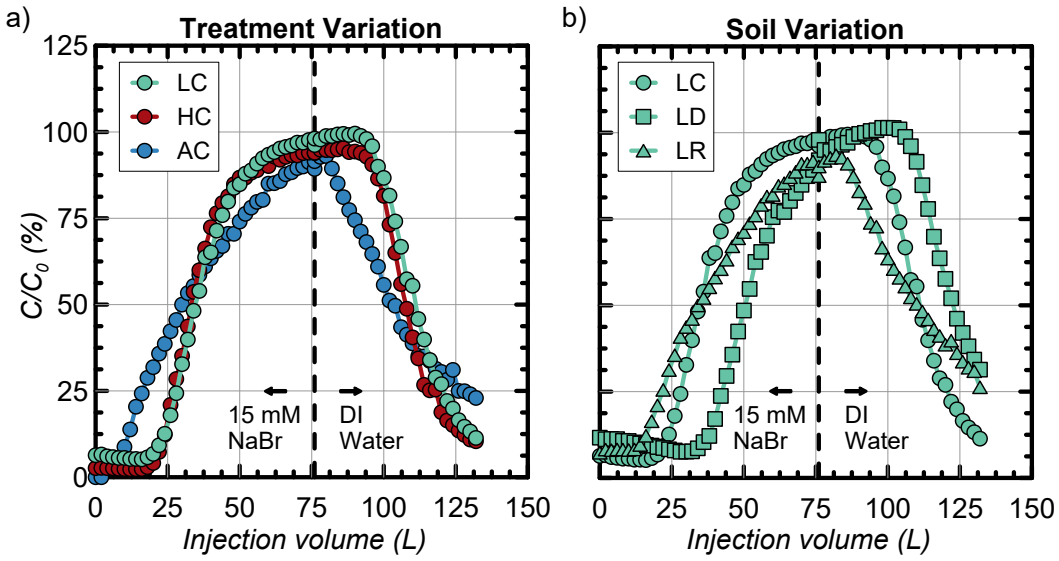

Figure 8.3. Measurements of C/C_0 versus injected volume from column outlet wells during passive tracer tests wherein a 15 mM NaBr solution was injected and rinsed with de-ionized (DI) water.

8.4 Results and Discussion

8.4.1 *Passive Tracer Testing*

Breakthrough curves obtained for all columns during passive tracer testing is presented in **Figure 8.3**. Passive tracer tests were used to evaluate the advective-dispersive transport differences between soil columns prior to biocementation treatments. All columns initially had C/C_0 values of less than 12%, likely resulting from background ion conductivities, with LD having the highest value. The higher initial C/C_0 value in LD is consistent with higher exchangeable cations measured in Delta Sand (Lee et al. 2019). Most soil columns, except for LD, had C/C_0 values above 20% after injecting only 20 to 30 L. In contrast, LD required near 42 L of injected solution before an increase in the C/C_0 value above 20% was detected. The lag in Br^- arrival for LD likely resulted from the larger porosity, 0.40, in this column. Despite this difference, all columns had C/C_0 values greater than 89% after injecting the daily treatment volume of 76 L of NaBr solution, with AC

having the lowest value with 89% and LD having the highest value with 98%. Columns HC and LC had similar breakthrough curves while the breakthrough curve for AC was more similar to LR despite containing a different sand material. This may be indicative of some variability in soil preparation and/or preferential flow.

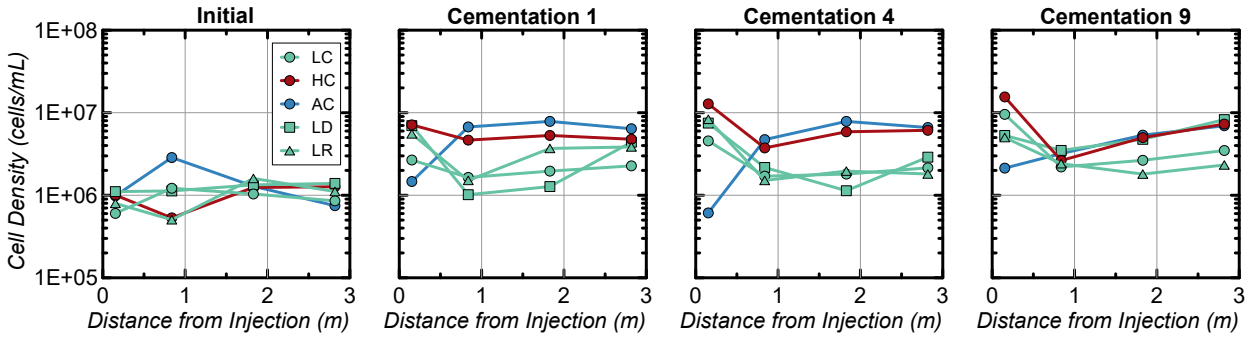

Figure 8.4. Aqueous cell densities versus distance from injection location for all columns during initial conditions (after saturation) and at the end of the 1st, 4th, and 9th cementation treatment.

8.4.2 *Biological Monitoring*

Measured aqueous cell densities along column lengths for select times including initial conditions (after saturation), and after the 1st, 4th, and 9th cementation treatment, are presented in **Figure 8.4**. As shown after saturation and prior to all stimulation treatments, cell densities along all columns ranged from ~5.0 x 10^5 to 2.9 x 10^6 cells/mL, showing similar initial conditions. After the 1st cementation treatment, however, cell densities across the length of HC were between 4.7 to 7.1 x 10^6 cells/mL, between 1.5 to 7.9 x 10^6 cells/mL for AC, and were significantly lower for all low rate stimulation columns (1.0 to 7.0 x 10^6 cells/mL). In general, all low rate stimulation columns had cell densities that were 2.5 to 4.5 x 10^6 cells/mL lower than high rate stimulation columns. This difference was per design as lower yeast extract concentrations were hypothesized to yield

lower ureolytic rates through reductions in total cell densities. It should be noted that attached cell populations could not be accounted for from solution measurements alone and may have also differed significantly between stimulation conditions. Additionally, cell density measurements account for all cells and do not differentiate between ureolytic and non-ureolytic cells.

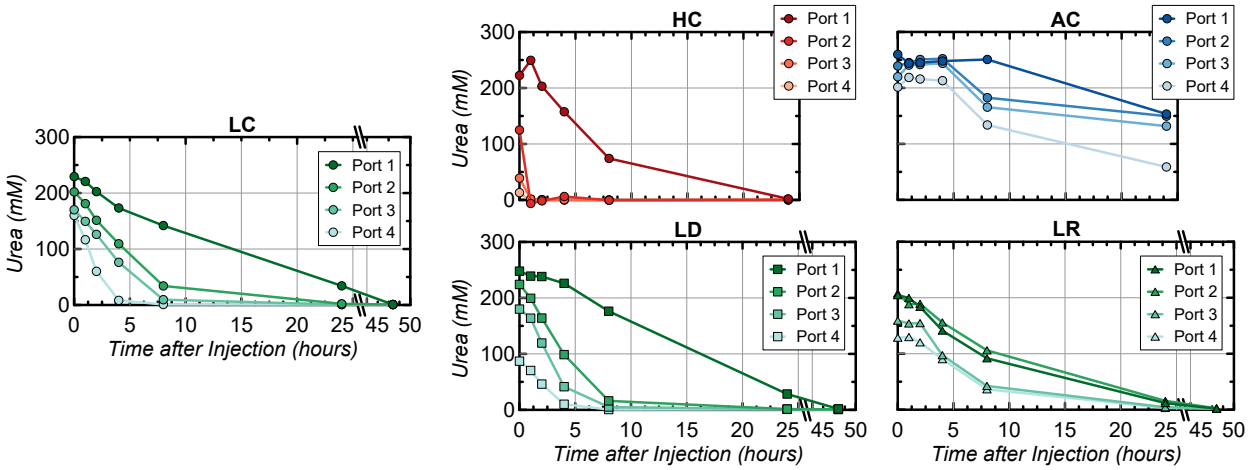

Figure 8.5. Concentrations of aqueous urea in time at all port locations in all columns during the 9th cementation treatment.

Figure 8.5 presents urea concentrations in time at different port locations along column lengths following the application of the ninth cementation injection, which was representative of other treatment residence periods. Aqueous samples were collected 0, 1, 2, 4, 8, and 24 hours after injection for all columns and 48 hours after injection for low rate stimulation columns (LC, LD, and LR). It is noted that results from Port 1 are not discussed in detail as lower ureolytic rates observed at this location may have resulted from either lower ureolytic bacteria densities due to detachment during injections or the mixing of unreacted solutions from the nearby solution reservoir during timed sampling. As shown, urea concentrations for all ports, except for Port 1, show urea concentrations lower than the injected concentration of 250 mM indicating both

reactions during transport and solution mixing. In the high rate stimulation column, HC, lower concentrations of urea at Ports 2, 3, and 4 of 125 mM, 39 mM, and 13 mM, respectively, were observed which indicates significant reactions during transport. In all low rate stimulation columns, higher concentrations of urea were observed from 203 mM to 224 mM at Port 2, from 159 mM to 180 mM at Port 3, and from 87 mM to 160 mM at Port 4. The presence of higher urea concentrations across the length of the low rate stimulation columns confirmed that more limited urea hydrolysis occurred during injection transport. Additionally, the ureolysis rate was higher in HC than LC with all urea hydrolyzed after 1 hour of retention in the column at all locations beyond Port 1. In comparison, all low rate stimulation columns had similar ureolytic rates with all ports, hydrolyzing injected urea within a 48-hour period. Significantly lower ureolytic rates observed in low rate stimulation columns LC, LD, and LR compared to the high rate stimulation column HC were expected to result in differences in soil calcite contents along column lengths due to differences in precipitation reactions occurring during solution transport. In AC, however, only 40% to 70% of injected urea was hydrolyzed across the length of the column after 24 hours. Limited ureolytic activity in all ports for AC with more urea degradation at the distal end was surprising and likely resulted from the second augmentation, which injected an additional 456 L of inoculum. Poor ureolysis was also observed following the first augmentation with most ureolytic activity localized to regions near the injection well (data not shown). Despite the unexpected lower ureolytic rate observed in AC, a high cell density was observed in this column similar to HC, which may have resulted from trace yeast extract remaining in the augmentation media used to culture *S. pasteurii* and microbial succession. Although a ureolytic rate similar to HC was expected in AC, this was not observed, suggesting that even more augmentation

treatments would have been necessary to achieve uniform ureolytic activity over large injection distances.

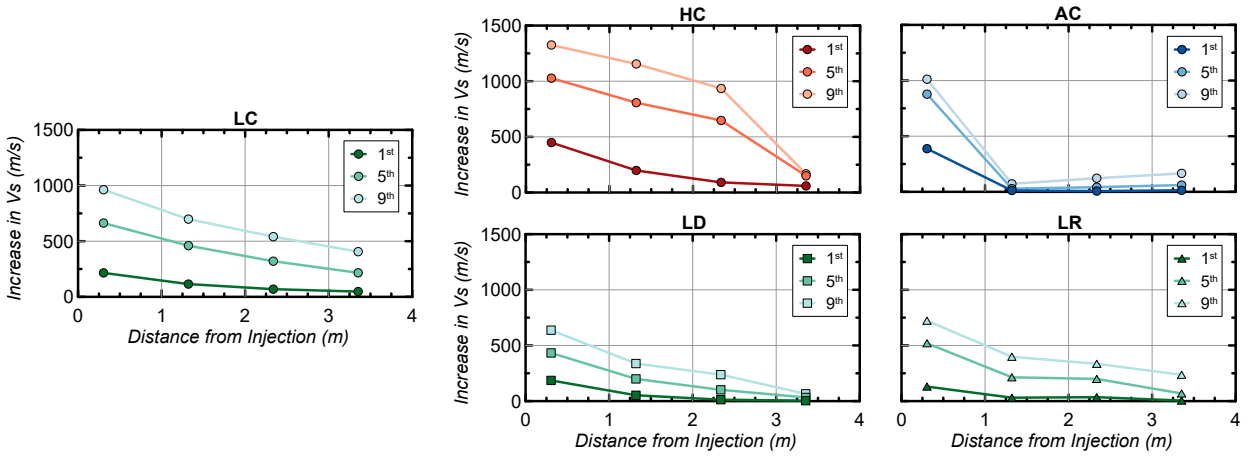

Figure 8.6. Spatial contours of soil V_s for all columns after the 1st, 5th, and 9th cementation injection.

8.4.3 *Shear Wave Velocity Measurements*

Increases in soil V_s measured along all column lengths following the 1st, 5th, and 9th cementation treatments is presented in **Figure 8.6**. The greatest increases in V_s were observed near injection wells for all columns and exceeded 637 m/s following nine cementation treatments. HC had the highest increase in V_s of about 1325 m/s near the injection location, however, near the end of the column (distance of 3.37 m) an increase of only 168 m/s occurred. When comparing columns HC and LC, a larger increase in V_s was observed in HC after 9 cementation treatments at locations closer to the injection well, however, in LC at a 3.37 m distance an improvement of 406 m/s was observed compared to only 168 m/s in HC. These results suggest that reductions in ureolytic activity were able to achieve more distal and uniform improvement compared to higher ureolytic rates for the given flow conditions. If soil columns had been longer than 3.7 meters and

representative of free-field conditions, LC would have been expected to have obtained a similar total mass of precipitation in a more distributed and uniform manner.

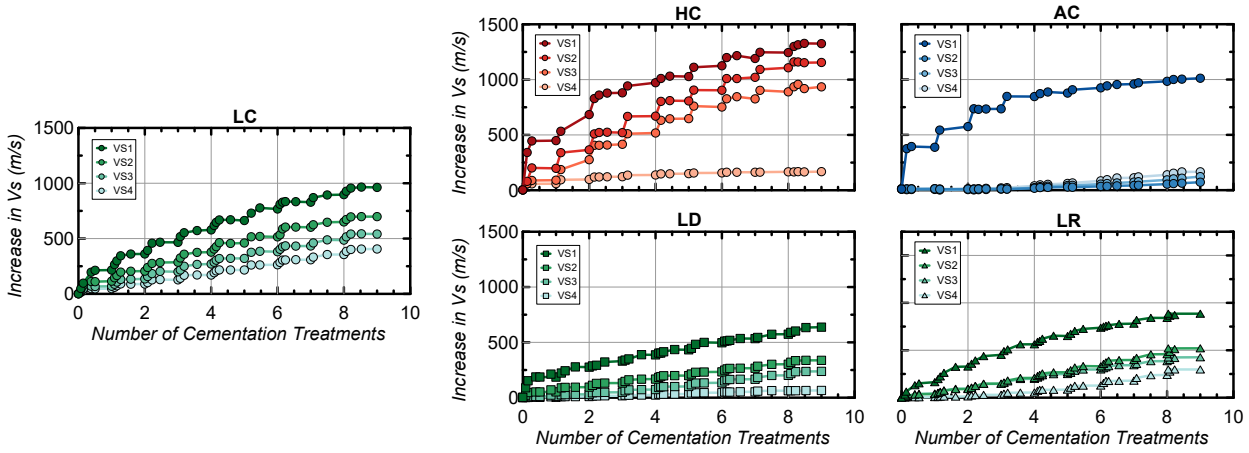

Figure 8.7. Increase in V_s in time at all sensor locations for all columns showing the progression of V_s with number of cementation treatments.

V_s increases versus cementation treatment number for all measurement locations in all columns is presented in **Figure 8.7**. As shown previously, more uniform increases in V_s across column lengths were observed in low rate stimulation columns with all measurement locations exhibiting similar behaviors in time. These results suggest that soil type can affect V_s improvements. However, the cause of this variation is not fully understood. Although similar bulk ureolytic rates were observed between all low rate stimulation columns, differences in V_s trends for similar treatments may have resulted from other biogeochemical differences (microbial communities, strain-specific ureolytic rates, soil fabric and minerology, etc.) and or differences in precipitate distributions at the particle scale. For both columns HC and AC, a rapid reduction in V_s improvement was observed with distance from the injection location. In AC, a large increase in V_s was only measured near the

injection port (distance of 0.31 m). Localized improvement near the injection well in AC was consistent with poor ureolytic activity observed at larger treatment distances.

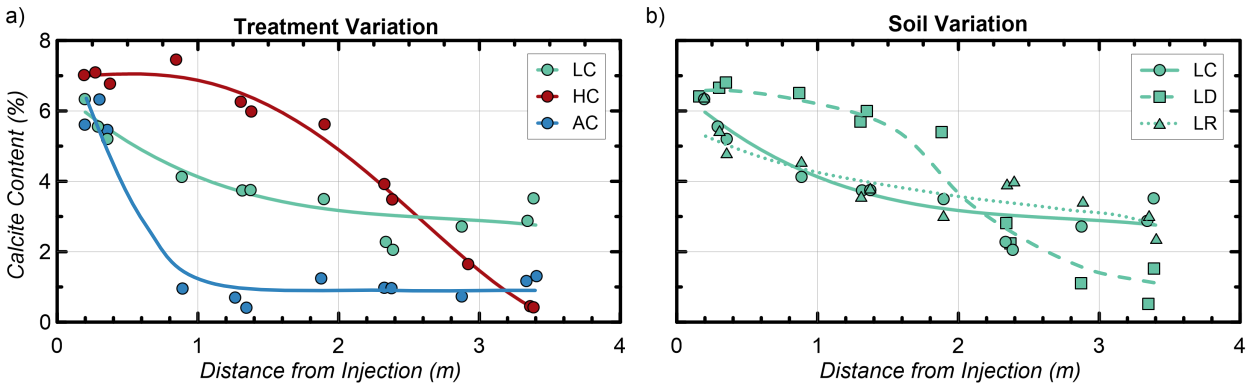

Figure 8.8. Comparison of calcite content spatial measurements with trend line interpretations for (a) Concrete Sand with different biological treatment types and (b) for low ureolytic rate stimulation treatments for different sands.

8.4.4 *Calcite Content Measurements*

Soil calcite content spatial contours for all columns from measurements obtained at bender element and sampling port locations is presented in **Figure 8.8**. Observed soil calcite content trends were consistent with V_s trends. Large decreases in calcite contents were observed after 2.3 m for HC and after 0.3 m for AC. Calcite contents across column lengths ranged from 0.4% to 7.5% for HC and 0.1% to 6.3% for AC. In contrast, calcite contents were more uniform for low rate stimulation columns with values ranging from 2.1% to 6.3% for LC, 0.5% to 6.8% for LD, and 2.4% to 6.4% for LR. Surprisingly, a low calcite content near 0.5% was measured at the distal end of LD and was consistent with minimal V_s improvement observed at this location. A more limited treatment extent in this column may have resulted from the significantly larger pore volume in LD.

Table 8.3. Comparison of Actual and Theoretical Calcite Contents (CC) for Columns

			Low reactions during transport	High reactions during transport
Column	**PV (L)**	**Measured Average CC (%)**	**Theoretical CC (%) with 1 PV**	**Theoretical CC (%) with 76 L* (~1.2 - 1.5 PVs)**
LC	48.5	3.72	3.38	5.20
HC	50.7	4.97	3.58	5.28
AC	50.6	1.80	3.61	5.32
LD	63	4.45	5.22	6.23
LR	50.3	4.01	3.71	5.50

*76 L represents the treatment injection volume for cementation treatments.

Table 8.3 provides a comparison of the measured average calcite contents (CC) for all columns with the theoretical values calculated assuming that either 1 PV of solution reacted to completion (low reactions during transport) or the entire injected volume (76 L) reacted to completion (high reactions during transport). The 1 PV theoretical value represents the maximum CC that can be achieved if no precipitation reactions occurred during transport and the 76 L theoretical value represents the maximum CC possible if all calcium were fully consumed through significant reactions during transport. The actual average calcite content across all columns was calculated by averaging the measured calcite content data along column lengths with distance. Values for HC suggest that significant reactions during transport occurred with the measured average CC (4.97%) being much closer to the 76 L theoretical CC (5.20%) than the 1 PV theoretical CC (3.58%). This indicated that minimal calcium remained unconsumed during treatments, and therefore almost no soluble calcium would be expected to be transported and precipitate at further distances with this formulation. However, for the low ureolytic columns, LC, LD, and LR, the measured average CC values (3.72%, 4.45%, and 4.01%, respectively) were significantly closer to the theoretical 1 PV CC values (3.38%, 5.22%, and 3.71%, respectively) rather than the injected volume 76 L theoretical CC values (5.20%, 6.23%, and 5.50%, respectively). This suggested that reactions

during transport were much more limited, thus soluble calcium could have been transported to precipitate at further distances if column lengths had exceeded the 3.7 meters tested. In AC, the average calcite content was near half of the theoretical 1 PV CC value, further confirming the conclusion that AC did not fully consume the urea and calcium that was transported and retained within the column after injections.

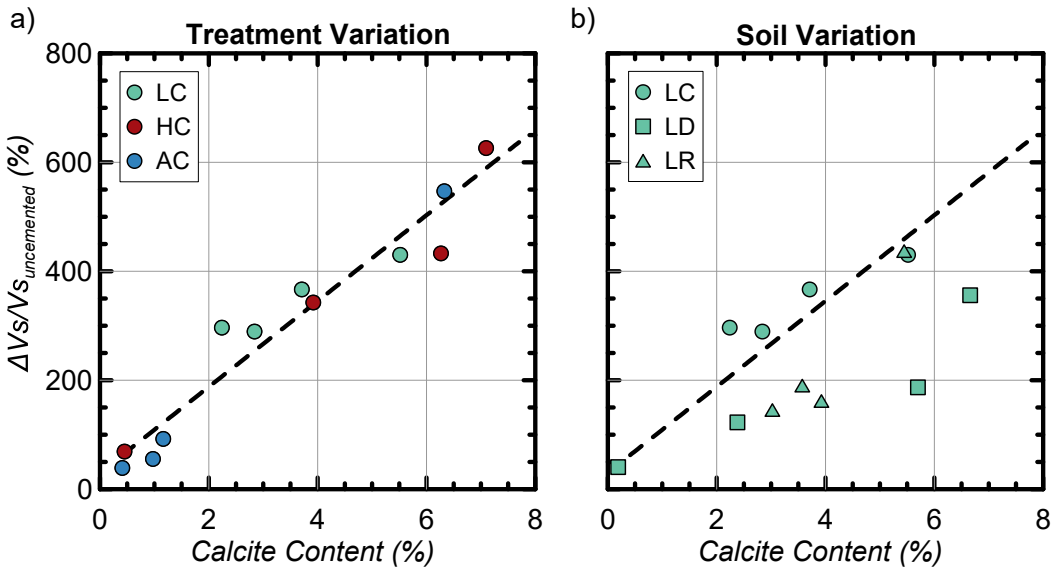

Figure 8.9. (a) Normalized shear wave velocity increases ($\Delta V_s/V_{s\ uncemented}$) versus soil calcite contents for columns with Concrete Sand with different biological treatment types and (b) columns with low ureolytic rate stimulation treatments for different sands. An interpreted linear trend line is shown on both plots for Concrete Sand columns.

Figure 8.9 presents corresponding soil calcite content measurements and V_s increases normalized by untreated soil V_s from all V_s measurement locations after 9 cementation treatments. A near linear trend occurred for Concrete Sand despite different stimulation methods. Concrete Sand columns generally had the highest normalized V_s increases of all tested soils for similar calcite contents with V_s increases near 500% when calcite contents were near 6%. When comparing

relationships for different soil types for the low ureolytic rate stimulation treatments, V_s increases were higher in LC when compared to LD and LR. The mechanism(s) responsible for these large differences in soil V_s improvements observed between different soils at similar calcite contents are not fully understood and merit future investigation.

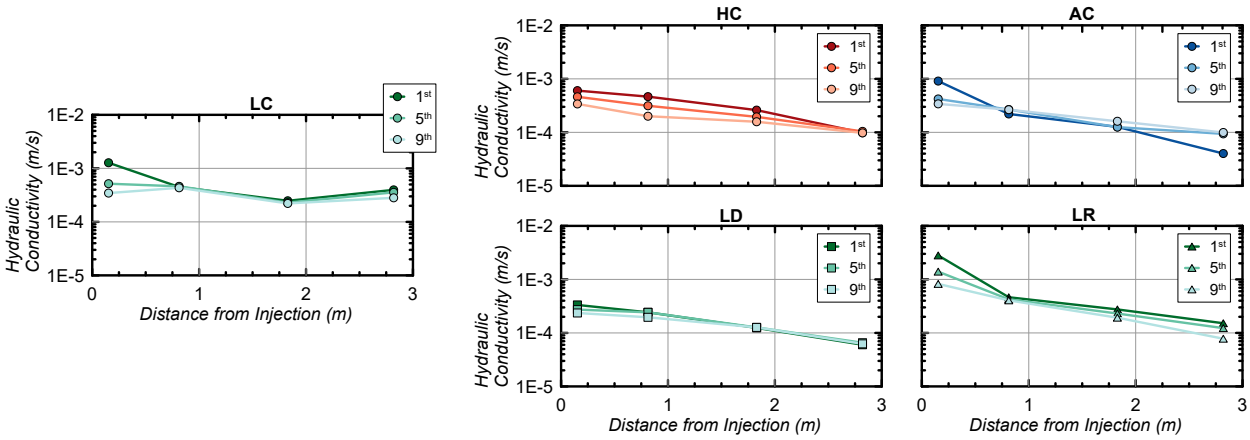

Figure 8.10. Soil hydraulic conductivities along column lengths during the 1st, 5th, and 9th cementation injection.

8.4.5 *Hydraulic Conductivity Measurements*

Soil hydraulic conductivities along column lengths during the 1st, 5th, and 9th cementation treatment calculated from pore pressure and flow rate measurements are presented in **Figure 8.10**. Despite increases in V_s values exceeding 637 m/s near the injection well in all columns, hydraulic conductivities across all columns had almost no observable changes. This suggested that the produced biocementation had little effect on solution transport and that additional cementation treatments could have been applied. For all columns, hydraulic conductivities were consistently lower at distances further from the injection location for all times. It is hypothesized that this may have resulted from either fines migration, incomplete saturation (i.e., presence of air pockets), soil

placement variation, or a combination thereof. It is also noted that soil hydraulic conductivities became more similar across the length of all columns as treatments proceeded and greater solution volumes were injected.

8.4.6 *Ammonium By-Product Removal*

Figure 8.11 presents solution total ammonium concentrations measured across columns before ammonium rinsing, after injecting 525 L of rinse solutions (700 min), and after an additional 12-hour residence period. Prior to ammonium by-product rinsing, concentrations of total ammonium in all enriched columns were near 500 mM, suggesting that near complete hydrolysis of the supplied 250 mM urea had occurred. Initial aqueous ammonium concentrations for AC were lower than other columns, again suggesting that injected urea was not fully hydrolyzed. During ammonium removal, concentrations of aqueous ammonium were generally lowest near the injection location and highest at the distal end of columns both 700 and 1440 min after the start of injections. After 1440 min, all columns had greater than 95.7% ammonium removal except for the distal end of AC, which showed only 90.6% removal. Total ammonium concentrations for all columns generally increased during the 12-hour residence period, likely due to desorption of ammonium from soil particle surfaces. Still, total ammonium concentrations for all columns were less than 20 mM at all locations. LD had the highest ammonium removal, which may be related to the higher concentrations of exchangeable cations measured in the Delta Sand that could have occupied soil sorption sites and prevented ammonium sorption. Lower percentages of ammonium removal were observed in AC and may have been related to incomplete hydrolysis of supplied

urea and the presence of more unoccupied sorption sites. V_s measurements were also obtained during rinsing and suggested that changes of only ± 50 m/s occurred.

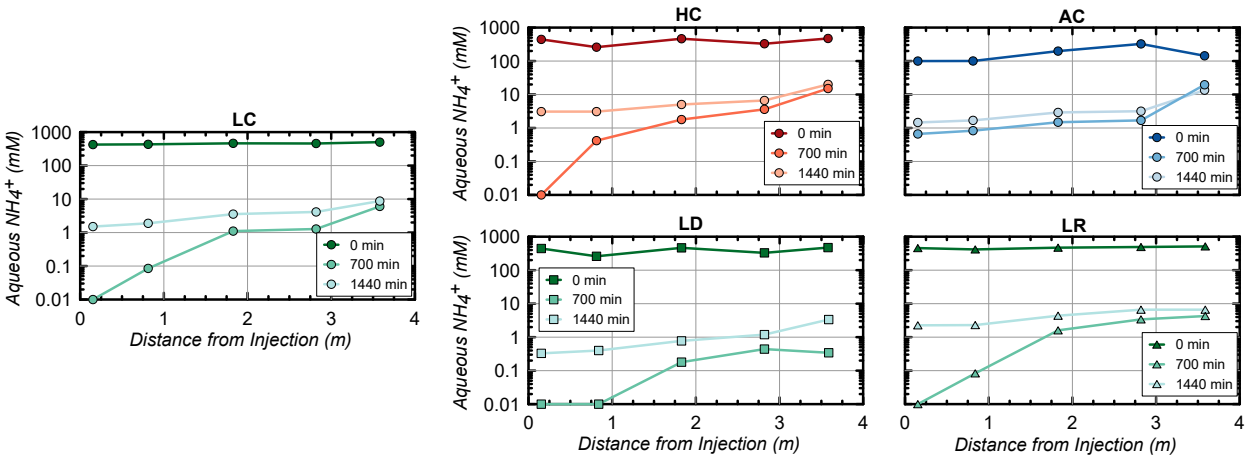

Figure 8.11. Aqueous ammonium concentrations versus distance from injection location for all columns at 0 min, 700 min, and 1440 min after the start of the ammonium by-product removal injections.

8.5 Conclusions

A study was completed using five 3.7-meter-long horizontal columns to (1) explore differences between biocementation treatment strategies intended to alter treatment uniformity and extent, (2) investigate the meter-scale success of MICP augmentation, stimulation, and cementation in different natural sands, (3) compare improvements between augmentation and stimulation, and (4) demonstrate the removal of ammonium by-products at meter-scale using a rinsing technique. Based on the results of this experiment, the following conclusions can be made:

- Ureolytic rates and suspended cell densities can be controlled during stimulation through changes in supplied yeast extract concentrations. For the given transport conditions, reductions in ureolytic rates resulted in greater cementation uniformity in LC across the full 3.7 m length

as indicated by calcite content and V_s measurements. In contrast, significant improvement was only observed up to 2.3 meters in HC.

- Treatment distance can be increased using low ureolytic rate stimulation approaches. In LC, reactions during transport were limited and unreacted calcium and urea exited the soil column and could have improved soils at further distances. This suggests that greater injection well spacings may be possible in the field using the low ureolytic rate stimulation approach.
- Successful stimulation and cementation were observed in all stimulation columns (HC, LC, LD, and LR) using 50 mM urea during stimulation and 1:1 urea to calcium chloride during cementation. This reduction in chemical usage during MICP may offer significant financial and environmental benefits.
- Columns containing different sands and receiving similar treatments (LC, LD, and LR) showed varying degrees of V_s improvement despite similar calcite contents. LC had the highest increase in V_s, ranging from 406 to 962 m/s, and LD had the lowest improvement, ranging from 65 to 637 m/s. The mechanism(s) responsible for these soil improvement differences remain poorly understood.
- Hydraulic conductivity measurements for all columns showed no significant reductions during treatments despite V_s improvements up to 1325 m/s and calcite contents up to 8%. This suggests that additional cementation treatments could have been applied.
- The HC treatment approach resulted in a more rapid and localized increase in improvement near the injection well. Mass balance calculations further suggested that near full consumption of injected calcium occurred in this column due to high reactions during solution transport.
- The augmented column, AC, showed improvement localized near the injection well. This was attributed to colloidal filtration occurring during non-nutritive *S. pasteurii* augmentation

injections. An effort to improve performance was then made by injecting 6X the initial augmentation volume before the 5th cementation treatment. These efforts produced insignificant improvements beyond 0.31 m from the injection well.

- The ammonium by-product rinsing strategy removed greater than 95.7% ammonium from aqueous solutions in all columns using a 525 L rinse solution volume. This rinsing process had insignificant effects on cementation integrity.

Chapter 9. INVESTIGATING AMMONIUM BY-PRODUCT REMOVAL FOR UREOLYTIC BIOCEMENTATION USING METER-SCALE EXPERIMENTS

This paper has been published in *Scientific Reports*. The paper is presented herein, with slight modifications.

Citation:

Lee, M., Gomez, M. G., San Pablo, A. C. M., Kolbus, C. M., Graddy, C. M. R., DeJong, J. T., & Nelson, D. C. (2019). Investigating Ammonium By-product Removal for Ureolytic Biocementation Using Meter-scale Experiments. *Scientific Reports*, *9*(1), 18313.

ABSTRACT

Microbially Induced Calcite Precipitation (MICP), or biocementation, is a promising bio-mediated technology that can improve the engineering properties of soils through the precipitation of calcium carbonate. Despite significant advances in the technology, concerns regarding the fate of produced NH_4^+ by-products have remained largely unaddressed. In this study, five 3.7-meter long soil columns each containing one of three different soils were improved using ureolytic biocementation, and post-treatment NH_4^+ by-product removal was investigated during the application of 525 L of a high pH and high ionic strength rinse solution. During rinsing, reductions in aqueous NH_4^+ were observed in all columns from initial concentrations between ≈100 mM to 500 mM to final values between ≈ 0.3 mM and 20 mM with higher NH_4^+ concentrations observed at distances furthest from the injection well. In addition, soil V_s measurements completed during rinse injections suggested that no significant changes in cementation integrity occurred during NH_4^+ removal. After rinsing and a 12 hour stop flow period, all column solutions achieved cumulative NH_4^+ removals exceeding 97.9%. Soil samples collected following rinsing, however, contained significant sorbed NH_4^+ masses that appeared to have a near linear relationship with

surrounding aqueous NH_4^+ concentrations. While these results suggest that NH_4^+ can be successfully removed from biocemented soils, acceptable limits for NH_4^+ aqueous concentrations and sorbed NH_4^+ masses will likely be governed by site-specific requirements and may require further investigation and refinement of the developed techniques.

9.1 Introduction

Microbially Induced Calcite Precipitation (MICP), or biocementation, has shown significant promise as an environmentally-conscious alternative to geotechnical ground improvement technologies, which have traditionally relied upon hazardous grouting chemicals, high mechanical energy, and energy-intensive materials to improve the engineering properties of soils (DeJong et al. 2013; Seagren and Aydilek 2010; El Mountassir et al. 2018). In the urea hydrolysis (ureolysis) driven process, microorganisms containing urease enzymes are used to catalyze a reaction that degrades urea, yielding total ammonium (NH_4^+), dissolved inorganic carbon, and hydroxide ions (Stocks-Fisher et al 1999) [Equation (9.1, 9.2, 9.3)]. When soluble calcium is available from either treatment solutions or groundwater, resulting alkalinity can supersaturate solutions with respect to calcium carbonate ($CaCO_3$) and initiate mineral precipitation on soil particle surfaces and contacts [**Equation (9.4)**]. Resulting biocementation can improve the engineering properties of soils through large increases in shear stiffness and strength with small reductions in hydraulic conductivity and porosity (DeJong et al. 2006; Gomez et al. 2017; 2018a; Montoyta and DeJong 2015. The process has been proposed for a variety of applications including mitigation of earthquake-induced soil liquefaction, general geotechnical soil improvement, subsurface flow manipulation, and divalent contaminant immobilization among other uses (DeJong et al. 2013; Fujita et al. 2004; Montoya et al. 2013; Minto et al. 2016; Phillips et al. 2016).

$$(NH_2)_2CO + 2H_2O \rightarrow 2NH_3 + H_2CO_3 \quad \textbf{[Equation (9.1)]}$$

$$NH_3 + H_2O \leftrightarrow NH_4^+ + OH^- \quad \textbf{[Equation (9.2)]}$$

$$H_2CO_3 \leftrightarrow HCO_3^- + H^+ \leftrightarrow CO_3^{-2} + 2H^+ \quad \textbf{[Equation (9.3)]}$$

$$Ca^{+2} + CO_3^{-2} \leftrightarrow CaCO_{3\,(solid)} \quad \textbf{[Equation (9.4)]}$$

Researchers have made significant advances in the technology in recent years, including identifying alternative treatment techniques (O'Donell et al. 2017; Gomez et al. 2018b), up-scaling the process to meter-scale (van Passen 2011; Smith et al. 2012; Gomez et al. 2015; 2017; Saneiyan et al. 2019), and characterizing the engineering behavior of biocemented soils (Montoya and DeJong 2015; Zamani and Montoya 2019). Despite these advances, environmental concerns regarding the fate of produced NH_4^+ by-products have remained largely unaddressed (DeJong et al. 2013; Gat et al. 2017). NH_4^+ is a commonly encountered source of inorganic nitrogen in soil systems, however, high aqueous NH_4^+ concentrations produced following ureolytic MICP may present serious environmental and human health concerns if left untreated in soils and groundwater. For example, the presence of high NH_4^+ in surface waters can encourage the growth of toxic algal blooms, which can decrease aquatic dissolved oxygen availability, produce high levels of toxins, and encourage bacterial growth, therefore threatening fish, humans, and other flora and fauna (Paerl 1997). While no maximum contaminant level has been established by the U.S. EPA for total NH_4^+ in drinking water, maximum concentrations for aquatic life of 17 mg/L (≈ 1 mM) and 1.9 mg/L (≈ 0.1 mM) total NH_4^+ for acute and chronic exposure, respectively, have been recommended (U.S. EPA 2013). During field-scale applications, aqueous NH_4^+ concentrations produced during biocementation will likely require removal to meet water quality standards and or maintain similar water quality as that present prior to treatments. NH_4^+ concentrations near twice the concentration

of applied urea are expected by reaction stoichiometry [**Equation (9.1)**], with many past experiments resulting in the production of NH_4^+ concentrations exceeding 500 mM. Limited understanding of post-treatment NH_4^+ removal has been a significant barrier for biocementation technology that has limited field-scale applications and environmental benefits. In order for MICP to be a truly environmentally beneficial technology, methods to manage, remediate, or remove NH_4^+ by-products following biocementation are needed.

While *in situ* nitrification of produced NH_4^+ to nitrite (NO_2^-) and nitrate (NO_3^-) (under aerobic conditions) and subsequent denitrification of NO_3^- to nitrogen gases (under anaerobic conditions) may offer a potential remediation strategy, these processes will be challenging and likely unpractical at field-scale due to the need for dramatic modifications in subsurface oxygen availability and chemical conditions. In addition, Gat et al. (2017) showed that *in situ* oxidation of NH_4^+ can have detrimental effects on biocementation integrity resulting from the generation of acidity in this process, further suggesting the need to address produced NH_4^+ following biocementation. Although few studies have examined and quantified the removal of NH_4^+ by-products following MICP, "rinse" solutions have been most commonly applied to remove NH_4^+ from treated areas with subsequent remediation of collected effluent completed *ex situ* at water reclamation facilities (Cuthbert et al. 2013; O'Donnell et al. 2017). Post-treatment rinsing may require significant energy and materials when applied at field scale, however, the technique can provide an effective strategy for NH_4^+ management following biocementation in the absence of other remediation processes and may provide an opportunity for NH_4^+ recovery. Recently, centimeter-scale soil column experiments were performed to further investigate and quantify the removal of NH_4^+ by-products following MICP in a clean poorly-graded Concrete Sand material

using rinse solution injections (Lee et al. 2019b). Results suggested that removal of positively-charged NH_4^+ ions from clean sands may be significantly more difficult due to interactions with negatively-charged soil particle surfaces. When rinse solutions of differing ionic strength and pH were applied, NH_4^+ removal was improved with increases in ionic strength, while pH had no detectable influence on removal. Improved removal was attributed to the exchange of NH_4^+ existing on soil surfaces with Ca^{2+} cations supplied from rinse solutions. A high pH (pH = 9.0) and high ionic strength (500 mM $CaCl_2$) rinse solution was identified that improved NH_4^+ removal while simultaneously limiting dissolution of biocementation. Although these results were promising, it remained unclear if these techniques would remain effective at meter-scale treatment distances.

In this study, five 3.7-meter long soil columns were improved using ureolytic biocementation, and post-treatment NH_4^+ by-product removal was investigated as a function of different soil materials and treatment techniques. Columns contained three different poorly-graded sand materials including: an alluvial sand (Column 1, 2, and 3), a marine sand (Column 4), and a second alluvial sand material (Column 5). Prior to biocementation, all columns received different biological treatments over the first six days intended to either enrich native ureolytic microorganisms or augment *Sporosarcina pasteurii* (*S. pasteurii*) bacteria uniformly across column lengths. Three different biological treatment strategies were applied to enrich native ureolytic microorganisms to achieve high (Column 1) and low bulk ureolytic rates (Column 2, 4, 5) and augment soils with S. pasteurii at a high cell density (Column 3) to obtain a high ureolytic rate similar to Column 1. Differences in achieved ureolytic rates were intended to examine the effect of urea hydrolysis rate on the spatial uniformity and extent of biocementation; the results of which are more extensively

described in a separate manuscript26. Following biological treatments, nine cementation injections containing identical calcium and urea concentrations were applied to all columns over nine (Column 1, 3) and eighteen (Column 2, 4, 5) days. All columns achieved differing degrees of biocementation with distance from the injection well. Following MICP treatments, 525 L of a high pH and high ionic strength rinse solution was applied to each column to remove produced NH4+. During rinse injections, changes in NH4+ by-product removal and **e**ffects on biocementation integrity were monitored. Following rinsing, physical soil samples were collected at various locations and sorbed NH4+ masses remaining on soil surfaces were quantified.

9.2 Materials and Methods

9.2.1 *Soil Materials*

Four different clean poorly-graded sands were used to prepare soil columns. Column 1, 2, and 3 contained the same alluvial Concrete Sand used in past experiments (Gomez et al. 2017; Lee et al. 2019b; Gomez et al. 2014; Graddy et al. 2018), Column 4 contained a marine Delta Sand, and Column 5 contained an alluvial Covelo Sand. In all columns, coarser Monterey Sand was placed at column ends as a filter material. Soil properties including USCS classification following ASTM D2487-10, depositional environment, D_{10}, D_{30}, D_{60}, fines content (%< #200 sieve), and minimum (e_{min}) and maximum (e_{max}) void ratios are summarized for all sands in **Table 9.1**.

Table 9.1. Summary of Soil Properties

Soil Material	USCS	Deposition	D_{10} (mm)	D_{30} (mm)	D_{60} (mm)	Fines Content (%)	e_{min}	e_{max}
Concrete Sand	SP	Alluvial	0.23	0.54	1.54	1.1	0.35	0.60
Delta Sand	SP	Marine	0.19	0.25	0.37	1.3	0.48	0.95
Covelo Sand	SP	Alluvial	0.23	0.52	1.55	1.6	0.38	0.59
Monterey Sand	SP	Alluvial	1.01	1.15	1.45	0	-	-

Table 9.2. Summary of Soil Column Properties and PHREEQC Model Parameters

		Experimental Measurements			PHREEQC Model Parameters	
Column No.	Soil Material	Porosity	Relative Density (%)	Total Pore Volume (L)	Porosity	Longitudinal Dispersivity (m)
1	Concrete Sand	0.31	56	50.7	0.23	0.3
2	Concrete Sand	0.30	67	48.5	0.23	0.3
3	Concrete Sand	0.32	56	50.6	0.25	1.5
4	Delta Sand	0.40	58	63.0	0.33	0.1
5	Covelo Sand	0.32	55	50.3	0.25	1.5

9.2.2 *Soil Columns*

Five 3.7-meter long hollow steel columns with square cross-sections (0.2 m by 0.2 m) contained 0.15 m^3 of sand and received treatment injections in one direction to simulate a single stream tube within a well-to-well half-space. Treatment wells (ID = 26.6 mm) were located on column ends and had valves, which allowed for pressurization of the injection well and removal of effluent solutions at the outlet well. Soils were placed in three ≈ 16 to 76 mm lifts, which allowed for bender element sensors to be placed at mid-height within columns during soil placement. Lifts

were moist tamped and surfaces were scarified to limit density differences between lifts. **Table 9.2** summarizes soil material types, soil column porosities, relative densities, and pore volumes determined from placed soil masses. In all columns, estimated porosities were between 0.30 and 0.40, relative densities were between 55% and 67%, and column pore volumes (PV) varied between 48.5 L and 63.0 L. Columns contained four bender element sensor pairs at distances of 0.31 m, 1.33 m, 2.35 m, and 3.37 meters from the injection location to monitor changes in soil shear wave velocities (V_s), indicative of biocementation. Four aqueous sampling ports were placed at distances of 0.15 m, 0.83 m, 1.82 m, and 2.81 m away from the injection location to monitor injection pressures and obtain solution samples at various times. Sampling ports consisted of 0.15 m long steel tubes (ID = 3.35 mm) with 25.4 mm diameter circular plastic filters (125-195 μm) open at mid-height within columns. A fifth drain port, consisting of a 60.3 mm ball valve with a porous filter material, was used to obtain additional samples and was located 3.58 m away from the injection location at the bottom of columns. **Figure 9.1** provides a detailed schematic and images of soil columns including treatment application systems, bender element and sampling port locations, and treatment wells.

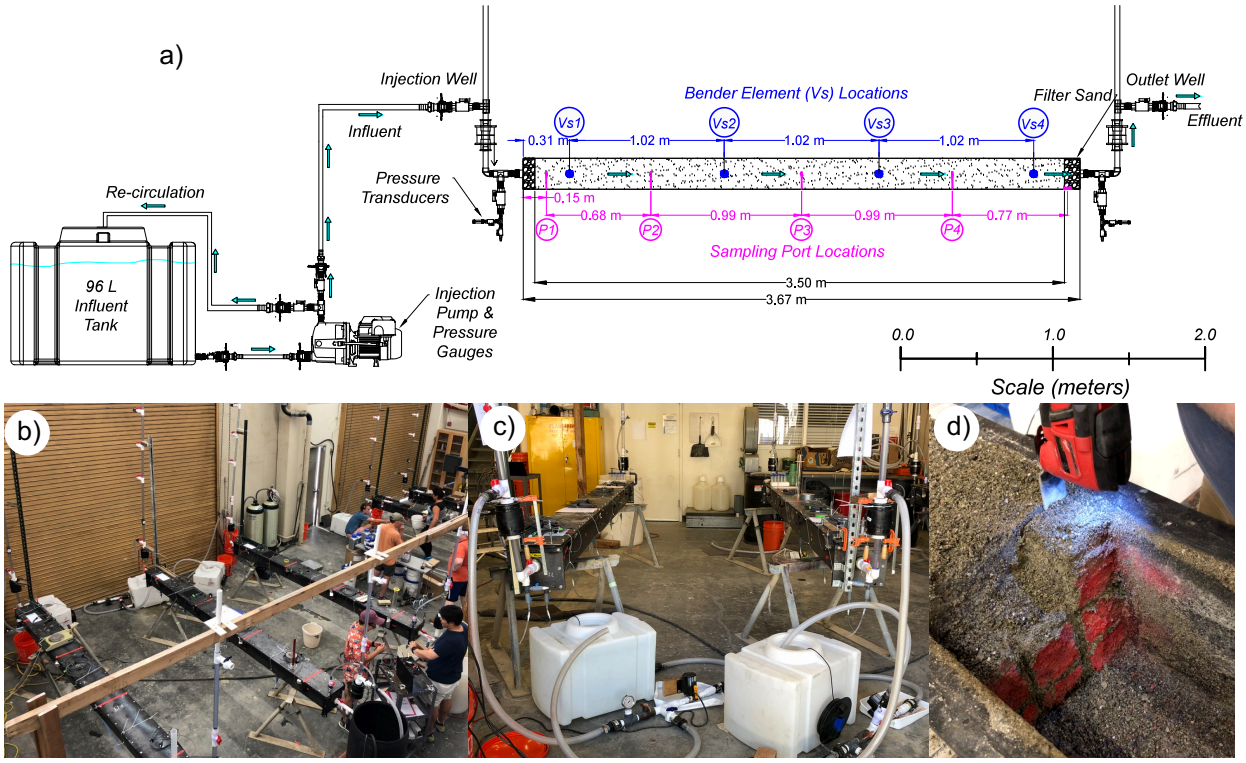

Figure 9.1. Overview of meter-scale experiments including: (a) schematic of meter-scale soil columns with treatment application systems, sampling ports, and bender element locations, (b) images of soil columns during treatments, (c) treatment solution injection systems, and (d) biocemented soil materials during post-rinsing soil sampling.

9.2.3 *Saturation and Bromide Passive Tracer Testing*

Prior to all treatments, columns were slowly saturated with an artificial ground water (AGW) solution containing 40 µM KNO_3, 450 µM $MgSO_4$, 1.75 mM $CaCl_2$, 40 µM $NaNO_3$, 1.1 mM $NaHCO_3$, and 60 µM $KHCO_3$ following Ferris et al. (2004). Immediately following saturation and before all biocementation treatments, columns received passive tracer injections to evaluate differences in solution transport between columns. During tracer testing, 76 L of a 15 mM NaBr solution was injected, followed by 76 L of de-ionized water to examine the arrival and removal of passive Br^- ions at the outlet well. A constant flow rate of 400 mL/min was used for injections and

solution samples were collected at outlet wells once every 5 minutes. Solution conductivities were measured and normalized by the conductivity of the injected NaBr solution to estimate normalized Br^- concentrations (C/C_0). One-dimensional advective-dispersive soil column transport models were developed using the geochemical software PHREEQC (Parkhurst and Appelo 2013) and were used to match passive tracer experimental observations by varying porosities and longitudinal dispersivities for all columns. All models were composed of 42 cells (0.089 meters each) and received NaBr and de-ionized water injections that were identical to the physical experiment.

9.2.4 *Treatment Injections*

Following passive tracer testing, all columns received different treatment solutions in a series of three treatment phases: (1) enrichment/augmentation, (2) cementation, and (3) NH_4^+ rinsing. **Table 9.3** presents a summary of treatment schemes including solution chemical constituents and concentrations, injection numbers and volumes, and injection and stop flow time durations for all columns. In the first treatment phase, solutions were applied to either enrich soil columns for native ureolytic microorganisms (Column 1, 2, 4, 5) or augment soils with the highly active ureolytic bacterium*, S. pasteurii* (Column 3). Enriched columns received six enrichment treatments once daily with varying concentrations of yeast extract intended to achieve different ureolytic activities. Column 1 received higher yeast extract concentrations (0.2 g/L) following past experiments (Gomez et al 2018b) wherein high ureolytic activities were targeted (hydrolysis of 250 mM urea within ≈8 hours). Columns 2, 4, and 5 received lower yeast extract concentrations (0.04 g/L) to obtain a low bulk ureolytic rate (hydrolysis of 250 mM urea within ≈ 48 hours). Column 3 was inoculated on the last day of enrichment treatments by injecting 76 L of an isotonic saline solution

(9 g/L NaCl) containing *S. pasteurii* (ATCC strain 11859) at a cell density of 9.36 x 10^7 cells/mL, intended to match the high ureolytic rate of Column 1. Due to lower ureolytic activity than expected along Column 3, a second augmentation injection consisting of 456 L of isotonic saline with 1.4 x 10^6 cells/mL was applied after the fourth cementation injection. Following all enrichment treatments, a flush solution that was identical to cementation solutions, but did not contain urea and Ca^{2+}, was applied to all enriched columns immediately before the first cementation treatment to remove high aqueous carbonate species expected after enrichment. Cementation treatments containing Ca^{2+} were then applied to all columns to initiate $CaCO_3$ precipitation for a total of nine injections. Columns 1 and 3 received cementation treatments once every 24 hours and Columns 2, 4, and 5 received treatments once every 48 hours to allow near full hydrolysis to occur. During enrichment, augmentation, and cementation treatments, injection volumes of 76 L were applied at a constant flow rate of 400 mL/min, during which injected solutions were continuously mixed within injection tanks. Following cementation treatments, a 200 mM $CaCl_2$ solution (initial pH ≈ 10.0) was applied to all columns to remove NH_4^+ following previously identified strategies (Lee et al. 2019b). During NH_4^+ by-product removal injections, a rinse solution volume of 525 L was injected into each column at a flow rate of 750 mL/min and lasted ≈700 minutes. Following rinse injections, columns remained saturated for 12 hours during a stop flow period until columns were disassembled. All solutions were injected using small pumps (Wayne Inc., 0.1 HP) with pressure gauges to monitor injection pressures.

Table 9.3. Summary of Solution Constituents and Injection Schemes for All Columns

Solution Constituent	Column 1		Column 2, 4, & 5		Column 3		All Columns
	Enrich-ment	Cement-ation	Enrich-ment	Cement-ation	Augment-ation	Cement-ation	NH_4^+ Rinsing
Calcium Chloride (mM)	-	250	-	250	-	250	200
Urea (mM)	50	250	50	250	-	250	-
Ammonium Chloride (mM)	100	12.5	100	12.5	-	12.5	-
Sodium Acetate (mM)	42.5	42.5	42.5	42.5	-	42.5	-
Yeast Extract (g/L)	0.2	0.2	0.04	0.02	-	-	-
Sodium Hydroxide (g/L)	1.28	-	1.28	-	-	-	-
NaCl (g/L)	-	-	-	-	9	-	-
S. pasteurii (cells/mL)	-	-	-	-	$9.36x10^{7*}$ $1.40x10^{6**}$	-	-
Initial Solution pH	9.0	8.4	9.0	8.4	≈ 7.0	8.4	10.0
Number of Injections	6	9	6	9	2	9	1
Injection Volume (L)	76	76	76	76	76* 456**	76	525
Injection Duration (min)	186	186	186	186	186* 1,140**	186	700
Stop Flow Period (hours)	20.8	20.8	20.8	44.8	24.5	20.8	12.3

**First augmentation treatment*

***Second augmentation treatment*

9.2.5 *Aqueous Sampling*

Before and immediately after treatment injections, aqueous samples of ≈ 10 mL were collected from all sampling ports. On select days, aqueous samples were also collected 1, 2, 4, and 8 hours after injections to monitor ureolytic activity and chemical changes in time. Prior to all sample collection events, 30 mL of solution was removed from ports and discarded to obtain representative samples. During NH_4^+ rinse injections, ≈10 mL samples were collected from outlet wells once

every 20 minutes and from all sampling ports and well locations once every 60 minutes. Aqueous samples were immediately frozen and stored at -20°C until subsequent chemical analyses.

9.2.6 *Shear Wave Velocity Measurements*

Shear wave velocity (V_s) measurements were obtained using horizontally-oriented bender element sensor pairs placed at mid-depth within columns at various distances from the injection well. V_s measurements were obtained at all locations before and immediately after all biological and cementation injections. Additional measurements were performed during NH_4^+ rinsing before, 120, 240, 480, and 700 minutes after the start of rinse injections and following a 12-hour stop flow period (24 hours after start of rinse injections). Bender elements were coated with epoxy, electronics wax, and an insulating coating to waterproof sensors following similar processes detailed in Gomez et al. (2017). Transmitting bender elements were excited with a 24V 100 Hz square wave and signals from receiving bender elements were measured and recorded using an oscilloscope at a sampling frequency of 1 MHz. Shear wave arrival times were interpreted visually and V_s values were calculated from measured sensor spacings.

9.2.7 *Aqueous Measurements*

Solution pH measurements were completed using a semi-micro pH electrode and meter system that was calibrated daily using a three-point buffer sequence (4.01, 7.00, 10.00) and had ± 0.01 pH unit accuracy. Total NH_4^+ measurements were completed using a salicylate reaction method similar to Krom (1980), wherein two reagents (Reagent A & B) were added to dilute sample

volumes and absorbance values were measured at 650 nm using a microplate spectrophotometer. Reagent A consisted of 1.9 mM sodium nitroprusside, 811 mM sodium salicylate, 387 mM sodium citrate, and 515 mM sodium tartrate in water. Reagent B consisted of 1.32 mM sodium hypochlorite and 1.5 M sodium hydroxide in water. Urea measurements were completed using a colorimetric urea assay similar to Knorst et al. (1997). A colorimetric reagent consisting of 216 mM p-dimethylaminobenzaldehyde, 2.32 M hydrochloric acid, and 13.83 M ethanol in water was added to dilute samples and absorbance values were measured at 422 nm using a microplate spectrophotometer. Conductivity measurements were completed using a conductivity probe and meter. Augmented cell densities were determined through direct counting (Hobbie et al. 1977).

9.2.8 *Cation Exchange Capacity and Exchangeable Cation Measurements*

Cation exchange capacity (CEC) and exchangeable cation measurements were completed for untreated sand materials using a process similar to U.S. EPA Method 9080 (U.S. EPA 1986). Soil CEC values reflect the capacity of negatively-charged soil surfaces to bind positively-charged ions, thus it was hypothesized that CEC differences between soils could influence NH_4^+ transport and removal following biocementation. During these measurements, 10 grams of untreated dry soil and 50 mL of a 1 M NH_4Cl solution were added to a plastic syringe. After a 12-hour residence period, soil solutions were extracted, collected, and select exchangeable cations were characterized using inductively coupled plasma mass spectrometry (ICP-MS). Remaining extracted soil samples were then rinsed with ethanol for 6 hours to remove NH_4^+ ions that may have remained in free solution. Finally, 50 mL of 1 M KCl solution was added to all samples and allowed to equilibrate for 12 hours to encourage replacement of sorbed NH_4^+. Soil solutions were then extracted again

and NH_4^+ concentrations in the extracted solution were quantified using the salicylate colorimetric assay. Measured NH_4^+ concentrations were used to calculate soil CEC values.

9.2.9 *Soil Sampling and Soil NH_4^+ Measurements*

Following all treatments, column top caps were removed, and soil samples were collected at various locations at the center of columns. At heavily cemented locations, soil samples required removal using an oscillating power saw (**Figure 9.1d**). Following sample collection, moist soil samples were frozen and stored at -20°C until subsequent chemical analyses could be completed. An extraction process was used to quantify NH_4^+ masses remaining within soil samples. Free soil solution was first removed from thawed moist soil samples using a centrifuge process wherein 30 grams of moist soil samples (of known water content) were added to conical centrifuge tubes with 0.45 micron nylon filter baskets and centrifuged at 3800 rpm for 20 minutes to extract solutions. A minimum volume of 2 mL was collected, frozen, and stored at -20° C until NH_4^+ concentrations were analyzed. Sorbed NH_4^+ masses remaining on soil particle surfaces were quantified using a KCl extraction process following Keeney & Nelson (1982). In this process, 10 gram moist soil samples (of known water content) were mixed with 20 mL of a 2 M KCl solution and allowed to equilibrate for at least 4 hours to facilitate removal of NH_4^+ ions. Soil solution mixtures were then added to another conical filter tube, centrifuged, and a 2 mL solution sample was collected, frozen, and stored at -20°C until NH_4^+ concentrations were analyzed. KCl extracted NH_4^+ measurements included NH_4^+ initially present in free soil solutions as well as NH_4^+ masses that were initially sorbed to soil surfaces. Sorbed NH_4^+ masses were therefore estimated by subtracting NH_4^+ masses

expected from free solution from NH_4^+ measurements following KCl extraction. Sorbed NH_4^+ masses were normalized per gram of dry soil.

9.3 Results and Discussion

Results from soil CEC and exchangeable cation measurements are summarized below in **Table 9.4** for all three sands. A fourth sample consisting of Concrete Sand augmented with 10% by mass reagent-grade $CaCO_3$ was also tested to assess the potential influence of $CaCO_3$ minerals on soil CEC. As shown, Delta Sand had the highest CEC (4.32 meq/100g) with Covelo Sand exhibiting the lowest CEC of tested sands (1.64 meq/100g). Additionally, when $CaCO_3$ was added to the Concrete Sand sample, no significant effects on CEC were observed suggesting that the presence of biocementation $CaCO_3$ minerals likely had little influence on the ability of soils to bind NH_4^+ ions. When examining exchangeable cation concentrations, sands generally had similar values for common soil cations. Delta Sand, however, had notably higher K^+, Mg^{2+}, Na^+, and S^{2+} concentrations than other tested sands, which was consistent with the marine depositional environment from which it was obtained. Exchangeable cations in Concrete Sand and Covelo Sand were most similar, however, Covelo Sand had significantly higher Al^{3+} and Ca^{2+} concentrations as well as much lower Mg^{2+} concentrations than other sands. While tested sands had minor CEC and exchangeable cation differences, values were generally consistent with those expected for clean quartz sands (Mengel 1980).

Table 9.4. Summary of Cation Exchange Capacity and Exchangeable Cation Analyses for Sands

Sand	CEC (meq per 100 g soil)	Exchangeable Cations (μg per gram of soil)									
		Al^{3+}	Ba^{2+}	Ca^{2+}	K^{+}	Mg^{2+}	Mn^{2+}	Na^{+}	S^{2+}	Si^{4+}	Zn^{2+}
Concrete Sand	2.58	< 0.1	21.4	277.7	18.9	191.5	< 0.1	23.9	3.6	9.9	< 0.1
Delta Sand	4.32	< 0.1	13.5	236.7	84.0	238.8	1.5	180.1	81.8	9.6	< 0.1
Covelo Sand	1.64	0.7	9.4	555.3	18.7	59.6	1.3	5.7	17.0	4.8	2.3
Concrete Sand w/ 10% CaCO3	2.52	< 0.1	14.8	910.1	16.7	129.5	< 0.1	17.8	3.7	6.7	< 0.1

Figure 9.2 presents measurements of normalized solution conductivity (C/C_0) versus injected NaBr tracer solution volume from samples obtained at outlet wells during passive tracer testing. Differences in C/C_0 values with injected volume are reflective of porous media advective-dispersive transport properties including porosity, hydrodynamic dispersion, and diffusion **(**Brusseau 1993**)**. Immediately after starting the 15 mM NaBr solution injection, most C/C_0 values were near zero with small values (< 10% C/C_0) observed exiting columns due to background soil solution conductivities. In Column 4, containing Delta Sand, notably larger initial C/C_0 values were observed and were consistent with the higher exchangeable cations measured previously (**Table 9.4**). After additional tracer solution was injected, C/C_0 values increased above background levels ($C/C_0 \approx 20\%$) in Column 1, 2, 3, and 5 after injecting ≈ 20 to 30 L (0.39 to 0.62 PV). Column 4 had a much more delayed arrival, however, with C/C_0 values increasing above ≈20% only after ≈ 42 L (0.66 PV). The delayed breakthrough in Column 4 was consistent with the higher porosity measured in this column (**Table 9.2**). After injecting the 76 L volume, C/C_0 values measured at

the outlet well were between 94% and 96% for Column 1 and 2, 89% and 90% for Column 3 and 5, and were 98% for Column 4. While it was expected that Column 1, 2, and 3, which all contained Concrete Sand, would have similar breakthrough curves, the Column 3 breakthrough was distinctly different. Column 3 and 5, however, were found to have very similar breakthrough curve behaviors despite containing different sands. While unexpected, both Concrete Sand and Covelo Sand had similar grain size distributions and differences in transport properties may have resulted from differences in soil preparation between columns and minor preferential flow at the column boundaries. To better quantify transport differences between columns one-dimensional advective-dispersive soil column transport models were calibrated to match experimental trends by varying column longitudinal dispersivities (α) and porosities (n). Modelled results are presented in **Figure 9.2** and porosity and dispersivity values used for models are summarized in Table 9.2. Modelled porosities were lower than those calculated from soil mass measurements for all columns, likely due to incomplete saturation, which could have reduced the apparent porosity of columns. When comparing dispersivity values between columns, a large increase in longitudinal dispersivities was observed between Column 1 and 2 (α = 0.3 m) and Column 3 and 5 (α = 1.5 m), despite having similar porosities. Column 4 had a similar dispersivity (α = 0.1 m) as Column 1 and 2, but a much larger modeled porosity (n_{model} = 0.33) as expected from soil mass measurements.

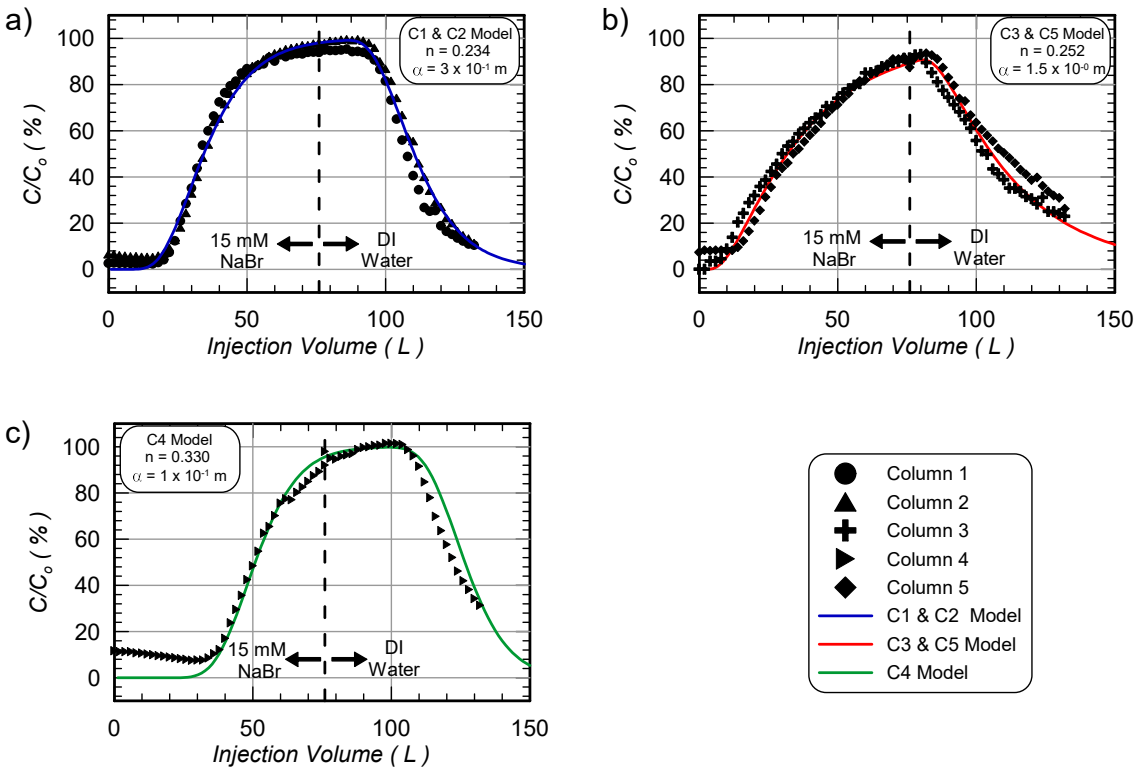

Figure 9.2. Measurements of normalized bromide concentrations (C/C_0) versus injected volume during passive tracer testing for (a) Column 1 and 2, (b) Column 3 and 5, and (c) Column 4 with PHREEQC modelled comparisons.

Figure 9.3 presents aqueous NH_4^+ concentrations in time following the ninth cementation injection for Column 1, 2, and 3 from measurements at all port locations, immediately after injections, and 1, 2, 4, 8, 24, and 48 hours (when applicable) after injections. Aqueous NH_4^+ concentrations were determined by difference and reaction stoichiometry from direct urea measurements in time. While similar data were also obtained for Column 4 and 5, only Column 2 data are shown and was representative of trends observed in all enriched low ureolysis rate columns (Column 2, 4, 5). As shown, similar NH_4^+ production trends in time were observed between columns at each port location. Immediately after injections, aqueous NH_4^+ concentrations were lowest at the 0.15 m port location and increased with distance from the injection well for all columns due to urea hydrolysis

occurring during solution transport as well as mixing with previously reacted solutions. At a distance of 0.15 m in the high ureolysis rate Column 1, NH_4^+ concentrations increased from post-treatment values near ≈ 50 mM to ≈ 500 mM over 24 hours, while ≈ 500 mM concentrations were achieved at all other ports within 1 hour after injections. In the low ureolysis rate Column 2, NH_4^+ concentrations increased from post-treatment values near ≈ 50 mM to ≈500 mM at a distance of 0.15 m within 48 hours, and to ≈500 mM at all other ports between 6 and 24 hours after injections. In the augmented Column 3, a slower rate of urea hydrolysis was consistently observed at all port locations relative to enriched columns. This resulted in significantly lower NH_4^+ concentrations between ≈200 mM and ≈400 mM residing after 24 hour treatment periods and a significant fraction of injected urea remaining non-hydrolyzed due to low ureolytic activity. Localization of ureolytic activity near injection well locations has been previously observed in augmented experiments (van Paassen 2010) and likely resulted from the colloidal filtration of *S. pasteurii* bacterial cells during augmentation of Column 3 (Ginn et al. 2002). Despite much lower NH_4^+ production observed in Column 3, all enriched columns (1, 2, 4, 5) achieved similar post-treatment NH_4^+ concentrations near ≈ 500 mM after 24 hour (Column 1) and 48 hour residence periods (Columns 2, 4, 5).

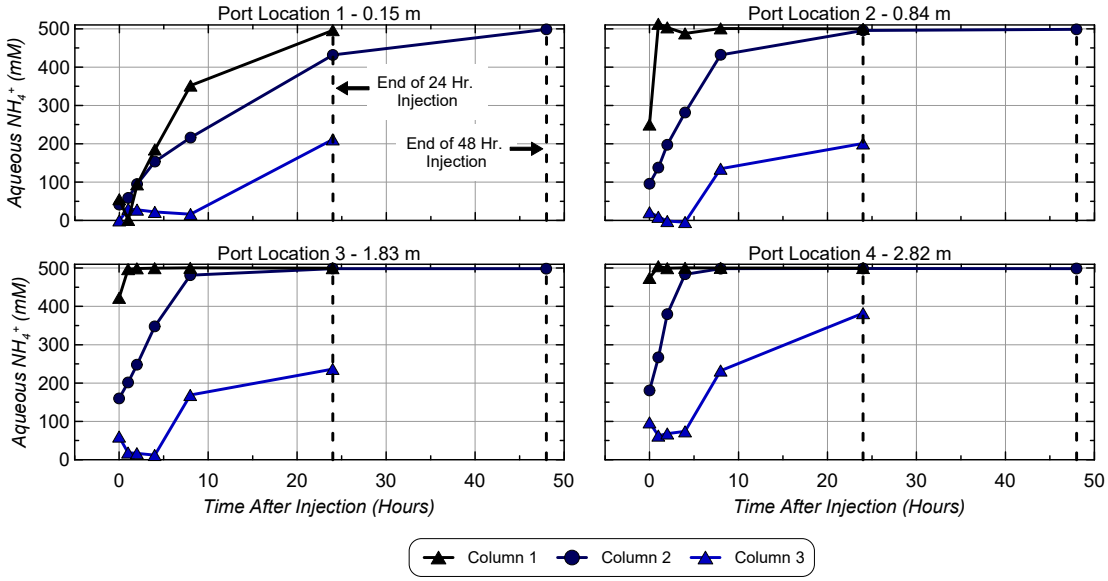

Figure 9.3. Changes in aqueous NH_4^+ concentrations in time at all aqueous sampling port locations during the ninth cementation treatment.

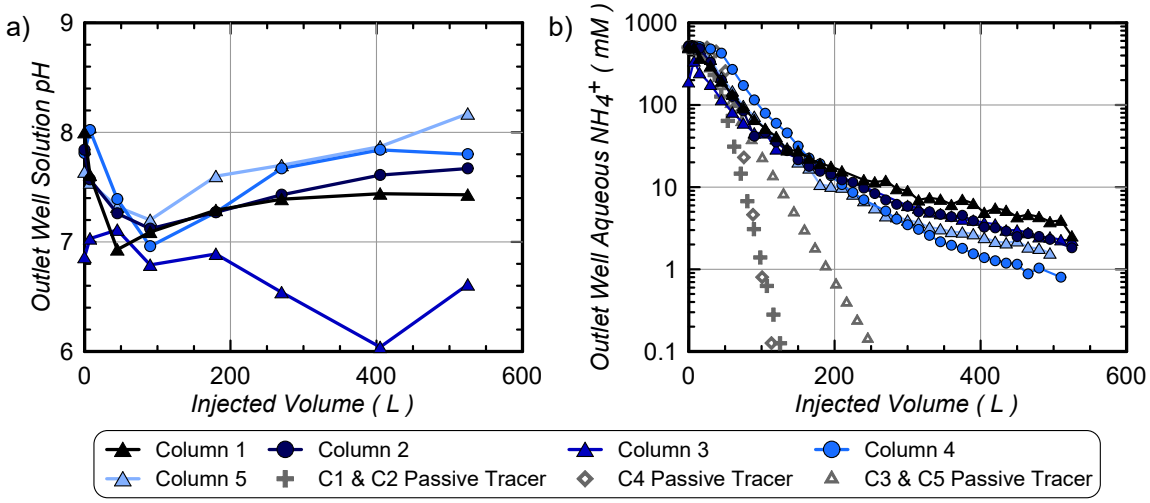

Figure 9.4. Measurements of outlet well (a) solution pH and (b) aqueous NH_4^+ concentrations versus injected rinse solution volume with PHREEQC modeled passive tracer comparisons.

Figure 9.4 presents solution pH and aqueous NH_4^+ concentration measurements for outlet well samples versus injected rinse solution volume. As shown in **Figure 9.4a**, solutions initially exiting all enriched columns had pH values between 7.6 and 8.0. This was consistent with previously observed solution pH values for cementation solutions with urea-to-calcium ratios of 1:1 following near full urea hydrolysis. In Column 3, however, initial pH values were significantly lower (near 6.8) due to limited generation of alkalinity from limited urea hydrolysis. As rinse injections proceeded, effluent pH values approached 7.0 for all columns after injecting 100 L. In all enriched columns (Column 1, 2, 4, 5), pH values then gradually increased to near steady values between 7.4 and 8.2 for the remainder of rinsing. The temporary reduction observed in outlet solution pH values was unexpected as the initial pH of the injected rinse solution was near 10. It is hypothesized that this pH reduction may have resulted from consumption of remaining carbonate species and some limited calcite precipitation upon the initial introduction of rinse solutions with 200 mM Ca^{2+}. Following the removal of sufficient solution alkalinity, increases in pH may then have occurred due to equilibration of high pH solutions with existing $CaCO_3$ and soil minerals. In Column 3, pH values remained lower than all enriched columns with final outlet well solution pH values near 6 to 6.5, which likely resulted from a lack of significant quantities of $CaCO_3$ minerals in this column.

Large reductions in effluent NH_4^+ from values between 497 mM and 524 mM (Column 1, 2, 4, 5) and ≈ 342 mM (Column 3) to values between ≈20 and 32 mM were observed in all columns at the outlet well after injecting 200 L (**Figure 9.4b**). Following the application of an additional 200 L, however, NH_4^+ concentrations were only reduced to values between 3.5 and 9.0 mM. At the end of the 525 L injection, all effluent NH_4^+ concentrations were between 0.8 and 2.5 mM. It is hypothesized that the limited improvement in NH_4^+ removal after injecting significantly more rinse

solution volume was influenced by soil-ion interactions and removal of sorbed NH_4^+ masses, though solution mixing via hydrodynamic dispersion may have also contributed. In order to evaluate the effect of these interactions on observed NH_4^+ trends, PHREEQC models were used to simulate passive tracer removal trends for all columns. As shown, concentrations were similar between measured NH_4^+ and modelled passive tracers early during rinsing due to limited breakthrough at the outlet well location, however, at injection volumes greater than 100 L, modeled passive tracer concentrations were significantly lower than experimentally observed NH_4^+ values. For example, reductions in passive ion concentrations to values below 10 mM required a maximum injection volume of 124 L for all models, however, physical experiments suggested that over twice that volume (≈ 280 L) was required to achieve these NH_4^+ levels. When integrating outlet well concentrations over injected volumes, measurements suggested the removal of 27.2, 27.2, 17.6, 38.6, and 28.2 moles of NH_4^+ occurred in Columns 1 through 5, respectively. This was equivalent to the removal of average pore fluid concentrations of 536 mM, 561 mM, 347 mM, 612 mM, and 560 mM NH_4^+ for Columns 1 through 5, respectively. Average pore fluid concentrations removed from Columns 1, 2, 4, and 5 exceeded the maximum expected NH_4^+ concentration of 500 mM and suggested that significant sorbed NH_4^+ masses must have been removed during rinsing. Retardation of NH_4^+ transport relative to passive ions was also previously observed in centimeter-scale experiments[25] and likely contributed to delayed NH_4^+ removal relative to passive tracer trends. Lastly, although NH_4^+ removal was expected to be reduced in Column 4 for similar rinse injection volumes due to a larger porosity, surprisingly, when injection volumes exceeded ≈200 L, an opposite trend was observed with much lower NH_4^+ concentrations exiting Column 4 compared to other columns. While unexpected, this was consistent with the greater NH_4^+ removal calculated for this column.

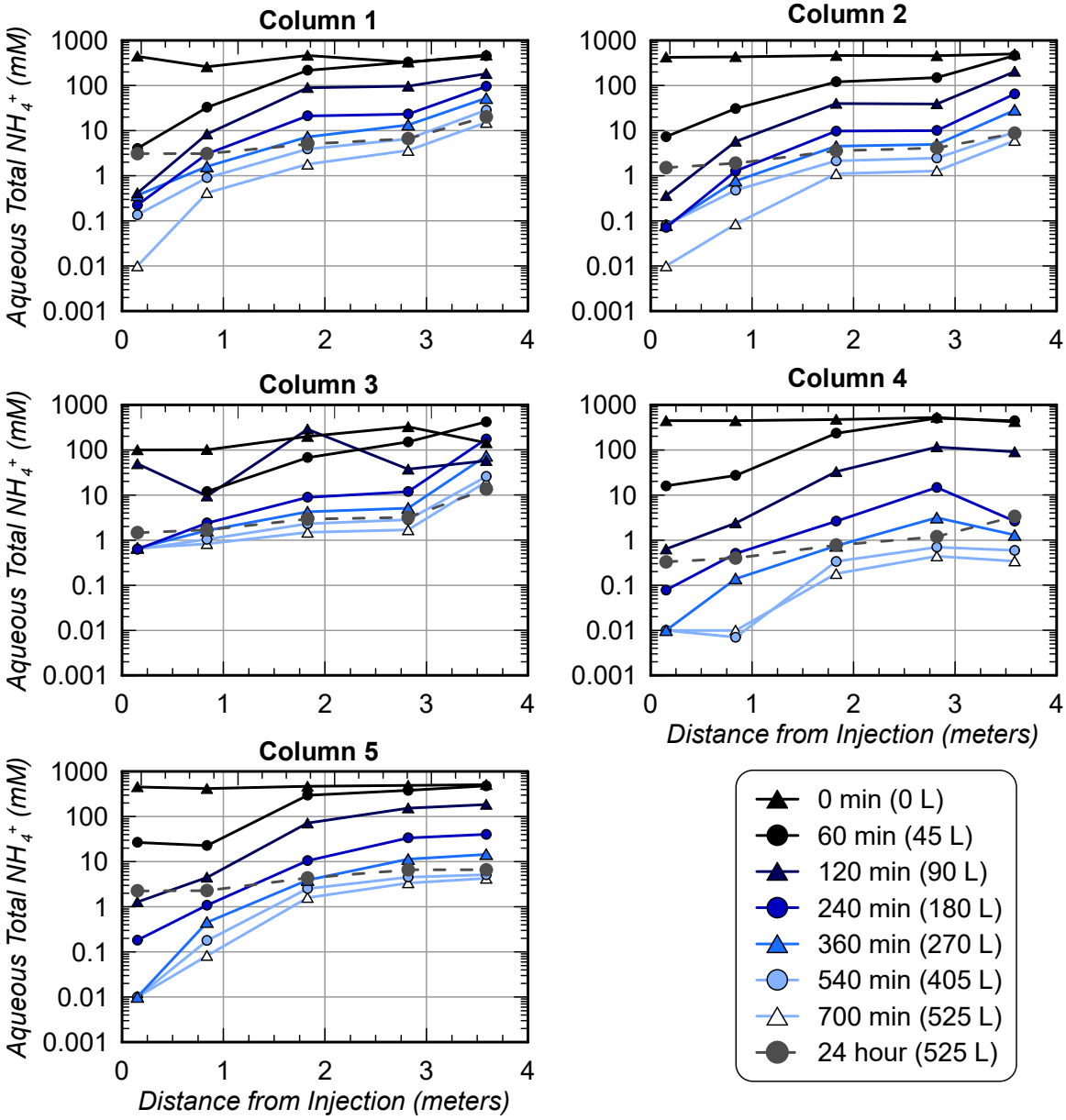

Figure 9.5. Contours of aqueous NH_4^+ concentrations within columns at all sampling port locations at various times during rinse injections. Measurement times after start of injections and cumulative injected rinse volumes are provided.

Figure 9.5 presents aqueous NH_4^+ concentrations measured spatially along soil columns at various points in time during rinse injections and 24 hours after rinse injections following a 12 hour stop

flow period. Pre-rinsing measurements reflected conditions following the ninth cementation treatment, wherein most locations in enriched columns had NH_4^+ concentrations between ≈400 and 500 mM due to near full hydrolysis of the previously applied 250 mM urea injection. In Column 3, however, much lower NH_4^+ concentrations between 100 mM and 324 mM were observed and were consistent with the lower ureolytic activity observed in the augmented column during cementation treatments (**Figure 9.3**). As rinse injections proceeded in time, significantly lower NH_4^+ concentrations were first observed at sampling locations closer to the injection well with large increases along column lengths. After injecting 45 L, almost no changes in NH_4^+ concentrations were observed near the outlet well (distance of 3.58 m), however, NH_4^+ concentrations were reduced to much lower values between 4 mM and 27 mM near the inlet well (distance of 0.15 m) in all columns. When comparing trends in time, spatial NH_4^+ concentrations were similar between Columns 1, 2, and 5, however, Column 3 and 4 trends were significantly different. Despite lower pre-treatment NH_4^+ concentrations in Column 3 prior to rinsing, trends in time were similar to other Concrete Sand columns when rinse volumes were less than ≈270 L. When additional rinse solution was applied to Column 3, however, continued reductions in NH_4^+ were not observed and most locations had concentrations exceeding 1 mM. Reduced NH_4^+ removal in Column 3 may have resulted from limited urea hydrolysis during the treatment period, the presence of more unoccupied cation exchange sites, and thus increased retardation of NH_4^+ transport. Additionally, lower pH values observed in this column during rinsing, may have resulted in more ammonium existing in the charged form NH_4^+ rather than NH_3. In Column 4, greater NH_4^+ removal was again observed for similar injection volumes, despite having a larger column pore volume. Higher exchangeable cation contents measured in Delta Sand may have prevented NH_4^+ from interacting with soil surfaces during rinsing, thus improving NH_4^+ removal efficiency. After

injecting 525 L of rinse solutions, NH_4^+ concentrations were below 15 mM, 6 mM, 19 mM, 0.4 mM, and 4 mM at all locations in Columns 1 through 5, respectively. Following the 12 hour stop flow period, however, NH_4^+ concentrations generally increased and gradients in concentrations across columns became less pronounced likely due to equilibration of solutions with sorbed NH_4^+ concentrations and diffusion. **Figure 9.6** presents changes in NH_4^+ concentrations during the stop flow period versus column length. Most locations had NH_4^+ increases between 1 and 5 mM during the stop flow period. Again, Column 1, 2, and 5 showed similar trends, with Column 3 and 4 differing. In Column 3, much smaller increases in NH_4^+ concentrations were observed with a single location achieving a 6.1 mM reduction during the retention period. Similarly, in Column 4, increases in concentrations were much lower than other columns and were generally near 0.3 mM. Smaller increases in NH_4^+ concentrations in these columns during the stop flow period may reflect more limited desorption of NH_4^+ resulting from less NH_4^+ exposure during treatments (Column 3) and saturation of sorption sites and limited NH_4^+ and soil interactions (Column 4).

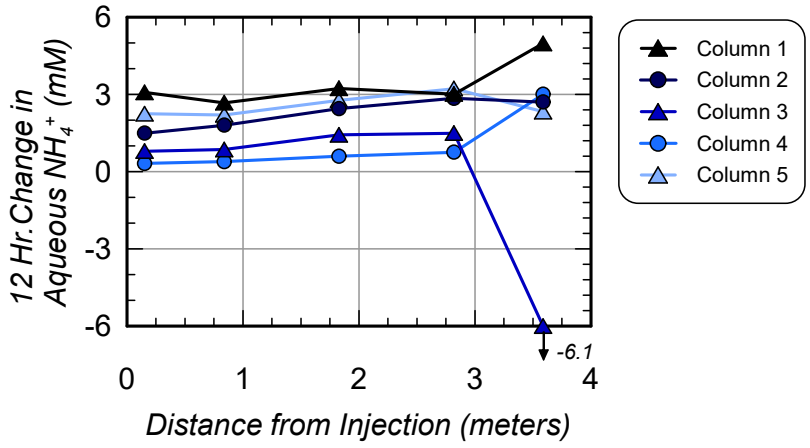

Figure 9.6. Changes in aqueous NH_4^+ concentrations following a 12 hour stop flow period after rinsing versus column length for all columns.

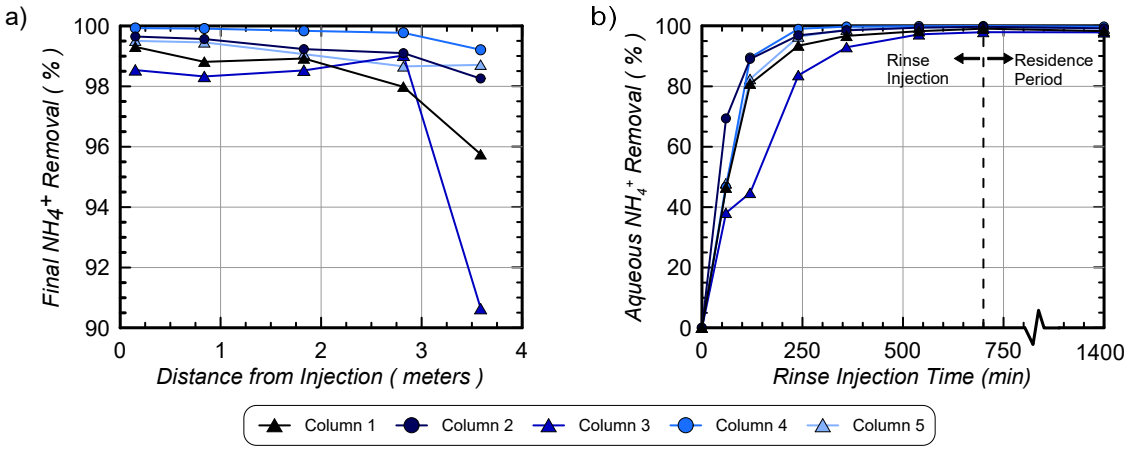

Figure 9.7. (a) Final NH_4^+ removal following the 12-hour stop flow period (in percent) versus column length and (b) cumulative NH_4^+ removal (in percent) versus rinse injection time.

Figure 9.7 presents (a) removal of pre-rinsing NH_4^+ concentrations (in percent) along column lengths and (b) cumulative NH_4^+ removal (in percent) for all columns in time. As shown in **Figure 9.7a**, all locations achieved greater than 95.7% NH_4^+ removal following rinsing and the 12-hour residence period, with the exception of the most distal location in Column 3 (90.6% removal). At distances less than 2.82 m, greater removal was observed with all columns achieving greater than 98.0% NH_4^+ removal. Column 4 achieved the highest NH_4^+ removal of all columns with all locations achieving values above 99.2% removal. In order to better understand temporal changes in NH_4^+ removal, spatial contours of NH_4^+ at various times (**Figure 9.5**) were integrated along column lengths to estimate cumulative NH_4^+ removal in time. As shown in **Figure 9.7b**, all columns started with 0% removal before rinsing, and achieved between 38% and 69% NH_4^+ removal after injecting only 45 L (60 min). With increased rinse injection volumes, columns exhibited similar removal trends with the exception of Column 3, which achieved less removal in time. In all enriched columns, greater than 80% removal was achieved after injecting 90 L (120 min) and greater than 93% removal was achieved after injecting 180 L (240 min). Column 3,

however, required near 270 L (360 min) to obtain 93% removal. Immediately following rinse injections, cumulative removal was 99.1%, 99.7%, 97.9%, 99.9%, and 99.6%, in Columns 1 through 5, respectively. However, after the stop flow period, removal percentages decreased by up to 0.9% and were 98.2%, 99.2%, 97.9%, 99.8%, and 99.1%, in Columns 1 through 5, respectively.

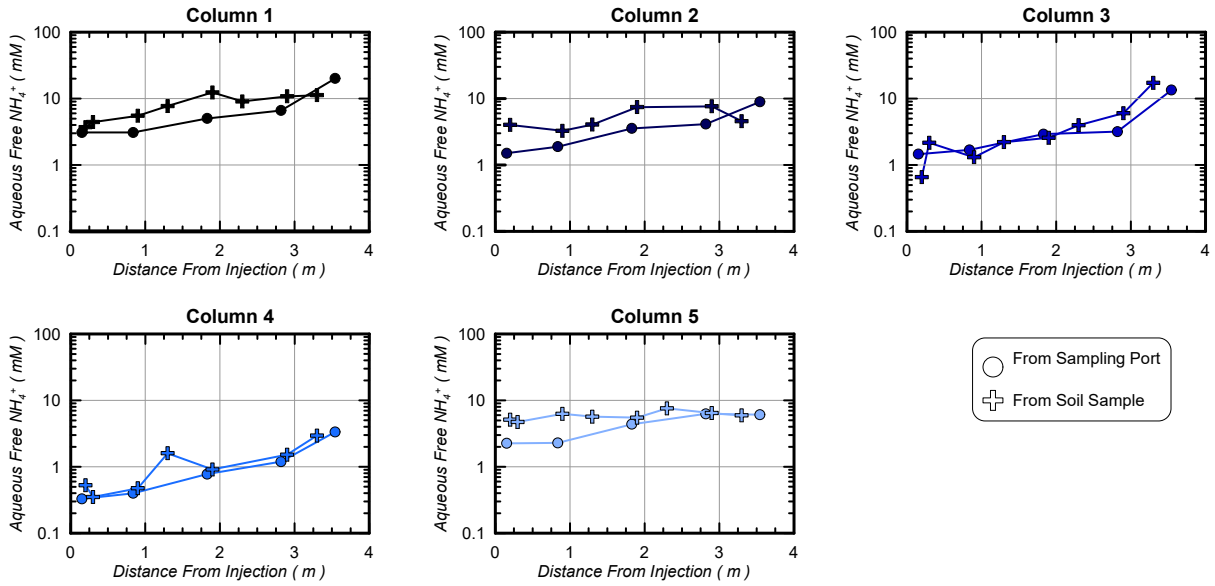

Figure 9.8. Comparison of aqueous NH_4^+ concentrations between solution samples obtained from aqueous sampling ports (after the 12 hour stop flow period) and physical soil samples obtained post-rinsing.

Figure 9.8 presents NH_4^+ concentrations measured in aqueous solutions obtained from sampling ports after the stop flow period as well as solutions extracted from moist soil samples obtained post-rinsing at various locations. As shown, values obtained from both methods resulted in similar magnitudes and trends in NH_4^+ concentrations along columns suggesting that aqueous samples obtained from sampling ports were generally representative of internal soil conditions. NH_4^+ concentrations from soil samples, however, were consistently slightly higher than sampling port values suggesting that greater concentrations of NH_4^+ may have resided more locally around soil

particle surfaces. Despite these differences, soil sample trends indicated post-rinsing NH_4^+ concentrations between 3.7 mM and 17 mM in Column 1, 2, 3, and 5 with greater removal and values between 0.3 mM and 2.9 mM in Column 4.

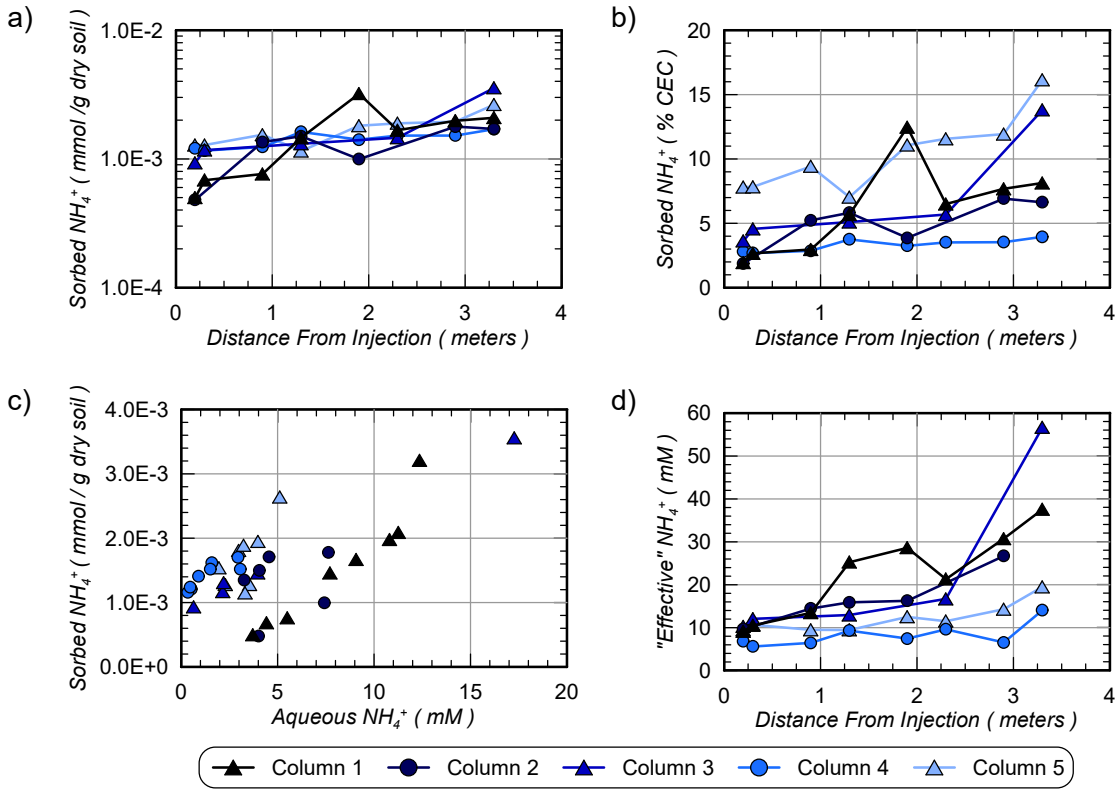

Figure 9.9. (a) Sorbed NH_4^+ masses versus column lengths, (b) sorbed NH_4^+ masses as a percentage of soil CEC versus column lengths, (c) sorbed NH_4^+ masses versus aqueous NH_4^+ concentrations, and (d) "effective" aqueous NH_4^+ concentrations versus column lengths.

Figure 9.9a presents measurements of sorbed NH_4^+ masses as determined from KCl extracted soil versus free solution NH_4^+ measurements (**Figure 9.8**). As shown, columns had measurable sorbed NH_4^+ masses that varied between 4.8×10^{-4} and 3.6×10^{-3} millimoles of NH_4^+ per gram of dry soil. In all columns, sorbed NH_4^+ masses increased with distance from the injection well location, suggesting reduced NH_4^+ removal from soil surfaces at larger distances. **Figure 9.9b** presents similar sorbed NH_4^+ masses as a percentage of soil cation exchange capacities. As shown, all

sorbed NH_4^+ masses were between 1.9% and 16.1% of the total CEC of soil materials. Large differences were observed between soil types with Concrete Sand columns (Column 1, 2, 3) achieving average sorbed NH_4^+ masses of 5.8% CEC, Covelo Sand (Column 5) achieving the highest average sorbed NH_4^+ masses of 10.3% CEC, and Delta Sand (Column 4) achieving the lowest average sorbed NH_4^+ masses of 3.3% CEC. **Figure 9.9c** presents measurements of sorbed NH_4^+ masses with corresponding aqueous NH_4^+ concentrations obtained from soil samples. As expected, for all soil materials, when aqueous NH_4^+ concentrations were higher, sorbed NH_4^+ masses also increased. The apparent linear relationship between sorbed NH_4^+ masses and aqueous NH_4^+ concentrations in equilibrium with soil surfaces suggested that NH_4^+ sorption in columns may be reasonably described by a Freundlich adsorption isotherm over the concentrations observed **(**Freundlich 1907). Linear relationships between free NH_4^+ concentrations and sorbed NH_4^+ masses have been similarly observed in other studies examining ammonium sorption kinetics in soils (Huang et al. 2010; Uğurlu and Karaoğlu 2011). Furthermore, this correlation suggests that sorbed NH_4^+ concentrations were likely higher prior to rinsing and were reduced during the rinsing process. This is consistent with the higher removed NH_4^+ concentrations estimated from outlet well measurements (**Figure 9.4**). In order to better understand the amount of NH_4^+ remaining on soil particle surfaces, “effective” aqueous NH_4^+ concentrations were calculated assuming that all sorbed NH_4^+ was instead available to surrounding aqueous solutions. **Figure 9.9d** presents “effective” NH_4^+ concentrations with distance along all columns computed from known column pore volumes and soil masses. As shown, effective NH_4^+ concentrations ranged between 5.6 mM and 56.6 mM for all columns. This suggested that if sorbed NH_4^+ masses entered into free solution, aqueous NH_4^+ concentrations would increase by 0.05 mM to 42.8 mM. Again, the highest effective NH_4^+ concentrations were calculated for Column 3 and the lowest effective NH_4^+ concentrations

were in Column 4. While these NH_4^+ ions remained sorbed to soils under conditions present during the stop flow period, sorbed NH_4^+ may present challenges related to desorption over time as groundwater solutions are transported through treated locations.

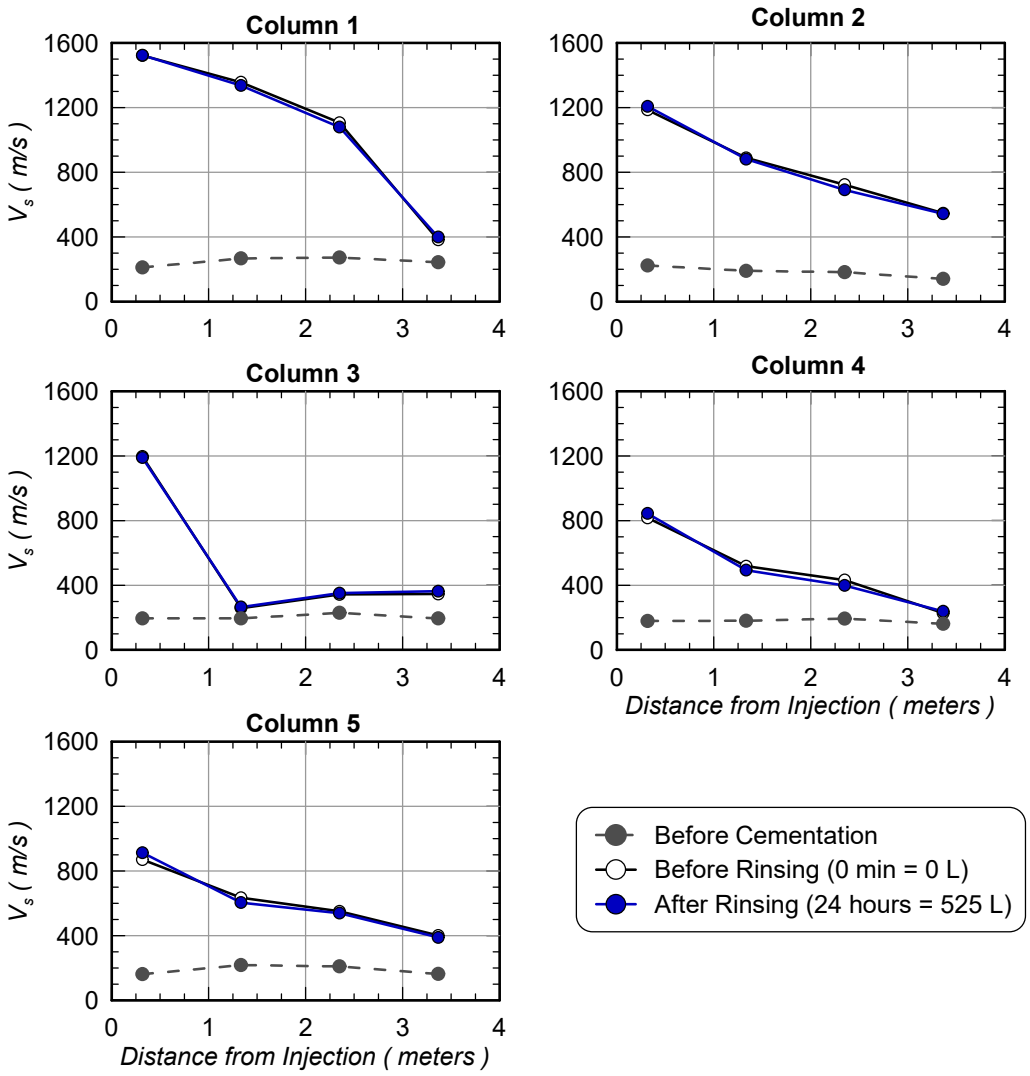

Figure 9.10. Soil shear wave velocities (V_s) versus column lengths for all columns before cementation, after cementation and immediately before rinsing, and after rinsing.

Figure 9.10 presents contours of soil V_s measured along columns lengths for all columns before cementation injections, after cementation but before rinsing, and after rinsing injections following

the stop flow period. All columns had similar initial V_s values, however, after cementation treatments, large differences in V_s distributions were observed between columns and were reflective of differences in biocementation distributions. In Column 1, which had the highest ureolytic activity, high magnitudes of cementation were observed at distances less than 2.35 m with V_s values ranging from 1107 m/s to 1522 m/s with a large reduction in V_s to 382 m/s at a distance of 3.37 m. In Column 2, which contained the same sand but had a lower ureolytic activity, V_s values ranged between 723 m/s and 1186 m/s at distances less than 2.35 m, however, a V_s of 546 m/s was obtained at 3.37 m, which was significantly greater than Column 1. In Column 3, which was augmented, a V_s of 1197 m/s was obtained near the injection well, however, little cementation was detected at distances greater than 0.31 m. In Column 4 and 5, which had lower ureolytic activity, similar trends were observed along column lengths as Column 2, with slightly lower V_s values between 817 m/s and 871 m/s measured at a distance of 0.31 m and values between 227 m/s and 401 m/s measured at a distance of 3.37 m. For all columns, V_s values before and after rinsing differed by no more than ± 50 m/s suggesting that little dissolution or precipitation had occurred. To further examine trends during rinsing, changes in V_s values were plotted in time during rinse injections for all columns and bender element locations (**Figure 9.11**). No consistent trends between columns or measurement locations were observed. Immediately after the start of injections, locations had changes in V_s values between -46 m/s and +14 m/s, however, following the stop flow period changes between -33 m/s and +43 m/s were observed. These V_s results suggest that rinse injections likely only resulted in minor changes in calcite contents between -0.2% and +0.3% by mass following previous relationships established by Gomez and DeJong (2017).

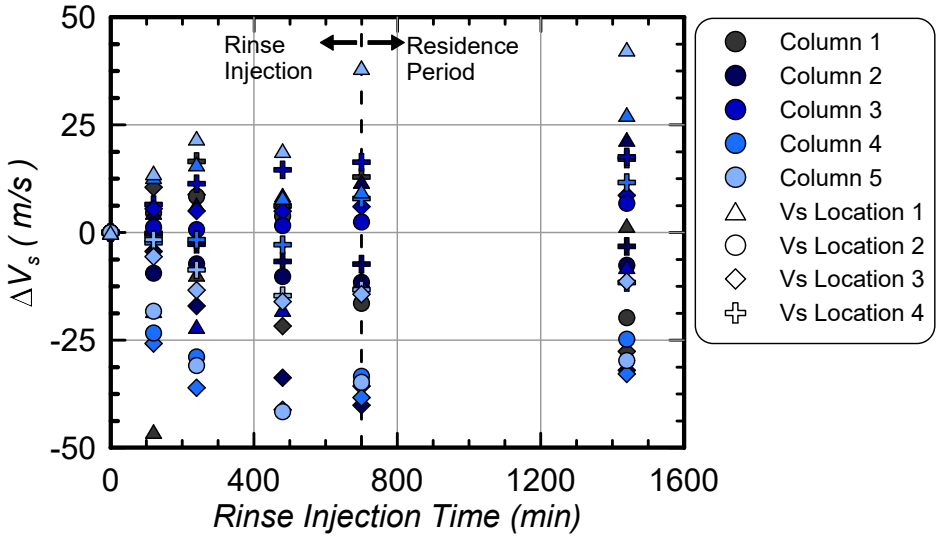

Figure 9.11. Changes in soil shear wave velocities (V_s) for all bender element sensor locations in all columns versus time since the start of rinsing injections.

9.4 Conclusions

The production of NH_4^+ by-products during ureolytic biocementation presents a significant challenge for the technology, which must be addressed if MICP is to attain widespread acceptance as an environmentally-conscious ground improvement alternative. In this study, five 3.7-meter long soil columns containing three different sandy soils were treated using different biocementation treatment techniques to investigate NH_4^+ by-product removal following ureolytic biocementation. During treatments, differences in enriched and augmented ureolytic activity were achieved and resulted in differences in biocementation distributions. While all enriched columns achieved near full hydrolysis of applied 250 mM urea injections over 24 hours (Column 1) and 48 hours (Column 2, 4, 5), the augmented Column 3 achieved limited urea hydrolysis and less NH_4^+ production during cementation treatments. The localization of ureolytic activity and cementation observed near the injection well in Column 3 was attributed to the filtration of *S. pasteurii* bacterial

cells during augmentation. Following cementation, a single 525 L volume of a high pH and high ionic strength rinse solution (200 mM $CaCl_2$, pH ≈ 10.0) was applied to each column and NH_4^+ removal and cementation integrity were monitored. NH_4^+ concentrations observed at the outlet well were compared to expected trends for a passive tracer and results suggest that NH_4^+ transport was retarded by soil-ion interactions with significantly greater NH_4^+ removal than expected due to removal of sorbed NH_4^+ from soil surfaces. When spatial changes in NH_4^+ concentrations were examined during rinsing, large gradients in NH_4^+ concentrations were observed across columns, however, NH_4^+ concentrations below 19 mM were observed at all locations immediately after rinsing. After a 12-hour stop flow period, increases in NH_4^+ concentrations between 1 and 5 mM at most locations were observed, with final cumulative NH_4^+ removal between 97.9% and 99.8%, achieved for all columns. Greater NH_4^+ removal observed in Column 4 was attributed to higher concentrations of exchangeable cations present in the marine soil, which may have limited interactions between NH_4^+ and soil minerals. In contrast, limited NH_4^+ removal observed in Column 3 was believed to have resulted from both the presence of more unoccupied sorption sites from limited urea hydrolysis and lower pH values observed during rinsing. Following KCl extraction of post-rinsing soil samples, measurements suggested that significant NH_4^+ remained sorbed to soil surfaces, which may present challenges related to NH_4^+ desorption over time. Finally, soil V_s measurements suggested that NH_4^+ removal had no significant effect on cementation integrity. While these results suggest that NH_4^+ can be successfully removed from aqueous solutions residing in biocemented soils, acceptable limits for aqueous NH_4^+ concentrations and sorbed NH_4^+ masses will likely be governed by site-specific requirements and may require further investigation of rinsing and management techniques.

Chapter 10. EFFECT OF BIOCEMENTATION ON THE LIQUEFACTION BEHAVIOR OF OTTAWA F-65 SAND

This chapter will be submitted as a journal paper to the *Soil Dynamics and Earthquake Engineering Journal* and be authored by Minyong Lee and Michael Gomez.

ABSTRACT

Biocementation is an environmentally-conscious ground improvement technique that can improve the engineering behavior of granular soils through the precipitation of calcium carbonate on soil particle surfaces and contacts. While the process has received significant attention as an earthquake-induced liquefaction mitigation technique, critical gaps have remained in our understanding of how liquefaction behaviors may shift with differences in applied loading magnitudes and cementation levels for loose poorly-graded clean sands. A series of direct simple shear tests were performed to examine the undrained monotonic and cyclic shearing behavior of biocemented Ottawa F-65 sand prepared to varying cementation levels corresponding to V_s increases up to 500 m/s and soil $CaCO_3$ contents up to 5% by mass. During monotonic undrained shearing, cementation dramatically increased material shear stiffness and strength, with minimal volumetric tendencies mobilized at peak strength, but increasingly dilative behaviors observed at larger strains once cemented bonds were deteriorated. During undrained cyclic shearing, the liquefaction triggering resistance of loose sand was dramatically improved with increases in cementation across a broad range of loading magnitudes (CSR = 0.1 to 1.5) and well exceeded improvements, which could be achieved through densification alone. At larger strains following triggering, however, more modest improvements in post-triggering strain accumulation and reconsolidation strain behaviors were observed, which could be primarily attributed to cementation-induced densification at low cementation levels (V_s < 150 m/s) but further enhanced

at higher cementation levels due to the presence of cemented bonds and particle surface coatings. Outcomes from this study improve our understanding of the liquefaction behaviors of biocemented soils, the metrics by which these behaviors can be effectively characterized, and the mechanisms responsible for these behavioral enhancements, ultimately furthering our understanding of how this technology may be employed for liquefaction mitigation applications.

10.1 Introduction

Conventional ground improvement methods used to mitigate earthquake-induced soil liquefaction include techniques which can cement soil particles together and improve material shear strengths, such as jet and permeation grouting, methods which can improve dissipation of excess pore pressures generated during dynamic loading thereby reducing the potential for liquefaction triggering, such as earthquake drains, and other approaches which act to densify soils thereby reducing contractive volumetric tendencies during shearing, such as deep dynamic compaction (Mitchell et al. 1995; Madabhushi et al. 2007). Although effective, such methods oftentimes necessitate energy-intensive materials and high mechanical energy with the potential for detrimental environmental impacts related to greenhouse gas emissions and effects on groundwater quality (Karol 2003; DeJong et al. 2010; Kendall et al. 2018). Recently bio-mediated soil improvement technologies have been identified that afford the potential to realize comparable engineering improvements as conventional techniques, while leveraging natural biogeochemical reactions to reduce environmental impacts. While the breadth of bio-mediated soil improvement technologies continues to expand, these processes generally either precipitate inorganic minerals to bond adjacent soil particles and coat soil particle surfaces, generate organic extracellular polymeric substances to block soil pore spaces and provide modest improvements in tensile

strength, or produce relatively insoluble gasses that can alter pore fluid compressibility and dampen dynamic pore pressure generation (DeJong et al. 2013). The application of these technologies for a variety of engineering purposes has allowed for continued development of treatment application techniques and improved characterization of the physical and mechanical properties of biocemented soils (Bernardi et al. 2014; Gomez et al. 2015; Gomez et al. 2019; Jiang et al 2019; Ghaseimi and Montoya 2020; San Pablo et al. 2020; Lee et al 2022). The use of bio-mediated soil improvement methods towards mitigating earthquake-induced soil liquefaction has remained one of the most prominent envisioned applications and has guided and motivated the development of such technologies specifically with respect to improvement of loose saturated granular soils (Sharma et al. 2020).

Ureolytic biocementation, or Microbially-induced Calcium Carbonate Precipitation (MICP), is the a Conventional ground improvement methods used to mitigate earthquake-induced soil liquefaction include techniques which can cement soil particles together, thereby improving material shear strength, such as jet and permeation grouting, methods which can improve the dissipation of excess pore pressures generated during dynamic loading, thereby reducing the potential for liquefaction triggering, such as earthquake drains, and other approaches which can densify soils, thereby reducing contractive volumetric tendencies during undrained shearing, such as deep dynamic compaction (Mitchell et al. 1995; Madabhushi 2007). Although effective, such methods oftentimes necessitate energy-intensive materials and/or high mechanical energy with the potential for detrimental environmental impacts related to greenhouse gas emissions and effects on groundwater quality (Karol 2003; DeJong et al. 2010; Kendall et al. 2018). Recently bio-mediated soil improvement technologies have been identified which can afford the potential to

realize comparable engineering improvements as conventional techniques, while leveraging natural biogeochemical reactions to reduce environmental impacts. While the breadth of bio-mediated soil improvement technologies continues to expand, these processes generally either precipitate inorganic minerals to bond adjacent soil particles and/or coat soil particle surfaces, generate organic extracellular polymeric substances to block soil pore spaces and provide a modest soil tensile strength, or produce relatively insoluble gasses that can alter pore fluid compressibility and dampen dynamic pore pressure generation (DeJong et al. 2013). In particular, the application of bio-mediated soil improvement methods towards mitigating earthquake-induced soil liquefaction has remained one of the most prominent envisioned use cases and has guided and motivated the development of such technologies specifically with respect to the improvement of loose saturated granular soils (Sharma et al. 2020). Ureolytic biocementation, or Microbially-induced Calcium Carbonate Precipitation (MICP), is the arguably the most well researched bio-mediated soil improvement process. During MICP, solutions containing urea and calcium salts are supplied to subsurface soils designated for improvement and soil microorganisms capable of hydrolyzing urea (ureolysis) are used to induce and control the precipitation of calcium carbonate ($CaCO_3$) minerals through the generation of carbonate species (Ferris et al. 1996; Stocks-Fischer et al. 1999; DeJong et al. 2006). The resulting biocementation coats soil particle surfaces and binds interparticle contacts, thereby dramatically increasing the shear strength and stiffness of soils (DeJong et al. 2006; Montoya and DeJong 2015; Gomez et al. 2018; Nafisi et al. 2020), while largely retaining porous soil fabrics and initial hydraulic conductivities when applied to clean granular soils (Gomez and DeJong 2017; San Pablo et al. 2020). The non-invasive nature of this process may afford important practical advantages over conventional soil improvement methods, particularly with respect to improving liquefiable soils underlying existing infrastructure.

Although past studies have improved our understanding of the undrained cyclic behavior of biocemented soils; knowledge gaps have persisted with respect to how liquefaction triggering and post-triggering behaviors may shift as a function of applied loading magnitudes and cementation levels for loose poorly-graded clean sands. At the element scale, several notable findings have been made. For example, Simatupang et al. (2018) investigated the undrained cyclic behavior of enzymatically cemented sands using undrained cyclic triaxial testing and found that generated $CaCO_3$ bonds governed small-strain behaviors and liquefaction triggering resistances, however, as bonds became progressively damaged at larger strains, increases in specimen densities and particle surface roughness governed responses and resulted in more minimal behavioral improvements following triggering. Xiao et al. (2018) performed similar undrained cyclic triaxial tests on biocemented and uncemented calcareous sands subjected to different confining stresses and observed reductions in triggering resistances with increases in applied confining stresses for all specimens due to increasingly contractive volumetric tendencies. Xiao et al. (2019) further compared biocemented and uncemented calcareous sands prepared to varying initial densities and found that biocemented specimens had triggering resistances larger than that which could be attributed to cementation-induced densification. Zamani & Montoya (2019) completed undrained cyclic direct simple shear (DSS) tests on biocemented silty sands (fines contents < 35%, ΔV_s < 400 m/s) and observed the highest improvements in cyclic resistances with added cementation at both lower (< 5%) and higher fines (≈ 35%) contents attributed to differences in cemented soil fabrics. Riveros and Sadrekarimi (2020a) examined the undrained cyclic response of biocemented Fraser River sand (ΔV_s ≈90 m/s) and observed increases in liquefaction triggering resistances and more limited pore pressure generation with added cementation. Lee et al. (2022) investigated the

liquefaction behavior of lightly biocemented loose Ottawa F-65 sand (ΔV_s < 100 m/s) using undrained cyclic DSS tests and observed log-linear increases in soil liquefaction triggering resistances with increases shear wave velocities (ΔV_s), but more minimal behavioral enhancements following triggering as weakly cemented bonds became increasingly deteriorated.

At a larger systems level, centrifuge and shake table tests have been used to examine the response of biocementation applied to discrete soil volumes as well as interactions between improved zones and overlying structures. Montoya et al. (2013) examined the dynamic response of centrifuge models that were uniformly cemented to various levels ($\Delta V_s \approx$ 100 and 730 m/s) and subjected to multiple shaking events, and observed large increases in triggering resistances and surface wave amplification with increasing cementation. Darby et al. (2019) performed centrifuge tests using similar uniformly biocemented specimens ($\Delta V_s \approx$ 140 to 590 m/s) and evaluated changes in soil liquefaction triggering resistances and post-triggering shear strain development during repeated cyclic loading events, with cone penetration tests and shear wave velocity measurements also performed to monitor progressive densification and changes in cementation integrity. Zhang et al. (2020) completed shake table tests with biocemented calcareous sands and observed increases in soil fundamental frequencies and triggering resistances with increasing cementation, but with reductions in soil damping ratios. Zamani et al. (2021) completed centrifuge tests investigating the effect of a constant biocementation level ($\Delta V_s \approx$ 420 to 500 m/s) applied to discrete soil volumes at various proximities to shallow foundations and other dense and loose untreated layers, and observed reductions in post-liquefaction reconsolidation settlements with increases in cemented zone thicknesses as well as more complex pore pressure dissipation interactions between

contractive uncemented loose liquefiable layers and more dilative dense uncemented and biocemented zones.

Although the above studies have formed the basis for our current understanding of the effect of biocementation on soil liquefaction behaviors, differences in the metrics by which researchers characterize the achieved biocementation (i.e., $CaCO_3$ content vs. ΔV_s vs. dry density vs. cementing solution composition), parent soil properties (i.e., gradation, fines content, mineralogy), specimen preparation procedures (i.e., cementation under constant stress vs. stress application following cementation) and loading conditions (i.e., cyclic direct simple shear vs. cyclic triaxial) have posed significant challenges with respect to providing a more universal understanding of these material behaviors as a function of isolated variables. As biocementation advances towards practical adoption for liquefaction mitigation applications, systematic investigations of the liquefaction triggering and post-triggering behaviors of biocemented loose clean sands remain needed for loading cycles representative of earthquake-induced demands (< 100 cycles). Such investigations will allow for changes in cementation level, confining stresses, loading demands, relative densities, and other field-representative factors to be rationally accounted for during MICP ground improvement designs and provide new insights regarding the metrics by which expected field-scale behaviors can be correlated to laboratory responses.

In this study, a series of DSS tests were performed to examine the monotonic and cyclic shearing behavior of biocemented Ottawa F-65 sand at varying cementation levels corresponding to ΔV_s increases between 0 and 500 m/s and soil $CaCO_3$ contents between 0 to 5% by mass. Drained and undrained monotonic DSS tests were first performed on biocemented loose specimens and

uncemented specimens of varying initial densities to examine differences in shear stiffness, shear strength, and volumetric tendencies as a function of differences in cementation level and dry density. Following all monotonic tests, forty-four undrained cyclic tests were performed on loose Ottawa F-65 sand specimens cemented to similar levels and subjected to cyclic stress ratios (CSRs) ranging from 0.1 to 1.75 intended to achieve liquefaction triggering within 100 cycles or less. Thirty-seven additional undrained cyclic tests were performed on uncemented specimens prepared to varying initial relative densities to compare the behaviors of the biocemented specimens to uncemented specimens at similar dry densities. Following all testing, relationships between specimen properties, including dry densities, $CaCO_3$ contents, and V_s values, and observed behaviors, including pre-triggering excess pore-pressure generation, post-triggering strain accumulation, post-shearing reconsolidation strains, and V_s changes following shearing were examined to better understand the mechanisms of improvement afforded by cementation and the metrics by which these behaviors can be effectively predicted.

10.2 Materials and Methods

10.2.1 *Sand Material*

Ottawa F-65 sand (U.S. Silica, Ottawa, IL) was used for all tests in this study following numerous other investigations by Ziotopoulou et al. (2018), Darby et al. (2019), Carey et al. (2020), Burdalski and Gomez (2020), El Ghoraiby et al. (2020), Lee et al. (2020, 2022) and others. Ottawa F-65 sand is primarily composed of quartz mineral, has a USCS classification of SP following ASTM D2487 (ASTM, 2017), a D_{50} of 0.21 mm, and contains no fines (Carey et al. 2020). Minimum and maximum void ratios for Ottawa F-65 sand are 0.51 and 0.78, respectively (Carey et al. 2020).

Ottawa F-65 sand was selected for this study, to allowed for earlier results from Lee et al. (2022), which examined the effect of light cementation levels on the liquefaction behaviors of this same soil, to be extended upon.

10.2.2 *Direct Simple Shear Apparatus*

All drained and undrained monotonic and undrained cyclic tests were performed using an electromechanical dynamic cyclic simple shear apparatus (EMDCSS, GDS Instruments, Hook, U.K.) similar to other past investigations (Lee et al. 2020, 2022). The apparatus measured applied axial forces (5-kN range and 0.045% accuracy), shear forces (5-kN range and 0.045% accuracy), axial displacements (25-mm range and 0.1% accuracy), and shear displacements (15-mm range and 0.1% accuracy) during tests using several load cells and LVDTs. All tests were performed using porous discs that had 2 mm long pins, which acted to mitigate potential localization of shear strains at the interface between soil specimens and end platens.

10.2.3 *Specimen Preparation*

All specimens were dry pluviated using a custom fabricated pluviation device and were 70.22 mm in diameter, near 22 mm in height, and were contained within latex membranes and stainless-steel rings. Prior to applying the initial confining stress, specimen top surfaces were vacuumed to be level and a pre-conditioning protocol was followed wherein a small vertical stress was first applied and a series of small-strain drained cycles were applied to engage specimens at the porous disc and soil interface and establish K_0 conditions throughout specimens, while avoiding the potential for specimen densification. A pre-conditioning protocol was selected for this study which was

consistent with recommendations by Humire et al. (2022), wherein the appropriate number of drained cycles needed to properly engage specimens without resulting in densification were identified by (1) analyzing changes in specimen relative densities and stiffnesses resulting from the application of varying numbers of small-strain drained cycles and (2) comparing the number of loading cycles required to trigger liquefaction for pre-conditioned specimens to past independent experimental datasets available for Ottawa F-65 sand (Ueda et al. 2018; Morales et al. 2021) to ensure consistency. The pre-conditioning protocol used for this work involved the application of a small vertical stress of 25 kPa immediately after specimen preparation followed by the application of 150 small-strain strain-controlled drained cycles with amplitude of 0.01 mm (≈ 0.05% shear strain), during which changes in specimen shear stiffness and volume were monitored to assess end platen engagement.

Immediately following pre-conditioning, specimens were saturated using de-aired de-ionized water which was injected into specimens from the bottom upwards for at least 30 minutes at a flow rate of 10 mL/min. Saturation injections were continued until no air bubbles were observed exiting specimens within a period of 10 minutes. For all tests, specimen D_r values changed by less than 2% following both pre-conditioning and saturation, suggesting that minimal densification occurred during these processes. After saturation, a vertical stress of 100 kPa was applied to specimens in order to simulate stress conditions near 10 meters within a saturated soil deposit. For drained monotonic tests, the 100 kPa vertical stress was maintained during shearing, however, for all undrained monotonic and cyclic tests, equivalent undrained conditions were achieved by maintaining constant volume conditions during shearing with related changes in applied vertical stresses indicative of expected changes in excess pore pressure generation. For untreated

specimens, shearing events occurred immediately after initial saturation once a vertical effective stress of 100 kPa was achieved. For biocemented specimens, however, biocementation injections were applied following initial saturation after applying the vertical stress of 100 kPa, with saturation injections repeated again after cementation treatments and immediately prior to shearing. The initial relative densities (D_r) and dry densities (ρ_{dry}) of all specimens were determined for the condition present following the application of the 100 kPa total stress and immediately prior to shearing by weighing oven-dried specimens after testing and accounting for additional added $CaCO_3$ masses for biocemented specimens. All specimens had pore volumes (PV) between 32 and 35 mL (porosity ≈ 40%).

10.2.4 *Biocementation Treatments*

Biocemented specimens were prepared using procedures similar to those described in Lee et al. (2022) wherein ureolytic bacterial cell suspensions were first applied to specimens and cementation injections were subsequently introduced to cement soils to varying cementation levels. All specimens were augmented with *Sporosarcina pasteurii* (*S. pasteuri*i, ATCC 11859) cells that were cultured in ATCC 11859 growth media (0.13M Tris Base, 20 g/L yeast extract, 10 g/L $(NH_4)_2SO_4$, pH-adjusted to 9.0), pelleted and rinsed using isotonic saline (9 g/L NaCl) and centrifugation, and added to augmentation solutions. Augmentation solutions were prepared in a 250 mL (8.3 PV) volume for all specimens and contained *Sporosarcina pasteurii* at a cell density between 10^7 and 10^8 cells/mL, 100 mM NH_4Cl, and 0.2 g/L yeast extract. In order to promote more uniform cell distributions throughout DSS specimens, augmentation solutions were applied in four phases. First, 75 mL (2.5 PV) of augmentation solution was injected from the bottom of specimens

upwards at a flow rate of 10 mL/min and all effluent was discarded. Next, 75 mL of augmentation solution was injected the top of specimens downwards and all generated effluent was collected and mixed with the remaining 100 mL of fresh augmentation solution. Lastly, 75 mL of this mixture was injected again from the bottom of specimens upwards and another 75 mL was injected from the top of specimens downwards, each time collecting and homogenizing effluent solutions. After all injections, augmentation solutions resided within specimens for at least 30 minutes to encourage cell attachment. Solution OD_{600} measurements performed before and after augmentation suggested that between 90% and 95% of the injected cells were retained within specimens.

After augmentation, calcium-containing cementation solutions were applied to all biocemented specimens to initiate the cementation process. Cementation solutions were applied in 150 mL (5 PV) cementation solution volumes that were injected from the bottom to the top of specimens at a flow rate of 10 mL/min. Cementation solutions contained 100 mM NH_4Cl and varying concentrations of urea and $CaCl_2$ between 50 mM and 750 mM formulated to mitigate spontaneous precipitation of $CaCO_3$ within specimen porous discs during repeated injections needed for more highly cemented specimens. Specimens prepared to light cementation magnitudes ($\Delta V_s < 100$ m/s), received single cementation solution injections containing $CaCl_2$ concentrations between 50 and 250 mM at urea-to-calcium concentration ratios of 1.5-to-1.0 (urea concentrations of 75 mM to 375 mM). For all higher cementation levels, urea-to-calcium concentration ratios were reduced to either 1-to-1 or 1-to-1.2, intended to supply excess calcium and achieved more limited excess carbonate in solutions following injections, which could react upon the application of calcium-rich solutions in subsequent injections. Similar techniques are described in Gomez et al. (2019) and

have been shown to mitigate the potential for spontaneous chemical precipitation of $CaCO_3$, which could have clogged specimen porous discs and resulted in cemented microstructures that were inconsistent between cementation levels. At the highest cementation level considered corresponding to a ΔV_s near 500 m/s, solutions with 750 mM $CaCl_2$ and 625 mM urea (1-to-1.2 ratio) were applied once daily over two to three days until the desired cementation level, as assessed by shear wave velocity changes, was obtained. Although differences in treatment solution compositions were employed, previous investigations by the authors have shown that when similar treatment approaches are used and applied urea and calcium concentrations are varied, no significant differences in reaction kinetics, $CaCO_3$ mineralogy, or $CaCO_3$ morphology are observed (Burdalski and Gomez 2020). All cementation solution injections resided within specimens for a minimum of 18 hours to ensure reaction completion. After cementation, specimens were then re-saturated using 450 mL injections of de-aired de-ionized water that was pH-adjusted to 7.0 using sodium hydroxide to limit the potential for $CaCO_3$ dissolution. Measurements of axial strains during treatments suggested that all performed injections had no detectable effects on specimen dry densities.

10.2.5 *Shear and Compression Wave Velocity Measurements*

In order to non-destructively monitor changes in cementation magnitudes during the treatment process, verify similarities between specimen initial conditions, and assess cementation damage following shearing events, shear wave velocity (V_s) measurements were performed for all specimens using bender-extender element sensors (Lings and Greening 2001). Transmitting and receiving bender-extender sensors were mounted within specimen top and bottom end platens and

were excited using a 24-volt 100 Hz square wave generated by a power supply and custom signal generator and data acquisition system. Measurements of voltage in time from receiving bender-extender sensors were recorded using an oscilloscope at a sampling frequency of 1 MHz. Soil V_s values were then determined from the time difference between transmitted and received waves and known sensor spacings. For all biocemented specimens, V_s measurements were performed (i) before and after augmentation, (ii) before, after, and ≈ 18 hours after cementation injections, (iii) before initiating shearing events, and (iv) following shearing and reconsolidation of specimens. For all uncemented specimens, V_s measurements were performed only (i) before shearing and (ii) following shearing and reconsolidation. Although tests were not fully undrained, bender-extender elements were also used to measure specimen compression wave velocities (V_p) prior to shearing to ensure sufficient saturation. All specimen V_p values exceeded 1500 m/s prior to drained and equivalent undrained shearing events.

10.2.6 *Drained and Undrained Monotonic Shearing*

All monotonic drained and undrained tests were performed using a shearing rate of 0.011 or 0.022 mm/min (approximately 0.05% or 0.1% shear strain per minute). All drained monotonic tests were completed while maintaining a vertical effective stress of 100 kPa. All undrained monotonic tests were completed under equivalent undrained (constant volume) conditions wherein changes in the vertical stress during constant volume shearing were assumed to be equivalent to excess pore pressures generated under fully undrained conditions. Shearing was performed until all specimens achieved single amplitude shear strains (SASS) of 24%, intended to induce a similar magnitude of damage to cemented specimens as undrained cyclic shearing events described later. For all tests,

displacement and stress measurements were recorded at a sampling frequency of 0.5 Hz. Following monotonic shearing, applied vertical stresses were unloaded (≈ 0 kPa), specimens were slowly re-centered to back to their initial positions (shear displacement ≈ 0%), and the initial vertical stress (100 kPa) was reapplied to reconsolidate specimens. Post-shearing shear wave velocities were measured once vertical displacements stabilized for at least 5 minutes after applying the reconsolidation stress.

10.2.7 *Undrained Cyclic Shearing*

Undrained cyclic shearing events involved the application of sinusoidal stress-controlled loading cycles under equivalent undrained (constant volume) conditions with no pore pressure measurements. During tests, differences in applied loading magnitudes were considered including cyclic stress ratios (CSR = $\tau/\sigma'_{v\ initial}$) of 0.1, 0.15, 0.2, 0.25, 0.3, 0.75, 1.0, 1.25, 1.5, and 1.75. Although differences in applied loading frequencies have been shown to have minimal effects on the undrained cyclic behavior of cohesionless soils, undrained cyclic loading was applied at frequencies between 0.005 and 0.05 Hz, depending on the cyclic loading magnitude and cementation level in order to improve the ability of the DSS apparatus to achieve the intended loading and obtain more resolved measurements. Displacement and stress measurements were recorded at a sampling frequency of 200 data points per cycle for all tests. All cyclic shearing events were terminated once specimens experienced a double amplitude shear strain (DASS) of 24%. During select tests on uncemented dense specimens, the accumulation of 24% DASS were never achieved and therefore tests were terminated after ≈ 100 cycles were applied following triggering once DASS values stopped increasing with further increases in applied cycles.

Following undrained cyclic shearing, specimens were slowly re-centered to back to their initial position (shear deformation ≈ 0%) while maintaining the current vertical stress after failure (≈ 0 kPa). The initial vertical stress of 100 kPa was then reapplied to reconsolidate specimens. Similar to monotonic tests, post-shearing shear wave velocities were measured once vertical displacements stabilized for at least 5 minutes after applying the reconsolidation stress. While it is acknowledged that field-representative post-liquefaction reconsolidation behaviors cannot be fully captured in equivalent undrained DSS tests, the reapplication of the vertical total stress in this testing program following cyclic loading was intended to interpret the potential for volume change in these materials following liquefaction.

10.2.8 *Dry Density & $CaCO_3$ Content Measurements*

Following all tests, soil specimens were freely drained, removed from the DSS apparatus, and oven-dried for at least 18 hours at 110 °C. Dry masses were measured and dry densities were determined by dividing dry masses by the total volume of specimens immediately prior to shearing. Specimens were then subsampled for $CaCO_3$ content measurements in order to assess cementation magnitudes and uniformity. Soil $CaCO_3$ contents were determined using a pressure chamber method following ASTM D4373 by reacting cemented soil subsamples (≈ 10 grams) with hydrochloric acid (ASTM, 2014). The dissolution of $CaCO_3$ minerals in acid generates CO_2 gas and therefore measured increases in test chamber pressures were used to determine soil $CaCO_3$ contents using calibration relationships. A minimum of three soil $CaCO_3$ content measurements were completed for each specimen with the average soil $CaCO_3$ content reported. $CaCO_3$ contents

measurements for the same specimen differed by no more than 0.1% by mass with coefficients of variation (COV) for measurements being less than 15% for nearly all specimens.

10.3 Results and Discussion

10.3.1 *Changes in Specimen V_s, $CaCO_3$ Contents, & Dry Densities with Biocementation*

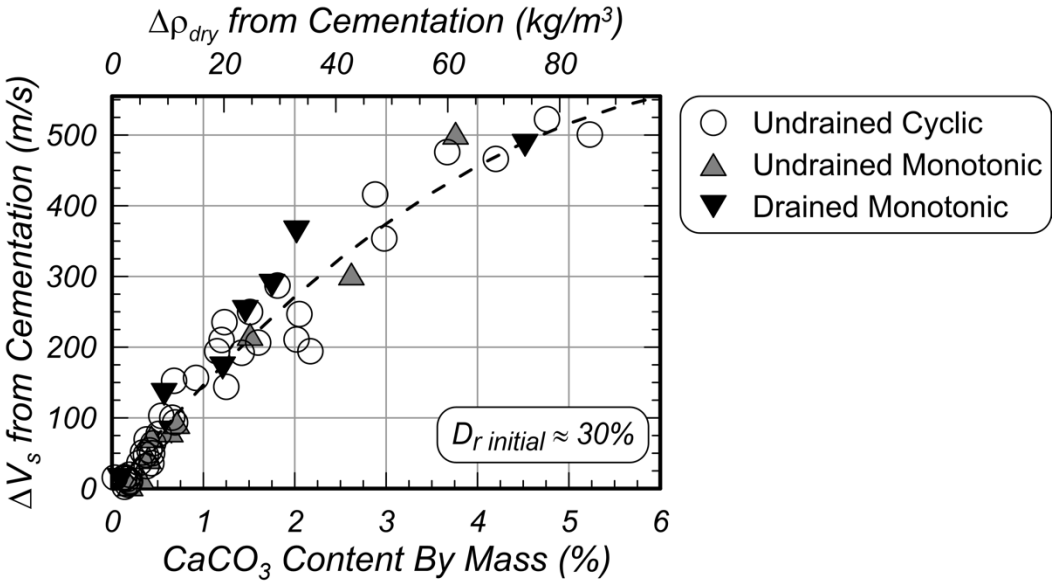

Figure 10.1. Relationships between cementation-induced shear wave velocity increases (ΔV_s), soil $CaCO_3$ contents, and changes in dry densities ($\Delta\rho_{dry}$) for all biocemented and uncemented loose ($D_{r\ initial} \approx 30\%$) Ottawa F-65 specimens.

Figure 10.1 presents relationships between cementation-induced increases in shear wave velocities (ΔV_s) and corresponding increases in soil $CaCO_3$ contents as well as bulk dry densities ($\Delta\rho_{dry}$). All specimens were prepared loose ($D_{r\ initial} \approx 30\%$) and were cemented to varying cementation levels with ΔV_s increases between 0 (uncemented) and 500 m/s, soil $CaCO_3$ contents between 0 and 5% by mass, and $\Delta\rho_{dry}$ increases between 0 and 85 kg/m^3. Values are provided for

specimens from all tests performed in this study including drained monotonic, undrained monotonic, and undrained cyclic tests. As shown above, all biocemented specimens exhibited comparable ΔV_s increases for similar cementation levels, indicated by soil $CaCO_3$ contents and $\Delta\rho_{dry}$ increases. Although past studies have shown a near-linear relationship between ΔV_s increases and soil $CaCO_3$ contents (Gomez & DeJong 2017; Gomez et al. 2018; Darby et al. 2019; Lee et al. 2020, 2022 and others), a near linear relationship was only observed at relatively low cementation levels ($CaCO_3$ contents < 1%), with higher levels of cementation achieving notably smaller increases in ΔV_s with increasing $CaCO_3$ contents. The consistency between ΔV_s and $CaCO_3$ content values observed for all specimens, however, suggested that the distribution of cementation on soil particle surfaces and contacts likely remained similar for specimens regardless of cementation level. This outcome also suggested that techniques intended to limit the spontaneous precipitation of $CaCO_3$ during repeated treatments were largely successful, with some differences observed at higher $CaCO_3$ contents (> 3%) potentially indicative of the presence of some $CaCO_3$ that did not as effectively contribute to shear stiffness enhancements.

10.3.2 *Effect of Biocementation on Drained Monotonic Behaviors*

A series of drained monotonic tests were performed on biocemented loose specimens and untreated specimens at varying initial densities to examine changes in stress-strain and volumetric behaviors as a function of cementation level and densification. **Table 10.1** summarizes results from all drained monotonic tests including specimen initial properties (e.g., targeted initial packing [loose, medium dense, dense], initial D_r, and initial V_s), post-cementation specimen properties (e.g., ΔV_s from cementation, $CaCO_3$ content by mass, coefficient of variation [COV] for $CaCO_3$ content

measures, dry density values before shearing [including contributions from cementation], and increases in dry densities attributed to cementation), and various parameters describing shearing and post-shearing behaviors (e.g. vertical reconsolidation strains, and ΔV_s changes after shearing and reconsolidation). For uncemented specimens, targeted initial densities were varied and included "loose" specimens with initial D_r values between 26.6% and 30.5% and initial V_s values between 138 m/s and 155 m/s, a single "medium-dense" specimen with an initial D_r value of 53.5% and an initial V_s value of 159 m/s, and a single "dense" specimen with an initial D_r value of 72.8% and an initial V_s value of 188 m/s. Eight biocemented specimens were prepared "loose" prior to cementation and had initial D_r values between 23.3% and 44.3% and initial V_s values between 141 m/s and 160 m/s, similar to other uncemented loose tests. Following preparation, these biocemented specimens were then cemented to achieve dry density increases up to 74 kg/m^3 and ΔV_s increases up to 485 m/s, which were consistent with the cementation levels subsequently investigated in undrained cyclic tests.

Table 10.1. Summary of Initial and Post-cementation Properties and Shearing and Post-shearing Behaviors for Drained Monotonic Tests Performed on Biocemented Loose Specimens and Uncemented Specimens at Varying Initial Densities

Specimen Initial Properties [1]				*Post-cementation Specimen Properties*					*Shearing and Post-shearing Behaviors*		
Specimen Type	**Packing**[2]	**D_r initial (%)**	**V_s initial (m/s)**	**ΔV_s from cementation (m/s)**	**$CaCO_3$ by mass (%)**	**COV of $CaCO_3$ (%)**[3]	**ρ_d (kg/m^3)**	**$\Delta\rho_d$ (kg/m^3)**	**Peak τ from 0 to 3% SASS (kPa)**	**Reconsolidation Strain (%)**[4]	**ΔV_s after shearing and reconsolidation (m/s)**
Uncemented	L	30.5	138	0	0.0	-	1561	-	39	-0.24	-2
Uncemented	L	26.6	155	0	0.0	-	1551	-	36	-0.21	-5
Uncemented	M	53.5	159	0	0.0	-	1620	-	49	-0.42	-17
Uncemented	D	72.8	188	0	0.0	-	1674	-	54	-1.03	-13
Cemented	L	29.3	154	13	0.1	22	1559	1.4	38	1.01	-9
Cemented	L	23.7	146	80	0.6	5	1554	10.1	46	1.60	-20
Cemented	L	43.5	149	133	0.6	7	1603	9.2	58	-0.78	-48
Cemented	L	23.3	142	171	1.2	1	1562	19.0	66	0.05	-74
Cemented	L	44.3	160	250	1.5	2	1620	23.6	59	-1.03	-86
Cemented	L	32.5	141	287	1.8	1	1594	27.9	72	-1.20	-99
Cemented	L	37.0	149	363	2.0	1	1610	32.5	79	-1.20	-310
Cemented	L	32.5	159	485	4.5	2	1640	74.1	143	-1.46	-407

[1]All specimens were initially consolidated to σ'_v = 100 kPa

[2]L= loose, M= medium-dense, D= dense

[3]Coefficient of variation for $CaCO_3$ contents measurements

[4]All specimens were reconsolidated back to σ'_v = 100 kPa

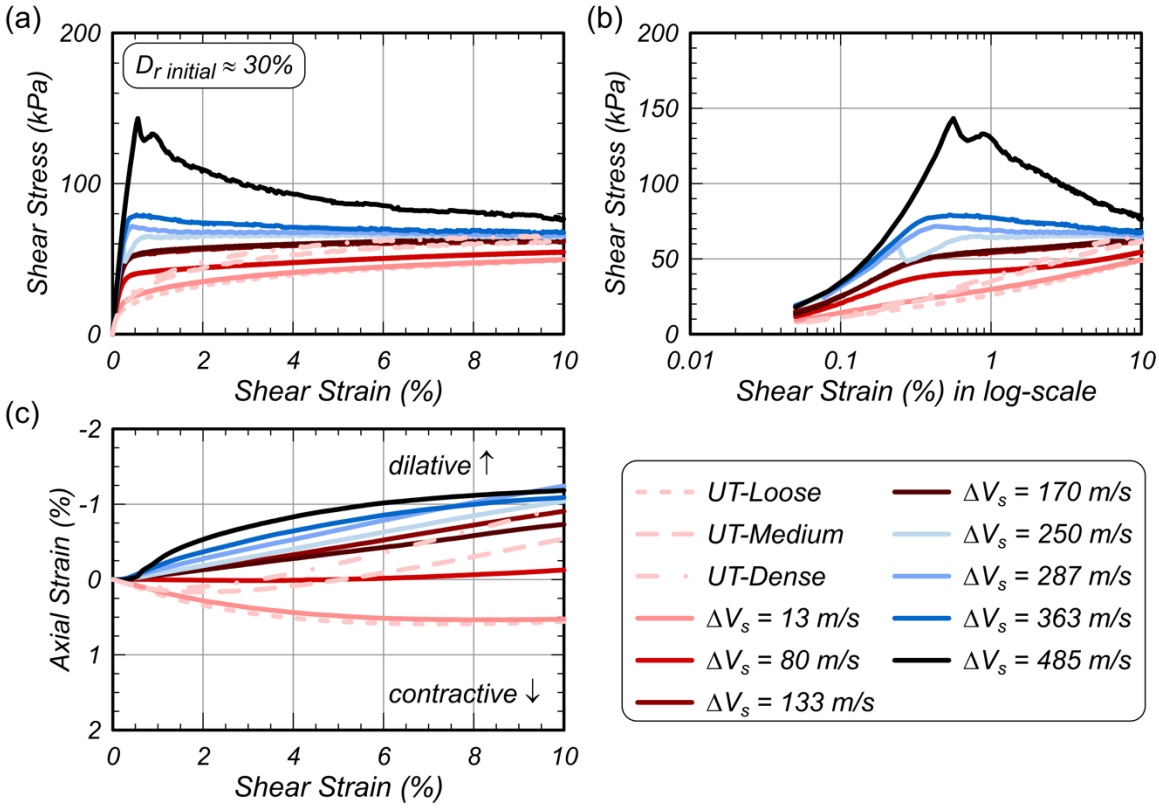

Figure 10.2. Results from drained monotonic tests for biocemented loose ($D_{r\ initial}$ ≈ 30%) specimens treated to varying cementation levels and uncemented specimens prepared to varying initial densities including plots of **(a)** shear stress versus shear strain, **(b)** shear stress versus shear strain (in log-scale), and **(c)** axial strain versus shear strain. All tests were performed under a constant vertical effective stress of 100 kPa.

Figure 10.2 presents drained monotonic shearing behaviors for both uncemented specimens at varying initial densities and biocemented loose specimens including shear stress versus shear strain responses (**Figure 10.2a, 10.2b**) and axial strain versus shear strain responses (**Figure 10.2c**). As shown, as cementation levels were progressively increased, initially loose specimens transitioned from strain-hardening to strain-softening responses with the presence a more prominent peak strength (**Figure 10.2a**). Peak shear strengths also consistently increased with increases in biocementation magnitudes from ≈50 kPa for the uncemented loose condition to ≈ 150 kPa for the most heavily cemented specimen (ΔV_s = 485 m/s). Interestingly, unlike uncemented specimens

wherein the peak dilation angle would be expected to correspond with the peak strength, minimal volumetric strains were observed in biocemented specimens at peak strength due to the presence of cemented bonds which restricted volumetric tendencies (**Figure 10.2c**). However, post-peak larger shear deformations were achieved (SASS > 0.5%), cemented bonds were increasingly damaged, and the dilatancy of the soil was further mobilized. At further strains (SASS ≈ 10%), shearing behaviors were also improved with increasing cementation, although to a lesser degree than peak strengths. When examining the shearing response of uncemented specimens prepared to different initial relative densities less significant increases in peak shear strength were observed with densification. For example, the dense (D_r ≈ 70%) uncemented specimen achieved a peak shear strength near 75 kPa that was comparable to the loose biocemented specimen with a ΔV_s of only 170 m/s, however, the dense specimen also required much greater shear strains to mobilize to this peak strength (≈ 6% vs. ≈ 0.5%). Significant differences in specimen shear stiffnesses upon the initiation of shearing (< 1% SASS) were also observed with increasing cementation and could be more easily observed when presenting shear strains in log-scale (**Figure 10.2b**). As shown, all uncemented specimens as well as the ΔV_s = 13 m/s biocemented specimen had comparable shear stiffnesses up to ≈ 0.5% shear strain. However, large increases in shear stiffnesses were observed over this same strain range (SASS < 0.5%), once ΔV_s values exceeded 80 m/s until ΔV_s values approached 250 m/s after which more minor increases in stiffnesses were observed as ΔV_s increased from 250 m/s to ≈ 500 m/s.

When examining volumetric behaviors during shearing (**Figure 10.2c**), all uncemented specimens contracted initially, with the loose specimen maintaining contractive volumetric strains at larger strains, but the medium dense and dense specimens transiting to dilative volumetric strains after ≈

5% and ≈ 3.5% shear strain, respectively. At low cementation, volumetric strains for the ΔV_s = 13 m/s specimen were comparable to the uncemented loose specimen, an outcome that was consistent with the minimal differences in stress-strain behaviors that were observed. However, near a ΔV_s of 80 m/s, a transition from initial contraction to more minimal volumetric changes at peak strength was observed, with increasingly dilative volumetric strains observed at shear strains exceeding ≈ 0.5% as specimen cementation levels increased. As expected, the strongest dilation was observed in the most heavily cemented ΔV_s of 485 m/s specimen, wherein dilative volumetric strains exceeding 1% were observed at shear strains greater than 6%. For all cemented specimens, the onset of significant volumetric changes occurred at higher shear strains than uncemented specimens, again reflective of the increased restriction of soil volumetric tendencies afforded by cemented bonds, with significant volumetric changes only observed in cemented specimens post-peak once cemented bonds were deteriorated and the frictional resistance and dilatancy of the specimens was mobilized.

10.3.3 *Effect of Biocementation on Undrained Monotonic Behaviors*

A series of undrained monotonic tests were performed on biocemented loose specimens and untreated specimens prepared to varying initial densities to further examine changes in stress-strain and pore pressure generation behaviors as a function of cementation level and densification. Results from undrained monotonic tests were also used to further augment insights obtained from undrained cyclic tests, particularly for high loading magnitudes (i.e., CSRs), as described later. **Table 10.2** summarizes results from all undrained monotonic tests including specimen initial properties (e.g., targeted initial packing [loose, medium dense, dense], initial D_r, and initial V_s),

post-cementation specimen properties (e.g., ΔV_s from cementation, $CaCO_3$ content by mass, coefficient of variation [COV] of $CaCO_3$ content measures, dry densities before shearing [including contributions from cementation], and increases in dry densities attributed to cementation), and various parameters describing shearing and post-shearing behaviors (e.g., peak shear stress from 0 to 3% SASS, corresponding CSR required to achieve 3% SASS in 0.25 cycles determined from the peak stress, vertical reconsolidation strains, and ΔV_s changes after shearing and reconsolidation events). Specimen properties employed in undrained monotonic tests were similar to those examined in the previous drained monotonic tests with differences initial relative density considered for uncemented specimens and differences in cementation levels considered for biocemented loose specimens up to a ΔV_s near 500 m/s. Uncemented "loose" specimens had initial D_r values between 30.0% and 33.3% and initial V_s values between 138 m/s and 149 m/s. A single uncemented "medium-dense" specimen had an initial D_r value of 59.4% and an initial V_s value of 150 m/s. A single uncemented "dense" specimen had an initial D_r value of 72.0% and an initial V_s value of 152 m/s. Nine biocemented loose specimens had initial D_r values between 26.5% and 36.5% and initial V_s values between 136 m/s and 152 m/s, which were again comparable to uncemented loose tests.

Table 10.2. Summary of Initial and Post-treatment Specimen Properties and Shearing and Post-shearing Behaviors for Undrained Monotonic Tests Performed on Biocemented Loose Specimens and Uncemented Specimens at Varying Initial Densities

Specimen Initial Properties [1]				*Post-cementation Specimen Properties*					*Shearing and Post-shearing Behaviors*			
Specimen Type	**Packing**[2]	**D_r initial (%)**	**V_s initial (m/s)**	**ΔV_s from cementation (m/s)**	**$CaCO_3$ by mass (%)**	**COV of $CaCO_3$ (%)**[3]	**ρ_d (kg/m^3)**	**$\Delta\rho_d$ (kg/m^3)**	**Peak τ from 0 to 3% SASS (kPa)**	**$CSR_{3\%\ SASS}$ in 0.25 cycles**	**Reconsolidation Strain (%)**[4]	**ΔV_s after shearing and reconsolidation (m/s)**
Uncemented	L	30.3	138	0	0.0	-	1560	-	17.7	0.18	2.73	-2
Uncemented	L	33.3	149	0	0.0	-	1582	-	16.3	0.16	0.87	-5
Uncemented	M	59.4	150	0	0.0	-	1636	-	34.9	0.35	-0.03	-17
Uncemented	D	72.0	152	0	0.0	-	1671	-	43.5	0.44	-0.06	-13
Cemented	L	33.3	139	5	0.2	35	1571	3.1	20.0	0.20	2.58	-9
Cemented	L	32.5	141	16	0.3	14	1571	5.0	24.0	0.24	2.55	-20
Cemented	L	27.5	140	44	0.4	10	1560	6.2	30.8	0.31	2.56	-48
Cemented	L	26.5	136	73	0.4	11	1558	6.7	32.9	0.33	2.58	-74
Cemented	L	28.3	152	81	0.6	9	1566	10.0	49.1	0.49	1.04	-86
Cemented	L	31.2	138	93	0.7	9	1574	11.2	72.0	0.72	2.20	-99
Cemented	L	36.4	147	218	1.5	3	1600	24.2	137.5	1.38	-0.35	-226
Cemented	L	35.2	147	303	2.6	2	1615	42.3	226.1	2.26	-0.79	-310
Cemented	L	32.7	152	502	3.8	2	1628	61.2	364.6	3.65	-1.44	-407

[1]All specimens were initially consolidated to σ'_v = 100 kPa

[2]L= loose, M= medium-dense, D= dense

[3]Coefficient of variation for $CaCO_3$ contents measurements

[4]All specimens were reconsolidated back to σ'_v = 100 kPa

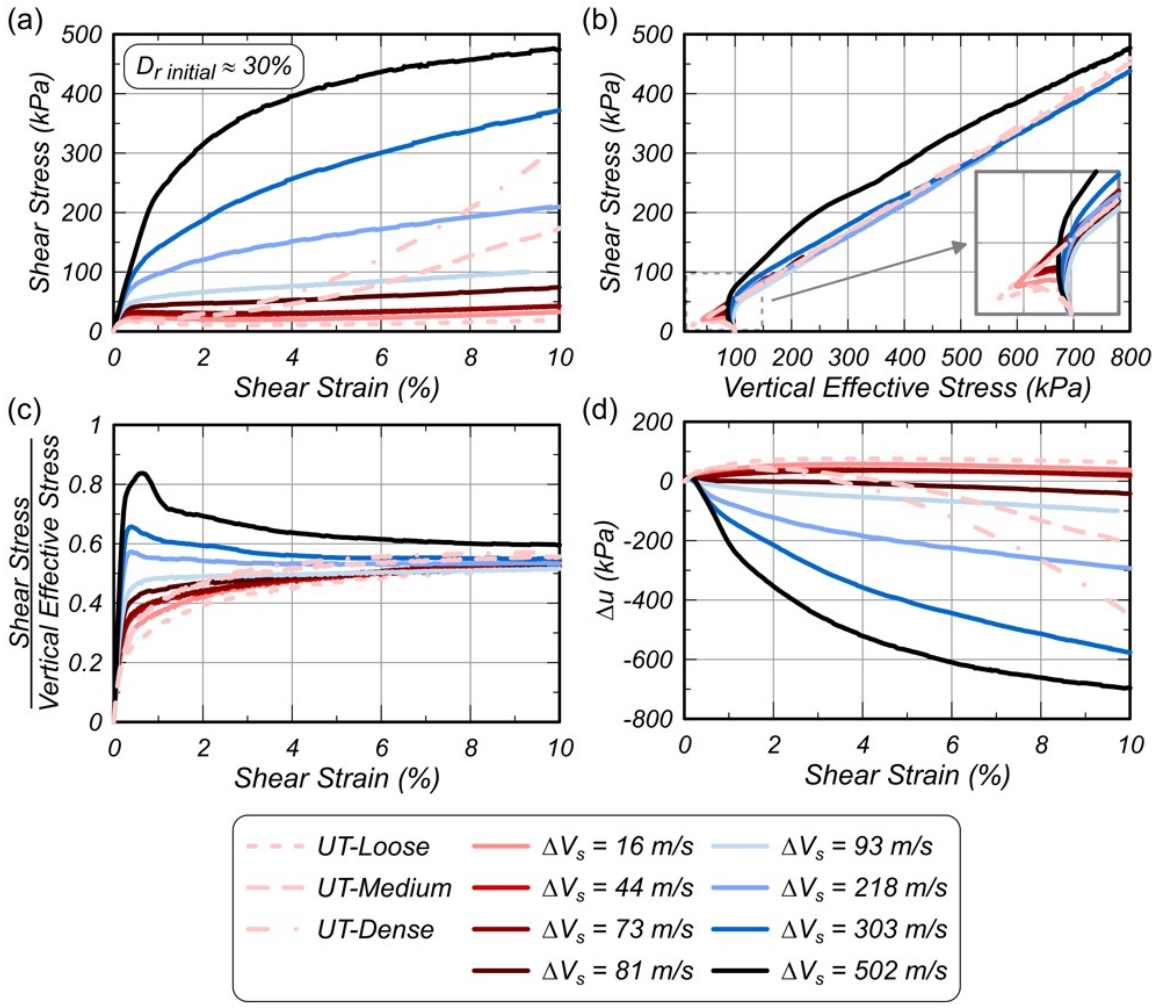

Figure 10.3. Results from undrained monotonic tests for biocemented loose ($D_{r\ initial} \approx 30\%$) specimens treated to varying cementation levels and uncemented specimens prepared to varying densities ($D_{r\ initial} \approx 30$ to 70%) including plots of **(a)** shear stress versus shear strain, **(b)** shear stress versus vertical effective stress, **(c)** stress-normalized shear stress versus shear strain, and **(d)** excess pore water pressure (Δu) versus shear strain. All tests were performed at an initial vertical effective stress of 100 kPa and were sheared under constant volume conditions.

Figure 10.3 presents undrained monotonic shearing behaviors for both uncemented specimens at varying initial densities and biocemented loose specimens including shear stress versus shear strain (**Figure 10.3a**), shear stress versus vertical effective stress (**Figure 10.3b**), stress-normalized shear stress versus shear strain (**Figure 10.3c**), and excess pore water pressure (Δu) versus shear strain

(**Figure 10.3d**) responses. As shown, higher shear strengths were observed at almost all strain levels with increasing biocementation (**Figure 10.3a**), in part due to increased dilative tendencies, which generated larger negative excess pores pressures and therefore increased vertical effective stresses (**Figure 10.3b, 10.3c**). In contrast, positive excess pores pressures were generated initially upon shearing in all uncemented specimens regardless of initial density as well as some lightly cemented specimens corresponding to ΔV_s values near and below 73 m/s. Similar to drained behaviors, a transition was observed near a ΔV_s value of 81 m/s from positive to negative excess pore pressure generation at larger shear strains (> 0.5%), highlighting the substantial contribution of even low cementation levels towards altering volumetric tendencies. When considering apparent changes in failure envelopes with added cementation (**Figure 3b**), no significant differences were observed between uncemented and cemented specimens until ΔV_s values approached 500 m/s, for which a clear upward shift in this envelope was observed when compared to other more lightly cemented specimens. The slope of the failure envelope (i.e., ϕ') for the ΔV_s = 502 m/s specimen appeared to reduce at higher stresses, however, suggesting that while there may be a large increase in apparent cohesion from cementation at lower stresses, at higher stresses, the effect of cementation may become diminished as cemented bonds are increasingly deteriorated. Similar to observations from other studies, the effect of cementation on failure envelopes did not appear to reflect a consistent shift in Mohr-Coulomb parameters (i.e., c, ϕ'), but rather appeared to illustrate more complicated shearing behaviors wherein cemented bonds can provide higher shear strengths at lower effective stresses, however, with progressive shearing these effects are diminished, the failure envelope collapses and shearing behaviors approach that expected for uncemented sands, albeit with small changes due to increased interparticle angularly and surface

roughness, which can increase critical state friction angles once a sufficient amount of cementation is present.

Once shear stress versus shear strain behaviors were stress-normalized (**Figure 10.3c**), behaviors were similar to drained monotonic tests, with normalize shear strengths and initial shear stiffnesses increasing dramatically with increasing ΔV_s, and transition from strain-hardening to strain-softening behaviors near a ΔV_s value of 93 m/s. At higher cementation levels, peaks in normalized shear strengths were observed at shear strains near ≈ 0.5%, despite minimal negative excess pore pressure generation, again reflective of increases in shear strengths afforded by cemented bonds. At larger strains, again cemented bonds deteriorated, with normalized strengths in all cemented tests approaching similar values to uncemented specimens. One exception was the ΔV_s of 502 m/s specimen, which still exhibited larger normalized strengths at shear strains near 10%, however, it remains unclear if such differences would have persisted due to particle level changes if samples were reliably sheared to higher strains, or if such behaviors would have further deteriorated towards the uncemented condition as cemented bonds were increasing broken. Finally, although the uncemented dense specimen exhibited a peak normalized strength comparable to the cemented loose specimen at a ΔV_s of 218 m/s, the shear strains required to mobilize this peak strength and associated dilatant volumetric behaviors in the dense uncemented specimen were near ≈ 6%, nearly twelve times greater than that required to achieve this peak strength in the cemented specimen (SASS ≈ 0.5%).

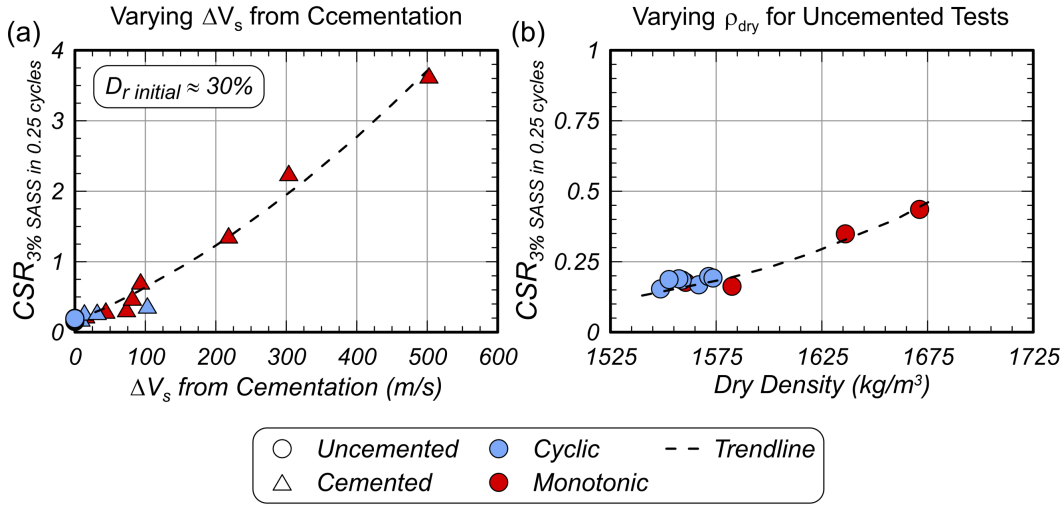

Figure 10.4. Applied CSRs required to achieve trigger liquefaction (3% SASS) in 0.25 cycles versus **(a)** ΔV_s values from cementation for loose ($D_{r\ initial} \approx 30\%$) uncemented and biocemented specimens of varying cementation levels and **(b)** dry density values for uncemented specimens of varying initial densities determined from a combination of both undrained monotonic and undrained cyclic DSS tests.

10.3.4 *Determination of 0.25 Cycle Triggering Resistances From Undrained Cyclic & Monotonic Tests*

During undrained cyclic loading, the minimum number of cycles that can be applied prior to triggering (3% SASS) while still achieving the intended cyclic shear stress is 0.25 cycles, which represents the accumulation of 3% SASS during the application of a monotonic shear stress. During select undrained cyclic tests performed in this study, the applied cyclic loading exceeded the specimen's monotonic triggering resistance and therefore the intended CSR was not achieved prior to accumulating 3% SASS (i.e., achieving triggering). Rather than considering data from these tests as achieving triggering at cycle numbers less than 0.25 cycles at the targeted CSR, instead the actual applied loading (i.e., CSR) which resulted in triggering (3% SASS) was

determined from these tests and was described as the CSR required to achieve monotonic triggering or triggering within 0.25 loading cycles ($CSR_{3\%\ SASS\ in\ 0.25\ cycles}$). Similar to undrained cyclic tests, undrained monotonic tests also achieved 3% SASS after applying some peak shear stress. Therefore, the peak shear stress applied from 0 to 3% SASS during undrained monotonic tests was normalized by the initial vertical effective stress (100 kPa) to determine an equivalent CSR that would have achieved monotonic triggering ($CSR_{3\%\ SASS\ in\ 0.25\ cycles}$). Collectively, a combination of both undrained monotonic and undrained cyclic test data was used to determine the CSRs required to trigger liquefaction (3% SASS) within 0.25 loading cycles ($CSR_{3\%\ SASS\ in\ 0.25\ cycles}$) for loose specimens of differing cementation levels and uncemented specimens with different dry densities. **Figure 10.4** presents these relationships and $CSR_{3\%\ SASS\ in\ 0.25\ cycles}$ values from these trends were subsequently used to develop liquefaction triggering resistance curves, as described later. **Figure 10.4a** presents $CSR_{3\%\ SASS\ in\ 0.25\ cycles}$ values obtained from both undrained cyclic and monotonic tests on loose uncemented and biocemented specimens versus ΔV_s increases from cementation. As shown, 0.25 cycle triggering resistances consistently increased with added cementation for all test specimens, with dramatic increases from values near a CSR of ≈ 0.15 for the uncemented condition to values near a CSR of ≈ 3.7 as cementation levels approached a ΔV_s near 500 m/s. Since only discrete CSR values were considered for undrained cyclic tests and the development of liquefaction triggering resistance curves, the presented trendline was used to interpret the required cementation level (ΔV_s increase) needed to achieve triggering (3% SASS) in 0.25 cycles for all discrete CSR magnitudes considered (i.e., CSR = 0.1, 0.15, etc.). For uncemented tests, a similar approach was used to determine the CSRs required to achieve monotonic triggering ($CSR_{3\%\ SASS\ in\ 0.25\ cycles}$) for specimens of differing initial densities. **Figure 10.4b** presents $CSR_{3\%\ SASS\ in\ 0.25\ cycles}$ values obtained from both undrained cyclic and monotonic

tests on uncemented specimens of varying initial densities versus specimen dry density. As expected, increases in dry densities resulted in more dilative volumetric responses during undrained shearing therefore increasing 0.25 cycle triggering resistances, albeit to much smaller degree than increases in cementation level. The developed trendline shown in **Figure 10.4b** was used to interpret the required CSR magnitudes needed to achieve triggering (3% SASS) after 0.25 cycles for the different dry density levels (loose, medium dense, dense) considered in these tests. Since the targeted CSR was never actually achieved for the undrained cyclic tests shown in **Figure 10.4**, all further results obtained from these tests were excluded in subsequent plots but were summarized in supplemental tables. **Supplemental Table 10.1** summarizes results from uncemented undrained cyclic tests, including specimen initial properties (e.g., targeted packing [loose, medium dense, dense], initial D_r, initial dry density, initial V_s, and monotonic triggering resistance [$CSR_{3\%\ SASS\ in\ 0.25\ cycles}$]), the applied loading ($CSR = \tau/\sigma'_{v\ initial}$), pre-triggering behaviors (e.g., cycles to excess pore-water pressure ratios ($r_u = \Delta u/\sigma'_{v\ initial}$) of 0.95, and cycles to 3% SASS), and post-triggering behaviors (e.g., cycles to 5% SASS, 9% SASS, and 24% DASS, vertical reconsolidation strains, and ΔV_s changes after shearing and reconsolidation events). **Supplemental Table 10.2** summarizes results from biocemented undrained cyclic tests including specimen initial properties (e.g., targeted initial density type [loose, medium, dense], initial D_r, and initial V_s), post cementation specimen properties (e.g., ΔV_s from cementation, $CaCO_3$ content by mass, COV for $CaCO_3$ content measurements, and dry densities prior to shearing [including cementation contributions], and monotonic triggering resistance [$CSR_{3\%\ SASS\ in\ 0.25\ cycles}$]), the applied cyclic loading (CSR), pre-triggering behaviors (e.g., cycles to r_u of 0.95, and cycles to 3% SASS), and post-triggering behaviors (e.g., cycles to 5% SASS, 9% SASS, and 24% DASS, vertical reconsolidation strains, and ΔV_s changes after shearing and reconsolidation events).

10.3.5 *Effect of Biocementation on Undrained Cyclic Behaviors*

Undrained cyclic tests were performed on loose biocemented specimens as well as uncemented specimens prepared to different initial densities to examine changes in liquefaction behaviors as a function of both densification and cementation level. **Table 10.3** summarizes results from all uncemented undrained cyclic tests including specimen initial properties (e.g., targeted initial density type [loose, medium dense, dense], initial D_r, initial dry density, initial V_s, and monotonic triggering resistance [$CSR_{3\%\ SASS\ in\ 0.25\ cycles}$]), the applied loading ($CSR = \tau/\sigma'_{v\ initial}$), pre-triggering behaviors (e.g., cycles to excess pore-water pressure ratios ($r_u = \Delta u/\sigma'_{v\ initial}$) of 0.95, and cycles to 3% SASS), and post-triggering behaviors (e.g., cycles to 5% SASS, 9% SASS, and 24% DASS, compliance rate, vertical reconsolidation strains, and ΔV_s changes after shearing and reconsolidation events). As shown, undrained cyclic tests on uncemented loose, medium dense, and dense specimens were only able to achieve the targeted cyclic shear stress prior to triggering (3% SASS) up to maximum CSR values near 0.15, 0.2, and 0.3, respectively, above which specimens experienced triggering before achieving the targeted CSR (**Figure 10.4b, Supplemental Table 10.2**). Uncemented specimens used for undrained cyclic tests had initial properties similar to monotonic tests with loose, medium dense, and dense specimens achieving average D_r values of 30.2% (standard deviation [σ] = 3.1%), 55.8% (σ = 6.5%), and 74.9% (σ = 3.4%), respectively. Uncemented loose, medium dense, and dense specimens also had average initial V_s values of 143 m/s (σ = 7 m/s), 157 m/s (σ = 10 m/s), and 166 m/s (σ = 4 m/s), respectively.

Table 10.4 summarizes results from all biocemented undrained cyclic tests including specimen initial properties (e.g., targeted initial density type [loose, medium, dense], initial D_r, and initial V_s), post cementation specimen properties (e.g., ΔV_s from cementation, $CaCO_3$ content by mass, COV for $CaCO_3$ content measurements, total relative densities prior to shearing [including added cementation masses], and dry densities prior to shearing [including added cementation masses]), the applied cyclic loading (CSR), pre-triggering behaviors (e.g., cycles to r_u of 0.95, and cycles to 3% SASS), and post-triggering behaviors (e.g., cycles to 5% SASS, 9% SASS, and 24% DASS, compliance rate, vertical reconsolidation strains, and ΔV_s changes after shearing and reconsolidation events). All biocemented specimens were prepared initially loose and had average initial D_r and V_s values of 33.7% (σ = 4.4%) and 147 m/s (σ = 8 m/s), respectively, similar to other uncemented loose tests. Following treatment, cemented specimens achieved $CaCO_3$ contents up to 5.2% by mass, dry density increases up to 87 kg/m^3, and ΔV_s increases up to 523 m/s.

Table 10.3. Summary of Specimen Initial Properties, Applied Loadings, and Pre-triggering and Post-triggering Behaviors for Undrained Cyclic Tests Performed on Uncemented Specimens at Varying Initial Densities

Specimen Initial Properties[1]					*Loading*	*Pre-triggering Results*		*Post-triggering Results*					
Packing[2]	D_r initial (%)	ρ_d (kg/m^3)	V_s initial (m/s)[3]	CSR $_{3\%\ SASS\ in\ 0.25\ cycles}$	CSR	Cycles to $r_u = 0.95$	Cycles to 3% SASS	Cycles to 5% SASS	Cycles to 9% SASS[4]	Cycles to 24% DASS[4]	Compliance rate (%/kPa)[4]	Reconsolidation Strain (%)[5]	ΔV_s after shearing and reconsolidation (m/s)[3]
L	27.1	1553	152	0.15	0.1	17.01	16.77	17.13	17.66	19.16	0.377	1.56	1
L	28.1	1555	150	0.15	0.1	23.51	23.19	23.62	24.22	25.61	0.372	2.36	14
L	30.8	1562	153	0.16	0.1	20.51	20.59	20.67	21.66	23.17	0.349	2.42	12
M	55.1	1625	155	0.29	0.1	20.02	20.59	21.60	24.65	29.28	0.104	1.73	-13
M	61.3	1641	160	0.34	0.1	19.04	19.60	20.66	25.73	38.73	0.047	1.63	-15
D	73.4	1675	167	0.46	0.1	33.01	35.72	41.71	62.21	115.73	0.011	1.69	-3
D	73.9	1677	173	0.47	0.1	58.02	63.18	71.20	107.22	N/A	N/A	1.82	-26
L	28.4	1556	137	0.15	0.15	0.99	0.77	0.80	0.80	1.14	1.622	2.06	3
L	29.9	1560	139	0.16	0.15	1.02	0.65	0.66	1.22	2.21	0.385	2.12	-3
L	33.5	1569	-	0.17	0.15	0.99	0.75	0.76	0.78	1.60	0.706	2.40	-
M	56.1	1627	143	0.30	0.15	3.01	2.69	3.64	6.66	N/A	N/A	1.63	-5
M	58.4	1634	157	0.32	0.15	3.51	3.66	5.62	10.74	18.27	0.041	1.68	-11
M	59.7	1637	160	0.33	0.15	0.84	2.71	3.67	6.71	11.15	0.071	1.58	-13
D	75.4	1681	163	0.48	0.15	5.03	7.68	22.23	80.20	174.25	0.004	1.31	-12
D	71.6	1670	165	0.44	0.15	2.03	5.66	9.70	25.79	42.23	0.016	1.37	-14
D	79.4	1693	-	0.53	0.15	6.52	10.21	35.24	N/A	N/A	N/A	0.24	-
M	48.0	1606	-	0.24	0.2	1.01	0.65	0.69	1.62	3.12	0.182	2.07	-
M	64.1	1649	171	0.37	0.2	1.27	2.61	4.66	16.69	33.74	0.014	1.17	-31
M	65.4	1653	171	0.38	0.2	1.28	2.60	4.66	14.72	27.22	0.018	1.11	-26
D	70.0	1666	-	0.42	0.2	2.02	2.65	6.21	29.24	100.25	0.005	1.60	-
D	77.1	1686	167	0.50	0.2	2.01	3.14	6.21	18.20	49.24	0.010	1.59	-5
M	63.8	1648	162	0.36	0.25	1.01	0.56	1.58	3.67	7.68	0.051	1.42	-18
D	78.2	1689	171	0.52	0.25	1.02	1.69	6.22	43.25	N/A	N/A	1.39	-33
D	78.8	1691	167	0.52	0.25	1.02	1.61	3.74	46.25	123.68	0.003	1.23	-25
D	69.8	1665	164	0.42	0.3	1.02	0.72	3.20	18.24	34.73	0.009	1.23	-15
D	76.5	1684	160	0.50	0.3	1.52	1.71	5.70	32.22	61.74	0.005	1.59	-11

[1] All specimens were initially consolidated to σ'_v = 100 kPa

[2] L= loose, M= medium-dense, D= dense

[3] V_s values are reported when bender element measurements were performed

[4] "N/A" denotes when 9% SASS or 24% DASS or compliance rate was not achieved (dense samples)

[5] All specimens were re-consolidated back to σ'_v = 100 kPa

Table 10.4. Summary of Specimen Initial and Post-treatment Properties, Applied Loadings, and Pre-triggering and Post-triggering Behaviors for Undrained Cyclic Tests Performed on Biocemented Loose Specimens

Specimen Initial Properties[1]			*Post-cementation Specimen Properties*						*Loading*	*Pre-triggering Results*	*Post-triggering Results*						
Packing[2]	D_r initial (%)	V_s initial (m/s)	ΔV_s from cementation (m/s)	$CaCO_3$ by mass (%)	COV of $CaCO_3$ (%)	Total D_r (%)[3]	ρ_d (kg/m^3)	$\Delta\rho_d$ (kg/m^3)	CSR	Cycles to r_u = 0.95[4]	Cycles to 3% SASS	Cycles to 5% SASS	Cycles to 9% SASS	Cycles to 24% DASS	Compliance rate (%/kPa)	Reconsolidation Strain (%)[5]	ΔV_s after shearing and reconsolidation (m/s)
L	34.0	158	6	0.17	17	35.0	1572	3	0.1	36.49	36.62	36.73	37.63	38.59	0.457	2.99	-6
L	37.1	167	14	0.13	13	37.9	1579	2	0.1	85.02	85.57	85.65	86.66	87.65	0.433	2.25	-22
L	31.0	150	14	0.13	13	31.8	1564	2	0.1	93.50	93.27	93.59	94.12	94.60	0.677	2.91	6
L	34.9	140	3	0.14	28	35.8	1574	2	0.15	1.49	1.21	1.22	1.23	1.56	1.714	2.75	0
L	31.2	142	10	0.20	15	32.4	1566	3	0.15	7.00	6.66	6.72	7.58	8.07	0.426	2.44	1
L	29.2	148	15	0.03	52	29.4	1558	0	0.15	3.01	3.06	3.08	3.18	3.72	0.909	2.32	-6
L	31.4	144	20	0.19	13	32.6	1566	3	0.15	24.00	23.66	23.73	24.14	24.61	0.632	2.77	-11
L	28.9	154	48	0.37	1	31.2	1563	6	0.15	10.97	73.17	73.60	74.14	74.60	0.420	2.05	-44
L	34.3	141	50	0.44	4	37.0	1577	7	0.15	44.54	44.62	44.73	45.59	46.08	0.411	3.04	-52
L	26.2	140	51	0.34	7	28.4	1556	5	0.15	26.02	25.76	26.13	26.58	27.06	0.462	2.74	-37
L	31.8	159	16	0.14	10	32.7	1566	2	0.2	1.01	0.68	0.68	1.11	1.56	0.511	2.25	-18
L	29.8	146	36	0.43	10	32.5	1566	7	0.2	8.02	7.21	7.66	8.65	9.61	0.188	2.03	-38
L	28.6	158	54	0.41	7	31.1	1563	6	0.2	11.51	11.17	11.64	12.60	13.19	0.223	2.11	-57
L	31.2	157	77	0.51	9	34.4	1571	8	0.2	47.01	47.14	47.62	48.17	49.08	0.232	2.57	-77
L	30.6	146	36	0.30	13	32.5	1566	5	0.25	2.01	1.64	1.68	2.15	2.58	0.383	2.37	-29
L	29.1	143	70	0.38	16	31.5	1563	6	0.25	3.01	2.71	2.71	3.12	3.55	0.429	2.32	-73
L	28.4	142	100	0.66	3	32.6	1566	10	0.25	47.52	47.59	47.70	48.61	49.15	0.231	2.28	-92
L	27.9	139	64	0.45	11	30.7	1561	7	0.3	3.01	2.64	2.68	3.13	3.56	0.326	2.41	-47
L	35.5	142	93	0.69	4	39.8	1584	11	0.3	4.03	3.72	4.21	4.65	5.55	0.164	2.26	-94
L	35.6	139	144	1.25	12	43.4	1594	20	0.3	10.49	50.52	51.56	53.53	54.69	0.072	1.52	-153
L	35.2	143	103	0.54	8	38.6	1594	9	0.5	0.04	0.14	0.22	0.62	1.02	0.205	1.72	-76
L	31.8	141	152	0.68	6	36.0	1575	11	0.5	1.01	2.13	2.54	2.69	3.56	0.126	1.86	-145
L	42.0	148	192	1.42	6	50.8	1613	23	0.5	6.98	28.15	29.61	31.67	34.00	0.031	1.83	-158
L	32.7	162	156	0.92	6	38.5	1581	15	0.75	0.99	0.66	1.10	1.62	2.12	0.082	1.82	-166
L	33.7	142	194	1.15	2	40.9	1587	18	0.75	1.50	2.20	2.66	3.61	4.12	0.063	1.94	-204
L	35.4	144	194	2.17	3	48.9	1608	35	0.75	6.50	11.63	13.65	16.23	18.13	0.018	1.38	-169
L	38.2	146	206	1.60	4	48.2	1606	26	0.75	4.52	8.78	10.65	12.68	14.17	0.022	1.41	-173
L	37.1	150	211	2.02	1	49.7	1610	33	0.75	8.99	19.27	21.13	23.18	24.65	0.022	1.24	-205
L	34.3	156	247	2.05	2	47.1	1603	33	0.75	6.51	29.19	33.24	38.18	40.18	0.011	1.66	-244
L	34.4	144	250	1.51	5	43.8	1595	24	1	3.00	2.16	3.10	4.15	5.12	0.030	1.64	-219
L	34.6	145	416	2.88	2	52.6	1618	47	1	9.00	16.12	19.02	22.17	27.11	0.008	1.12	-397
L	34.8	150	235	1.23	6	42.5	1591	20	1.25	0.51	0.75	0.76	0.81	1.61	0.084	0.90	-239
L	37.6	143	466	4.20	3	63.7	1648	69	1.25	7.99	10.21	12.11	18.52	24.52	0.005	0.23	-434
L	38.5	154	287	1.81	3	49.8	1610	29	1.5	1.50	1.14	1.67	2.64	3.16	0.030	1.54	-295
L	46.9	149	476	3.67	3	69.4	1664	61	1.5	9.99	9.64	11.72	15.68	19.66	0.006	0.21	-252
L	41.5	165	523	4.76	0	70.9	1668	79	1.5	N/A	16.21	23.71	36.21	43.21	0.002	-0.43	-414
L	33.4	144	354	2.98	5	52.0	1616	48	1.75	2.00	3.13	4.22	7.17	7.77	0.011	0.03	-296
L	38.3	148	501	5.23	4	70.7	1668	87	1.75	8.52	8.71	12.23	16.17	17.80	0.006	0.36	-260

[1]All specimens were initially consolidated to σ'_v = 100 kPa

[2]L= loose, M= medium-dense, D= dense

[3]This calculation accounts for added masses from cementation and assumes that e_{min} and e_{max} do not chage

[4]"N/A" denotes when r_u of 0.95 was not achieved

[5]All specimens were re-consolidated back to σ'_v = 100 kPa

During undrained cyclic testing of biocemented specimens, changes in pre-triggering and post-triggering behaviors were observed as a function of both cementation level and applied loading magnitudes. **Figure 10.5** presents representative undrained cyclic responses for biocemented loose specimens of varying biocementation levels (ΔV_s = 0, 48, 194, 247, 287, and 476 m/s) that were subjected to applied CSRs of either 0.15, 0.75, or 1.5. In this figure, rows (a) through (f) present responses for specimens treated to different biocementation levels with specimens from rows (a) and (b) being subjected to a CSR of 0.15, specimens from rows (c) and (d) being subjected to a CSR of 0.75, and specimens from rows (e) and (f) being subjected to a CSR of 1.5. Conversely, columns (i) through (iv) in **Figure 10.5** present responses for these tests including (i) shear stress versus vertical effective stress, (ii) shear stress versus shear strain, (iii) applied shear stress versus cycle number, and (iv) excess pore pressure ratio (r_u) versus cycle number. Due to large differences in resistances as a function of cementation level, specimens cemented to ΔV_s values from 0 to 500 m/s could not be tested at the same cyclic loading magnitudes (i.e., CSRs). Therefore, differences in behaviors with changes in biocementation level are shown by comparing two specimens subjected to the same cyclic loading magnitude (i.e., CSR), but which had different cementation levels (e.g., comparison of row (a) to row (b), etc.). As expected, with increases in cementation level for the same applied loading, the number of cycles required to trigger liquefaction (SASS = 3% or r_u = 0.95) increased dramatically. For example, for a CSR of 0.15, the uncemented specimen triggered near 0.7 cycles, while a specimen cemented to achieve a small ΔV_s of only 48 m/s required 73 cycles to trigger, with delayed positive excess pore pressure generation early on during cyclic loading and noticeable improvements in post-triggering resistances when compared to the uncemented condition (**Figure 10.5a and 10.5b**). As cementation levels were further increased to between 200 and 250 m/s, a higher applied CSR of 0.75 was required to trigger liquefaction within 100 loading cycles and further changes in elemental behaviors were observed. The specimen with

a ΔV_s of 194 m/s required 0.7 cycles to trigger liquefaction, while the ΔV_s of 247 m/s specimen required 29 cycles (**Figure 10.5c and 10.5d**). Large negative excess pore pressures were generated in both specimens ($r_u \approx -0.5$) upon initiating cyclic loading, reflective of strongly dilative volumetric tendencies, in stark contrast to the positive excess pore pressures observed immediately upon shearing at lower cementation levels and applied loadings. Observed failure envelopes also appeared to shift during the undrained cyclic loading sequence, likely indicative of progressive damage to cemented bonds. Post-triggering behaviors were also improved with added cementation. At the highest CSR shown (CSR = 1.5), specimens cemented to a ΔV_s of 287 m/s and 476 m/s required near 1 and 10 cycles to trigger liquefaction, respectively, with strong negative excess pore pressures again generated initially during shearing with r_u values between -1.5 and -2 observed initially during shearing (**Figure 10.5e and 10.5f**). Again, some abrupt shifts in failure envelopes were observed with progressive loading and post-triggering resistances were again improved with added cementation, reflective of the more dilative tendencies afforded by increases in specimen dry densities from added $CaCO_3$ solids and potential changes in inter-particle frictional resistances due to the coating of particles with cementation. Lastly for all tests, large biases in the direction of post-triggering shear strain accumulation were not observed immediately following triggering, suggesting that specimens achieved relatively homogenous cemented conditions prior to shearing, with only minimal biases observed for higher cementation levels at larger strains likely reflective of progressive damage and localization of shear strains within specimens.

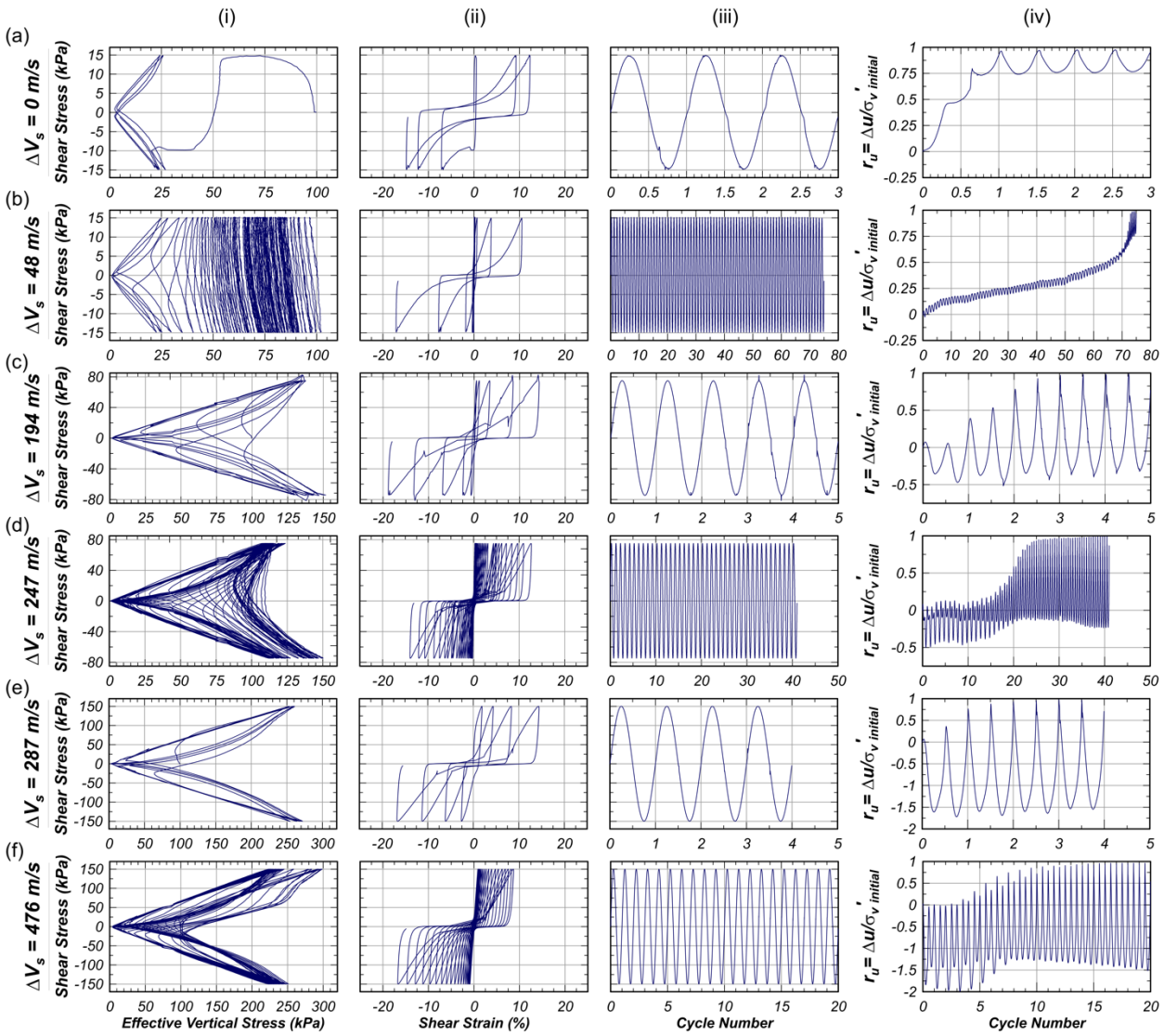

Figure 10.5. Results from undrained cyclic DSS tests performed on loose ($D_{r\ initial} \approx 30\%$) Ottawa F-65 specimens of varying cementation levels (assessed by ΔV_s) subjected to a CSR of **(a, b)** 0.15, **(c, d)** 0.75, and **(e, f)** 1.5. Plots show **(i)** shear stress versus vertical effective stress, **(ii)** shear stress versus shear strain, **(iii)** shear stress versus cycle number, and **(iv)** r_u ($= \Delta u/\sigma'_{vo}$) versus cycle number.

10.3.6 *Effect of Biocementation on Pre-triggering Behaviors*

Differences in excess pore pressure generation were investigated for different cementation levels as a function of developed shear strains. **Figure 10.6** shows relationships between the maximum r_u values that a specimen experienced prior to achieving a given shear strain magnitude for biocemented loose specimens with ΔV_s values from 194 to 294 m/s subjected to a CSR of 0.75 (**Figure 10.6a, b**) and ΔV_s values from 287 to 523 m/s subjected to a CSR of 1.5 (**Figure 10.6c, d**). As shown, specimens treated to higher biocementation levels were able to tolerate higher r_u values prior to developing significant increases in shear strains. For example, when considering the biocemented specimens subjected to a CSR of 0.75, shear strains increased rapidly in the specimen cemented to a ΔV_s of 194 m/s after r_u values exceeded ≈ 0.1, however, a specimen cemented to a ΔV_s of 294 m/s did not start rapidly accumulating shear strains until r_u values exceeded ≈0.9. Similar behaviors were observed at the higher CSR value of 1.5, with again shear strains rapidly increasing in a specimen cemented to a ΔV_s of 287 m/s after r_u values exceeded ≈ 0.1 with the specimen cemented to a higher ΔV_s of 523 m/s rapidly accumulating shear strains only after r_u values exceeded ≈ 0.8. These results were consistent with observations made at lower cementation levels (Lee et al. 2022) and suggested that more highly biocemented specimens may experience more minimal deformations at higher r_u values prior to triggering, due to the presence of stiff cemented bonds which provide a stress-independent tensile strength. With increasing cementation level or ΔV_s, the tensile strength afforded by these cemented bonds becomes larger and therefore further reductions in effective stresses (increases in r_u values) are needed prior to onset of significant shear deformations. However, once the vertical effective stress is reduced to some critical value (some threshold r_u value), these cemented bonds may provide insufficient strength towards preventing shear strain development, resulting in bond failure, rapid shear strain

accumulation, and further mobilization of contractive volumetric tendencies as indicated by further increases in r_u.

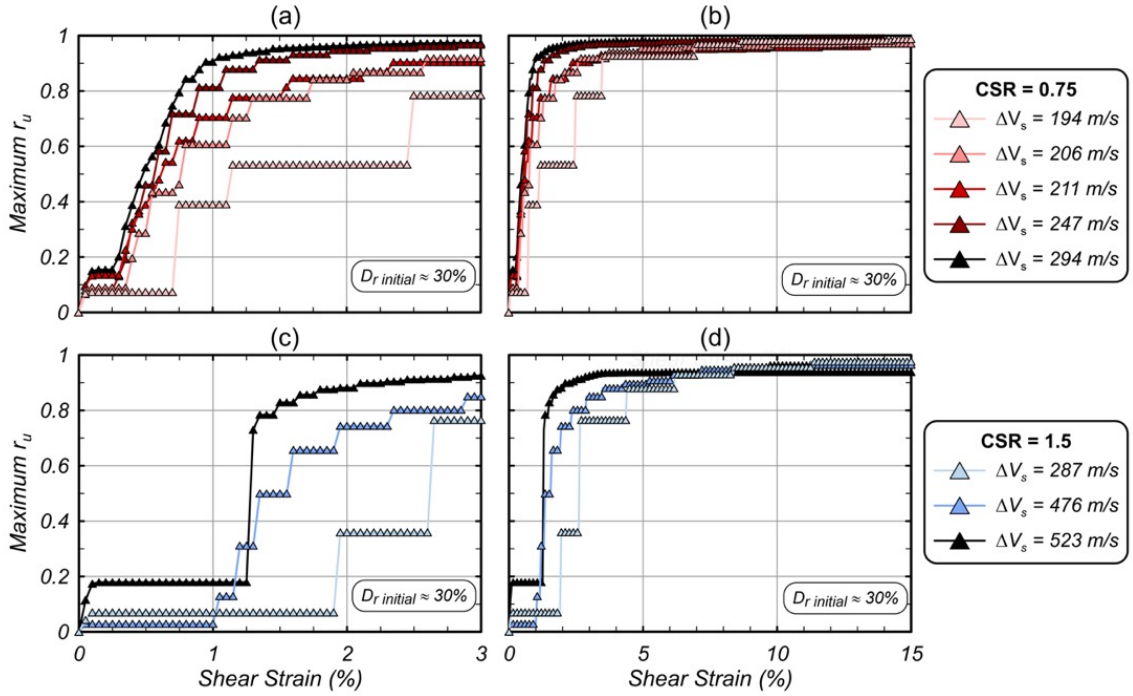

Figure 10.6. Changes in maximum excess pore pressure ratios ($r_u = \Delta u/\sigma'_{vo}$) with shear strain for loose specimens of varying cementation levels subjected to CSRs of **(a, b)** 0.75 and **(c, d)** 1.5. The maximum excess pore pressure ratio (r_u) indicates the largest r_u value that a specimen has experienced prior to achieving different shear strain magnitudes. Plots present similar data for shear strains from **(a, c)** 0 to 3% and **(b, d)** 0 to 15%. Data points were evaluated at discrete shear strain increments of 0.05%.

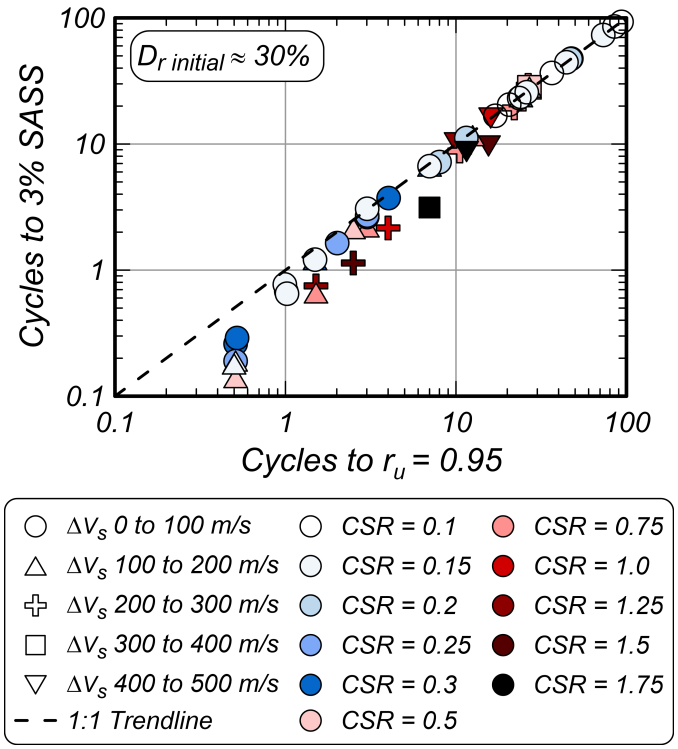

Figure 10.7. Comparison of liquefaction triggering criteria including number of cycles to 3% SASS versus number of cycles to r_u = 0.95 for tests involving loose specimens at varying biocementation levels (as indicated by ΔV_s) subjected to different applied CSRs. Points plotting near the 1:1 trendline provided are reflective of perfect agreement between criteria.

In order to examine changes in soil liquefaction resistances as a function of varying biocementation levels, dry densities, and applied cyclic loading magnitudes, two different liquefaction triggering criteria were considered including (i) the number of loading cycles required to achieve a SASS of 3% (Ishihara 1993), and (ii) the number of loading cycles required to achieve a r_u of 0.95 (Ishihara 1993; Wu et al. 2004). The r_u = 0.95 excess pore pressure generation-based criterion was used instead of r_u = 1.0 to account for potential variations in laboratory measurements, as recommended by Wu et al. (2004). All test data was analyzed in accordance with both criteria and relationships between the number of loading cycles required to achieve a SASS of 3% and a r_u value of 0.95 were compared for all biocemented loose specimens subjected to different applied loading

magnitudes (**Figure 10.7**). As shown, both liquefaction triggering criteria were consistent with data from almost all specimens plotting near the 1:1 trendline. Results between criteria diverged only slightly when specimens were subjected to high CSR values relative to the level of cementation and triggering occurred within less than one cycle. Since no significant differences were observed between criteria as a function of cementation level or loading magnitudes and given that all tests were completed under equivalent-undrained conditions with no direct pore pressure measurements, the number of loading cycles to 3% SASS was used for all subsequent analyses to evaluate changes in liquefaction triggering resistances.

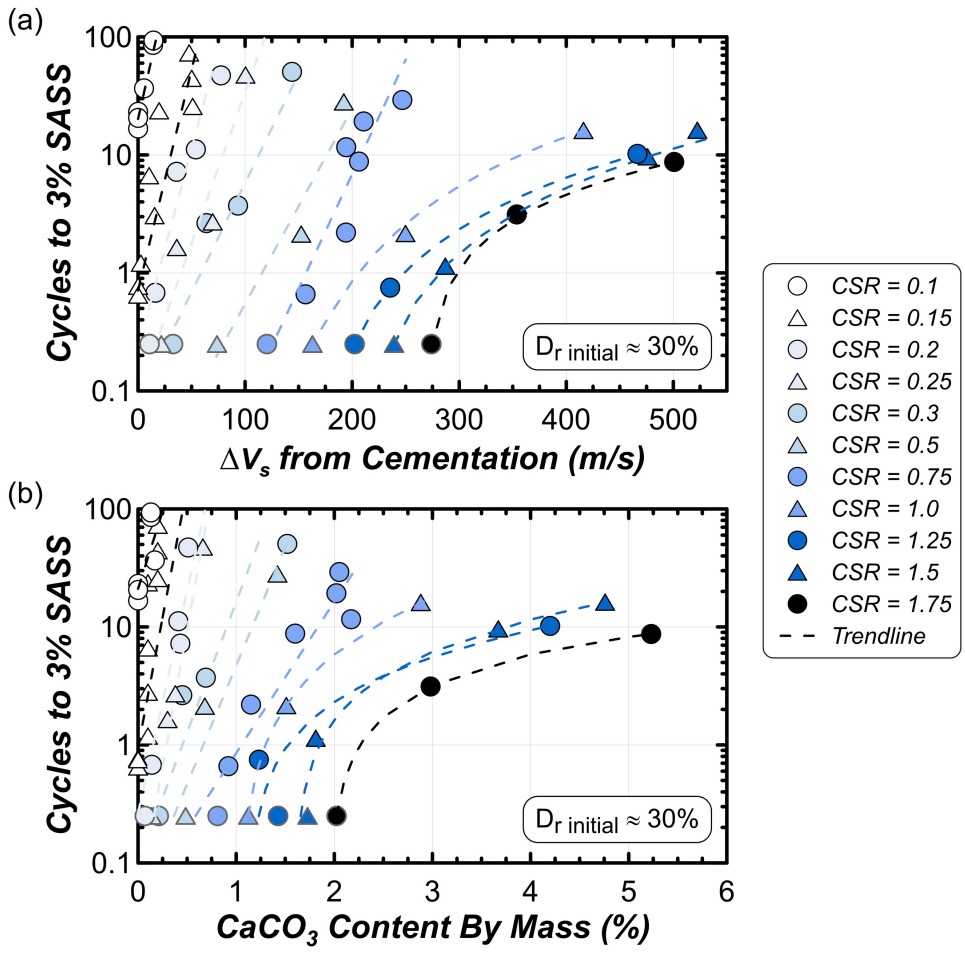

Figure 10.8. Number of cycles to 3% SASS versus **(a)** ΔV_s from biocementation and **(b)** $CaCO_3$ contents for loose ($D_{r\ initial} \approx 30\%$) specimens of varying biocementation levels.

Figure 10.8 presents relationships between the number of cycles to liquefaction triggering (SASS = 3%) and ΔV_s increases from cementation (**Figure 10.8a**) and soil $CaCO_3$ contents (**Figure 10.8b**) for all loose uncemented and biocemented specimens subjected to varying applied CSRs. The performed tests examined liquefaction triggering behaviors for cycles to triggering from 0.25 to 100 cycles, with the upper bound of 100 cycles considered due to the limited relevance of higher cycle numbers to earthquake-induced liquefaction mitigation applications. Conversely, the lower bound value of 0.25 cycles corresponded to failure during monotonic loading, as described previously. Since it was not possible to prepare specimens to the exact cementation level which

corresponded to 0.25 cycle triggering resistances for all of the CSR values considered, earlier relationships between $CSR_{3\%\ SASS\ in\ 0.25\ cycles}$ and ΔV_s increases **(Figure 10.4)** were instead used to determine the ΔV_s values corresponding to triggering in 0.25 cycles for all CSRs considered and are shown in **Figure 10.8a**. These ΔV_s values were also related to expected $CaCO_3$ contents using the earlier ΔV_s and $CaCO_3$ content relationship (**Figure 10.1)** and were used to plot values shown in **Figure 10.8b**. $CSR_{3\%\ SASS\ in\ 0.25\ cycles}$ values interpreted from **Figure 10.4** are outlined in gray in **Figure 10.8** to differentiate them from the other test data, which was determined from individual tests. As shown in **Figure 10.8**, for the same applied CSR magnitude, increases in biocementation, as indicated by either ΔV_s or $CaCO_3$ content increases, resulted in large increases in the number of cycles required to trigger liquefaction. Similar to relationships observed by Lee et al. (2022) for lower cementation levels (ΔV_s < 100 m/s), log-linear increases in the number of cycles to trigger liquefaction were observed with increases in ΔV_s, although only when applied CSRs were less than ≈ 0.75. At higher CSR values (CSR ≥ 1.0), trends between different CSR values appeared to converge with relationships between the number of cycles required to trigger liquefaction and ΔV_s values for a given CSR being better approximated by second-order polynomials, suggesting that increases in cementation levels had more minimal impacts on triggering resistances as applied CSRs increased. For example, for a CSR of 0.15, the number of cycles to trigger liquefaction increased by 2 orders of magnitude as ΔV_s values increased from ≈ 0 to 50 m/s, however, when a CSR of 0.75 was applied, liquefaction triggering resistances increased by only 1 order when ΔV_s values increased by a similar magnitude from ≈ 150 to 200 m/s. Furthermore, at a CSR of 1.75, the number of cycles to trigger liquefaction increased by less than half an order of magnitude as ΔV_s values were increased more significantly from ≈ 350 to 500 m/s (≈ 150 m/s increase).

Interestingly, the diminishing effect of added cementation on liquefaction resistances appeared to occur most dramatically once the applied cyclic shear stresses approached and exceeded the initial vertical effective stress (CSR ≥ 1.0). Under these conditions, significant increases in confining pressures were required to apply these large shear stress magnitudes while maintaining constant volume conditions. In the most heavily cemented experiments, the applied vertical stresses during shearing approached nearly three times the initial overburden stress (≈ 300 kPa) (**Figure 10.5f).** It is hypothesized that a combination of both large applied cyclic loading demands, which resulted in more immediate plastic deformations, and the application of higher confining pressures needed to achieve these high CSRs under constant volume conditions may have resulted in greater deterioration of cementation at high cementation levels and applied CSRs, thereby resulting in the convergence of triggering resistance versus ΔV_s relationships at high CSR and ΔV_s values. When examining triggering resistance relationships as a function of $CaCO_3$ content instead of ΔV_s values, greater scatter in relationships was observed, particularly for specimens treated to higher cementation levels. Accordingly, relationships between cycles to 3% SASS and $CaCO_3$ contents were less reliable, with regressed trendlines for higher CSRs intersecting one another and inconsistent with expected trends. Similar to conclusions made by Lee et al. (2022), this outcome suggested that soil $CaCO_3$ contents may be less reliable than ΔV_s values towards predicting the triggering resistances of biocemented sands due to the inability of soil $CaCO_3$ contents to provide information regarding where cementation may exist on soil particle surfaces and contacts. In contrast, V_s provides a more direct indication of the formation of cemented interparticle bonds and their associated effects on soil initial shear stiffnesses. From this context, ΔV_s values may be a preferred metric for the assessment of triggering behaviors for biocemented sands, when compared to other mass-based characterizations of cementation levels.

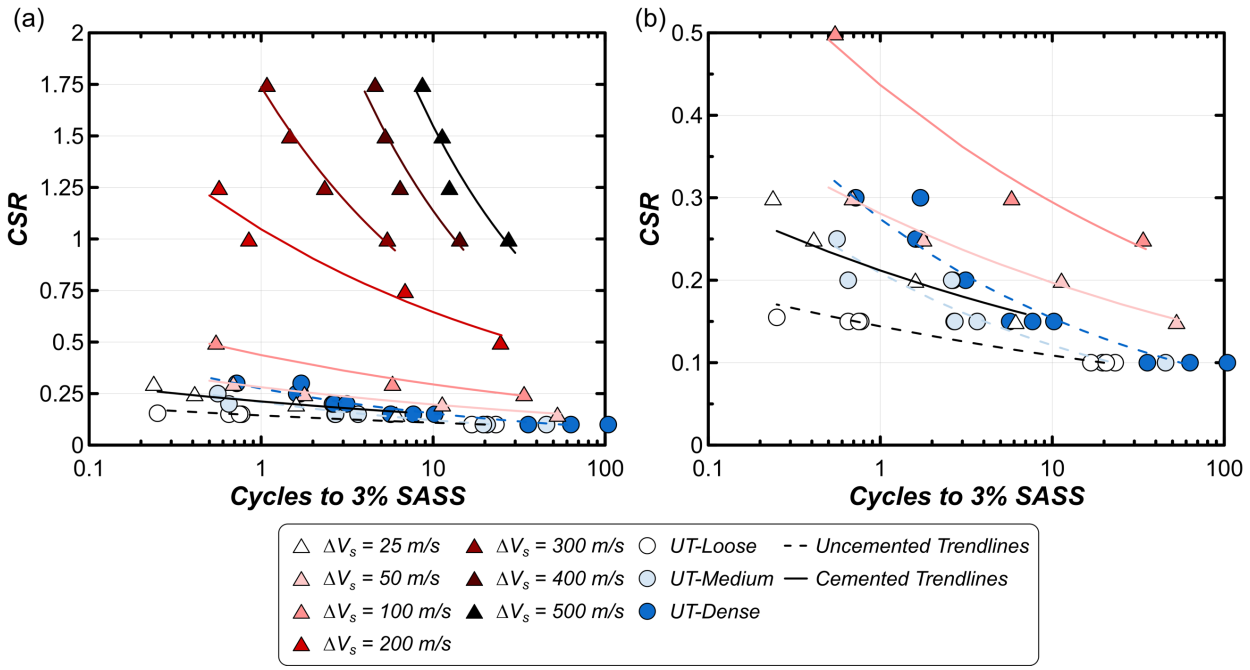

Figure 10.9. Relationships between applied CSRs versus number of cycles to 3% SASS for loose ($D_{r\ initial} \approx 30\%$) biocemented specimens of varying biocementation levels (ΔV_s = 25, 50, 100, 200, 300, 400, 500 m/s) and uncemented specimens prepared to varying initial dry densities.

Figure 10.9 presents liquefaction resistance curves (applied CSRs versus number of cycles to liquefaction triggering [3% SASS]) for loose biocemented specimens of varying cementation levels and uncemented specimens of varying initial densities for two different CSR ranges. Since it was not possible to prepare biocemented specimens at exactly the same ΔV_s values for different applied CSRs, relationships between the number of cycles to 3% SASS and ΔV_s values (**Figure 10.8a**) were used to determine the number of cycles to 3% SASS for specific ΔV_s increments from 0 m/s to 500 m/s, which were then used to determine liquefaction resistance curves. All curves were fitted using a power law function ($CSR = a \cdot N_L^{-b}$) wherein N_L is the number of cycles to liquefaction triggering for a given CSR value, the a-value controls the vertical position of the curve, and the b-value controls the slope of the curve. All fitted parameters are summarized in **Table 10.5**

for uncemented and cemented liquefaction resistance curves. As expected, all curves illustrated large increases in the number of cycles to 3% SASS with increasing ΔV_s values for the same applied CSR. When examining curves with changes in uncemented dry densities, improvements in the number of cycles to 3% SASS were observed with densification but were relatively modest compared to those observed with added cementation with the dense specimens exhibiting resistances comparable to specimens cemented to a ΔV_s of less than 50 m/s. When comparing curve parameters, increases in both a- and b-values were observed with increases in cementation level as well as initial relative densities for uncemented specimens. Large increases in b-values were particularly noteworthy with increasing cementation; increasing from 0.122 for the uncemented loose condition to 0.210 for a ΔV_s of ≈ 200 m/s, and 0.461 for a ΔV_s of ≈ 500 m/s. Past studies have universally agreed that curve a-values consistently increase with greater cementation, however, expected changes in b-values with increasing cementation have been somewhat inconclusive. For example, gradual increases in both a- and b-values with increasing cementation were observed by Riveros and Sadrekarimi (2020a), however, Xiao et al. (2018) and Xiao et al. (2019) observed increasing a-values with cementation, but no significant changes in b-values with increasing cementation. Increases in b-values observed in this study, however, suggest that as cementation levels increase, materials may become less sensitive to changes in applied loading demands. Although b-value increases were consistently observed with increases in cementation, it should also be mentioned that the behavior of more highly cemented specimens was only examined at high CSR values and therefore the observed b-value trends may have differed, had lower CSRs been considered.

Table 10.5. Fitted Parameters for Liquefaction Resistance Curves for Uncemented Specimens at Varying Initial Densities and Biocemented Specimens at Various ΔV_s Increases

Curve Parameters[1]	*Uncemented Specimens*			*ΔV_s (m/s) of Cemented Specimens*						
	UT-L	UT-M	UT-D	25	50	100	200	300	400	500
a	0.144	0.209	0.274	0.212	0.281	0.437	1.047	1.737	3.197	4.474
b	0.122	0.236	0.251	0.147	0.154	0.171	0.210	0.340	0.449	0.461

[1]Liquefaction resistance curve, $CSR = a \cdot N_L^{-b}$, where N_L is number of cycles to liquefaction

10.3.7 *Effect of Biocementation on Post-triggering Behaviors*

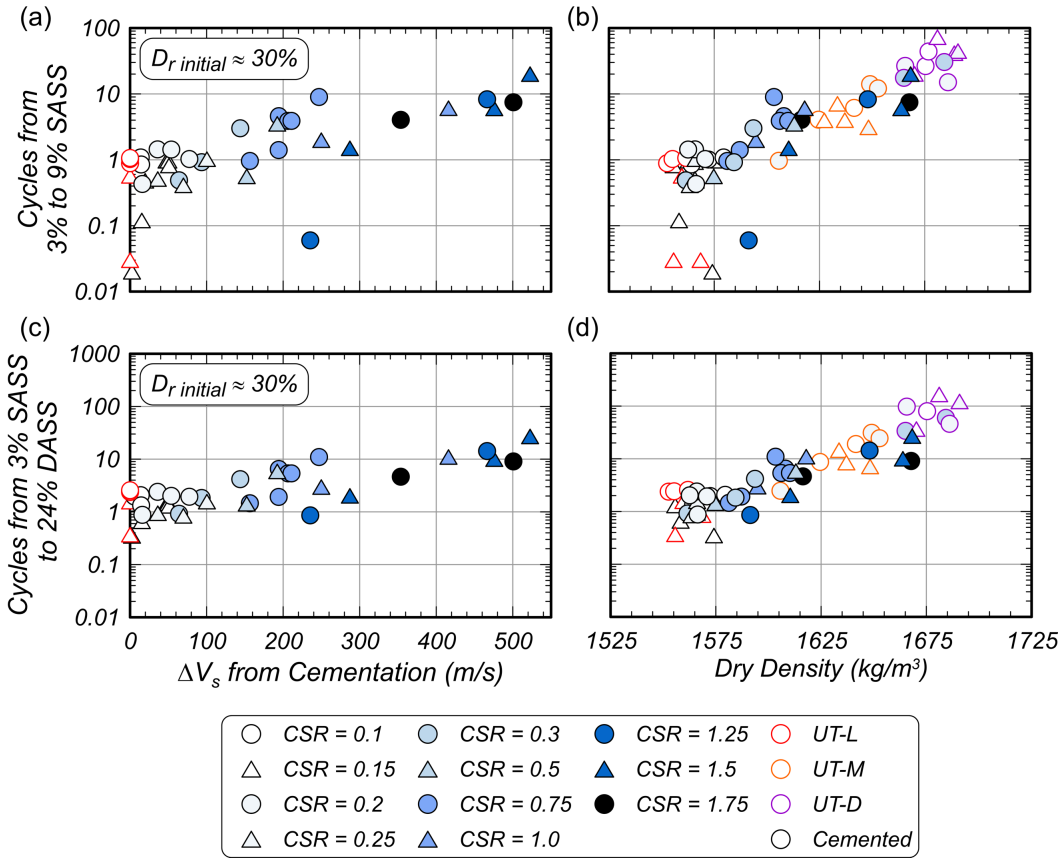

Figure 10.10. Number of cycles from **(a, b)** 3% to 9% SASS and **(c, d)** 3% SASS to 24% DASS versus **(a, c)** ΔV_s from cementation for loose ($D_{r\ initial} \approx 30\%$) specimens of varying biocementation levels and **(c, d)** dry density for all biocemented specimens and uncemented specimens prepared at varying initial dry densities.

In order to explore changes in post-triggering behaviors with differences in cementation magnitudes and specimen dry densities, the number of cycles to different shear strain thresholds following liquefaction triggering (SASS > 3%) were examined. **Figure 10.10** presents the number of cycles from 3% to 9% SASS (**Figure 10.10a, c**) and 3% SASS to 24% DASS (**Figure 10.10b, d**) versus ΔV_s from cementation (**Figure 10.10a, b**) and dry density differences (**Figure 10.10c, d**). As shown in **Figures 10.10a and 10.11c**, more highly cemented specimens achieved significant increases in the number of cycles required to achieve similar magnitudes of post-triggering strain accumulation regardless of the particular strain levels considered. For example, while uncemented specimens required between 0.9 and 2.4 cycles to increase strains from 3% SASS to 24% DASS, more heavily cemented specimens near ΔV_s values of 500 m/s required over 10 cycles to achieve this same post-triggering strain accumulation. This outcome was particularly noteworthy, given the significantly higher shear stresses (CSR > 1.25) applied to the more heavily cemented specimens when compared to uncemented specimens (CSR < 0.2). In order to better assess the effect of cementation-induced densification on post-triggering behaviors, post-triggering strain accumulation was also compared between biocemented and uncemented specimens on the basis of dry density differences (**Figures 10.10b and 10.10d**). As shown, trends between uncemented and cemented specimens were consistent when plotted versus dry density regardless of differences in cementation levels and applied CSRs. The densest specimens had dry densities near 1675 kg/m^3 achieved by either cementing loose specimens to higher cementation levels or preparing uncemented specimens to denser initial packings and exhibited nearly two orders of magnitude improvement in the number of cycles required to accumulate strains from 3% SASS to 24% DASS when compared to uncemented loose specimens (dry densities ≈ 1575 kg/m^3). Although simultaneous increases in applied CSRs and cementation levels obfuscated the ability to observe

differences in post-triggering strain accumulation behaviors as a function of cementation level alone, collectively these trends suggested that improvements in post-triggering behaviors were obtained with increasing biocementation either due to cementation-induced densification of soils from the precipitation process (as best captured by $CaCO_3$ contents or dry densities) and/or the addition of cemented bonds and particle coatings (as best captured by ΔV_s increases).

Although previous trends showed improvements in post-triggering strain accumulation could be achieved with added cementation, simultaneous increases in applied CSRs at higher cementation levels made these behaviors difficult to compare as a function of cementation level alone and the mechanisms responsible for these enhancements remained relatively unknown. In order to compare differences in post-triggering strain accumulation behaviors while accounting for differences in applied cyclic loading magnitudes, the stress-normalized post-triggering strain accumulation framework proposed by Tasiopoulou et al. (2019) was followed wherein a stress-normalized compliance rate was computed ($\Delta\gamma_{postliq\ per\ cycle}/\tau_{cyc}$), which describes the expected increase in post-triggering shear strain per cycle ($\Delta\gamma_{postliq\ per\ cycle}$) normalized by the applied cyclic shear stress (τ_{cyc}) in order to account for differences in post-triggering strain accumulation behaviors independent of the applied cyclic shear stress. Post-triggering shear strain increases per cycle ($\Delta\gamma_{postliq\ per\ cycle}$) were determined for all tests following **Equation (10.1)** by considering the increase in strain after triggering from 3% SASS to 12% SASS and dividing this strain increment by the number of cycles required to achieve this post-triggering shear strain increase ($N_{cyc,3\%\ to\ 12\%\ SASS}$).

$$\Delta\gamma_{postliq\ per\ cycle} = \frac{\gamma_{postliq}}{N_{cyc,postliq}} = \frac{12\%\ SASS - 3\%\ SASS}{N_{cyc,3\%\ to\ 12\%\ SASS}} \qquad \text{Equation (10.1)}$$

Figure 10.11 presents increases in post-triggering strains ($\gamma_{postliq}$) and stress-normalized post-triggering strain accumulation ($\gamma_{postliq}/\tau_{cyc}$) for ten different DSS tests involving specimens prepared to five different cementation levels subjected to differences in applied cyclic shear stresses (i.e., CSRs). As shown in **Figure 10.11a,** when post-triggering strains were compared for similar cementation levels versus number of cycles, post-triggering shear strains accumulated much more rapidly in samples subjected to higher CSRs, as expected. However, when these same post-triggering shear strains were normalized by the applied cyclic shear stresses ($\gamma_{postliq\ per\ cycle}/\tau_{cyc}$), trendlines became similar for all specimens treated to similar cementation levels, suggesting that the approach could successfully remove the effect of applied loading magnitudes on post-triggering shear strain accumulation (**Figure 10.11b**). The slope of the trendlines shown in **Figure 10.11b**, known as the compliance rate ($\Delta\gamma_{postliq\ per\ cycle}/\tau_{cyc}$), were also relatively constant during all tests with increases in cycles and provided a means by which improvements in shear strain accumulation behaviors could be quantified and compared between tests.

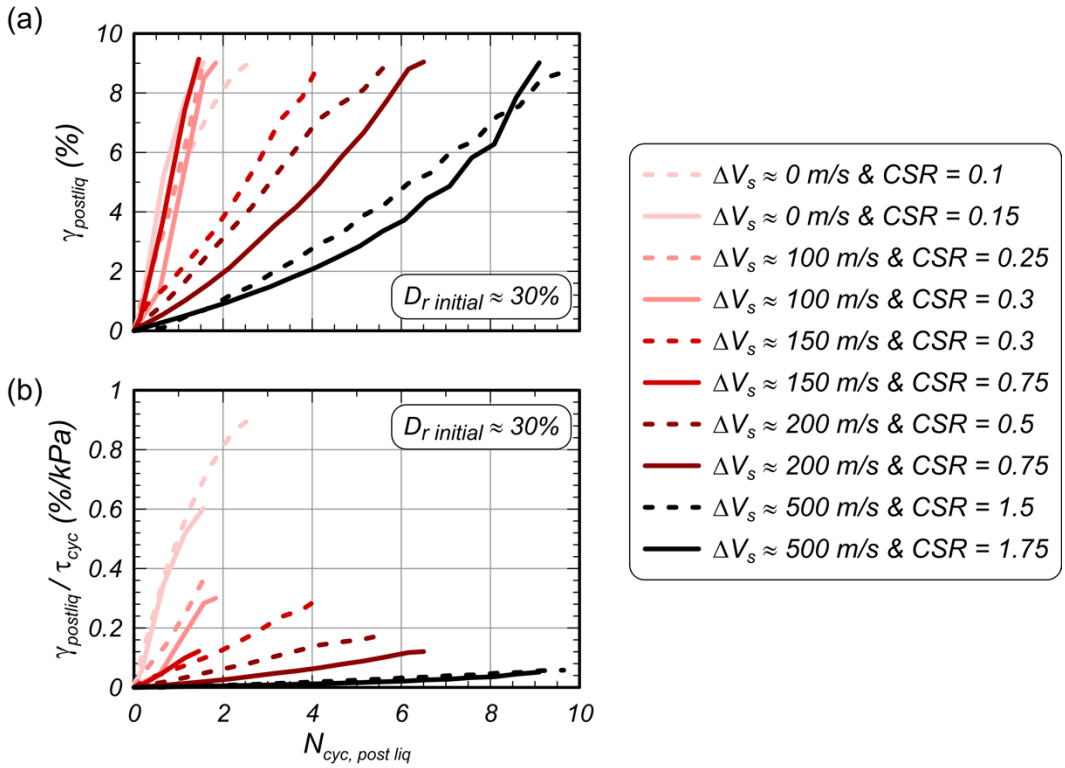

Figure 10.11. (a) Post-triggering shear strain ($\gamma_{postliq}$) and **(b)** stress-normalized post-triggering shear strain ($\gamma_{postliq}/\tau_{cyc}$) accumulation versus number of applied loading cycles ($N_{cyc,\ post\ liq}$) for select undrained cyclic DSS tests prepared to five different cementation levels ($\Delta V_s \approx$ 0, 100, 150, 200, 500 m/s) and subjected to different applied cyclic shear stresses (i.e., CSRs). Data presented follows the framework proposed by Tasiopoulou et al. (2019).

In order to further examine the effect of biocementation on post-triggering shear strain accumulation behaviors, compliance rates ($\Delta\gamma_{postliq\ per\ cycle}/\tau_{cyc}$) were compared as a function of cementation levels (ΔV_s), dry densities, and total relative densities (accounting for added solids from cementation) for uncemented and cemented Ottawa F-65 sand specimens from this study as well as other uncemented clean sand specimens from other studies compiled by Tasiopoulou et al. (2019) including tests on Monterey Sand (Wu 2002), Fraser River Sand (Sriskandakumar 2004), Nevada Sand (Kammerer et al. 2000; Arulmoli et al. 1992; Ziotopoulou and Boulanger 2016), Ottawa F-65 Sand (Ziotopoulou et al. 2018; Parra Bastidas 2016), and Toyoura Sand (Tatsuoka et

al. 1986; Kiyota et al. 2008, 2010; Zhang and Wang 2012; Chiaro et al. 2012; De Silva et al. 2015; Umar et al. 2016). **Figure 10.12** presents compliance rates versus ΔV_s values from cementation for all uncemented and biocemented loose Ottawa F-65 specimens from this study (**Figure 10.12a**), dry densities for all biocemented loose specimens and uncemented Ottawa F-65 specimens prepared to varying initial densities from this study as well as data from other studies considering Ottawa F-65 Sand specimens (**Figure 10.12b**), and total relative densities for all biocemented loose Ottawa F-65 specimens from this study as well as uncemented sand specimens prepared to varying initial densities including Ottawa F-65 Sand as well as other uncemented sands compiled by Tasiopoulou et al. (2019) (**Figure 10.12c**). As shown in **Figure 10.12a**, uncemented loose specimens had compliance rates between 0.35 and 1.62 %/kPa with detectable decreases in compliance rates once ΔV_s values exceeded 50 m/s and large compliance rate reductions with further increases in cementation to values near 0.03 %/kPa at a ΔV_s near 200 m/s and 0.004 %/kPa at a ΔV_s near 500 m/s, reflective of nearly three orders of magnitude of improvement. Although increases in cementation were shown to significantly reduce compliance rates once ΔV_s values exceeded 50 m/s, it was unclear if these post-triggering improvements were the result of cemented bonding or dry density increases afforded by added cementation.

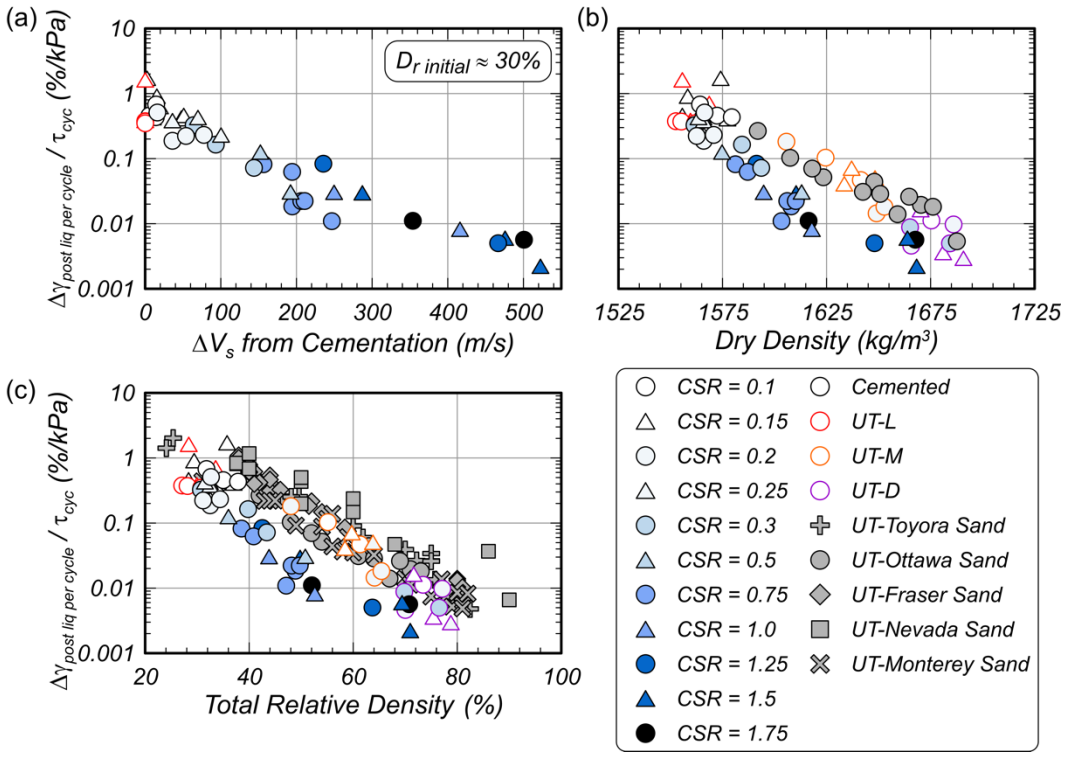

Figure 10.12. Post-triggering compliance rates versus **(a)** ΔV_s from cementation for loose ($D_{r\ initial}$ ≈ 30%) Ottawa F-65 specimens of varying biocementation levels, **(b)** dry densities for all biocemented specimens and uncemented Ottawa F-65 specimens prepared at varying initial dry densities including uncemented Ottawa F-65 sands from other studies, and **(c)** total relative densities for all biocemented specimens and uncemented Ottawa F-65 specimens prepared at varying initial dry densities including various other uncemented sands compiled by Tasiopoulou et al. (2019).

In order to further explore the effect of densification on post-triggering shear strain accumulation, compliance rates were compared on the basis of dry density for both uncemented and biocemented Ottawa F-65 sand specimens including data obtained from other studies (Ziotopoulou et al. 2018, Parra Bastidas 2016) (**Figure 10.12b**). as well as on the basis of differences in total relative densities for biocemented and uncemented Ottawa F-65 sands as well as other clean uncemented sands compiled from other studies by Tasiopoulou et al. (2019) (**Figure 10.12c**). As shown in

Figure 10.12b, decreases in compliance rates were observed with increases in dry density for all Ottawa F-65 sand specimens regardless of cementation level. When comparing data for uncemented Ottawa F-65 sand from this study, compliance rates were consistent with values from other studies and indicated a nearly two orders of magnitude reduction in compliance rates could be obtained as specimen densities increased from the "loose" to "dense" condition. Although cemented and uncemented compliance rates were comparable at similar dry densities at low cementation levels, once dry densities approached values above ≈ 1575 kg/m^3, corresponding to ΔV_s values exceeding 150 m/s, compliance rates for cemented specimens were detectably lower than uncemented specimens for similar dry densities. At higher cementation levels, compliance rates for cemented specimens were between 0.5 and 1 order of magnitude lower than uncemented specimens at similar dry densities, suggesting that although post-triggering improvements afforded by cementation could be largely attributed to dry density increases, the presence of cemented bonds and particle coatings further improved behaviors beyond which could be attributed to densification alone. Compliance rates were further compared on the basis of differences in total relative densities for biocemented and uncemented Ottawa F-65 sands as well as other clean uncemented sands compiled from other studies by Tasiopoulou et al. (2019) (**Figure 10.12c**). Total relative densities were computed by considering added masses from cementation, but assuming minimal changes in e_{min} and e_{max} occurred. Although not strictly correct for more highly cemented materials, the use of total relative densities allowed compliance rates for biocemented specimens from this study to be compared to a broader set of compliance rates for other uncemented sands. As shown, similar compliance rates were observed for all uncemented sands with changes in total relative densities. When comparing compliance rates between uncemented and biocemented sands, however, values were similar until total relative densities exceeded values near 40% ($\Delta V_s \approx 150$ m/s). With further

increases in cementation levels, however, compliance rates were consistently lower for biocemented specimens when compared to uncemented specimens at similar total relative densities. Collectively, these trends suggested that: (i) detectable improvements in post-triggering strain accumulation behaviors could be observed for cemented specimens once ΔV_s values exceeded 50 m/s, (ii) at low cementation levels, corresponding to ΔV_s values between 50 and 150 m/s, improvements in post-triggering strain accumulation responses could be largely attributed to cementation-induced densification, and (iii) at higher cementation levels, corresponding to ΔV_s values above 150 m/s, improvements in post-triggering strain accumulation exceeded that attributable to dry density increases alone with the presence of cemented bonding and particle coatings further enhancing behaviors.

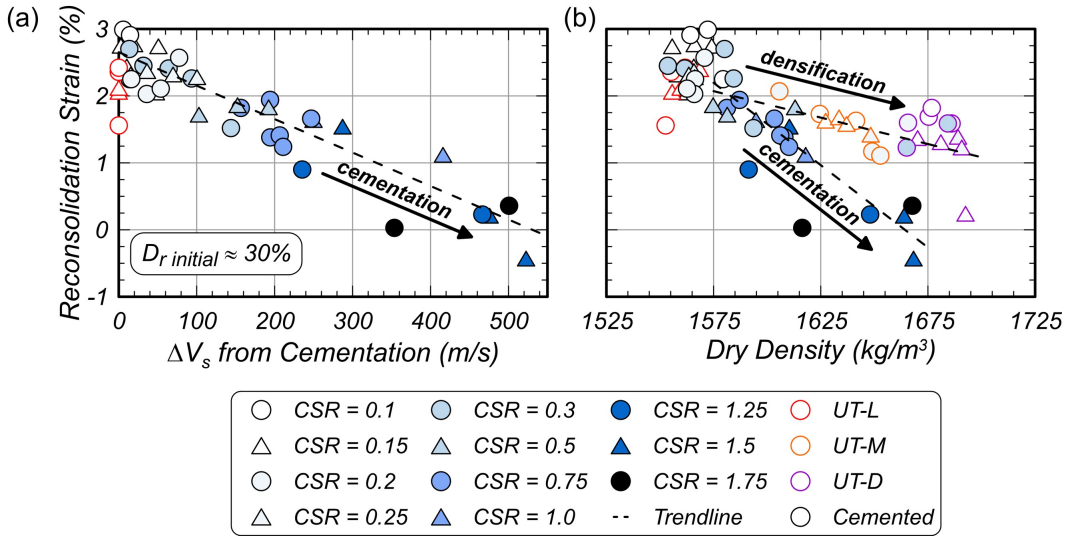

Figure 10.13. Vertical reconsolidation strains versus **(a)** ΔV_s from cementation for loose ($D_{r\ initial}$ ≈30%) specimens of varying biocementation levels and **(b)** dry density differences for all biocemented loose specimens and uncemented specimens prepared to varying initial densities.

In addition to changes in strain accumulation behavior, changes in vertical reconsolidation behaviors were also examined as a function of cementation levels, which occurred following shearing to 24% DASS, upon the reapplication of the initial vertical effective stress ($\sigma' = 100$ kPa). **Figure 10.13** presents vertical reconsolidation strains versus ΔV_s from cementation (**Figure 10.13a**) for all uncemented and biocemented loose specimens and dry density (**Figure 10.13b**) differences for all biocemented loose specimens and uncemented specimens at varying initial densities. As shown in **Figure 10.13a**, uncemented loose specimens had reconsolidation strains between 1.6 and 2.7%, however, detectable decreases in reconsolidation strains were observed as cementation levels exceeded ΔV_s values of ≈ 250 m/s, with reconsolidation strains near 1% at ΔV_s values near 300 m/s and near 0% at ΔV_s values near 500 m/s. When examining reconsolidation strain trends as a function of dry density differences instead (**Figure 10.13b**), clear differences between cemented and uncemented specimens were observed once cementation levels increased dry densities above ≈ 1575 kg/m^3, with uncemented specimens exhibiting consistently higher reconsolidation strains than cemented specimens at similar dry densities. This suggested that while reconsolidation strains were similar between uncemented and cemented specimens on the basis of dry density at low cementation levels, more highly cemented specimens ($\Delta V_s > 250$ m/s) were able to achieve improvements in reconsolidation behaviors beyond those attributable to density increases alone and remained stiffer in vertical compression following shearing to 24% DASS. This outcome may have resulted from the increased localization of shear strains within more highly cemented specimens as observed by other past studies (Tagliaferri 2011; DeJong et al. 2017; Lin et al. 2020), which could have enabled more highly cemented specimens to retain cemented zones following shearing that contributed towards enhancing reconsolidation responses.

Figure 10.14 presents relationships between ΔV_s changes following shearing and reconsolidation events and ΔV_s increases from cementation for all biocemented loose specimens. As shown, ΔV_s changes measured following shearing and reconsolidation events were reflective of the cumulative impact of both V_s decreases from cementation damage during shearing events as well as V_s increases from minor soil densification following reconsolidation. All specimens experienced similar shear-strain magnitudes following cyclic events (24% DASS) prior to reconsolidation. As shown, for biocemented specimens, ΔV_s increases from cementation and ΔV_s decreases following shearing and reconsolidation events closely followed the 1:1 trendline up to ΔV_s increases from cementation near 300 m/s, suggesting that small-strain stiffness improvements from biocementation were largely erased following shearing events at lower cementation levels, irrespective of differences in applied CSRs. At higher cementation levels (ΔV_s > 300 m/s), however, greater scatter was observed with some highly biocemented specimens plotting above the 1:1 trendline, suggesting that some cementation integrity (i.e., bonding) was retained following shearing. Interestingly, this cementation level threshold (ΔV_s > 300 m/s), was largely consistent with the ΔV_s values at which reconsolidation trends were shown to deviate between uncemented and biocemented specimens as a function of dry density (**Figure 10.14b**). Collectively, these results suggested that while more lightly cemented specimens behaved more similarly to denser uncemented specimens at larger strains, at higher cementation levels, some degree of cementation integrity was retained following shearing, thereby affording improvements in larger-strain behaviors beyond those which could be attributed to dry density increases alone.

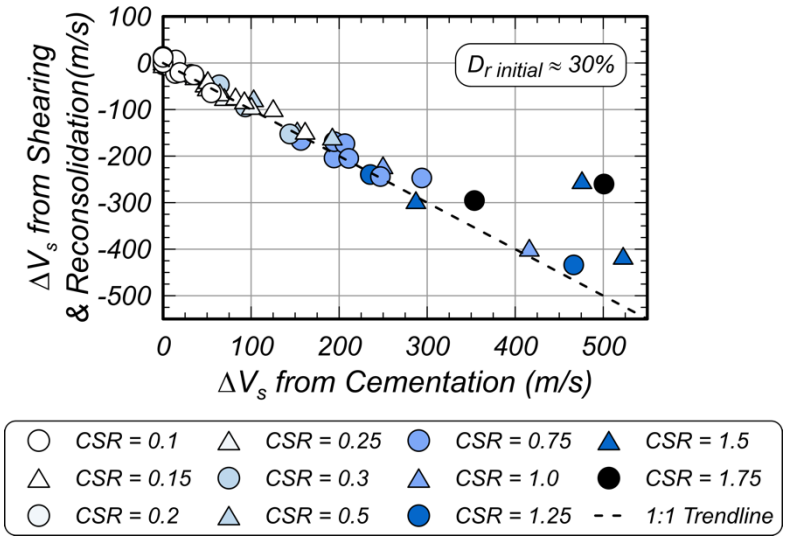

Figure 10.14. Shear wave velocity changes (ΔV_s) following shearing and reconsolidation events versus shear wave velocity increases (ΔV_s) from cementation for loose ($D_{r\ initial} \approx 30\%$) specimens of varying cementation subjected to different applied CSRs. Data points plotting near the 1:1 trendline suggest that increases in V_s from cementation were eliminated following shearing and reconsolidation events.

10.4 Conclusions

A study was performed to investigate the monotonic and cyclic shearing behavior of biocemented loose poorly-graded sands relevant to liquefaction mitigation applications. All specimens were cemented to achieve varying cementation levels corresponding to ΔV_s increases from 0 to 500 m/s and $CaCO_3$ contents between 0 and 5% by mass at a confining stress of 100 kPa and subsequently sheared. Undrained and drained monotonic tests examined differences in specimen stiffness, strength, and volumetric tendencies with increases in cementation level and changes in specimen initial densities for similar uncemented specimens. During undrained cyclic tests, similar biocemented and uncemented specimens were subjected to varying cyclic loading magnitudes (CSR = 0.1 to 1.75) intended to achieve liquefaction triggering for all specimens at cycle numbers

relevant to earthquake-induced loadings (cycles < 100) and compare the pre-triggering and post-triggering behaviors of specimens at similar dry densities. From the results of this study, the following conclusions can be made:

- Improvements in drained and undrained monotonic shearing behaviors were consistently observed with increases in cementation magnitudes. Stress-strain, excess pore pressure, and volumetric strain responses reflected a transition from contractive to dilative volumetric tendencies above a ΔV_s of 80 m/s, with greater dilation observed with increased cementation. Cemented specimens exhibited peak shear strengths at considerably smaller strains (≈ 0.5%) than uncemented specimens (≈ 5%) with minimal volumetric changes observed at peak strength, but volumetric tendencies increasingly mobilized at larger strains once cemented bonds were deteriorated.
- During undrained cyclic shearing, more highly cemented specimens were able to tolerate higher r_u values prior to accumulating significant shear strains reflective of the stress-invariant cohesive strength afforded by cemented bonds, which allowed specimens to retain higher shear stiffnesses at lower effective stresses during cycles applied prior triggering.
- Similar to results by Lee et al. (2022), increases in biocementation corresponding to ΔV_s increases between 0 and 500 m/s were shown to dramatically increase the number of cycles required to trigger liquefaction. While log-linear improvements in liquefaction resistances were observed with ΔV_s increases at lower cyclic demands (CSR < 0.75), at higher applied CSRs (CSR > 1.0), the effect of cementation was diminished, and heavily cemented specimens appeared to somewhat be insensitive to changes in applied loading demands. Furthermore, triggering resistances were found to correlate better with ΔV_s increases as

opposed to soil $CaCO_3$ contents, an outcome reflective of the improved ability of shear wave velocity measurements to assess differences in interparticle bonding and contact stiffnesses when compared to more rudimentary mass-based characterizations.

- When examining liquefaction resistance curves as a function of cementation level, power curve parameters exhibited consistent shifts with increasing cementation, with large increases in both a- and b-values. Although some significant discrepancies remain between studies regarding how these parameters may change, observations from this study were consistent with those by Riveros and Sadrekarimi (2020a) and suggest that the triggering resistances of biocemented specimens may become less sensitive to changes in applied CSRs with increasing cementation.
- Post-triggering strain accumulation behaviors were compared between uncemented and biocemented specimens subjected to different applied loadings using the compliance rate framework proposed by Tasiopoulou et al. (2019), wherein post-triggering shear strain accumulation rates per cycle were determined and normalized by the applied shear stress. Although low cementation levels (50 m/s < ΔV_s < 150 m/s) were shown to afford detectable improvements in post-triggering strain accumulation behaviors, these improvements were more modest than earlier triggering enhancements and could be largely attributed to cementation-induced densification. In contrast, at higher cementation levels (ΔV_s > 150 m/s), cemented specimens exhibited further reductions in post-triggering shear strain accumulation rates when compared to uncemented specimens at similar dry densities, thereby suggesting that additional improvements in post-triggering behaviors may be afforded by the presence of cemented bonds and cemented particle coatings once a sufficient magnitude of cementation is present.

- When comparing differences in reconsolidation behaviors following undrained cyclic shearing events, large reductions in vertical reconsolidation strains were observed with increasing cementation. While improvements afforded by cementation appeared to be largely attributable to densification at lower cementation levels, at higher cementation levels ($\Delta V_s > 300$ m/s) cemented specimens exhibited lower vertical reconsolidation strains than uncemented specimens at similar dry densities. This outcome suggests that cemented zones may have remained intact in more heavily cemented specimens following shearing events due to increased localization of shear strains at higher cementation levels. Although these intact cemented regions may have provided more limited benefits with respect to restraining shear deformations, such zones may have contributed substantially towards enhancing reconsolidation behaviors.
- Following shearing and reconsolidation events, changes in soil V_s values suggested that initial shear stiffness enhancements resulting from biocementation were largely eliminated in more lightly cemented specimens, however at higher cementation levels ($\Delta V_s > 300$ m/s), some amount of cementation integrity could be retained post-shearing. This outcome was consistent with the post-triggering behavioral improvements also observed at these higher cementation levels.

Although the results of this study significantly improve our understanding of the liquefaction behaviors of poorly-graded loose sands, further work remains needed to more fully characterize these behaviors and investigate the effect of field relevant factors including initial relative density differences prior to cementation, changes in applied loadings, the influence of static shear stresses, confining stress differences, and independent changes in specimen dry densities and V_s increases for biocemented specimens, among other factors.

Chapter 11. FUTURE WORK

In this research program, (1) the liquefaction behavior of biocemented loose clean sands was characterized as a function of cementation levels and loading magnitudes, (2) techniques were developed to control the spatial distribution of biocementation soil improvement and manage generated ammonium by-products, and (3) the efficacy of the developed treatment techniques and by-product management approaches was investigated at meter-scale through a combination of both physical experiments and numerical modeling. Although insights achieved during this research are expected to further advance biocementation towards field-scale deployment for practical liquefaction mitigation applications, many areas remain for which future research is recommended. Although not exhaustive, some recommendations for future research are presented as follows:

11.1 Continued Characterization of the Undrained Cyclic Behavior and Dynamic Properties of Biocemented Sands

Previous investigations explored the shearing behavior of biocemented loose sand specimens across a broad range of cementation levels (ΔV_s from 0 to 500 m/s) relevant to practical engineering applications. Although significant insights were achieved, knowledge gaps still persist regarding the influence of a variety of field-relevant factors including specimen initial relative densities prior to cementation, confining stress differences, and applied static shear stresses as well as the particular mechanisms responsible for the behavioral enhancements observed at small- and large-strains. While systematic mechanical testing may be used to investigate these isolated variables using testing venues similar to those present in this work (i.e., DSS, triaxial testing), the use of other microscale analyses may also be important towards better understanding potential

differences in soil fabrics and particle surface roughness with added cementation. Furthermore, results from previous investigations suggest that while biocementation may significantly improve triggering resistances, comparable post-triggering behaviors can be obtained for uncemented specimens prepared to similar dry densities. From this perspective, other techniques used to densify soils during or prior to treatments may afford further enhancements in large-strain engineering behaviors while minimizing associated environmental impacts. Finally, results from previous systems level investigations have shown the ability of biocementation to improve soil liquefaction resistances, with some important related effects regarding site response. In order for these effects to be better anticipated and designed for at field-scale, characterizations of the low-strain dynamic properties of biocemented soils including modulus degradation and damping behaviors as a function of strain level remain needed.

11.2 Optimization of Rinse Injection Sequencing and Solution Compositions for Post-treatment Ammonium By-product Removal

Although previous experiments examined the application of either continuous 12 PV or daily 1 PV staged rinse injections to remove generated ammonium by-products following biocementation, results from these experiments suggested that the majority of ammonium concentrations are removed early during injections via advection with further reductions at lower aqueous concentrations requiring cation exchange to remove sorbed ammonium masses. Moving forward, additional experiments may consider combinations of continuous and staged rinse injections to minimize pumping effort while achieving similar removal efficiencies as daily staged injections. In this approach, continuous injections could be applied early on to displace aqueous concentrations with stop-flow daily injections applied near the end of rinsing to progressively

remove sorbed ammonium masses. Lastly, although varying concentrations of Ca^{2+} and Na^{+} were considered in earlier rinsing experiments, K^{+} ions shown to achieve the greatest removal were only tested at a single 200 mM concentration. While past rinsing experiments also suggested that changes in applied rinse solution cation concentrations had minimal effects on ammonium removal, future experiments should be performed using rinse solutions with lower K^{+} concentrations in order to further reduce required materials.

11.3 Investigation of Biological Nitrogen Transformations for By-product Management

Research work in this study examined the ability of rinse solution injections to remove ammonium by-products generated during the MICP process. Moving forward ammonium by-product management will remain critical towards enabling deployment of biocementation at actual field sites. While rinse injections provide one approach by which ammonium by-products can be managed, microbial metabolic processes may also be employed to transform generated nitrogen by-products into more benign chemical species, such as dinitrogen gas. Although not yet demonstrated, such techniques may require significantly less materials and energy than current rinsing techniques.

11.4 Deployment, Monitoring, and Verification of Biocementation at Field-scale

Although investigations performed in this research examined the deployment of new treatment techniques and process monitoring tools using centimeter- and meter-scale physical experiments, deployment of such approaches at field sites remains critical towards demonstrating and verifying

their efficacy at practical scales. Field sites present conditions and complexities which cannot be fully replicated in the lab including (1) differences in subsurface stratigraphy and inherent soil spatial variability, (2) environmental differences including changes in groundwater chemistry, parent soil mineralogy, oxygen and nutrient availability, and temperature fluctuations, and (3) differences in solution injection strategies due to increased solution dispersion and radial flow conditions. Moving forward, field testing will provide an important opportunity to verify that treatment processes can be reliably controlled to alter cementation spatial distributions and magnitudes, by-products can be effectively managed, removed, and monitored, and geophysical, geotechnical, and geotechnical measurements can be used to characterize the location, magnitude, and permanence of improvement. Although field trials may also provide some limited information regarding systems-level mechanical improvements through blasting trials and/or other means, geotechnical centrifuge testing will also continue to afford new opportunities to better understand the systems-level response of biocementation improved soils needed to calibrate and advance numerical models and inform future treatment designs.

BIBLIOGRAPHY

[1] Akili, W., & Al-Joulani, N.M.A. (1988). Cone penetration tests on artificially cemented sands. In International Symposium on penetration testing; ISOPT-1. 1 (pp. 607-613).

[2] Almajed, A., Khodadadi Tirkolaei, H., & Kavazanjian, E. (2018). Baseline Investigation on Enzyme-Induced Calcium Carbonate Precipitation. Journal of Geotechnical and Geoenvironmental Engineering, 144(11), 04018081. https://doi.org/10.1061/(ASCE)GT.1943-5606.0001973

[3] Arulmoli, K., K. K. Muraleetharan, M. M. Hossain, and L. S. Fruth. 1992. *VELACS: Verification of liquefaction analysis by centrifuge studies, laboratory testing program*. Soil Data Rep., Project No. 90–0562. Irvine, CA: Earth Technology Corporation.

[4] ASTM. (2017). "Standard Practice for Classification of Soils for Engineering Purpose.", ASTM D2487-17e1, West Conshohocken, PA.

[5] ASTM. (2014). "Standard Test Method for Rapid Determination of Carbonate Content of Soils." *ASTM D4373-14*, West Conshohocken, PA

[6] ASTM. (2016a). "Standard Test Methods for Maximum Index Density and Unit Weight of Soils Using a Vibratory Table." *ASTM D4253-16e1*, West Conshohocken, PA.

[7] ASTM. (2016b). "Standard Test Methods for Minimum Index Density and Unit Weight of Soils and Calculation of Relative Density" *ASTM D4254-16*, West Conshohocken, PA.

[8] Bachus, R.C., Clough, G.W., Sitar, N., Shafii-Rad, N., Crosby, J., and Kaboli, P. (1981). Behavior of weakly cemented soil slopes under static and seismic loading conditions,

Vol. II (Open-File Report) [Open-File Report]. U.S.G.S. Rep. No. 51, July, U.S. Geological Survey.

[9] Bang, S.S., Bang, S., Frutiger, S., Nehl, L.M., & Comes, B.L. (2009). Application of Novel Biological Technique in Dust Suppression.

[10] Bang, S., Min, S.-H., & Bang, S. S. (2011). Application of Microbiologically Induced Soil Stabilization Technique for Dust Suppression. International Journal of Geo-Engineering, 3(2), 27–37.

[11] Bernardi, D., DeJong, J. T., Montoya, B. M., & Martinez, B. C. (2014). Bio-bricks: Biologically cemented sandstone bricks. Construction and Building Materials, 55, 462–469. https://doi.org/10.1016/j.conbuildmat.2014.01.019

[12] Bhattacharya, A., Naik, S. N., & Khare, S. K. (2018). Harnessing the bio-mineralization ability of urease producing Serratia marcescens and Enterobacter cloacae EMB19 for remediation of heavy metal cadmium (II). Journal of Environmental Management, 215, 143–152. https://doi.org/10.1016/j.jenvman.2018.03.055

[13] Bolton, M. D. (1986). The strength and dilatancy of sands. Géotechnique, 36(1), 65–78. https://doi.org/10.1680/geot.1986.36.1.65

[14] Brusseau, M. L. (1993). The influence of solute size, pore water velocity, and intraparticle porosity on solute dispersion and transport in soil. Water Resources Research, 29(4), 1071–1080. https://doi.org/10.1029/92WR02595

[15] Burbank, M. B., Weaver, T. J., Green, T. L., Williams, B. C., & Crawford, R. L. (2011). Precipitation of Calcite by Indigenous Microorganisms to Strengthen Liquefiable Soils. Geomicrobiology Journal, 28(4), 301–312. https://doi.org/10.1080/01490451.2010.499929

[16] Burbank, M., Weaver, T., Lewis, R., Williams, T., Williams, B., & Crawford, R. (2013). Geotechnical Tests of Sands Following Bioinduced Calcite Precipitation Catalyzed by Indigenous Bacteria. Journal of Geotechnical and Geoenvironmental Engineering, 139(6), 928–936. https://doi.org/10.1061/(ASCE)GT.1943-5606.0000781

[17] Burdalski, R. J., & Gomez, M. G. (2020). Investigating the Effect of Microbial Activity and Chemical Concentrations on the Mineralogy and Morphology of Ureolytic Biocementation. Geo-Congress 2020, 83–95. https://doi.org/10.1061/9780784482834.010

[18] Burdalski, R. J., II. (2020). Investigating the Effect of Biological and Chemical Factors on the Reaction Kinetics and Mineralogy of Ureolytic Biocementationf [Master's thesis]. University of Washington, Seattle, WA, USA.

[19] Carey, T. J., Stone, N., & Kutter, B. L. (2020). Grain Size Analysis and Maximum and Minimum Dry Density Testing of Ottawa F-65 Sand for LEAP-UCD-2017. In B. L. Kutter, M. T. Manzari, & M. Zeghal (Eds.), Model Tests and Numerical Simulations of Liquefaction and Lateral Spreading (pp. 31–44). Springer International Publishing. https://doi.org/10.1007/978-3-030-22818-7_2

[20] Chiaro, G., J. Koseki, and T. Sato. 2012. "Effects of initial static shear on liquefaction and large deformation properties of loose saturated Toyoura sand in undrained cyclic

torsional shear tests." *Soils and Foundations*, 52 (3): 498–510. https://doi.org/10.1016/j.sandf.2012.05.008.

[21] Choi, S.-G., Wang, K., & Chu, J. (2016). Properties of biocemented, fiber reinforced sand. Construction and Building Materials, 120, 623–629. https://doi.org/10.1016/j.conbuildmat.2016.05.124

[22] Clarà Saracho, A., Haigh, S. K., & Ehsan Jorat, M. (2021). Flume study on the effects of microbial induced calcium carbonate precipitation (MICP) on the erosional behaviour of fine sand. Géotechnique, 71(12), 1135–1149. https://doi.org/10.1680/jgeot.19.P.350

[23] Clough, G. W. (1989). Influence of Cementation on Liquefaction of Sands. 16.

[24] Clough, G. W., & Bachus, R. C. (1981). An investigation of sampling disturbance in weakly cemented soils. In *Proc. Engineering Foundation Conf in Updating Subsurface Sampling and In-situ Testing, Santa Barbara, California*.

[25] Clough, G. W., Sitar, N., Bachus, R. C., & Rad, N. S. (1981). Cemented Sands under Static Loading. Journal of the Geotechnical Engineering Division, 107(6), 799–817. https://doi.org/10.1061/AJGEB6.0001152

[26] Cuthbert, M. O., McMillan, L. A., Handley-Sidhu, S., Riley, Michael. S., Tobler, D. J., & Phoenix, Vernon. R. (2013). A Field and Modeling Study of Fractured Rock Permeability Reduction Using Microbially Induced Calcite Precipitation. Environmental Science & Technology, 47(23), 13637–13643. https://doi.org/10.1021/es402601g

[27] Darby, K. M., Hernandez, G. L., DeJong, J. T., Boulanger, R. W., Gomez, M. G., & Wilson, D. W. (2019). Centrifuge Model Testing of Liquefaction Mitigation via Microbially Induced Calcite Precipitation. Journal of Geotechnical and Geoenvironmental Engineering, 145(10), 04019084. https://doi.org/10.1061/(ASCE)GT.1943-5606.0002122

[28] De Muynck, W., Debrouwer, D., De Belie, N., & Verstraete, W. (2008). Bacterial carbonate precipitation improves the durability of cementitious materials. Cement and Concrete Research, 38(7), 1005–1014. https://doi.org/10.1016/j.cemconres.2008.03.005

[29] De Muynck, W., Verbeken, K., De Belie, N., & Verstraete, W. (2010). Influence of urea and calcium dosage on the effectiveness of bacterially induced carbonate precipitation on limestone. Ecological Engineering, 36(2), 99–111. https://doi.org/10.1016/j.ecoleng.2009.03.025

[30] DeJong, J. T., Fritzges, M. B., & Nüsslein, K. (2006). Microbially Induced Cementation to Control Sand Response to Undrained Shear. Journal of Geotechnical and Geoenvironmental Engineering, 132(11), 1381–1392. https://doi.org/10.1061/(ASCE)1090-0241(2006)132:11(1381)

[31] DeJong, J. T., & Kavazanjian, E. (2019). Bio-mediated and Bio-inspired Geotechnics. In N. Lu & J. K. Mitchell (Eds.), Geotechnical Fundamentals for Addressing New World Challenges (pp. 193–207). Springer International Publishing. https://doi.org/10.1007/978-3-030-06249-1_7

[32] DeJong, J. T., Mortensen, B. M., Martinez, B. C., & Nelson, D. C. (2010). Bio-mediated soil improvement. Ecological Engineering, 36(2), 197–210. https://doi.org/10.1016/j.ecoleng.2008.12.029

[33] DeJong, J. T., Soga, K., Kavazanjian, E., Burns, S., Van Paassen, L. A., Al Qabany, A., Aydilek, A., Bang, S. S., Burbank, M., Caslake, L. F., Chen, C. Y., Cheng, X., Chu, J., Ciurli, S., Esnault-Filet, A., Fauriel, S., Hamdan, N., Hata, T., Inagaki, Y., … Weaver, T. (2013). Biogeochemical processes and geotechnical applications: Progress, opportunities and challenges. Géotechnique, 63(4), 287–301. https://doi.org/10.1680/geot.SIP13.P.017

[34] De Silva, L. I. N., J. Koseki, G. Chiaro, and T. Sato. 2015. "A stress–strain description of saturated sand under undrained cyclic torsional shear loading." *Soils and Foundations*, 55 (3): 559–574. https://doi.org/10.1016/j.sandf.2015.04.008.

[35] Department of Human Services Environmental Toxicology Section. (2000). Technical Bulletin-Health Effects Information: Ammonia. Portland, Oregon

[36] Dhami, N. K., Mukherjee, A., & Reddy, M. S. (2016). Micrographical, minerological and nano-mechanical characterisation of microbial carbonates from urease and carbonic anhydrase producing bacteria. Ecological Engineering, 94, 443–454. https://doi.org/10.1016/j.ecoleng.2016.06.013

[37] Dorich, R. A., & Nelson, D. W. (1983). Direct Colorimetric Measurement of Ammonium in Potassium Chloride Extracts of Soils. Soil Science Society of America Journal, 47(4), 833–836. https://doi.org/10.2136/sssaj1983.03615995004700040042x

[38] Dorofeyeva, L. V. (1975). Obtaining of measles virus haemagglutinin from strain L-16 grown in primary cell cultures. Acta Virologica, 19(6), 497.

[39] Dupraz, S., Parmentier, M., Ménez, B., & Guyot, F. (2009). Experimental and numerical modeling of bacterially induced pH increase and calcite precipitation in saline aquifers. Chemical Geology, 265(1–2), 44–53. https://doi.org/10.1016/j.chemgeo.2009.05.003

[40] El Ghoraiby, M., Park, H., & Manzari, M. T. (2020). Physical and Mechanical Properties of Ottawa F65 Sand. In B. L. Kutter, M. T. Manzari, & M. Zeghal (Eds.), Model Tests and Numerical Simulations of Liquefaction and Lateral Spreading (pp. 45–67). Springer International Publishing. https://doi.org/10.1007/978-3-030-22818-7_3

[41] El Mountassir, G., Minto, J. M., van Paassen, L. A., Salifu, E., & Lunn, R. J. (2018). Applications of Microbial Processes in Geotechnical Engineering. In Advances in Applied Microbiology (Vol. 104, pp. 39–91). Elsevier. https://doi.org/10.1016/bs.aambs.2018.05.001

[42] El Kortbawi, M., Ziotopoulou, K., Gomez, M.G., and Lee, M. (2022). "Mechanical Behaviour of Artificially Cemented Sands: Experimental and Numerical Developments." *Canadian Geotechnical Journal*, (Under Review).

[43] European Union. (2020). Directive (EU) 2020/2184 of the European Parliament and of the Council of 16 December 2020 on the Quality of Water Intended for Human Consumption. Off. J. Eur. Union, 435, 1-62.

[44] Fang, C., Mi, T., & Achal, V. (2021). Sustainable bio-bricks prepared with synthetic urine enabled by biomineralization reactions. Letters in Applied Microbiology, 73(6), 793–799. https://doi.org/10.1111/lam.13574

[45] Feng and Montoya—2017—Quantifying Level of Microbial-Induced Cementation.pdf. (n.d.).

[46] Feng, K., & Montoya, B. M. (2016). Influence of Confinement and Cementation Level on the Behavior of Microbial-Induced Calcite Precipitated Sands under Monotonic Drained Loading. Journal of Geotechnical and Geoenvironmental Engineering, 142(1), 04015057. https://doi.org/10.1061/(ASCE)GT.1943-5606.0001379

[47] Feng, K., & Montoya, B. M. (2017). Quantifying Level of Microbial-Induced Cementation for Cyclically Loaded Sand. Journal of Geotechnical and Geoenvironmental Engineering, 143(6), 06017005. https://doi.org/10.1061/(ASCE)GT.1943-5606.0001682

[48] Ferris, F. G., Phoenix, V., Fujita, Y., & Smith, R. W. (2004). Kinetics of calcite precipitation induced by ureolytic bacteria at 10 to 20°C in artificial groundwater. Geochimica et Cosmochimica Acta, 68(8), 1701–1710. https://doi.org/10.1016/S0016-7037(03)00503-9

[49] Ferris, F. G., Stehmeier, L. G., Kantzas, A., & Mourits, F. M. (1996). Bacteriogenic Mineral Plugging. Journal of Canadian Petroleum Technology, 35(08). https://doi.org/10.2118/96-08-06

[50] Freundlich, H. (1907). Über die Adsorption in Lösungen. Zeitschrift Für Physikalische Chemie, 57U(1), 385–470. https://doi.org/10.1515/zpch-1907-5723

[51] Frossard, A., Hammes, F., & Gessner, M. O. (2016). Flow Cytometric Assessment of Bacterial Abundance in Soils, Sediments and Sludge. Frontiers in Microbiology, 7. https://doi.org/10.3389/fmicb.2016.00903

[52] Frydman, S., Shaal, B., Baker, R., Steinbach, J., Horn, H., & Hendron, D. (1980). Liquefaction Study of Cemented Sand. Journal of the Geotechnical Engineering Division, 106(3), 275–297. https://doi.org/10.1061/AJGEB6.0000933

[53] Fujita, Y., Ferris, F. G., Lawson, R. D., Colwell, F. S., & Smith, R. W. (2000). Subscribed Content Calcium Carbonate Precipitation by Ureolytic Subsurface Bacteria. Geomicrobiology Journal, 17(4), 305–318. https://doi.org/10.1080/782198884

[54] Fujita, Y., Redden, G. D., Ingram, J. C., Cortez, M. M., Ferris, F. G., & Smith, R. W. (2004). Strontium incorporation into calcite generated by bacterial ureolysis. Geochimica et Cosmochimica Acta, 68(15), 3261–3270. https://doi.org/10.1016/j.gca.2003.12.018

[55] Fujita, Y., Taylor, J. L., Gresham, T. L. T., Delwiche, M. E., Colwell, F. S., McLing, T. L., Petzke, L. M., & Smith, R. W. (2008). Stimulation Of Microbial Urea Hydrolysis In Groundwater To Enhance Calcite Precipitation. Environmental Science & Technology, 42(8), 3025–3032. https://doi.org/10.1021/es702643g

[56] Gao, Y., Hang, L., He, J., & Chu, J. (2019). Mechanical behaviour of biocemented sands at various treatment levels and relative densities. Acta Geotechnica, 14(3), 697–707. https://doi.org/10.1007/s11440-018-0729-3

[57] Gat, D., Ronen, Z., & Tsesarsky, M. (2016). Soil Bacteria Population Dynamics Following Stimulation for Ureolytic Microbial-Induced CaCO 3 Precipitation.

Environmental Science & Technology, 50(2), 616–624. https://doi.org/10.1021/acs.est.5b04033

[58] Gat, D., Ronen, Z., & Tsesarsky, M. (2017). Long-term sustainability of microbial-induced CaCO3 precipitation in aqueous media. Chemosphere, 184, 524–531. https://doi.org/10.1016/j.chemosphere.2017.06.015

[59] Gat, D., Tsesarsky, M., Wahanon, A., & Ronen, Z. (2014). Ureolysis and MICP with Model and Native Bacteria: Implications for Treatment Strategies. Geo-Congress 2014 Technical Papers, 1713–1720. https://doi.org/10.1061/9780784413272.168

[60] Ghasemi, P., & Montoya, B. M. (2020). Field Application of the Microbially Induced Calcium Carbonate Precipitation on a Coastal Sandy Slope. Geo-Congress 2020, 141–149. https://doi.org/10.1061/9780784482834.016

[61] Ginn, T. R., Wood, B. D., Nelson, K. E., Scheibe, T. D., Murphy, E. M., & Clement, T. P. (2002). Processes in microbial transport in the natural subsurface. Advances in Water Resources, 26.

[62] Gomez, M. G., Anderson, C. M., DeJong, J. T., Nelson, D. C., & Lau, X. H. (2014). Stimulating In Situ Soil Bacteria for Biocementation of Sands. Geo-Congress 2014 Technical Papers, 1674–1682. https://doi.org/10.1061/9780784413272.164

[63] Gomez, M. G., Anderson, C. M., Graddy, C. M. R., DeJong, J. T., Nelson, D. C., & Ginn, T. R. (2017). Large-Scale Comparison of Bioaugmentation and Biostimulation Approaches for Biocementation of Sands. Journal of Geotechnical and Geoenvironmental Engineering, 143(5), 04016124. https://doi.org/10.1061/(ASCE)GT.1943-5606.0001640

[64] Gomez, M. G., & DeJong, J. T. (2017). Engineering Properties of Biocementation Improved Sandy Soils. Grouting 2017, 23–33. https://doi.org/10.1061/9780784480793.003

[65] Gomez, M. G., DeJong, J. T., & Anderson, C. M. (2018). Effect of biocementation on geophysical and cone penetration measurements in sands. Canadian Geotechnical Journal, 55(11), 1632–1646. https://doi.org/10.1139/cgj-2017-0253

[66] Gomez, M. G., Graddy, C. M. R., DeJong, J. T., & Nelson, D. C. (2019). Biogeochemical Changes During Biocementation Mediated by Stimulated and Augmented Ureolytic Microorganisms. Scientific Reports, 9(1), 11517. https://doi.org/10.1038/s41598-019-47973-0

[67] Gomez, M. G., Graddy, C. M. R., DeJong, J. T., Nelson, D. C., & Tsesarsky, M. (2018). Stimulation of Native Microorganisms for Biocementation in Samples Recovered from Field-Scale Treatment Depths. Journal of Geotechnical and Geoenvironmental Engineering, 144(1), 04017098. https://doi.org/10.1061/(ASCE)GT.1943-5606.0001804

[68] Gomez, M. G., Martinez, B. C., DeJong, J. T., Hunt, C. E., deVlaming, L. A., Major, D. W., & Dworatzek, S. M. (2015). Field-scale biocementation tests to improve sands. Proceedings of the Institution of Civil Engineers - Ground Improvement, 168(3), 206–216. https://doi.org/10.1680/grim.13.00052

[69] Gowthaman, S., Mohsenzadeh, A., Nakashima, K., & Kawasaki, S. (2021). Removal of ammonium by-products from the effluent of biocementation system through struvite

precipitation. Materials Today: Proceedings, S2214785321058089. https://doi.org/10.1016/j.matpr.2021.09.013

[70] Graddy, C. M. R., Gomez, M. G., Kline, L. M., Morrill, S. R., DeJong, J. T., & Nelson, D. C. (2018). Diversity of Sporosarcina -like Bacterial Strains Obtained from Meter-Scale Augmented and Stimulated Biocementation Experiments. Environmental Science & Technology, 52(7), 3997–4005. https://doi.org/10.1021/acs.est.7b04271

[71] Hamdan, N., & Kavazanjian, E. (2016). Enzyme-induced carbonate mineral precipitation for fugitive dust control. Géotechnique, 66(7), 546–555. https://doi.org/10.1680/jgeot.15.P.168

[72] Hamdan, N., Kavazanjian, E., Rittmann, B. E., & Karatas, I. (2017). Carbonate Mineral Precipitation for Soil Improvement Through Microbial Denitrification. Geomicrobiology Journal, 34(2), 139–146. https://doi.org/10.1080/01490451.2016.1154117

[73] Han, Z., Cheng, X., & Ma, Q. (2016). An experimental study on dynamic response for MICP strengthening liquefiable sands. Earthquake Engineering and Engineering Vibration, 15(4), 673–679. https://doi.org/10.1007/s11803-016-0357-6

[74] He, J., Chen, X., Zhang, Q., & Achal, V. (2019). More effective immobilization of divalent lead than hexavalent chromium through carbonate mineralization by Staphylococcus epidermidis HJ2. International Biodeterioration & Biodegradation, 140, 67–71. https://doi.org/10.1016/j.ibiod.2019.03.012

[75] Hernandez, G. L. (2018). Centrifuge model testing of liquefaction mitigation via microbially induced calcite precipitation. https://search.proquest.com/docview/2135254681?accountid=14505

[76] Hobbie, J. E., Daley, R. J., & Jasper, S. (1977). Use of nuclepore filters for counting bacteria by fluorescence microscopy. Applied and Environmental Microbiology, 33(5), 1225–1228. https://doi.org/10.1128/aem.33.5.1225-1228.1977

[77] Huang, H., Xiao, X., Yan, B., & Yang, L. (2010). Ammonium removal from aqueous solutions by using natural Chinese (Chende) zeolite as adsorbent. Journal of Hazardous Materials, 175(1–3), 247–252. https://doi.org/10.1016/j.jhazmat.2009.09.156

[78] Humire, F., M. Lee, K. Ziotopoulou, M. G. Gomez, and J. T. DeJong. 2022. "Development and Evaluation of Preconditioning Protocols for Sand Specimens in Constant-Volume Cyclic Direct Simple Shear Tests." *Geotech. Test. J.*, 45 (3): 20210028. https://doi.org/10.1520/GTJ20210028.

[79] Idriss, I. M., & Boulanger, R. W. (2008). Soil liquefaction during earthquakes. Earthquake Engineering Research Institute (EERI).

[80] Ishihara, K. (1993). Liquefaction and flow failure during earthquakes. Géotechnique, 43(3), 351–451. https://doi.org/10.1680/geot.1993.43.3.351

[81] Islam, M. T., Chittoori, B. C. S., & Burbank, M. (2020). Evaluating the Applicability of Biostimulated Calcium Carbonate Precipitation to Stabilize Clayey Soils. Journal of Materials in Civil Engineering, 32(3), 04019369. https://doi.org/10.1061/(ASCE)MT.1943-5533.0003036

[82] Ismail, M. A., Joer, H. A., Sim, W. H., & Randolph, M. F. (2002). Effect of Cement Type on Shear Behavior of Cemented Calcareous Soil. Journal of Geotechnical and Geoenvironmental Engineering, 128(6), 520–529. https://doi.org/10.1061/(ASCE)1090-0241(2002)128:6(520)

[83] Jiang, N.-J., Liu, R., Du, Y.-J., & Bi, Y.-Z. (2019). Microbial induced carbonate precipitation for immobilizing Pb contaminants: Toxic effects on bacterial activity and immobilization efficiency. Science of The Total Environment, 672, 722–731. https://doi.org/10.1016/j.scitotenv.2019.03.294

[84] Jiang, N.-J., & Soga, K. (2017). The applicability of microbially induced calcite precipitation (MICP) for internal erosion control in gravel–sand mixtures. Géotechnique, 67(1), 42–55. https://doi.org/10.1680/jgeot.15.P.182

[85] Kammerer, A. M., J. Wu, J. M. Pestana, M. Riemer, and R. B. Seed. 2000. *Cyclic simple shear testing of Nevada sand for PEER center project 2051999*. Geotechnical Engineering Rep. No. UCBGT-2000-01. Berkeley, CA: Univ. of California, Berkeley.

[86] Karol, R. H. 2003. *Chemical grouting and soil stabilization*. Civil and environmental engineering. New York: M. Dekker.

[87] Kendall, A., Raymond, A. J., Tipton, J., & DeJong, J. T. (2017). Review of life-cycle-based environmental assessments of geotechnical systems. Proceedings of the Institution of Civil Engineers - Engineering Sustainability, 171(2), 57–67. https://doi.org/10.1680/jensu.16.00073

[88] Kiyota, T., T. Sato, J. Koseki, and M. Abadimarand. 2008. “Behavior of Liquefied Sands Under Extremely Large Strain Levels in Cyclic Torsional Shear Tests.” *Soils and Foundations*, 48 (5): 727–739. https://doi.org/10.3208/sandf.48.727.

[89] Knorst, M. T., Neubert, R., & Wohlrab, W. (1997). Analytical methods for measuring urea in pharmaceutical formulations. Journal of Pharmaceutical and Biomedical Analysis, 15(11), 1627–1632. https://doi.org/10.1016/S0731-7085(96)01978-4

[90] Krom, M. D. (1980). Spectrophotometric determination of ammonia: A study of a modified Berthelot reaction using salicylate and dichloroisocyanurate. The Analyst, 105(1249), 305. https://doi.org/10.1039/an9800500305

[91] Kumari, D., Qian, X.-Y., Pan, X., Achal, V., Li, Q., & Gadd, G. M. (2016). Microbially-induced Carbonate Precipitation for Immobilization of Toxic Metals. In Advances in Applied Microbiology (Vol. 94, pp. 79–108). Elsevier. https://doi.org/10.1016/bs.aambs.2015.12.002

[92] Lee, M., Gomez, M. G., El Kortbawi, M., & Ziotopoulou, K. (2022). Effect of Light Biocementation on the Liquefaction Triggering and Post-Triggering Behavior of Loose Sands. Journal of Geotechnical and Geoenvironmental Engineering, 148(1), 04021170. https://doi.org/10.1061/(ASCE)GT.1943-5606.0002707

[93] Lee, M., Gomez, M. G., El Kortbawi, M., & Ziotopoulou, K. (2020). Examining the Liquefaction Resistance of Lightly Cemented Sands Using Microbially Induced Calcite Precipitation (MICP). Geo-Congress 2020, 53–64. https://doi.org/10.1061/9780784482834.007

[94] Lee, M., Gomez, M. G., San Pablo, A. C. M., Kolbus, C. M., Graddy, C. M. R., DeJong, J. T., & Nelson, D. C. (2019). Investigating Ammonium By-product Removal for Ureolytic Biocementation Using Meter-scale Experiments. Scientific Reports, 9(1), 18313. https://doi.org/10.1038/s41598-019-54666-1

[95] Lee, M., Kolbus, C. M., Yepez, A. D., & Gomez, M. G. (2019). Investigating Ammonium By-Product Removal following Stimulated Ureolytic Microbially-Induced Calcite Precipitation. Geo-Congress 2019, 260–272. https://doi.org/10.1061/9780784482117.026

[96] Li, L., Wen, K., Bu, C., & Amini, F. (2020). Enhancement of Bio-Sandy Brick through Discrete Randomly Distributed Fiber. Geo-Congress 2020, 39–45. https://doi.org/10.1061/9780784482834.005

[97] Li, M., Fu, Q.-L., Zhang, Q., Achal, V., & Kawasaki, S. (2015). Bio-grout based on microbially induced sand solidification by means of asparaginase activity. Scientific Reports, 5(1), 16128. https://doi.org/10.1038/srep16128

[98] Li, M., Li, L., Ogbonnaya, U., Wen, K., Tian, A., & Amini, F. (2016). Influence of Fiber Addition on Mechanical Properties of MICP-Treated Sand. Journal of Materials in Civil Engineering, 28(4), 04015166. https://doi.org/10.1061/(ASCE)MT.1943-5533.0001442

[99] Li, M., Wen, K., Li, Y., & Zhu, L. (2018). Impact of Oxygen Availability on Microbially Induced Calcite Precipitation (MICP) Treatment. Geomicrobiology Journal, 35(1), 15–22. https://doi.org/10.1080/01490451.2017.1303553

[100] Lin, H., M. T. Suleiman, and D. G. Brown. 2020. “Investigation of pore-scale CaCO3 distributions and their effects on stiffness and permeability of sands treated by microbially induced carbonate precipitation (MICP).” *Soils and Foundations*, 60 (4): 944–961. https://doi.org/10.1016/j.sandf.2020.07.003.

[101] Lin, H., Suleiman, M. T., Brown, D. G., & Kavazanjian, E. (2016). Mechanical Behavior of Sands Treated by Microbially Induced Carbonate Precipitation. Journal of Geotechnical and Geoenvironmental Engineering, 142(2), 04015066. https://doi.org/10.1061/(ASCE)GT.1943-5606.0001383

[102] Lin, H., Suleiman, M. T., Jabbour, H. M., Brown, D. G., & Kavazanjian, E. (2016). Enhancing the Axial Compression Response of Pervious Concrete Ground Improvement Piles Using Biogrouting. Journal of Geotechnical and Geoenvironmental Engineering, 142(10), 04016045. https://doi.org/10.1061/(ASCE)GT.1943-5606.0001515

[103] Lings, M. L., & Greening, P. D. (2001). A novel bender/extender element for soil testing. Géotechnique, 51(8), 713–717. https://doi.org/10.1680/geot.2001.51.8.713

[104] Madabhushi, Gopal. S. P. 2007. “Ground improvement methods for liquefaction remediation.” *Proceedings of the Institution of Civil Engineers - Ground Improvement*, 11 (4): 195–206. https://doi.org/10.1680/grim.2007.11.4.195.

[105] Martinez, B. C., & DeJong, J. T. (2009). Bio-Mediated Soil Improvement: Load Transfer Mechanisms at the Micro- and Macro- Scales. Advances in Ground Improvement, 242–251. https://doi.org/10.1061/41025(338)26

[106] Martinez, B. C., DeJong, J. T., Ginn, T. R., Montoya, B. M., Barkouki, T. H., Hunt, C., Tanyu, B., & Major, D. (2013). Experimental Optimization of Microbial-Induced Carbonate Precipitation for Soil Improvement. Journal of Geotechnical and Geoenvironmental Engineering, 139(4), 587–598. https://doi.org/10.1061/(ASCE)GT.1943-5606.0000787

[107] Mengel, D. B. 1980. Fundamentals of soil cation exchange capacity (CEC). Purdue Univ. Coop. Ext. Ser. AY-238. 2 p.

[108] Meyer, F. D., Bang, S., Min, S., Stetler, L. D., & Bang, S. S. (2011). Microbiologically-Induced Soil Stabilization: Application of Sporosarcina pasteurii for Fugitive Dust Control. Geo-Frontiers 2011, 4002–4011. https://doi.org/10.1061/41165(397)409

[109] Minto, J. M., Lunn, R. J., & El Mountassir, G. (2019). Development of a Reactive Transport Model for Field-Scale Simulation of Microbially Induced Carbonate Precipitation. Water Resources Research, 55(8), 7229–7245. https://doi.org/10.1029/2019WR025153

[110] Minto, J. M., MacLachlan, E., El Mountassir, G., & Lunn, R. J. (2016). Rock fracture grouting with microbially induced carbonate precipitation: ROCK FRACTURE GROUTING WITH MICP. Water Resources Research, 52(11), 8827–8844. https://doi.org/10.1002/2016WR018884

[111] Minto, J. M., Tan, Q., Lunn, R. J., El Mountassir, G., Guo, H., & Cheng, X. (2018). 'Microbial mortar'-restoration of degraded marble structures with microbially induced

carbonate precipitation. Construction and Building Materials, 180, 44–54. https://doi.org/10.1016/j.conbuildmat.2018.05.200

[112] Mitchell, A. C., & Ferris, F. G. (2005). The coprecipitation of Sr into calcite precipitates induced by bacterial ureolysis in artificial groundwater: Temperature and kinetic dependence. Geochimica et Cosmochimica Acta, 69(17), 4199–4210. https://doi.org/10.1016/j.gca.2005.03.014

[113] Mitchell, J. K. (2008). AGING OF SAND – A CONTINUING ENIGMA? 22.

[114] Mitchell, J. K., & Santamarina, J. C. (2005). Biological Considerations in Geotechnical Engineering. Journal of Geotechnical and Geoenvironmental Engineering, 131(10), 1222–1233. https://doi.org/10.1061/(ASCE)1090-0241(2005)131:10(1222)

[115] Mitchell, J. K., Baxter, C. D., & Munson, T. C. (1995, October). Performance of improved ground during earthquakes. In *Soil improvement for earthquake hazard mitigation* (pp. 1-36). ASCE.

[116] Mobley, H. L. T., Island, M. D., & Hausinger, R. P. (1995). Molecular Biology of Microbial Ureases. MICROBIOL. REV., 59, 31.

[117] Mohsenzadeh, A., Aflaki, E., Gowthaman, S., Nakashima, K., Kawasaki, S., & Ebadi, T. (2021). A two-stage treatment process for the management of produced ammonium by-products in ureolytic biocementation process. International Journal of Environmental Science and Technology, 19(1), 449–462. https://doi.org/10.1007/s13762-021-03138-z

[118] Montoya, B. M., & DeJong, J. T. (2015). Stress-Strain Behavior of Sands Cemented by Microbially Induced Calcite Precipitation. Journal of Geotechnical and Geoenvironmental Engineering, 141(6), 04015019. https://doi.org/10.1061/(ASCE)GT.1943-5606.0001302

[119] Montoya, B. M., Dejong, J. T., & Boulanger, R. W. (2013). Dynamic response of liquefiable sand improved by microbial-induced calcite precipitation. Géotechnique, 63(4), 302–312. https://doi.org/10.1680/geot.SIP13.P.019

[120] Montoya, B. M., DeJong, J. T., Boulanger, R. W., Wilson, D. W., Gerhard, R., Ganchenko, A., & Chou, J.-C. (2012). Liquefaction Mitigation Using Microbial Induced Calcite Precipitation. GeoCongress 2012, 1918–1927. https://doi.org/10.1061/9780784412121.197

[121] Montoya, B. M., Do, J., & Gabr, M. M. (2018). Erodibility of Microbial Induced Carbonate Precipitation-Stabilized Sand under Submerged Impinging Jet. IFCEE 2018, 19–28. https://doi.org/10.1061/9780784481592.003

[122] Montoya, B. M., Gerhard, R., DeJong, J. T., Wilson, D. W., Weil, M. H., Martinez, B. C., & Pederson, L. (2012). Fabrication, Operation, and Health Monitoring of Bender Elements for Aggressive Environments. Geotechnical Testing Journal, 35(5), 103300. https://doi.org/10.1520/GTJ103300

[123] Morales, B., Humire, F., & Ziotopoulou, K. (2021). Cyclic Direct Simple Shear Tests—Ottawa F50 and F65 Sands [Data set]. Designsafe-CI. https://doi.org/10.17603/DS2-9CXW-KQ20

[124] Moug, D., Khosravifar, A., Preciado, M., Sorenson, K., Stokoe, K., Menq, F., ... & Wang, Y. (2020). Field Evaluation of Microbially Induced Desaturation for Liquefaction Mitigation of Silty Soils. In 17th World Conference on Earthquake Engineering (17WCEE), Sendai, Japan.

[125] Mujah, D., Shahin, M. A., & Cheng, L. (2017). State-of-the-Art Review of Biocementation by Microbially Induced Calcite Precipitation (MICP) for Soil Stabilization. Geomicrobiology Journal, 34(6), 524–537. https://doi.org/10.1080/01490451.2016.1225866

[126] Nafisi, A., Liu, Q., & Montoya, B. M. (2021). Effect of stress path on the shear response of biocemented sands. Acta Geotechnica, 16(10), 3239–3251. https://doi.org/10.1007/s11440-021-01286-7

[127] Nafisi, A., Montoya, B. M., & Evans, T. M. (2020). Shear Strength Envelopes of Biocemented Sands with Varying Particle Size and Cementation Level. Journal of Geotechnical and Geoenvironmental Engineering, 146(3), 04020002. https://doi.org/10.1061/(ASCE)GT.1943-5606.0002201

[128] Nassar, M. K., Gurung, D., Bastani, M., Ginn, T. R., Shafei, B., Gomez, M. G., Graddy, C. M. R., Nelson, D. C., & DeJong, J. T. (2018). Large-Scale Experiments in Microbially Induced Calcite Precipitation (MICP): Reactive Transport Model Development and Prediction. Water Resources Research, 54(1), 480–500. https://doi.org/10.1002/2017WR021488

[129] O'Donnell, S. T., Rittmann, B. E., & Kavazanjian, E. (2017). MIDP: Liquefaction Mitigation via Microbial Denitrification as a Two-Stage Process. I: Desaturation. Journal of Geotechnical and Geoenvironmental Engineering, 143(12), 04017094. https://doi.org/10.1061/(ASCE)GT.1943-5606.0001818

[130] Paerl, H. W. (1997). Coastal eutrophication and harmful algal blooms: Importance of atmospheric deposition and groundwater as "new" nitrogen and other nutrient sources. Limnology and Oceanography, 42(5part2), 1154–1165. https://doi.org/10.4319/lo.1997.42.5_part_2.1154

[131] Parkhurst, D. L., & Appelo, C. A. J. (2013). Description of input and examples for PHREEQC version 3—A computer program for speciation, batch-reaction, one-dimensional transport, and inverse geochemical calculations (Techniques and Methods) [U.S. Geological Survey Techniques and Methods, book 6, chap. A43, 497 p.].

[132] Parra Bastidas, A. M. 2016. "Ottawa F-65 sand characterization." Ph.D. dissertation. Dept. of Civil and Environmental Engineering, Univ. of California, Davis.

[133] Phillips, A. J., Cunningham, A. B., Gerlach, R., Hiebert, R., Hwang, C., Lomans, B. P., Westrich, J., Mantilla, C., Kirksey, J., Esposito, R., & Spangler, L. (2016). Fracture Sealing with Microbially-Induced Calcium Carbonate Precipitation: A Field Study. Environmental Science & Technology, 50(7), 4111–4117. https://doi.org/10.1021/acs.est.5b05559

[134] Phillips, A. J., Troyer, E., Hiebert, R., Kirkland, C., Gerlach, R., Cunningham, A. B., Spangler, L., Kirksey, J., Rowe, W., & Esposito, R. (2018). Enhancing wellbore cement

integrity with microbially induced calcite precipitation (MICP): A field scale demonstration. Journal of Petroleum Science and Engineering, 171, 1141–1148. https://doi.org/10.1016/j.petrol.2018.08.012

[135] Puppala, A. J., Acar, Y. B., & Senneset, K. (1993). Cone Penetration in Cemented Sands: Bearing Capacity Interpretation. Journal of Geotechnical Engineering, 119(12), 1990–2002. https://doi.org/10.1061/(ASCE)0733-9410(1993)119:12(1990)

[136] Rad, N., & Tumay, M. (1986). Effect of Cementation on the Cone Penetration Resistance of Sand: A Model Study. Geotechnical Testing Journal, 9(3), 117. https://doi.org/10.1520/GTJ10617J

[137] Rad, N.S., and Clough, G.W. (1982). The influence of cementation on the static and dynamic behavior of sands (No. 59). John A. Blume Earthquake Engineering Center.

[138] Ramachandran, S. K., V. Ramakrishnan, & Sooke S. Bang. (2001). Remediation of Concrete Using Microorganisms. ACI Materials Journal, 98(1). https://doi.org/10.14359/10154

[139] Ramakrishnan, V., Bang, S.S., & Deo, K.S. (1998). "A novel technique for repairing cracks in high performance concrete using bacteria." *Proc. Int. Conf. on HPHSC 1998*, Perth, Australia, 597–618.

[140] Ramakrishnan, V., Panchalan, R. K., & Bang, S. S. (2005). IMPROVEMENT OF CONCRETE DURABILITY BY BACTERIAL MINERAL PRECIPITATION. In Proc. ICF, (Vol. 11, pp. 357-67).

[141] Ramakrishnan, V., Ramesh, K. P., & Bang, S. S. (2001). Bacterial concrete (A. R. Wilson & H. Asanuma, Eds.; pp. 168–176). https://doi.org/10.1117/12.424404

[142] Raymond, A.J., Kendall, A., DeJong, J.T., Gomez, M.G., & San Pablo, A.C.M., Lee, M., Graddy, C.M.R., Nelson, D.C. (2020). "Life Cycle Sustainability Assessment of Microbially Induced Calcite Precipitation (MICP) Biocementation Techniques". *Environmental Research: Infrastructure and Sustainability,* Under Review.

[143] Riveros, G. A., & Sadrekarimi, A. (2020a). Liquefaction resistance of Fraser River sand improved by a microbially-induced cementation. Soil Dynamics and Earthquake Engineering, 131, 106034. https://doi.org/10.1016/j.soildyn.2020.106034

[144] Riveros, G. A., & Sadrekarimi, A. (2020b). Effect of microbially induced cementation on the instability and critical state behaviours of Fraser River sand. Canadian Geotechnical Journal, 57(12), 1870–1880. https://doi.org/10.1139/cgj-2019-0514

[145] Rodriguez-Navarro, C., Rodriguez-Gallego, M., Ben Chekroun, K., & Gonzalez-Muñoz, M. T. (2003). Conservation of Ornamental Stone by Myxococcus xanthus- Induced Carbonate Biomineralization. Applied and Environmental Microbiology, 69(4), 2182–2193. https://doi.org/10.1128/AEM.69.4.2182-2193.2003

[146] San Pablo, A. C. M., Lee, M., Graddy, C. M. R., Kolbus, C. M., Khan, M., Zamani, A., Martin, N., Acuff, C., DeJong, J. T., Gomez, M. G., & Nelson, D. C. (2020). Meter-Scale Biocementation Experiments to Advance Process Control and Reduce Impacts: Examining Spatial Control, Ammonium By-Product Removal, and Chemical Reductions.

Journal of Geotechnical and Geoenvironmental Engineering, 146(11), 04020125. https://doi.org/10.1061/(ASCE)GT.1943-5606.0002377

[147] Saneiyan, S., Ntarlagiannis, D., Ohan, J., Lee, J., Colwell, F., & Burns, S. (2019). Induced polarization as a monitoring tool for in-situ microbial induced carbonate precipitation (MICP) processes. Ecological Engineering, 127, 36–47. https://doi.org/10.1016/j.ecoleng.2018.11.010

[148] Saxena, S. K., & Lastrico, R. M. (1978). Static Properties of Lightly Cemented Sand. Journal of the Geotechnical Engineering Division, 104(12), 1449–1464. https://doi.org/10.1061/AJGEB6.0000728

[149] Saxena, S. K., Reddy, K. R., & Avramidis, A. S. (1988). Liquefaction Resistance of Artificially Cemented Sand. Journal of Geotechnical Engineering, 114(12), 1395–1413. https://doi.org/10.1061/(ASCE)0733-9410(1988)114:12(1395)

[150] Seagren and Aydilek. (2010). Seagren, E. A., & Aydilek, A. H. (2010). Biomediated geomechanical processes. Environmental microbiology, 319-348.

[151] Sharma, M., N. Satyam, and K. R. Reddy. 2020. “State of the Art Review of Emerging and Biogeotechnical Methods for Liquefaction Mitigation in Sands.” *J. Hazard. Toxic Radioact. Waste*, 25 (1): 03120002. https://doi.org/10.1061/(ASCE)HZ.2153-5515.0000557.

[152] Sieczka, A., & Koda, E. (2016). Kinetic and Equilibrium Studies of Sorption of Ammonium in the Soil-Water Environment in Agricultural Areas of Central Poland. Applied Sciences, 6(10), 269. https://doi.org/10.3390/app6100269

[153] Simatupang, M., & Okamura, M. (2017). Liquefaction resistance of sand remediated with carbonate precipitation at different degrees of saturation during curing. Soils and Foundations, 57(4), 619–631. https://doi.org/10.1016/j.sandf.2017.04.003

[154] Simatupang, M., Okamura, M., Hayashi, K., & Yasuhara, H. (2018). Small-strain shear modulus and liquefaction resistance of sand with carbonate precipitation. Soil Dynamics and Earthquake Engineering, 115, 710–718. https://doi.org/10.1016/j.soildyn.2018.09.027

[155] Smith, R. W., Fujita, Y., Hubbard, S., & Ginn, T. R. (2012). Field Investigations of Microbially Facilitated Calcite Precipitation for Immobilization of Strontium-90 and Other Trace Metals in the Subsurface (Technical Report DEO/ER64404; pp. 1–20). US Department of Energy.

[156] Sriskandakumar, S. 2004. “Cyclic loading response of Fraser River sand for validation of numerical models simulating centrifuge tests.” M.Sc. thesis. Dept. of Civil Engineering, Univ. of British Columbia.

[157] Stocks-Fischer, S., Galinat, J. K., & Bang, S. S. (1999). Microbiological precipitation of CaCO3. Soil Biology and Biochemistry, 31(11), 1563–1571. https://doi.org/10.1016/S0038-0717(99)00082-6

[158] Tagliaferri, F., J. Waller, E. Andò, S. A. Hall, G. Viggiani, P. Bésuelle, and J. T. DeJong. 2011. “Observing strain localisation processes in bio-cemented sand using x-ray imaging.” *Granular Matter*, 13 (3): 247–250. https://doi.org/10.1007/s10035-011-0257-4.

[159] Tao, J., Li, J., Wang, X., & Bao, R. (2018). Nature-Inspired Bridge Scour Countermeasures: Streamlining and Biocementation. Journal of Testing and Evaluation, 46(4), 20170517. https://doi.org/10.1520/JTE20170517

[160] Tasiopoulou, P., K. Ziotopoulou, F. Humire, A. Giannakou, J. Chacko, and T. Travasarou. 2019. "Development and Implementation of Semiempirical Framework for Modeling Postliquefaction Shear Deformation Accumulation in Sands." *J. Geotech. Geoenviron. Eng.*, 146 (1): 04019120. https://doi.org/10.1061/(ASCE)GT.1943-5606.0002179.

[161] Tatsuoka, F., K. Ochi, S. Fujii, and M. Okamoto. 1986. "Cyclic Undrained Triaxial and Torsional Shear Strength of Sands for Different Sample Preparation Methods." *Soils and Foundations*, 26 (3): 23–41. https://doi.org/10.3208/sandf1972.26.3_23.

[162] Terzis, D., Laloui, L., Dornberger, S., & Harran, R. (2020). A Full-Scale Application of Slope Stabilization via Calcite Bio-Mineralization Followed by Long-Term GIS Surveillance. Geo-Congress 2020, 65–73. https://doi.org/10.1061/9780784482834.008

[163] Tobler, D. J., Cuthbert, M. O., Greswell, R. B., Riley, M. S., Renshaw, J. C., Handley-Sidhu, S., & Phoenix, V. R. (2011). Comparison of rates of ureolysis between Sporosarcina pasteurii and an indigenous groundwater community under conditions required to precipitate large volumes of calcite. Geochimica et Cosmochimica Acta, 75(11), 3290–3301. https://doi.org/10.1016/j.gca.2011.03.023

[164] Tobler, D. J., Cuthbert, M. O., & Phoenix, V. R. (2014). Transport of Sporosarcina pasteurii in sandstone and its significance for subsurface engineering technologies. Applied Geochemistry, 42, 38–44. https://doi.org/10.1016/j.apgeochem.2014.01.004

[165] Tziviloglou, E., Wiktor, V., Jonkers, H. M., & Schlangen, E. (2016). Bacteria-based self-healing concrete to increase liquid tightness of cracks. Construction and Building Materials, 122, 118–125. https://doi.org/10.1016/j.conbuildmat.2016.06.080

[166] Ueda, K., Vargas, R. R., & Uemura, K. (2018). LEAP-Asia-2018: stress–strain response of Ottawa sand in cyclic torsional shear tests.

[167] Uğurlu, M., & Karaoğlu, M. H. (2011). Adsorption of ammonium from an aqueous solution by fly ash and sepiolite: Isotherm, kinetic and thermodynamic analysis. Microporous and Mesoporous Materials, 139(1–3), 173–178. https://doi.org/10.1016/j.micromeso.2010.10.039

[168] Umar, M., G. Chiaro, and T. Kiyota. 2016. “On the influence of initial static shear on large deformation behavior of very loose Toyoura sand in undrained cyclic torsional shear tests.” *In Proc., 6th Japan-Korea Geotechnical Workshop*. Tokyo: Japanese Geotechnical Society.

[169] U.S. Environmental Protection Agency. Aquatic Life Ambient Water Quality Criteria for Ammonia – Freshwater (EPA Publication No. 822-R-13-001). Washington, DC, 1–255 (2013)

[170] van Paassen, L. A. (2009). Biogrout: Ground improvement by microbially induced carbonate precipitation. [s.n.].

[171] van Paassen, L. A. (2011). Bio-Mediated Ground Improvement: From Laboratory Experiment to Pilot Applications. Geo-Frontiers 2011, 4099–4108. https://doi.org/10.1061/41165(397)419

[172] van Paassen, L. A., Daza, C. M., Staal, M., Sorokin, D. Y., van der Zon, W., & van Loosdrecht, Mark. C. M. (2010). Potential soil reinforcement by biological denitrification. Ecological Engineering, 36(2), 168–175. https://doi.org/10.1016/j.ecoleng.2009.03.026

[173] van Paassen, L. A., Ghose, R., van der Linden, T. J. M., van der Star, W. R. L., & van Loosdrecht, M. C. M. (2010). Quantifying Biomediated Ground Improvement by Ureolysis: Large-Scale Biogrout Experiment. Journal of Geotechnical and Geoenvironmental Engineering, 136(12), 1721–1728. https://doi.org/10.1061/(ASCE)GT.1943-5606.0000382

[174] van Paassen, L. A., Pham, V., Mahabadi, N., Hall, C., Stallings, E., & Kavazanjian, E. (2017). Desaturation via Biogenic Gas Formation as a Ground Improvement Technique. PanAm Unsaturated Soils 2017, 244–256. https://doi.org/10.1061/9780784481677.013

[175] Wang, L., van Paassen, L., Gao, Y., He, J., Gao, Y., & Kim, D. (2020). Laboratory Tests on Mitigation of Soil Liquefaction Using Microbial Induced Desaturation and Precipitation. Geotechnical Testing Journal, 44(2), 20190432. https://doi.org/10.1520/GTJ20190432

[176] Wang, Y.-J., Han, X.-L., Jiang, N.-J., Wang, J., & Feng, J. (2020). The effect of enrichment media on the stimulation of native ureolytic bacteria in calcareous sand.

International Journal of Environmental Science and Technology, 17(3), 1795–1808. https://doi.org/10.1007/s13762-019-02541-x

[177] Whiffin, V. S., van Paassen, L. A., & Harkes, M. P. (2007). Microbial Carbonate Precipitation as a Soil Improvement Technique. Geomicrobiology Journal, 24(5), 417–423. https://doi.org/10.1080/01490450701436505

[178] Wu, J. 2002. "Liquefaction triggering and post-liquefaction deformation of Monterey 0/30 sand under uni-directional cyclic simple shear loading." Ph.D. dissertation. Dept. of Civil and Environmental Engineering, Univ. of California, Berkeley.

[179] Wu, J., Kammerer, A., Riemer, M., Seed, R., & Pestana, J. (2004). Laboratory Study of Liquefaction Triggering Criteria. 13th World Conference on Earthquake Engineering, Vancouver, BC, Canada, Paper (No. 2580), 14.

[180] Xiao, P., Liu, H., Stuedlein, A. W., Evans, T. M., & Xiao, Y. (2019). Effect of relative density and biocementation on cyclic response of calcareous sand. Canadian Geotechnical Journal, 56(12), 1849–1862. https://doi.org/10.1139/cgj-2018-0573

[181] Xiao, P., Liu, H., Xiao, Y., Stuedlein, A. W., & Evans, T. M. (2018). Liquefaction resistance of biocemented calcareous sand. Soil Dynamics and Earthquake Engineering, 107, 9–19. https://doi.org/10.1016/j.soildyn.2018.01.008

[182] Xiao, Y., Chen, H., Stuedlein, A. W., Evans, T. M., Chu, J., Cheng, L., Jiang, N., Lin, H., Liu, H., & Aboel-Naga, H. M. (2020). Restraint of Particle Breakage by Biotreatment Method. Journal of Geotechnical and Geoenvironmental Engineering, 146(11), 04020123. https://doi.org/10.1061/(ASCE)GT.1943-5606.0002384

[183] Xiao, Y., He, X., Evans, T. M., Stuedlein, A. W., & Liu, H. (2019). Unconfined Compressive and Splitting Tensile Strength of Basalt Fiber–Reinforced Biocemented Sand. Journal of Geotechnical and Geoenvironmental Engineering, 145(9), 04019048. https://doi.org/10.1061/(ASCE)GT.1943-5606.0002108

[184] Yu, X., Chu, J., Yang, Y., & Qian, C. (2021). Reduction of ammonia production in the biocementation process for sand using a new biocement. Journal of Cleaner Production, 286, 124928. https://doi.org/10.1016/j.jclepro.2020.124928

[185] Zamani, A., Liu, Q., & Montoya, B. M. (2018). Effect of Microbial Induced Carbonate Precipitation on the Stability of Mine Tailings. IFCEE 2018, 291–300. https://doi.org/10.1061/9780784481615.024

[186] Zamani, A., & Montoya, B. M. (2019). Undrained cyclic response of silty sands improved by microbial induced calcium carbonate precipitation. Soil Dynamics and Earthquake Engineering, 120, 436–448. https://doi.org/10.1016/j.soildyn.2019.01.010

[187] Zambare, N. M., Lauchnor, E. G., & Gerlach, R. (2019). Controlling the Distribution of Microbially Precipitated Calcium Carbonate in Radial Flow Environments. Environmental Science & Technology, 53(10), 5916–5925. https://doi.org/10.1021/acs.est.8b06876

[188] Zamani, A., P. Xiao, T. Baumer, T. J. Carey, B. Sawyer, J. T. DeJong, and R. W. Boulanger. 2021. “Mitigation of Liquefaction Triggering and Foundation Settlement by MICP Treatment.” *J. Geotech. Geoenviron. Eng.*, 147 (10): 04021099. https://doi.org/10.1061/(ASCE)GT.1943-5606.0002596.

[189] Zhang, J.-M., and G. Wang. 2012. “Large post-liquefaction deformation of sand, part I: physical mechanism, constitutive description and numerical algorithm.” *Acta Geotech.*, 7 (2): 69–113. https://doi.org/10.1007/s11440-011-0150-7.

[190] Zhang, X., Y. Chen, H. Liu, Z. Zhang, and X. Ding. 2020. “Performance evaluation of a MICP-treated calcareous sandy foundation using shake table tests.” *Soil Dynamics and Earthquake Engineering*, 129: 105959. https://doi.org/10.1016/j.soildyn.2019.105959.

[191] Zhang, Z., Qu, Y., Li, S., Feng, K., Wang, S., Cai, W., Liang, Y., Li, H., Xu, M., Yin, H., & Deng, Y. (2017). Soil bacterial quantification approaches coupling with relative abundances reflecting the changes of taxa. Scientific Reports, 7(1), 4837. https://doi.org/10.1038/s41598-017-05260-w

[192] Ziotopoulou, K., Montgomery, J., Bastidas, A. M. P., & Morales, B. (2018). Cyclic Strength of Ottawa F-65 Sand: Laboratory Testing and Constitutive Model Calibration. Geotechnical Earthquake Engineering and Soil Dynamics V, 180–189. https://doi.org/10.1061/9780784481486.019

[193] Ziotopoulou, K., Montgomery, J., Parra Bastidas, A.M., and Morales, B. (2018). “Cyclic response of Ottawa F-65 Sand: Laboratory and numerical investigation.” Proc. *Geotechnical Earthquake Engineering and Soil Dynamics V* (GEESDV 2018), June 10 – 13, 2018, Austin, Texas.

[194] Ziotopoulou, K., and R. W. Boulanger. 2016. “Plasticity modeling of liquefaction effects under sloping ground and irregular cyclic loading conditions.” *Soil Dynamics and Earthquake Engineering*, 84: 269–283. https://doi.org/10.1016/j.soildyn.2016.02.013.

APPENDIX A. CHAPTER 5 SUPPLEMENTARY TABLES AND FIGURES

Supplemental Table 5.1. Summary of Stimulation and Cementation Solutions for Experiment Sets A and B Columns

		Yeast Extract Additions		Stimulation Solutions				Cementation Solutions			
Exp.	Column	YE (g/L)	YE Frequency	Urea (mM)	NH_4Cl (mM)	NaOAc [1] (mM)	Initial pH	Urea (mM)	$CaCl_2$ (mM)	NH_4Cl (mM)	NaOAc [1] (mM)
A	1	0.2	daily	50	100	42.5	9	350	250	100	42.5
A	2	0.07	daily	50	100	42.5	9	350	250	100	42.5
A	3	0.01	daily	50	100	42.5	9	350	250	100	42.5
A	4	0.07	alternating	50	100	42.5	9	350	250	100	42.5
B	1	0.2	daily	50	100	42.5	9	250	250	100	42.5
B	2	0.08	daily	50	100	42.5	9	250	250	100	42.5
B	3	0.04	daily	50	100	42.5	9	250	250	100	42.5
B	4	0.02	daily	50	100	42.5	9	250	250	100	42.5
B	5	0.2	alternating	50	100	42.5	9	250	250	100	42.5
B	6	0.08	alternating	50	100	42.5	9	250	250	100	42.5
B	7	0.04	alternating	50	100	42.5	9	250	250	100	42.5
B	8	0.02	alternating	50	100	42.5	9	250	250	100	42.5

[1] Sodium acetate is abbreviated as “NaOAc”

Supplemental Table 5.2. Summary of Treatment Variations and Post-treatment Improvements for Experiment Set A Columns

	Treatment Solutions		$CaCO_3$ Measurements			
Column	YE (g/L)	YE Frequency	Distance From Injection (mm)	Section Average $CaCO_3$ By Mass (%)	Standard Deviation of Section $CaCO_3$ Measurements (%)	Column Average $CaCO_3$ by Mass (%)
1	0.2	daily	0 to 38	4.92	0.221	4.41
			38 to 76	5.06	0.236	
			76 to 114	4.15	0.109	
			114 to 152	3.52	0.032	
2	0.07	daily	0 to 38	4.24	0.212	4.28
			38 to 76	4.46	0.397	
			76 to 114	4.65	0.722	
			114 to 152	3.79	0.685	
3	0.01	daily	0 to 38	3.61	0.728	1.84
			38 to 76	1.65	0.209	
			76 to 114	0.92	0.075	
			114 to 152	1.18	0.127	
4	0.07	alternating	0 to 38	5.23	0.178	4.91
			38 to 76	4.88	0.311	
			76 to 114	5.50	0.370	
			114 to 152	4.05	0.566	

Supplemental Table 5.3. Summary of Treatment Variations and Post-treatment Improvements for Experiment Set B Columns

	Treatment Solutions		$CaCO_3$ Measurements				Vs Measurements
Column	YE (g/L)	YE Frequency	Distance From Injection (mm)	Section Average $CaCO_3$ By Mass (%)	Standard Deviation of Section $CaCO_3$ Measurements (%)	Column Average $CaCO_3$ by Mass (%)	∆Vs (m/s)
1	0.2	daily	0 to 38	4.84	0.105	3.72	592
			38 to 76	4.04	0.243		
			76 to 114	3.37	0.320		
			114 to 152	2.62	0.802		
2	0.08	daily	0 to 38	4.97	0.028	3.93	595
			38 to 76	4.25	0.138		
			76 to 114	3.82	0.192		
			114 to 152	2.69	0.200		
3	0.04	daily	0 to 38	5.37	0.261	4.12	448
			38 to 76	4.29	0.144		
			76 to 114	3.50	0.109		
			114 to 152	3.32	0.241		
4	0.02	daily	0 to 38	4.71	0.191	4.14	555
			38 to 76	4.83	0.031		
			76 to 114	3.52	0.475		
			114 to 152	3.49	0.299		
5	0.2	alternating	0 to 38	4.10	0.004	3.52	550
			38 to 76	4.07	0.152		
			76 to 114	2.98	0.173		
			114 to 152	2.94	0.108		
6	0.08	alternating	0 to 38	4.99	0.226	3.96	573
			38 to 76	3.95	0.566		
			76 to 114	3.18	0.129		
			114 to 152	3.74	0.156		
7	0.04	alternating	0 to 38	5.16	0.635	4.42	464
			38 to 76	4.85	0.478		
			76 to 114	4.39	0.276		
			114 to 152	3.26	0.128		
8	0.02	alternating	0 to 38	5.21	0.128	4.60	521
			38 to 76	4.99	0.088		
			76 to 114	4.42	0.056		
			114 to 152	3.79	0.274		

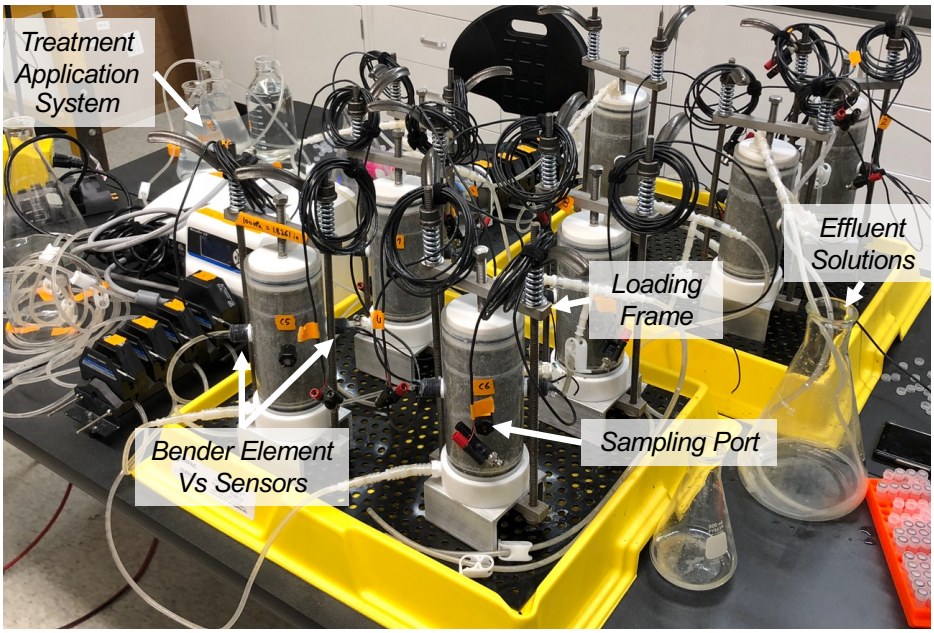

Supplemental Figure 5.1. Image of soil column experiments including locations of bender element V_s sensors, sampling ports, loading frames, the treatment application system, and collected effluent solutions.

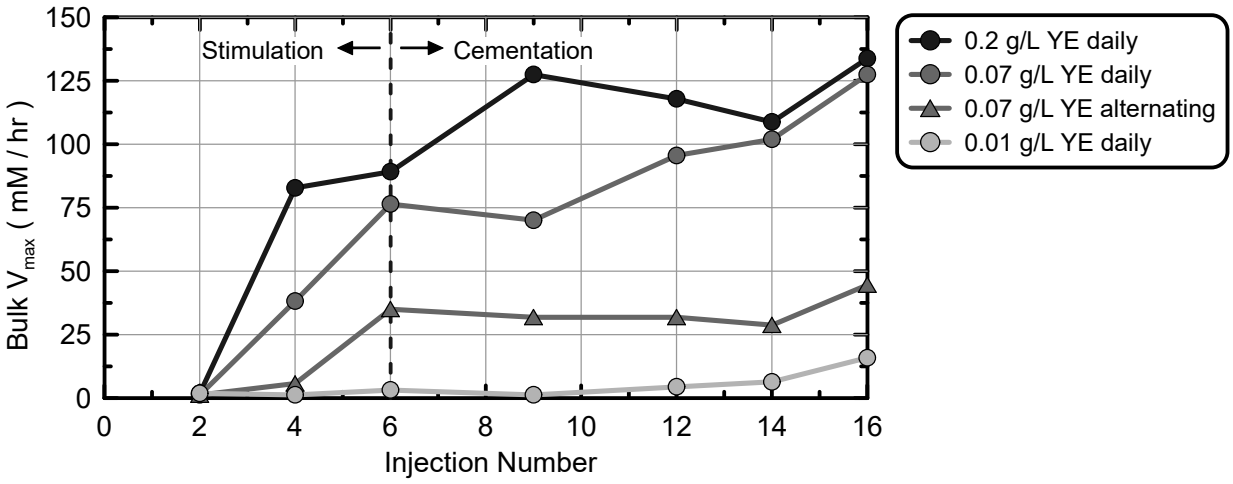

Supplemental Figure 5.2. Fitted bulk V_{max} values for all experiment set A columns during stimulation and cementation injections.

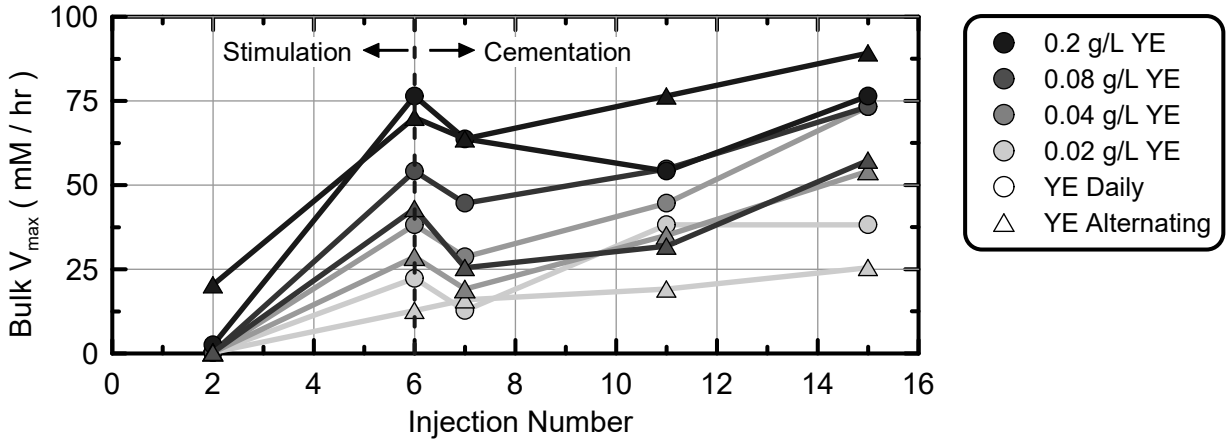

Supplemental Figure 5.3. Bulk V_{max} values for all columns from experiment set B during stimulation and cementation injections.

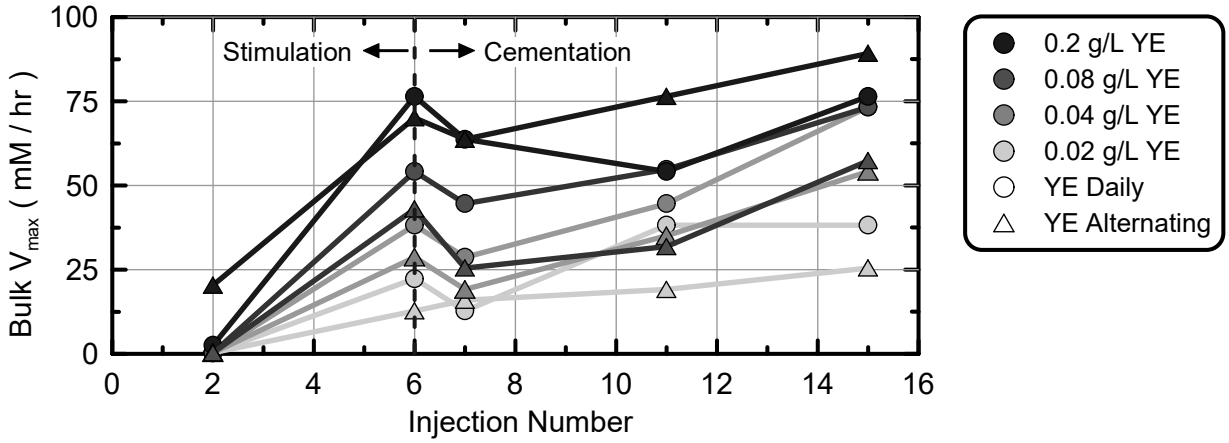

Supplemental Figure 5.4. Comparison of normalized bromide concentrations (C/C_0) measured at the column outlet in physical 3.67-meter-long soil column experiments and simulated values from the calibrated PHREEQC advective-dispersive soil column numerical model (n = 0.234, α_L = 0.3 m).

APPENDIX B. CHAPTER 7 SUPPLEMENTARY FIGURE

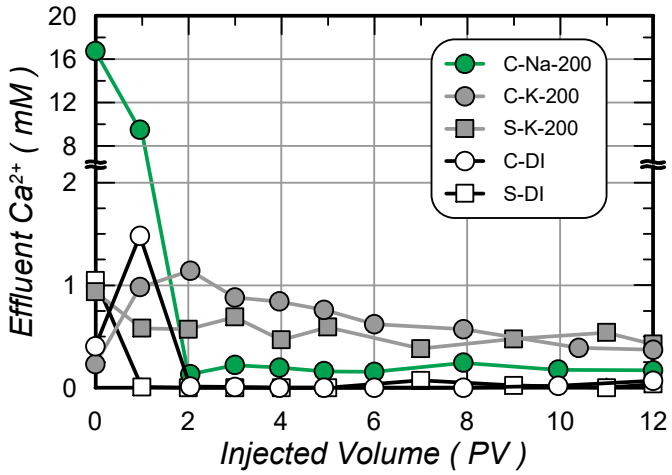

Supplemental Figure 11.1. Measurements of aqueous Ca^{2+} concentrations in effluent solutions during rinse injections versus injected volume for five select soil columns.

APPENDIX C. CHAPTER 10 SUPPLEMENTARY TABLES

Supplemental Table 1. Summary of Initial Specimen Properties, Applied Loadings, and Pre-triggering and Post-triggering Behaviors for Undrained Cyclic Tests Performed on Uncemented Specimens at Varying Initial Densities Achieving 3% SASS Prior To Reaching the Target CSR

Specimen Initial Properties [1]					*Loading*	*Pre-triggering Results*			*Post-triggering Results*				
Packing[2]	D_r initial (%)	ρ_d (kg/m^3)	V_s initial (m/s)[3]	CSR $_{3\% \text{ SASS in 0.25 cycles}}$	CSR	Cycles to r_u = 0.475	Cycles to r_u = 0.95	Cycles to 3% SASS	Cycles to 5% SASS	Cycles to 9% SASS	Cycles to 24% DASS	Reconsolidation Strain (%)[4]	ΔV_s after shearing and reconsolidation (m/s)[3]
L	25.5	1549	151	0.14	0.2	0.17	0.51	0.18	0.18	0.19	0.63	2.21	-4
L	32.8	1567	-	0.17	0.2	0.17	0.50	0.17	0.17	0.17	1.06	2.37	-
L	34.7	1571	139	0.18	0.2	0.25	0.50	0.26	0.26	0.57	1.06	2.28	7
M	43.8	1595	142	0.22	0.2	0.21	0.52	0.25	0.60	1.58	2.18	2.13	18
L	29.7	1559	142	0.16	0.25	0.15	0.51	0.15	0.15	0.16	0.61	2.00	3
L	29.0	1557	133	0.15	0.25	0.15	0.50	0.15	0.16	0.17	0.58	2.26	13
M	52.5	1618	164	0.27	0.25	0.18	0.53	0.20	0.64	1.65	3.16	1.89	-12
L	27.2	1553	141	0.15	0.3	0.12	0.49	0.12	0.12	0.13	0.55	2.52	32
L	35.5	1573	139	0.18	0.3	0.12	0.49	0.12	0.12	0.13	0.54	2.74	18
M	52.0	1616	147	0.27	0.3	0.42	0.53	0.21	0.62	1.64	3.63	1.56	-7
M	56.2	1627	153	0.30	0.3	0.43	1.02	0.23	0.62	1.65	3.64	1.47	-16

[1]All specimens were initially consolidated to σ'_v = 100 kPa

[2]L= loose, M= medium-dense, D= dense

[3]V_s values are reported when bender element measurements were performed

[4]All specimens were re-consolidated back to σ'_v = 100 kPa

Supplemental Table 2. Summary of Initial Specimen Properties, Post-treatement Specimen Properties, Applied Loadings, and Pre-triggering and Post-triggering Behaviors for Undrained Cyclic Tests Performed on Biocemented Loose Specimens Achieving 3% SASS Prior To Reaching the Target CSR

Specimen Initial Properties [1]			*Post-cementation Specimen Properties*						*Loading*	*Pre-triggering Results*			*Post-triggering Results*				
Packing[2]	D_r initial (%)	V_s initial (m/s)	ΔV_s from cementation (m/s)	$CaCO_3$ by mass (%)	COV of $CaCO_3$ (%)	ρ_d (kg/m^3)	$\Delta\rho_d$ (kg/m^3)	CSR $_{3\% \text{ SASS in } 0.25 \text{ cycles}}$	CSR	Cycles to r_u = 0.475	Cycles to r_u = 0.95	Cycles to 3% SASS	Cycles to 5% SASS	Cycles to 9% SASS	Cycles to 24% DASS	Reconsolidation Strain (%)[3]	ΔV_s after shearing and reconsolidation (m/s)
L	30.9	135	9	0.19	22	1565	1	0.19	0.25	0.17	0.51	0.19	0.20	0.21	0.55	3.03	-4
L	37.0	144	14	0.17	9	1580	1	0.21	0.3	0.24	0.51	0.26	0.27	0.28	0.56	2.70	-14
L	25.1	139	32	0.38	12	1554	2	0.30	0.3	0.37	0.52	0.29	0.29	0.58	1.04	2.45	-24
L	35.2	143	103	0.54	8	1594	9	0.65	0.5	0.47	0.04	0.14	0.22	0.62	1.02	1.72	-76

[1]All specimens were initially consolidated to σ'_v = 100 kPa

[2]L= loose, M= medium-dense, D= dense

[3]All specimens were re-consolidated back to σ'_v = 100 kPa